Ensilication of tetanus toxin C fragment for the development of thermostable vaccines

Doekhie, Aswin

Award date:
2019

Awarding institution:
University of Bath

Ensilication of tetanus toxin C fragment for the development of thermostable vaccines

submitted by

Aswin Doekhie

for the degree of Doctor of Philosophy

of the

University of Bath

Department of Chemistry

June 2019

Contents

Summary

The majority of vaccines consist of proteins derived from pathogens that, upon vaccination, provide humans with long-term immunity against infectious disease. Vaccine proteins are susceptible to environmental changes. Fluctuations in temperature are the foremost cause of protein degradation and will result in vaccines being ineffective. In short, many vaccines lack thermal stability. Vaccine manufacturer's therefore store and transport vaccines under continuous refrigeration (2 – 8 °C), known as the "cold-chain". This increases the longevity of vaccines but is also a very costly procedure. Studies have shown several operational problems within cold-chain and this is reflected in the high prevalence of vaccine-preventable diseases, especially in developing countries.

This project investigated the application of a previously developed method, ensilication, to stabilise vaccine proteins with use of silica to prevent thermal denaturation. This could provide an alternative to freeze-drying (lyophilisation) as some vaccines use excipients to improve efficacy which makes them unsuitable for lyophilisation. The 'sol-gel' method on which ensilication is based uses an inorganic compound, tetra-ethyl ortho-silicate (TEOS), to produce a polymer particle which can link around and interact with biomolecules present in buffered aqueous solution. This protects against temporal fluctuations in dry powdered form. After storage, the ensilicated protein can be released using a chemical method that removes the silica shell. Recombinant tetanus toxin c fragment (TTCF) was the model protein (antigen) utilised here to establish the feasibility of vaccine ensilication.

Structural and physical analysis of ensilicated TTCF, pre- (native) and post-ensilication (released), showed the retention of protein structure and functional properties. Additionally, *in vivo* animal experiments confirmed retention of released TTCF immunogenicity in mice. This included ensilicated TTCF that was subjected to extreme heat, displaying the thermal resilience of ensilicated material. Finally, synchrotron small angle x-ray scattering (SAXS) experiments elucidated the mechanism of stabilisation. Overall, this study shows a promising application of ensilication for the development of thermostable vaccines.

Acknowledgements

I would like to thank Dr Asel Sartbaeva for giving me the opportunity to conduct this project in her group. Her scientific understanding and positive motivation has been of great help and inspiration during my PhD. My gratitude goes out to Prof. Jean van den Elsen for his scientific guidance on structural biology matters and the *in vivo* studies, and for being a fellow Dutchman of course. Many thanks to Dr Francoise Koumanov for setting me up in her lab and providing invaluable support throughout my PhD with biology related topics. Thanks are also due to Dr Kevin Marchbank, his immunological expertise was a major asset to this project.

To the Annett Trust, words cannot describe the gratitude for the financial support throughout my PhD.

I am indebted to my fellow PhDs, Dr Yun-Chu Chen and Dr Antony Nearchou for their help. To Ayla, I am thankful for your support and discussions over many topics. Special thanks to Dr Jean-Michel Carter for the informal scientific discussions and interactions, in and out of the lab. Thanks go to Dr Rajeev Dattani for being instrumental in his guidance on SAXS. Not to forget, thanks to all the Masters' students that have been involved in this project with me. I thank Dr Chase Zexin Chen for his guidance on the protein purification and crystallography. Many thanks to all my colleagues during my time as research technician in industry at Crucell and Mymetics which led me to this PhD project.

To my parents and brother, their help and support have been of significant importance in my pursuit of academic interests. Thanks go to Rachel's family for their continued support. Last but not least, I thank Rachel for supporting me during my PhD and for always being there. To my newborn sons, Jake and Alfie, writing this thesis while they were born was challenging, but the time that it gave me to spend with them was totally worth it.

Declaration of work done in conjunction with others

The animal work done for the *in vivo* studies TTCF and lysozyme were performed by Dr Yi Yang and Dr Joshua Paulin under supervision of Dr Kevin Marchbank from the Department of Cellular Immunity, School of Medicine, Newcastle University.

The released lysozyme x-ray diffraction acquisition and model refinement were done by Dr Chase Zexin Chen and Dr Susan Crennell from the Department of Biology and Biochemistry at the University of Bath.

Publications

Doekhie, A., Chen, YC., Koumanov, F., van den Elsen, J. and Sartbaeva, A.
Enhancing the thermal stability of vaccines using silica
Conference Paper, Nov. 2016, XXIV International Conference on Bioencapsulation.

Chen, Y.-C., Smith, T., Hicks, R. H., **Doekhie, A.**, Koumanov, F., Wells, S. A., Edler, K. J., van den Elsen, J., Holman, G. D., Marchbank, K. J. & Sartbaeva, A.
Thermal stability, storage and release of proteins with tailored fit in silica.
Scientific reports, 2017, 7, 46568, doi: 10.1038/srep46568

Doekhie, A., Dattani, R., Chen, Y.-C., Yang, Y., Smith, A., Silve, A. P., Koumanov, F., Edler, K. J., Marchbank, K. J., van den Elsen, J. & Sartbaeva, A.
Time-resolved SAXS study of in situ silica stabilized tetanus antigen with retained immunogenicity in vivo (submitted for publication)

Ayla Wahid, **Aswin Doekhie**, Asel Sartbaeva, Jean van den Elsen
Ensilication Improves the Thermal Stability of the Tuberculosis Antigen Ag85b and a Sbi-Ag85b Vaccine Conjugate (submitted for publication)

Aswin Doekhie, Lucy Cliff, Matthew N. Slade, Remi Castaing, Karen J. Edler, Francoise Koumanov, Jean van den Elsen and Asel Sartbaeva.
Calorimetric analysis confirms thermal resilience of silica stabilised, 'ensilicated', lysozyme. (manuscript in preparation)

List of Figures

List of Tables

List of Abbreviations

1D	One dimensional
2D	Two dimensional
30-DTRs	30 day digital temperature recorders
ANOVA	Analysis of variance
APBS	Adaptive Poisson-Boltzmann solver
APS	Ammoniumpersulphate
ATR	Attenuated total reflectance
AU	Arbitrary units
BCA	Bicinchoninic acid
BSA	Bovine Serum Albumin
CCM	Cold chain monitoring
CD	Circular dichroism
CSM	Central spectral mass
DAWN	Data Analysis WorkbeNch
dd	Double distilled
DLS	Dynamic light scattering
DMSO	Dimethylsulfoxide
DNA	Deoxyribonucleic acid
DSC	Differential scanning calorimetry
DTA	Differential thermal analysis
DTP	Diphteria, tetanus and pertussis
DTT	Dithiothreitol
EDTA	Ethylenediaminetetraacetic acid
ELISA	Enzyme linked immunosorbent assay
EM	Electron microscopy
EPI	Expanded programme on immunisation
ESRF	European synchrotron research facility
FE-SEM	Field emission scanning electron microscopy
FPLC	Fast protein liquid chromatography
FT-IR	Fourier transform infra-red
GRAS	Generally regarded as safe
HB	Hepatitis B

HC	Heavy chain
HiB	Heamofillus Influenza B
HOMO	Highest occupied molecular orbital
HRP	Horseradish peroxidase
IEP/Pi	Isoelectric point
IgG	Immunogammaglobulin G
ILR	Ice-lined refrigerators
IMAC	Immobilised metal-ion chromatography
IPTG	β-D-1-thiogalactopyranoside
IPV	Inactivated polio virus
JEV	Japanese encaphelitis virus
kDa	KiloDalton
LB	Luria broth
LC	Light chain
LPS	Lipopolysaccharide
LUMO	Lowest unoccupied molecular orbital
MHC	Major histocompatibility complex
MS	Mass spectrometry
mV	Millivolt
MWCO	Molecular weight cut off
NMR	Nuclear magnetic resonance
OD	Optical density
PA	Protective antigen
PBS	Phosphate buffered saline
PDB	Protein data bank
PLGA	Poly(lactic-co-glycolic acid)
PRRS	Porcine reproductive and respiratory syndrome
rpm	Rounds per minute
SANS	Small angle neutron scattering
SAXS	Small angle x-ray scattering
SDS-PAGE	Sodium-dodecyl-sulphate polyacrylamide gel electrophoresis
SLD	Scattering length density
SNR	Signal-to-noise ratio
SOP	Standard operating procedure
TEOS	Tetra-ethyl orthosilicate
TGA	Thermogravimetric analysis

TMB	Tetra-methyl-benzidine
TT	Tetanus toxoid/toxin
TTCF	Tetanus toxin C fragment
UK	United Kingdom
UV	Ultra-violet
UVRR	UV resonance Raman
VFD	Vacuum foam drying
VVM	Vaccine vial monitoring
WB	Western blot
WHO	World health organisation
XRD	X-ray diffraction

Chapter 1

Introduction

1.1 Vaccines

One of humanity's greatest achievements in reducing microbial infections was the discovery of vaccines. Dr Edward Jenner (17 May 1749 – 26 January 1823) is the inventor of the first vaccine[1]. The word vaccine is derived from the Latin word for cow, 'vacca' and was used as recognition of Dr Jenners exceptional work in improving global health. He studied the transmittance of *Variolae Vaccinae*, cowpox, from horses to cows and subsequently to humans. Local farm staff were unknowingly spreading the disease from horses which were being tended due to a heel infection in which the virus was present. Without understanding of hygiene, the farm hands and milk maidens transferred the cowpox virus via their hands to the nipples of cows. Soon after, those who were infected started producing pustules at the site of infection. The disease would last for several days until it settled down. Unfortunately, it was highly contagious and spread quickly to other animals and disrupted daily operation.

The critical observation that Dr Jenner made was the inferred protection these people gained against smallpox after exposure to cowpox. He studied twenty-three cases with people of all genders and ages and inoculated them with effluvia (liquid from pustule) and subcutaneous injection of either cowpox and smallpox infectious material. Those who previously had been exposed to cowpox and were inoculated with smallpox displayed some clinical symptoms associated with smallpox but these did not progress towards the normal severity of this disease. He also inoculated children, who had not been exposed to cowpox, with exudate collected from a cowpox pustule on the hand of farm workers and subsequently tested whether these children were protected once exposed to smallpox. He found that all those who were

exposed to cowpox, either recently or in their younger years were protected against smallpox.
Thanks to his efforts and of those who improved the smallpox vaccine efficacy, this disease has been completely eradicated[2]. However, it should be noted that smallpox was a human specific pathogen with no additional reservoir species that could transmit it through the population. It was also a highly stable virus that was not prone to mutate. The key property of the vaccine was its stability at room temperature and this was imperative to worldwide eradication.

1.1.1 Cold-Chain: Vaccine transportation

One of the crucial issues with vaccines is the instability they possess. They, as many biological compounds, are not thermally stable (figure 1-1)[3–8]. Despite this, with the success of smallpox vaccinations, the Expanded Programme on Immunisation (EPI) set out to vaccinate every child before the 1990s. Therefore, the World Health Organisation (WHO) set out to introduce a straightforward way of increasing vaccine shelf-life, the 'cold-chain' (figure 1-2). This logistics network, built out of refrigerated components, would ensure vaccine distribution at 2-8 °C from manufacturer to patient administration[9]. As with many large-scale projects, there were and still are several challenges at hand which cause about 50% of vaccines transported today being wasted[11]. In more detail, in 1977, researchers established an action plan to fulfil the EPI strategy[12]. Monitoring of vaccine storage conditions was the first challenge. Initially, refrigeration temperature was recorded by health workers reading and documenting fridge temperatures. This was a highly unreliable method and was difficult to maintain. This issue was resolved when cold-chain monitoring (CCM) tools were developed. For example, blue wax absorption was able to indicate whether a vaccine had been exposed to heat. Shortly after came an improved version: A sticker, containing a polymer, that would change colour after heating and this reaction could not be reversed. It was a major success that helped health workers to identify redundant vials. The only obstacle left for CCM was identification of vials that had been exposed to freezing.
Currently, the cold-chain utilises 30 day digital temperature recorders (30-DTRs) which can be read at any time. This has drastically improved the vaccine vial monitoring (VVM) system[13,14]. The following challenges were of infrastructural nature. Electricity, or the lack thereof, was a considerable problem in the early days. Absorption-refrigerators used fuel to cool vaccines. Although used, they did not have the per-

formance to meet the required cooling standard for vaccines. Additionally, due to problems with the grid, electric-compression refrigerators could not be used as these would not remain cool for more than several hours. Another challenge was the intermediate forms of small-scale transport. Insulated boxes helped to cool vaccines but would only last 48 hours. Therefore, engineers developed a way to improve cooling. They lined both normal cooled-boxes and fridges with ice. These cooled-boxes could now keep vaccines cool up to 5 days and ice-lined refrigerators (ILR) were able to maintain cooling up to 8 hours without electricity thus making them the ideal machine to utilise. With the addition of solar panels, the ILRs are now mainly used in areas with poor infrastructure[15].

The last problem with cold-chain is the operators or health workers. Inadequate handling, documentation and under-staffing has led to significant losses of vaccines[11]. The WHO set up courses and training facilities in order to improve this aspect of cold-chain. An important development was the shake-test. Vaccine vials exposed to freezing conditions could form ice crystals after being shaken. This method allowed elimination of those affected vials, instead of using these in immunisation programmes with no efficacy. As staffing is a difficult theme to tackle, elimin-

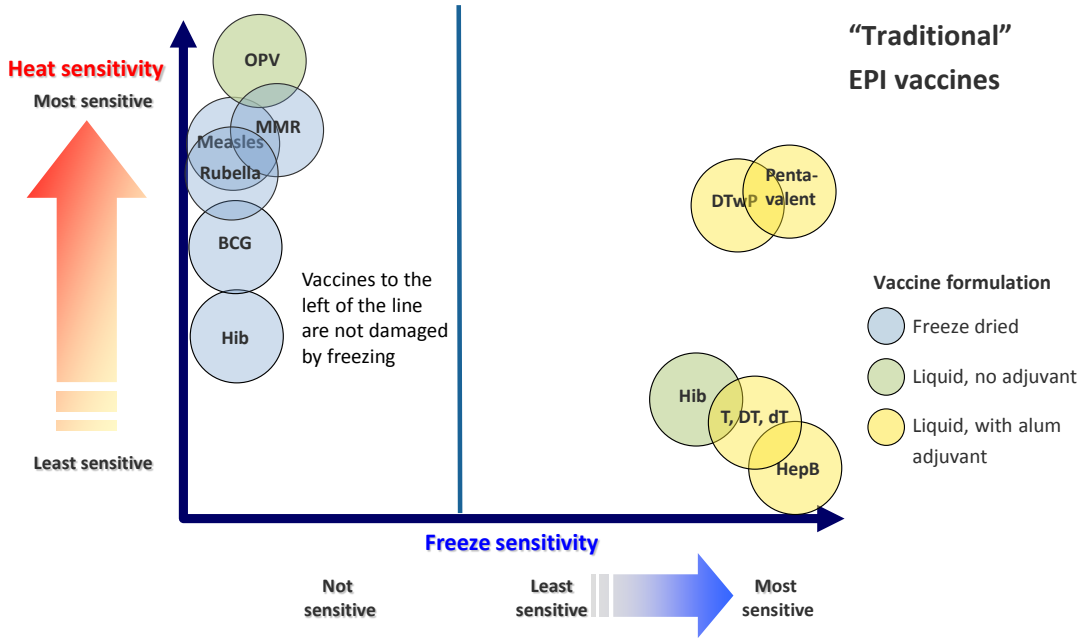

Figure 1-1: Thermal stability of EPI vaccines. Evident here is the segregation of liquid and freeze-dried formulated vaccines. DTP and the pentavalent vaccine are both freeze and heat sensitive. OPV: Oral polio vaccine; MMR: Measles, mumps and rubella; HiB: Haemophilus influenzae type b; BCG: Bacille Calmette-Guerin (against tuberculosis); T: Tetanus; D: Diphteria; wP: whole Pertussis; HepB: Hepatitis B.[10]

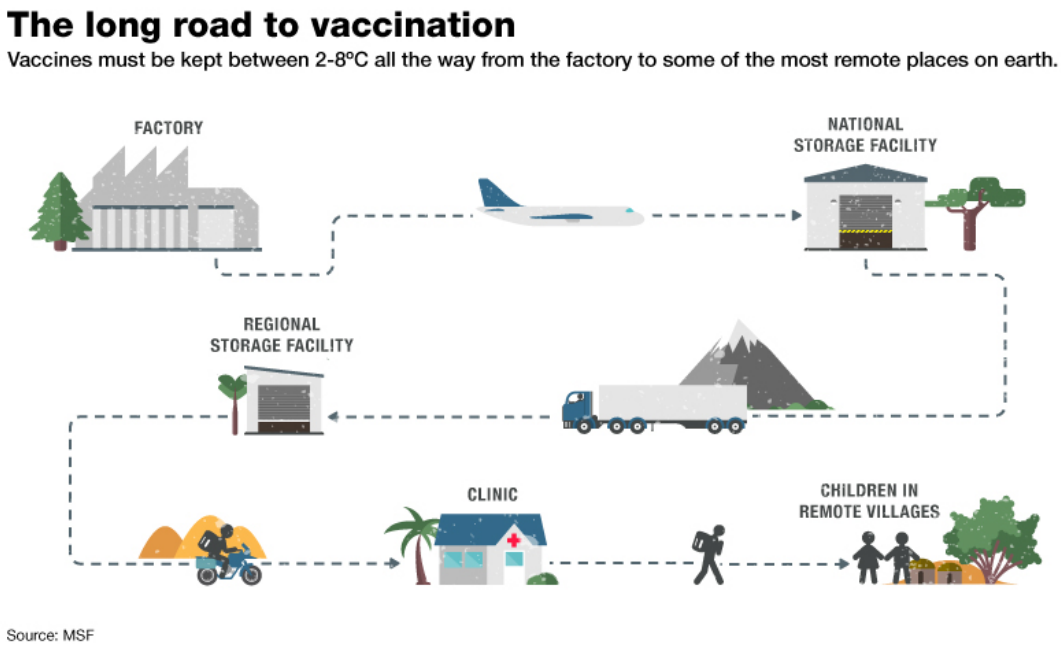

Figure 1-2: Cold-chain distribution. The logistics of vaccines requires strict conditions. From factory to patient, temperature must be regulated and maintained between 2-8 °C. The cold-chain is as strong as its weakest link which is situated at the end, the last leg of vaccine journey. In many cases this is from either a warehouse or hospital to the patients in difficult to reach areas and therefore require cooled-boxes for transportation which have limited cooling capability.[11].

ating the cold-chain over time with the development of more thermostable vaccines is one of their main priorities. This will ease handling and prevent errors plaguing the cold-chain infrastructure.

In 2011 the WHO set up the Global Vaccine Action Plan (GVAP) for 2011-2020. This 'Decade of Vaccines' was aimed to provide vaccination for all those in need by 2020 and beyond. The WHO set up six guiding principles which would help developing countries to take charge of their own vaccination programmes[10].

A vaccine coverage survey from 2014 (table 1-3) showed high levels of vaccination in developed regions. However, there are still a number of challenges in Asia and Africa which have lower levels of vaccination[16]. Vaccination is most effective against vaccine-preventable infectious diseases when a high percentage of the population (80 - 95 %) is vaccinated, providing herd-immunity. This helps to prevent infectious diseases from spreading within a population[17,18]. Therefore, attaining high vaccination levels in communities acts as the first line of defence against epidemics. To achieve this, vaccines must be readily available, however in many occasions the distribution of vaccines to and within countries with poor infrastructure *is* comprom-

Vaccination coverage									
WHO region	HepB BD	HepB3	DTP3	Hib3	Rota last	PCV3	Rubella	MCV1	MCV2
Total (worldwide)	38	82	86	56	19	31	46	85	56
African	10	77	77	77	30	50	10	73	11
Americas	69	88	90	90	71	83	92	92	51
Eastern Mediterranean	24	83	82	72	22	45	42	77	66
European	39	82	95	85	7	44	94	94	84
South-East Asia	29	75	84	30	0	0	12	84	59
Western Pacific	80	92	96	21	1	2	91	97	93

Figure 1-3: Vaccination coverage by vaccine and WHO region — worldwide, 2014*. HepB BD = hepatitis B vaccine birth dose; HepB3 = 3 doses of hepatitis B vaccine; DTP3 = 3 doses of diphtheria-tetanus-pertussis vaccine; Hib3 = 3 doses of Haemophilus influenzae type b vaccine; Rota last = last dose of rotavirus series; PCV3 = 3 doses of pneumococcal conjugate vaccine; MCV1 = 1st dose of measles containing vaccine; MCV2 = second dose of measles-containing vaccine. Numbers represent % vaccine coverage.* Weighted regional average.[16]

ised[19–21]. At present, the incidence of mortality due to vaccine preventable disease, mainly caused by ineffective vaccine transport, is approximately equal to the number of lives, 2.5 million, saved by vaccination yearly. Half of the deaths (approximately 1.5 million) are of children aged under 5 years[22]. This all relates to the share of vaccines that loses efficacy during the last stage of cold-chain and accounts for about 45 % of all vaccines transported[23]. The most recent report on the Decade of Vaccines, written by a group of experts at request of the WHO, concluded that the aims will not be met by 2020[24]. This conclusion came from observations that overshadowed successes gained. Especially, the outbreaks of measles and diphtheria in areas which held elimination status were major setbacks and displayed a novel difficult problem[24].

Vaccine complacency and hesitancy have been a growing issue over the past few years[25–28]. This resulted in pockets of low vaccination coverage in developed countries and were followed by these outbreaks. Not only these problems influence vaccination coverage. The volatile and uncertain political environment in many countries today affects budget spending on national immunisation programs[24]. All these factors combined results into a fragile system of protection. The experts advised that all countries should improve their efforts towards vaccination, in whichever form that may be.

1.1.1.1 Case studies

Several published case studies elucidated the weak links, illustrating the problems within cold-chain. Early investigations into the cold-chain performance in South Africa showed that vaccines were kept at optimal conditions within a hospital. However, vaccines were exposed to heat for a longer duration than allowed once they needed to be sent out to remote locations. It was found that 18% and 90% of the stored and transported vaccines, respectively, were exposed to heat that could detrimentally affect their potency[29].

Surveys undertaken to investigate the cold-chain integrity during transportation of vaccines between Sydney and Hunter, Australia, showed an average temperature to be above 10°C. This inadequacy was also found within the storage conditions. Only 25% of the used refrigerators were described to be effective. These reports raised serious concerns regarding the efficacy of these distributed vaccines[30]. These conditions were also reflected in rural Tanzania[31].

Another investigation focused on trained cold-chain personnel in Madrid and showed their unawareness of the freezing effect on vaccines[32]. This was an understandable outcome for the researchers as much effort had been put towards the prevention of vaccine exposure to elevated temperatures. They found approximately 50% of staff to be unaware of the freezing effect on DTP vaccine and only 32% knew how to perform the vial shake test. The study concluded that more effort should have been put towards identifying frozen vials.

Freezing was also found to be a serious problem to Hepatitis B vaccine transportation in Indonesia with 75% of shipments recording temperatures below 0°C[33]. The cold-chain in Bolivia was monitored in an extensive investigation for the DTP-HB-HiB vaccine[21]. Shipments to numerous communities from three central stores were monitored. All recorded shipments displayed freezing temperatures up to 50% of the shipment duration. In Thailand there was a similar problem at hand. Vaccines were exposed to freezing conditions, however only mildly. The temperature recorded on average was -0.5 °C for Hepatitis B vaccines. The vial shake test confirmed no damage had been inflicted[19]. Several other studies showed good vaccine storage conditions, however had infrastructure that needed to be improved or required additional staff training[34,35]. Overall, there is a trend in vaccine exposure to heating in warmer climates. This is then combated with extra refrigeration that over-performs and inflicts freezing. The solution required is the development of thermostable vaccines as this would solve all of the above.

1.1.2 Immunology of vaccination

The field of immunology established itself from the efforts undertaken by scientists working on vaccines[36–39]. Researchers discovered a vast and complex system of cells present in human blood which would serve as guardians of the human body. This was the immune system and it was established that it possessed two main divisions: the innate and adaptive immune system[40]. The former consists of natural borders such as mucus membranes, stomach acid, skin, ubiquitous proteins and a number of other factors. The latter was described following the observation that immunity was developed after vaccination. Therefore, something must have adapted or changed within the human body. White blood cells (leukocytes) were discovered during infection and elucidated to be the active part of the adaptive immune system. White blood cells recognise pathogens they have encountered before and eliminate such threats. The most important of these is the memory B-cell, a subset of leukocytes that is responsible for providing latent protection.

During an infection, a pathogen enters the human body and is identified by the adaptive immune system (figure 1-4). Crucial to this process is antigen recognition. Antigens are proteins that possess antigenic determinants, epitopes. These can be

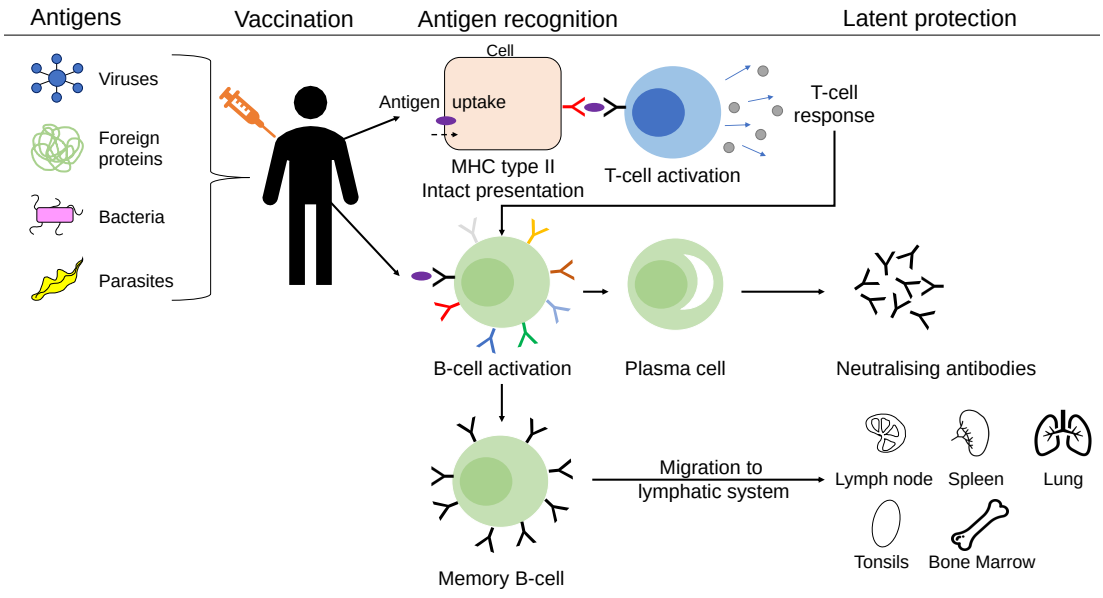

Figure 1-4: Vaccine antigen recognition. After vaccination, two major pathways are involved with antigen processing. MHC type 2 and B-cell activation allow for class switching of B-cells into memory B-cells. These subsequently migrate to the lymphatic system and remain there to provide latent protection.

classified as continuous; recognition of a exposed linear sequence in the peptide chain, or discontinuous; recognition of exposed amino acids formed by native folding of the antigen[41]. The latter is found in the majority of antigenic proteins. The recognition elicits an immune response which is mediated by antibodies[42] present on the surfaces of B-cells[43]. These cells were named after the Bursa of Fabricius where they were originally discovered[44]. Activated B-cells switch to produce a single kind of antibody[45], unique against a specific antigen. Other activated B-cells will proceed towards a lymph node and linger there. These will keep producing the soluble specific antibody which will provide latent protection and become memory-B-cells.
B-cell activation can also be achieved when cells utilise the Major Histocompatibility Complex (MHC) as another way for antigen recognition[46]. The MHC allows for uptake and processing of foreign proteins which are then presented on cell surfaces. These proteolytically cleaved epitopes span around 8 - 11 amino acids and are recognised by another subset of immune cells, T-cells, matured in the thymus[47] (hence T) which mediate the cellular immune response. Specifically, CD4+ T-cells (T-helper cells) recognise the foreign peptide processed by an antigen presenting cell (APC) , part of the innate immune system, and recruit more cells to induce an immunological response. Both pathways are necessary for generating a sufficient immune response to provide long term immunity.
Vaccination utilises this process by mimicking a natural infection using the immunogenic part of the pathogen, thereby inducing both T- and B-cell responses. It results in the formation of memory-B-cells without clinical disease occurring. The majority of vaccines consisting of antigens require adjuvants to induce latent protection.

1.1.2.1 Adjuvants

Vaccine adjuvants aid or enhance the development of protective immunity after vaccination[48]. These compounds are necessary for many vaccines that only consist of antigens compared to those with attenuated (weakened) pathogens. Although antigens themselves may elicit an immune-response this often lacks sufficient immunogenicity, therefore the necessity for adjuvants. Mineral salts, Freund's adjuvant, oil in water/water-in-oil emulsions, saponins, particles etc. are examples of adjuvants used today in various types of vaccines[49–51].
In particular, alum ($AlOH_3$) has been used for decades[52]. The mechanism of action for this compound is still relatively unknown. It was suggested that the aluminate gel used in vaccine formulations provided a sustained load of antigen release at site of injection (also referred as "the depot effect")[52]. This resulted in improved

uptake of the antigen by APCs and increased immunological activity around the site of injection. This initial understanding was amended after several studies found the depot effect not to be the key event for providing the immune response[49,50].
Another type of adjuvant is Freunds' adjuvant[53]. This is a crude cocktail of bacterial fragments created during the purification process previously used in the vaccination against bacterial toxins. It provides an excellent immunological stimuli but has had several concerns regarding safety and side-effects.
Oil-in-water/water-in-oil emulsions have exclusively been used as adjuvants in veterinary vaccines[49,51]. Dependent on the formulation some might cause local reactions on site of injection, this and other concerns are the reasoning behind the exclusivity. Adjuvants not only improve immune-response they also reduce the amount of antigen needed, therefore lowering the cost of vaccine manufacturing.
In contrast, there are concerns regarding vaccine stability, specifically alum adjuvanted vaccines. This is highlighted in section 1.3.2.

1.1.3 Protein structure

Vaccines come in many flavours as they may consist of proteins, sugars, genomic structures, viral particles or whole organisms[54]. Here, focus will be given towards protein-based vaccines.
Proteins are technically polypeptides, polymers of linked amino acids in a sequence. Their structure and function is based on the specific arrangement of nucleotides within genomic DNA that encodes for the amino acids[55]. DNA, read by specific enzymes, is transcribed and subsequently translated into a protein using the pro- and eukaryotic machinery present for this purpose[56].
Proteins have four levels of structure[57]. The linear amino acid polypeptide is the primary structure. There are 20 different amino acids commonly found in proteins (figure 1-5). These are subdivided in four groups: non-polar (hydrophobic), polar (uncharged), acidic and basic. They all possess the fundamental structure of an amino acid with their specific group, R, attached. This is made of an (alpha)α-carbon bound with an amino, H_3N^+ and carboxyl group, COO^- with the side-chain R for defining the amino acid in a tetrahedral conformation. This gives most amino acids chirality and is due to the asymmetry inherent. Polypeptides are formed by reacting the carboxyl group of an amino acid with the amino group of another (amide)[57]. This forms a (poly)peptide bond with the direction from N- to C-terminus, also known as the peptide backbone (figure 1-6).

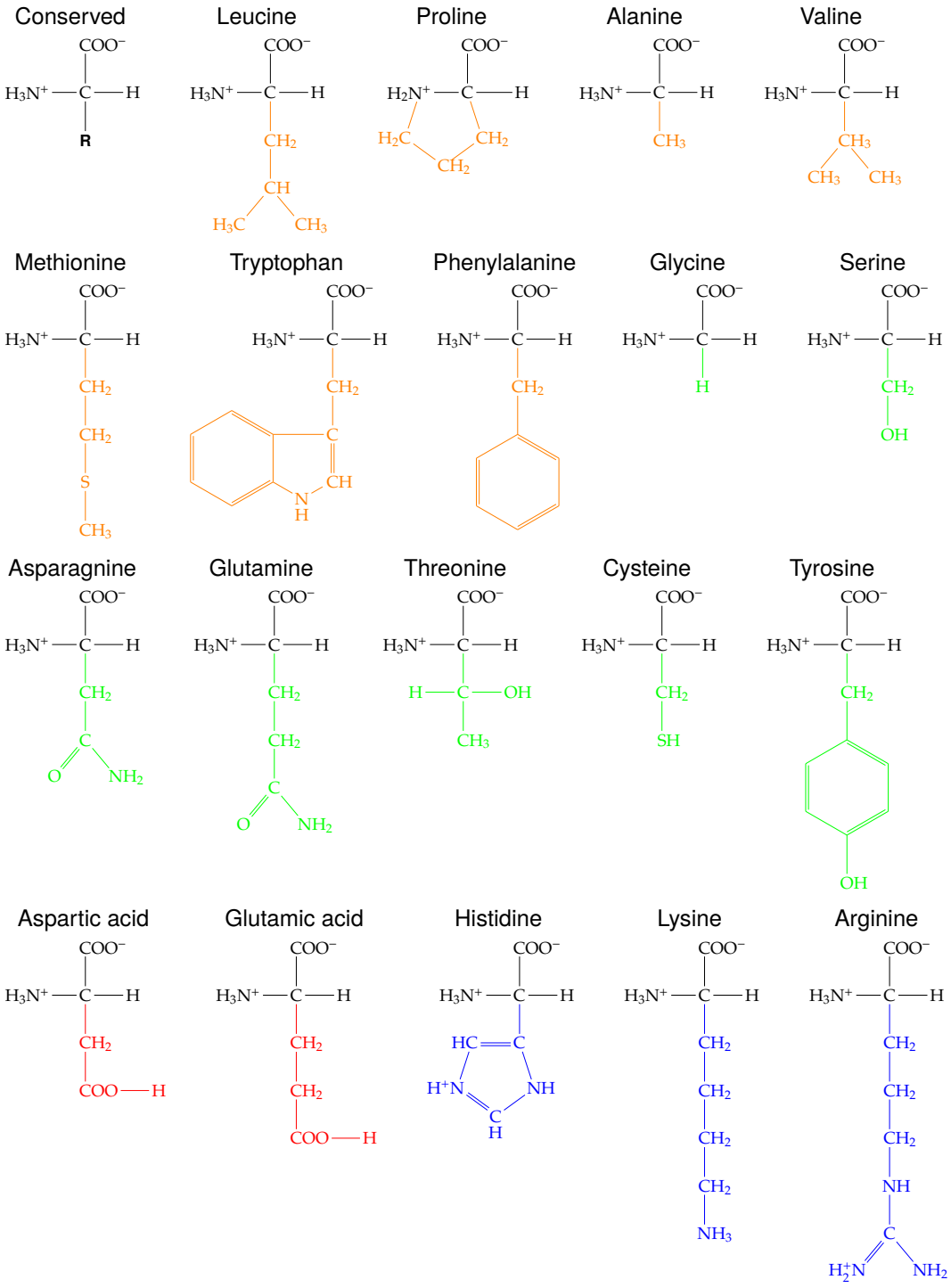

Figure 1-5: Commonly found amino acids in proteins. The conserved model shows the amino and carboxyl group with specific R-group attached. These can be subdivided based on their R group as non-polar hydrophobic (orange), polar (green), acidic (red) and basic (blue).

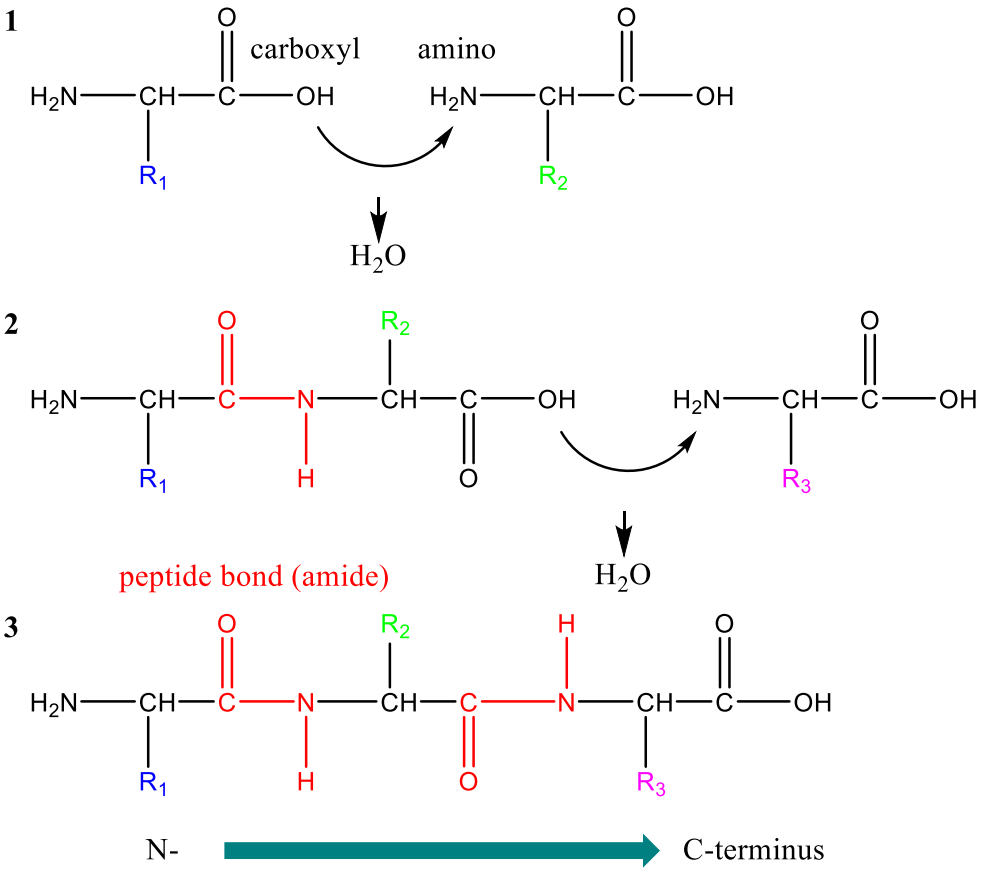

(a) peptide bond formation

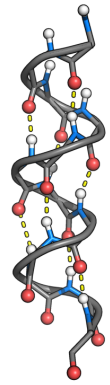

(b) alpha-helix

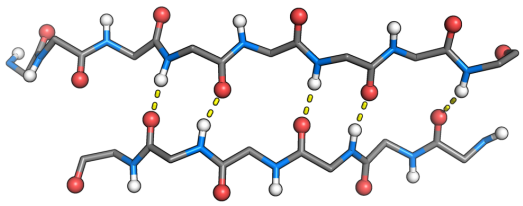

(c) beta-sheet

Figure 1-6: Polypeptide bond formation and super secondary structures. (a) peptide bond (amide) formation via the hydrolysis of a carboxyl group with an amino. (b & c) intra-chain hydrogen bonding (yellow dotted) between oxygen (red sphere) and hydrogen (white sphere) forms two major secondary structures: α-helix and β-sheet.

The secondary structure is a convolution of α-helices, (beta) β-sheets and random coils[57]. The first two have a major role in protein structure. They are formed by the intra-chain hydrogen bonding between amino acids. An α-helix is formed of one polypeptide whereas the β-sheet can consist of two or more (intra- and inter-chain). Both of these structures are periodic and possess a repetition interval. For alpha-helices, there is a turn every 3.6 Å. Here, the hydrogen bonding is parallel to the helix axis and provides the rigidity of this structure.

Within the β-sheet, the peptide backbone is nearly linear. This allows for parallel or anti-parallel hydrogen bonding, perpendicular to the peptide backbone and forms a pleated sheet. There are additional regions of combined α-helices and β-sheets forming super-secondary structures labelled motifs. β- meanders and β-barrels are two notable ones. Secondary structures influence the tertiary level. Proteins mainly consisting of either α-helices or β-sheets will form fibrous proteins. Others with good proportion of both secondary components will form globular structures which tend to be soluble in aqueous solutions. In comparison, fibrous proteins are insoluble. This clear distinction evidently shows the influence of peptide backbone arrangement.

Tertiary structure is the conformationally active form of a protein in which it carries out its function[57]. Proteins maintain their folding via several factors (figure 1-7). Hydro-

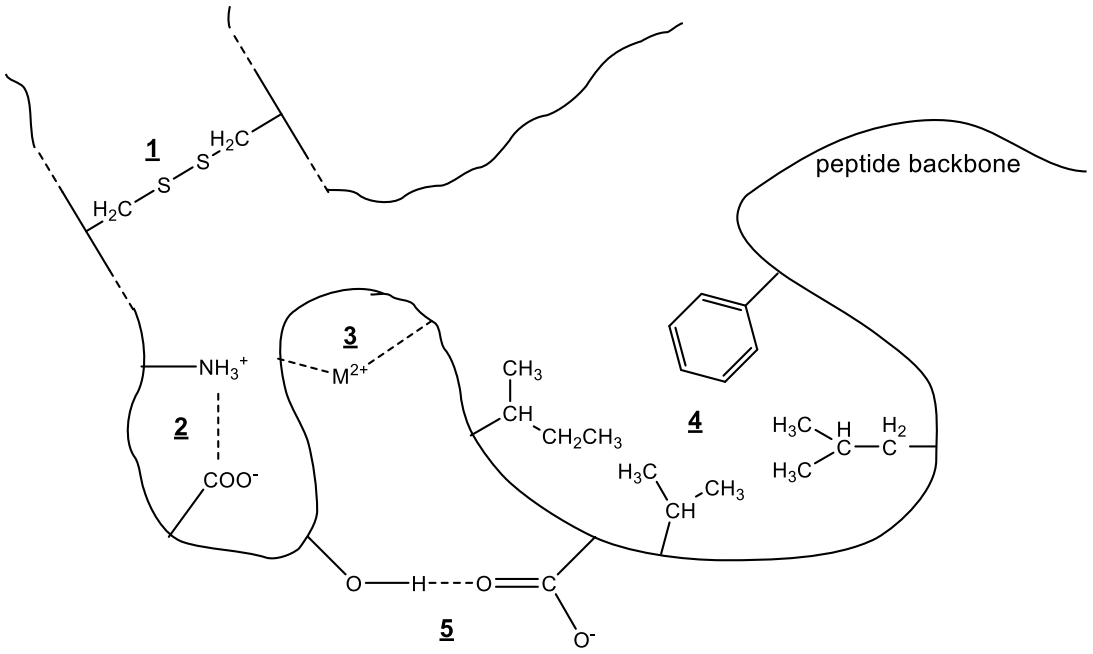

Figure 1-7: Tertiary protein structure factors.(1) Covalent bonding, disulphide bridge (2) Electrostatic interaction (3) Metal ion coordination (4) Hydrophobic interactions (5) Side chain hydrogen bonding.

gen bonding has been related to secondary structures, however within the tertiary level it plays an important role with the hydrogen bonding of amino acid side chains. This also involves salt-bridges between amino acid residues and solvent interactions. Charged groups use electrostatic attractions to stabilise the overall protein structure. This can be between amino acids and ionic ligands present. Hydrophobic interactions of non-polar side chains on the peptide backbone will obscure them from the aqueous environment[58]. This will expose the hydrophilic polar regions to the solution. Van der Waals (or covalent) bonding, disulphide bridges, will reinforce the protein structure via conformational restriction. In all, the native state of a protein is present when the combined energy of all atoms at its lowest. Notably, hydrophobic interactions are a major factor of protein folding and occur spontaneously, governed by entropy: $\Delta S_{universe} > 0$.
Quaternary structure, the fourth level, is applicable when multiple proteins combine into one larger structure. This can be applicable for enzymes. The same forces at tertiary level maintain this structure.
Heating and freezing of proteins leads to protein unfolding (denaturation) by disruption of hydrogen bonds and weakening of hydrophobic interactions[55,59]. In both cases, there is a change of energy that affects the native state of the protein.

1.1.3.1 Thermodynamics of protein folding

The change from polypeptide towards a folded state is associated with the change in (Gibbs) free energy[60] (ΔG) which cannot be calculated. However, the change is measurable using the formula for calculation of ΔG (kJ/mol). This is a combination of the first two laws of thermodynamics:

$$\Delta G = \Delta H - T\Delta S \tag{1.1}$$

Here, the change in enthalpy ΔH (kJ/mol) is described as the heat of a reaction at constant pressure. T is temperature, in Kelvin (K), and ΔS (J·mol^{-1}·K^{-1}) is the entropy of a system. Entropy (S), disorder, can be explained as, for example, the mobility of a molecule. The more dispersed in space, the higher a molecule's entropy. The levels of protein structure have various values, with polypeptide having the highest amount of entropy, decreasing with each increasing level. When ΔG is negative, a reaction occurs spontaneously and is responsible for the hydrophobic effect[61]. This can be achieved when $\Delta H > 0$ & $\Delta S > 0$ or $\Delta H < 0$ & $\Delta S > 0$.
Proteins exist in the folded (F) and unfolded (U) state in solution[60]. Whether the

system favours folded or unfolded state, the chemical equilibrium ratio constant K can be identified by establishing the relationship between K_{eq} and the free energy change at standard conditions ΔG^{o} in the form of:

$$K_{eq} = \frac{[F]}{[U]} \qquad \text{relates to} \qquad \Delta G^{o} = -RT \ln(K_{eq}) \tag{1.2}$$

Where R is the gas constant, 8.314 $J{\cdot}mol^{-1}{\cdot}K^{-1}$, T is temperature, in Kelvin (K). When $K_{eq} > 1$ the folded state is preferred and when $K_{eq} < 1$ the unfolded state is preferred . When $K_{eq} = 1$, there is an equilibrium between both states and this results in $\Delta G^{o} = 0$ as there is no change occurring.

Protein unfolding is frequently observed as a two-state transition[60,62]. This can be measured using fluorescence, UV absorbance, circular dichroism (CD), nuclear magnetic resonance (NMR) etc. The output of measurement, F (y), can be plotted against temperature, T (x). The data would allow for calculation of the apparent equilibrium constant (K_{app}) via non-linear least squares fitting of appropriate models. These could define the heat capacity, ΔC_p, and van 't Hoff enthalpy change, ΔH_{VH}, which would provide the heat constant required for the reaction and cooperative units per mole for unfolding.

Fitting would also accurately define the mid-point of transition temperature, T_m, which is influenced by buffer composition, changes in folding and other chemical contributors, and is a key parameter of protein stability.

1.1.4 Vaccine formulation and stability

Vaccines come in two formulations: liquid and dried. Liquid formulations have several key parameters which influence protein stability: pH, ionic strength, osmolarity and excipients[57].

pH is simply defined as the 10-base logarithm of $[H^+]$ ions in an aqueous solution. This is applicable to strong acids and bases. pH of a solution defines the acidity or alkalinity and affects protein folding. Usage of the Henderson-Hasselbach equation allows for calculating the pH of, for example, a buffer with consideration of weak bases and acids. It is written as followed:

$$-\log[H^+] \text{ or } [H_3O^+] = -\log K_a - \log \frac{\text{conjugate base } [HA]}{\text{acid } [A^-]} \tag{1.3}$$

$$pH = pK_a + \log \frac{[A^-]}{[HA]} \tag{1.4}$$

The [HA] and [A^-] are in molar concentration. pK_a is defined as the dissociation constant, similar to pH value, at which the acid and basic forms of a particular compound are equally dissociated in solution. pH influences the protonation and de-protonation of exposed amino acids invariably affecting hydrogen bonding and salt bridges. Researchers found that pH close to the isoelectric point, the pH at which the protein has zero charge, maintains native structure. Changes in pH can also have a detrimental effect on proteins. The hydrolysis of peptide bonds occurs at low pH and deamidation at high pH result in chemical degradation which is irreversible.
Ionic strength is defined as the capability of ions in solution to provide a shielding charge. This effect neutralises particle charges in solution and is defined as:

$$I = \frac{1}{2} \sum_{allions} m_i z_i^2 \tag{1.5}$$

where the sum of all ions with concentration m_i in molar and valency z_i^2 squared provides the ionic strength I. The higher this value, the greater the capacity of ions to mask charges present on proteins that could cause the protein to fold in an alternative conformation.
Osmolarity is related to ionic strength. It is defined as the individual compounds of a solute when dissolved in an aqueous solution. For example, 1 molar of NaCl is 1 mole of each ion in 1 litre, which is molarity. However, the osmolarity of NaCl gives each ionic component 1 osmole in 1 litre which gives rise to two osmole in 1 litre total as Na^+ and Cl^- are recognised as individual contributors to the solution. This difference between these two properties accounts for additional aspects of soluble compounds.

As noted previously, efforts towards stabilising vaccines are mainly aimed at solution stability. However, vaccines are also prepared in dried powdered form. There are several methods that are utilised: freeze-drying (lyophilisation), Xerovac™, spray drying or spray freeze-drying.
Lyophilisation or freeze-drying is the foremost used method in dried preparation of proteins[63–65]. Using the triple point of water (0.01 °C), a solution is rapidly frozen to form ice crystals, of which size is dependent on the cooling rate[66–68]. Under vacuum, the frozen water molecules move from solid to gaseous phase, sublimation takes place (primary drying)[69,70]. Hereafter, the mixture is further dried to remove non-frozen bound water attached to the protein (secondary drying)[71]. The resultant material has "a cake" like appearance. This procedure can be harsh on many pro-

teins. Several factors that support native structure are affected by the removal of water. Concentration, viscosity, ice crystal formation, pH and ionic strength are considerably altered during lyophilisation[65,69,71]. Therefore, most formulations require cryo-protectants and other chemical modulators to ensure retention of protein after reconstitution[65].

Xerovac™is a similar technique compared to freeze-drying which utilises a two staged drying process, without sublimation[72]. The powder is formed purely using dehydration with fluctuations of product temperature. It forms a foamy glass-like matrix. This method was utilised to develop a rinderpest vaccine[72–74].

Spray drying is performed as its name[75]. The mixture of interest is fed into an atomiser that sprays small droplets into a drying chamber filled with inert gas. The dried particles are collected into a glass vial. Spray freeze-drying is identical to this method with the major difference that particles are formed at subzero temperatures[75]. Both methods were evaluated for use in developing influenza vaccines that could be delivered nasally via inhalation[76–78].

1.1.5 Stabilising excipients in vaccines

Excipients are added to vaccines for the purpose of increasing protein stability, solubility, pH control, preventing aggregation and limiting degradation[79]. There are numerous excipients currently employed for various types of vaccines, both liquid and dried. Commonly used excipients are: glycine, thimerosal, gelatin, formaldehyde, Tween-80, sucrose, human/bovine albumin, phenol, glycerol, Triton X-100, formalin and sorbitol.

Glycine ($C_2H_5NO_2$, 75.067 g/mol) is an amino acid (figure 1-8) that functions as an osmolyte which cells employ to regulate osmotic pressure. Preferential hydra-

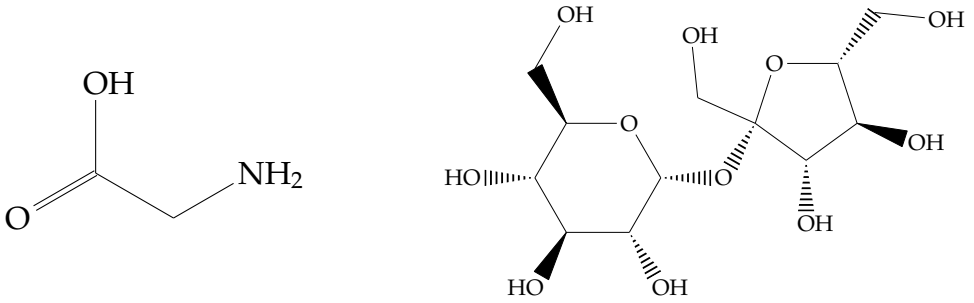

Figure 1-8: Structure of glycine and sucrose. (left) A non-essential amino acid. It is the simplest of amino acids. Regulates osmotic pressure by influencing hydration of proteins. (right) Sucrose, a form of sugar, lowers the surface tension of water and affects protein in the same way glycine operates.

tion[80–84] of a protein in solution occurs with the addition of glycine. This favours a protein to retain its native conformation and is due to the change in free energy of the solution. Another compound which employs a similar mode of action is sucrose.

Thimerosal ($C_9H_9HgNaO_2S$, 404.811 g/mol), UIPAC: sodium (2-carboxylatophenyl) sulfanyl-ethylmercury, is a controversial excipient used in vaccines (figure 1-9). This compound was developed in the 1930s and brought on the market as Merthiolate™.[85–91] It contains 50% mercury by weight, possesses anti-fungal and anti-

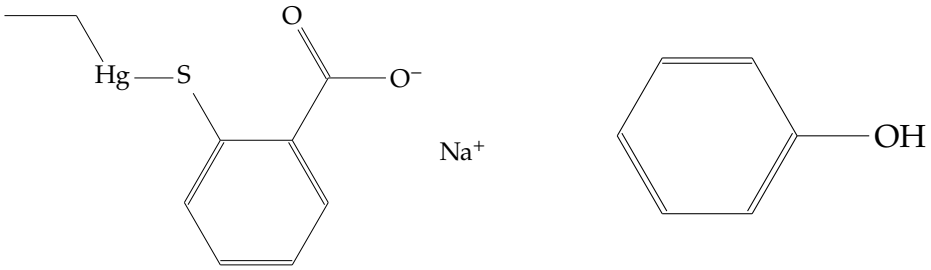

Figure 1-9: Structure of thimerosal (left) and phenol (right). Preservatives used in vaccines. The anti-fungal and antibacterial function of these compounds enhances the lifespan of vaccines.

bacterial properties that enhances vaccine lifespan. Notably, the incidence of autism was correlated with the use of thimerosal in vaccines. This publicly accepted conclusion at the time is still debated with many studies showing no evidence that thimerosal, at its low-dose present in vaccines, is the causative agent[92–94]. At higher concentrations, thimerosal has shown to impair neurological development *in vivo*[95–97]. This caused vaccine manufacturers to reconsider their formulations, either switching to phenol (C_6H_5OH, 94.113 g/mol), 2-phenoxyethanol[98] or benzethonium chloride as preservatives. The National Health Service (NHS) in the UK does not use thimerosal in any of their vaccines during immunisation programmes.

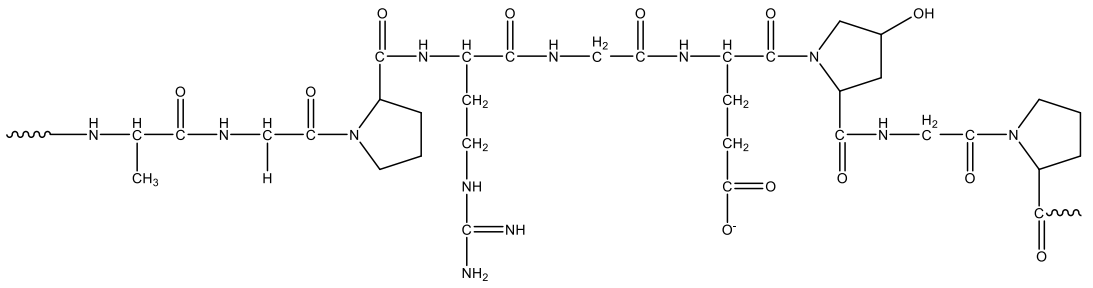

Figure 1-10: Structure of gelatin. Gelatin has protein stabilising capacity which have not been elucidated.

Gelatin is another generally regarded as safe (GRAS) stabiliser frequently used in vaccines[99] (figure 1-10). Obtained from the degradation of porcine skin, its macromolecular structure finds its basis from collagen. The mechanism of stabilisation for (vaccine) proteins has not been elucidated thus far. The use of gelatin has had some controversy as several individuals have allergic responses towards it. Other considerations are those of religious reasons.
Sorbitol and glycerol are noted stabilisers used in vaccine formulations[100] (figure 1-11). As co-solvents, they increase the aqueous phase viscosity and strengthen repelling forces between protein particles via electrostatics. This aids to prevent aggregation and help maintain the folding of hydrophobic regions to prevent inter-particle absorption.

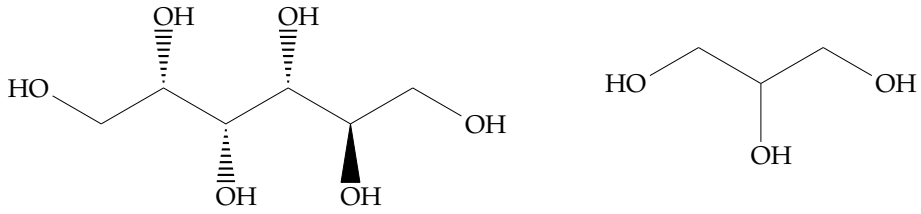

Figure 1-11: Structure of sorbitol (left) and glycerol (right). Both co-solvents exercise their function through hydrogen bonding, electrostatics and solute viscosity.

Human or bovine serum albumin (HSA/BSA) is a ubiquitous protein found in blood. Its function is the trafficking of several ionic ligands around the human body for the purpose of increasing protein solubility[101–103]. It also possesses chaperone-like functionality, preventing aggregation in solution when the environment is exposed to heat or other physical types of stress. However, there are consequences of using blood products in vaccines. There is an increased, theoretical, risk of microbial infection and the European Medicines Agency is pursuing blood product free vaccines[92,104].
Regardless of these measures influencing vaccine stability, those which come liquid formulated will have limited shelf life once exposed to temperatures outside storage conditions.

1.1.6 Efforts in thermostabilisation of vaccines

Stabilisation of vaccines, specifically providing increased thermal resilience, has been a key topic in vaccine development. One of the earliest reported studies showed deuterated (heavy) water, D_2O, improve the thermal stability of live virus vaccines[105]. The authors contributed this to the increased strength between pro-

tein side chains and deuterium compared to hydrogen bonding. With the addition of magnesium chloride ($MgCl_2$) they observed an even greater stability and retention of infectivity[106,107]. This study was conducted on the three strains of poliovirus used in the vaccine and was supported by another study which investigated yellow fever virus[108,109].

Magnesium displayed its stabilising capacity in another study which investigated the thermal stability of lethal anthrax toxin. Here, researchers studied the effect of additives to improve antigen uptake. They found magnesium sulphate ($MgSO_4$) to provide 82.7% recovery of functionality. Other additives showed reasonable values of retention. The mode of action was contributed to the increase in surface tension and increased energy for solvent cavity formation. This in effect prevented the exposure of hydrophobic regions present in the anthrax toxin proteins, therefore improved thermal stability when exposed to elevated temperatures[110].

The mechanism of D_2O-$MgCl_2$ was elucidated in a subsequent study. It was found via utilisation of tryptophan fluorescence spectroscopy (295 nm) and circular dichroism of secondary structures. The results showed decreased interaction of the viral capsid of poliovirus with the aqueous solvent, therefore maintaining native capsid state. This would prevent deformation when the solvent environment was heated, thus presenting the thermostabilising effect of this conjugate system[111].

All of these findings led to a study that investigated the thermostabilisation of egg grown influenza virus strains A and B with the utilisation of D_2O[112]. The study found optimal retention of viral infectivity with use of 90% deuterium oxide. A striking result was the thermal inactivation of influenza virus with a 2-log reduction of D_2O stabilised compared to 7-log decrease in minimal essential medium at 56 °C for up to 30 minutes. Researchers proposed three hypotheses for the increase in stabilisation. The first two have been described earlier which stated the increased strength of hydrogen bonding. Secondly, the decreased exposure to the aqueous environment and thirdly, the suggested effect of D_2O on proteolytic enzymes present in allantoic eggs. This reduced their enzymatic activity due to the presence of D_2O could relate to the survival of a higher percentage of viral particles.

Another study into the stabilisation of protective antigen (PA) of anthrax improved the formulation design to utilise glycerol and other polyols to prevent aggregation[113]. This was found to be the causative event detrimental to the protein when monitored at 20 °C. The half-life of PA increased 6-fold when heated at 40 °C in the presence of glycerol and NaCl compared to no additives. This dramatic increase in thermal stability was very promising in stabilising the recombinant vaccine against anthrax.

Researchers developed a novel approach to thermostabilisation of vaccines with the employment of carbohydrate glass[114]. This study used sugars such as sucrose and trehalose, known to aid protein stabilisation, mixed with viral particles in solution. During drying of this mixture, it underwent vitrification. This formed a sugar-glass matrix (powder) in which virus was embedded. The study displayed retention of infectivity up to 6 months stored at 45 °C for an adenovector type virus. As many vaccine manufacturers use adenovirus as a vector based system to produce pathogen-derived proteins, it suggested a major impact on vaccine production. The investigators suggest this platform to be suitable for developing countries with poor infrastructure.

The usage of sugar-glass was extended to the preparation of a porcine reproductive and respiratory syndrome (PRRS) vaccine[115]. The researchers employed several excipients mixed with the live attenuated virus and performed vacuum foam drying (VFD). With significant increase in thermal stability, the researchers found similar titres comparable to the commercial lyophilised vaccine.

Another interesting study utilised poly(lactic-co-glycolic acid, PLGA) to form micro-particles with vaccine proteins embedded[116–119]. This was aimed to improve drug delivery while providing enhanced thermal stability. Researchers made micro-particles that would encapsulate inactivated polio virus (IPV) with required excipients[120]. PLGA is made up of glycolic and lactic acid monomers giving it an overall negative charge. It has been approved by the Federal Drug Administration (FDA, USA) for usage of vaccine delivery. The micro-particles are made by addition of protein in aqueous buffer to an organic solvent containing the PLGA polymer. This mixture is added to a final aqueous buffer containing a stabilising agent which upon evaporation activates the precipitation of PLGA subsequently forming solid micro-particles[121]. Lyophilisation of the formed solution produces the final material. By varying formulation composition, the researchers achieved a good release profile with protective levels of immunological markers. These were the first studies where a polymer was introduced with the intention of vaccine thermostabilisation[116,121].

A more recent study into the preparation of buffalopox vaccine investigated the optimal formulation for freeze-drying and reconstitution[122]. Researchers found that the live attenuated virus in combination with lactalbumin hydralysate and sucrose was the optimum formulation to be freeze-dried. Reconstitution with identical formulation showed retention of efficacy after extended storage.

Overall, the development of thermostabilisation strategies for vaccines have become widespread. From simple molecular osmolytes, polyols and ionic effectors towards

polymer matrices and micro-capsules it is apparent that researchers are employing interesting approaches towards tailor made solutions. Unfortunately, these methods have their own limitations concerning heating or freezing during vaccine transportation. Especially the strategies for solution stability will have no avail against handling errors and thermal fluctuations. PLGA and sugar-glass methodologies have shown to be very promising for future use. However, the production of PLGA using organic solvents and lyophilisation at the end does raise concerns regarding the retention of antigen conformation not to mention the energy cost required. Sugar-glass matrices also present some difficulties. Reconstitution of this material produced some large fragments which do not dissolve. The researchers aim to use a filter syringe for injection. Importantly, carbohydrate-glass could be a nutrient source if there is a microbial contaminant present which would require strict verification of produced material.

1.2 Silica, an inorganic matrix

Silica, silicon dioxide, SiO_2 (60.083 g/mole), has many uses in modern society. Ceramics, glasses and a range of other compounds are made out of silica. It is the most abundant form of silicon (Si) found in the earth's crust which is a semi-metal on the periodic table. Its electronic configuration is $[Ne]3s^2 3p^2$ with a molecular weight of 28.086 g/mole. Pure silica is found in nature in the form of quartz, which grows naturally with a highly crystalline structure. It contains a SiO_2 chain giving rise to the classical helical arrangement of tetrahedral along the channels in one crystallographic direction. Each turn has three silicon and oxygen atoms with six of them forming the characteristic hexagonal shape. The exact repetition of this structure throughout the material defines quartz as crystalline. Glass, used for windows, contains silica molecules randomly linked with others in a non-uniform pattern that defines it as an amorphous material. These differences in molecular arrangement help to classify materials (figure 1-12).

Structurally, silica has a tetrahedral configuration with each tetrahedron consisting of a silicon atom and four oxygen ions or atoms[123]. These tetrahedra are considered almost rigid and have bond angles of 109.5° and Si-O bond distances of 1.61 Å. Other kind of familiar silicate glasses are borosilicate (Pyrex™) or lead crystal used for producing wine glasses.

There are also many living organisms who employ silica for survival, defence or longevity approaches. A few notable ones are; nettles have silicate needles for pro-

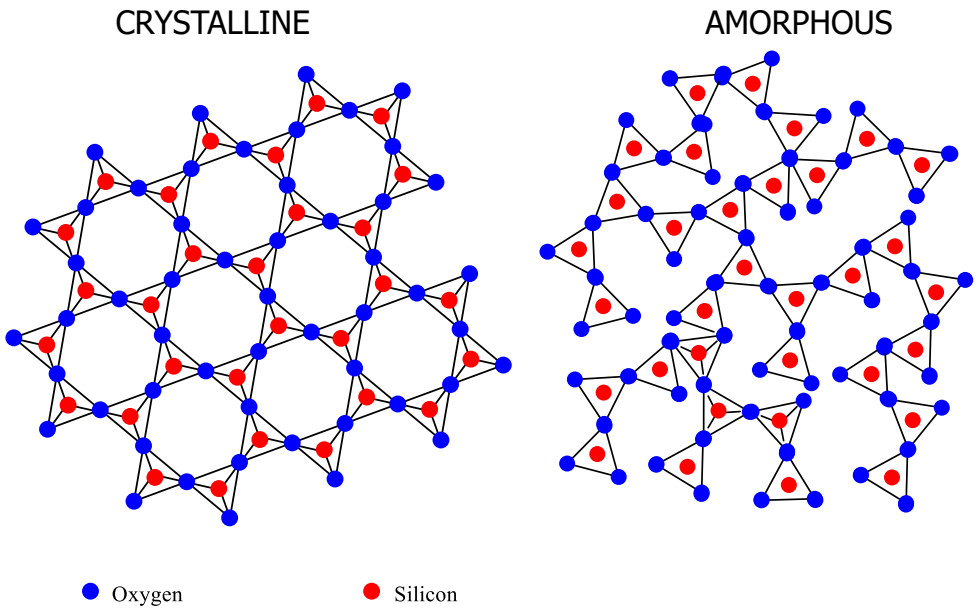

Figure 1-12: Molecular arrangement of silica. (left) Quartz (β-quartz here), the crystalline and most common form of silica. (right) Amorphous, random, arrangement of silica molecules. This material forms common glass used in windows.

tection;[124] diatoms make their shells from silica[125–127] and tardigrades coat themselves in glass to prevent death[128].

The use of silica in biological applications showed that silica, utilised via the sol-gel process, enhances protein stability. There has been extensive research on this topic with a particular focus on enzymes. The use of silica substrates to drastically increase the catalytic properties of enzymes has been a key interest of the pharmaceutical industry[129].

Silica-based materials have gained more popularity in biomedical applications due to their biocompatibility[130]. 3D scaffolds for soft and hard tissue regeneration, biomolecule entrapment matrices and mesoporous silica nanoparticles are a few examples[131–134].

1.2.1 Sol-gel processing of silica precursors

The start of sol-gel science, around 150 years ago, can be credited to several researchers. The work of Graham (1864) on silica sols[135], Ebelmen (1846) on the production of transparent glass using $SiCl_4$ and EtOH[136], Patrick (1912) on the development of a rapid sol-gel method to up scale silica gel production[137] and Kistler (1931) who synthesised the first "aerogel"[138], a highly porous network of silica. Gra-

ham was also the first to coin the term "sol-gel".
Sol-gel, short for solution-gelation, is a processing technique that utilises a metal alkoxide (MOCHx) to form a gelated (gelled, gel) solution[139]. The sol consists of colloidal (1-1000 nm) particles in solution. These are formed by reacting metal alkoxide with water. The subsequently hydrolysed molecules interact with each other forming larger structures with water and alcohol released as by-products of condensation. Depending on the precursor molecule, the number of bonds it can form defines the connected structure. Precursors that have 2 bonds available are bi-functional and create a linear polymer. This is defined as the macromolecular structure of monomers attached to one another. Hydrolysed metal alkoxides having more than 2 bonds, poly-functional, can create complex branched 3D structures. This formation is defined at random and excludes crystalline materials. The gel is formed once a continuous skeleton of polymer extends throughout the solution and allows for a semi-solid state. The basis of this is the static aggregate formed by polymer interactions. This display of percolation sets the fundamental theory behind this transition. Once the gel has formed, shrinkage via evaporation, heating or sublimation creates different types of materials. Aero-gels, xerogels and several types of ceramics can be made with this method. Most ceramics formed will be of amorphous nature after drying.

1.2.2 Ensilication for thermostabilisation

Ensilication, encapsulation in silica, is based upon the acid-catalysed hydrolysis of tetra-ethyl orthosilicate (TEOS)[139]. This compound has a central Si atom bound with oxygen's linking to a total of four ethyl groups. TEOS is made by dissolving SiO_2 in HCl which forms silica-tetrachloride SiCl4. By reacting $SiCl_4$ with ethanol CH_3CH_2OH it undergoes alcholysis and forms TEOS $Si(OCH_2CH_3)_4$. Hydrolysis of this compound results in the formation of silicic acid species $Si(OH)_{4-n}$[123,139–141](figure 1-13). This soluble form of silica is able to condensate and polymerise with itself under the right conditions. This chemical reaction is derived from sol-gel technology and has been widely used in many industrial applications such as the production of silica spheres for use in column packing. In general, sol-gel is the condensation and polymerisation of a monomeric species to form particles which link with each other to form a gel. Mixing water and TEOS in a 1:1 ratio and adding HCl as a catalyst results in the hydrolysis of ethyl groups. This biphasic system will proceed to react until the miscible solutions turn homogeneous.

- 1. Hydrolysis:

$$Si(O\mathbf{R})_4 + H_2O \xrightarrow[H+]{} Si(O\mathbf{R})_{4-n}(OH)_n + {}_n(\mathbf{R}O)$$

- 2. Condensation:

$$\mathbf{2}\,Si(O\mathbf{R})_{4-n}(OH)_n \longrightarrow Si(O\mathbf{R})_{4-n}-O-(\mathbf{R}O)_{4-n}Si + H_2O$$

$$Si(O\mathbf{R})_{4-n}(OH)_n + Si(O\mathbf{R})_{4-n} \longrightarrow Si(O\mathbf{R})_{4-n}-O-(\mathbf{R}O)_{4-n}Si + {}_n(\mathbf{R}OH)$$

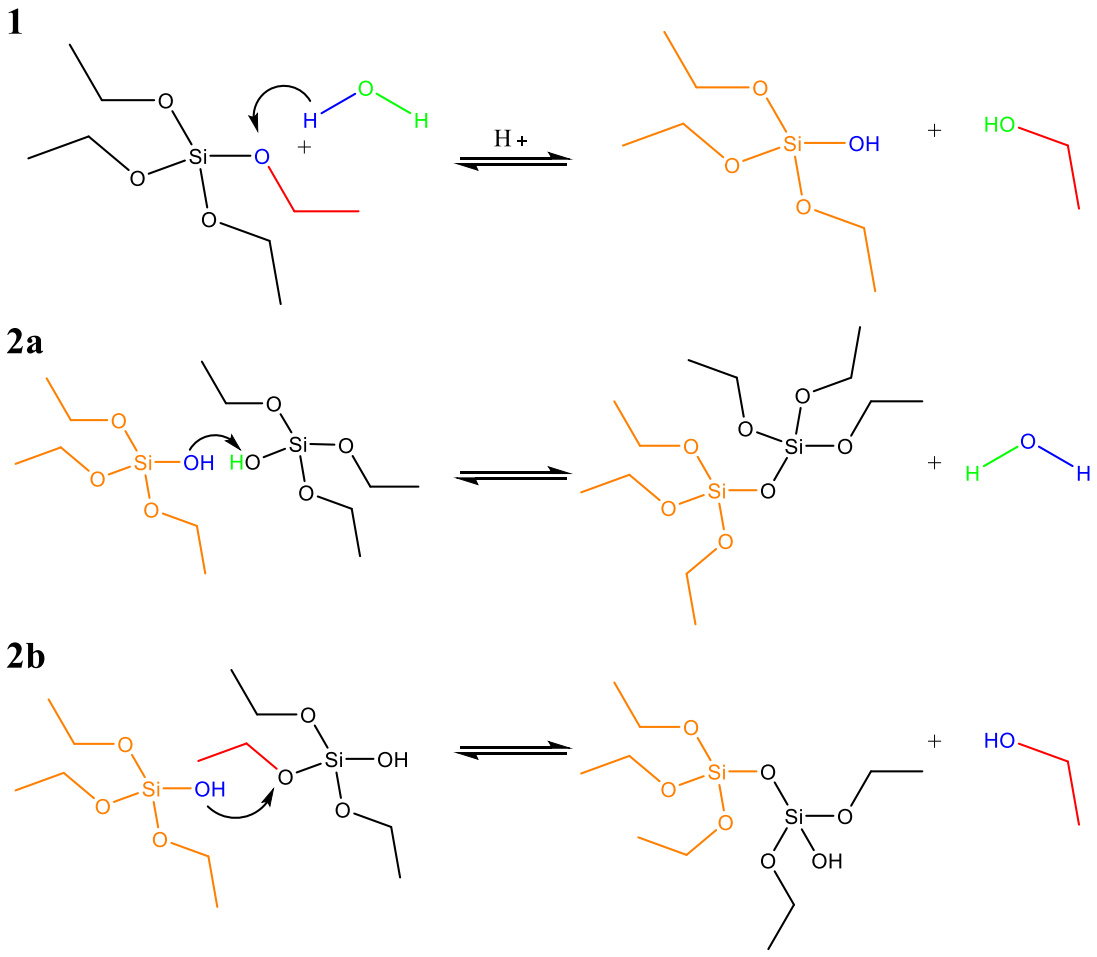

Figure 1-13: Sol-gel chemical reactions. Initial hydrolysis of TEOS mixed with water in an acidified environment. The subsequent reactions creates particles with water and ethanol as by-products. **R** = CH_2CH_3.

Our application intends to form nano-particles of protein and silica which stabilise before the solution gels. This technique physically immobilises the protein inside silica, rendering it unable to unfold when exposed to heating and freezing. The silica shell can be later removed using a buffer to dissolve the silica and release the protein into solution. Added benefit is the ability of performing this technique at ambient temperatures or lower which favours protein native state. Ensilication is further described in Chapter 3.

1.3 Tetanus as a model for thermostabilisation

Tetanus is the clinical name of the disease acquired by an infection caused by the bacterium *Clostridium Tetani*[142–144]. This bacterial pathogen is a ubiquitous Gram$^+$ bacillus normally found in soil and the stool of domesticated animals. It has not been identified within humans. It grows under anaerobic conditions in necrotic or infected tissues. *C.tetani* has abilities such as sporulation and motility using flagella. It has a distinct tennis racket like appearance when it contains a spore (figure 1-14). Its virulence comes from the exotoxins it produces[145]. DNA for these are encoded on

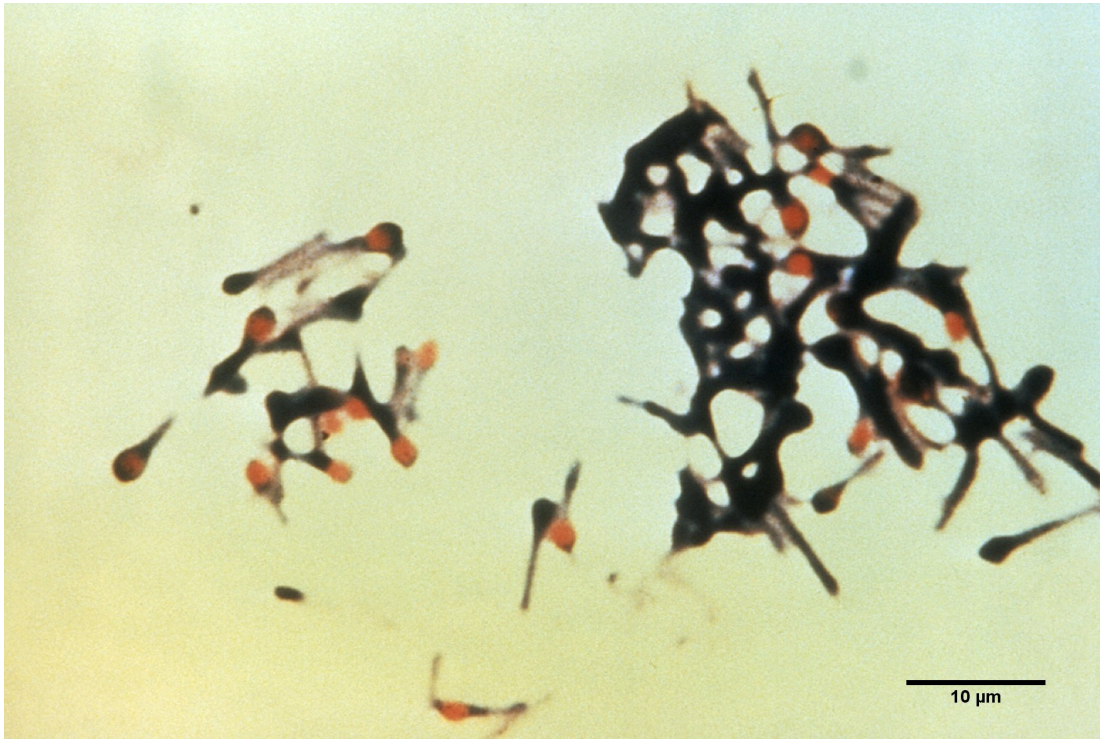

Figure 1-14: Clostridium Tetani. A Gram$^+$ bacteria found in soil and animal stool. Infection with this organism causes tetanus. Source: Centre for Disease Control (CDC).

a plasmid that is circulated between various strains. The two toxins produced are tetanospasmin and tetanolysin[146–148]. The latter destroys healthy tissue, releasing nutrients which allows the infection to spread. The former causes clinical disease. Tetanospasmin binds to neurological receptors present on nerve cells[149,150]. Once bound, the toxin is internalised by endocytosis and transported to motor neuron cells in the spinal cord[151]. Here, it blocks neurotransmitters from being released and this causes clinical symptoms such as lockjaw[152,153]. The mode of action is similar to that of botulism toxin where the toxoid, inactivated toxin: Botox, is used in plastic surgery[154,155]. The mode of action of the toxin results in acute spasm. This leads to death in infected individuals. Treatment of tetanus is not possible, prevention is.

1.3.1 Tetanospasmin, tetanus toxin C fragment

Tetanospasmin has a molecular size of 150 kDa and can be separated into two fragments[156]. This two-chain polypeptide has a 50 kDa light chain (L, fragment A) responsibly for blocking neurotransmitter release at the site of infection and a 100 kDa heavy chain (H) which binds to nerve cells and allows for cell uptake. If the toxin load is high, tetanospasmin might enter the bloodstream causing body wide symptoms. Furthermore, the heavy chain (H) can fragmented in to three segments (figure

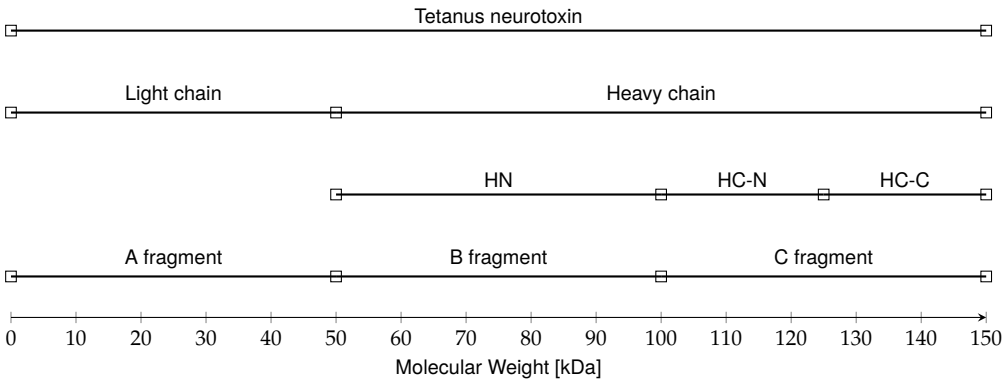

Figure 1-15: Protein segments of tetanus neurotoxin. TTCF is composed of two HC fragments of 25 kDa. These help binding to ganglioside receptors and mediate cell toxin uptake.

1-15). These make up a 50- and two 25 kDa fragments. The first fragment at the N-terminus is labelled HN (fragment B). The second and third are HC-N and HC-C. These latter two fragments together are named the tetanus toxin C fragment (TTCF) displayed in figure 1-16. The function of HC-C has been elucidated where HC-N has yet to be resolved. HC-C is responsible for ganglioside binding and allows the

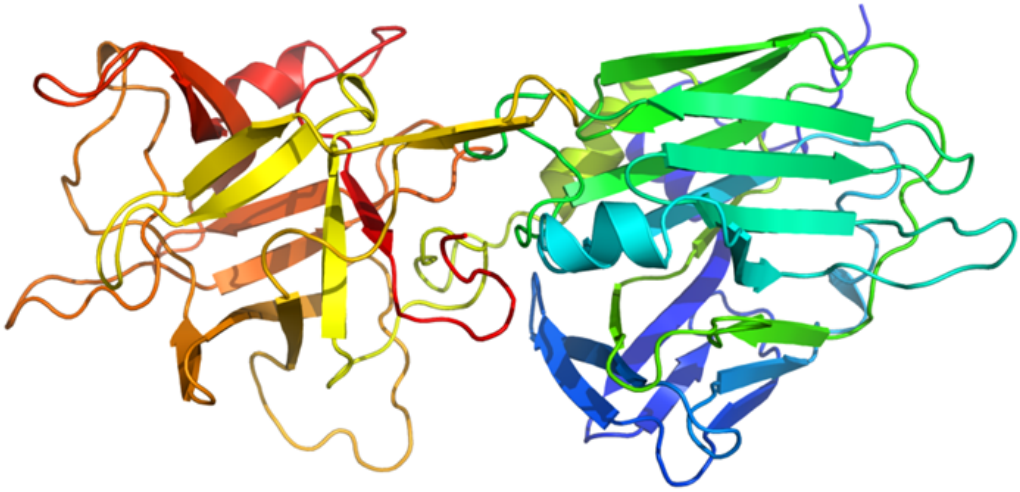

Figure 1-16: TTCF 3D structure from the Protein Database Bank (PDB):1A8D.[164] Resolved structure of TTCF showing the two linked HC-N and HC-C fragments.

toxin to bind with the membrane of peripheral motor axons[157–161]. As well as studies into the toxicity and tetanospasmin mode of action, TTCF has triggered interest from researchers looking at central nervous system diseases such as amyotrophic lateral sclerosis (ALS, also named motor neuron disease)[162,163]. In this setting, it is used as a non-toxic carrier or reporter protein to understand processes occurring in various stages of this disease.

1.3.2 Vaccination against tetanus

The first vaccine against tetanus was available in 1923 with routine vaccination starting, in the UK, in 1961. At 2 months of age, vaccination is initiated after which a secondary (booster) shot is given one month after. This second immunisation induces latent immunity. A final booster shot at 5 years of age extends the duration of immunisation over a longer period. During pregnancy and early neonatal stage, the infant is protected by maternal antibodies which are passed on from the mother. The vaccine is routinely administered to children and comes in the form of a diphtheria, tetanus and pertussis vaccine (DTP)[16]. However, for people that are bitten by wildlife there is a tetanus only vaccine available.

The current vaccine for tetanus (DTP, or TT) contains tetanus toxoid. This inactive form, of the full length neurotoxin containing the TTCF fragment, is created by formaldehyde treatment of the protein. It induces multiple inter-chain crosslinkages and renders tetanospasmin inactive but remains highly immunogenic[165]. Both TT vac-

cines contain an alum salt, $AlOH_3$, adjuvant[166,167]. The purpose of this is to boost the immune response. However, the adjuvant has a detrimental effect on its thermal stability during storage and transportation.

Freezing has a particular effect on the aluminium adjuvant which is used in the DTP vaccine formulation. It causes a morphological change which results in the formation of conglomerates of adsorbed aluminium[168–171]. These crystalline flocculates sediment due to the increase in size each time a freeze-thaw cycle occurs. The vial "shake test" is the only method to quickly asses vaccine vial freezing. The WHO studied the freezing times at various temperatures. Researchers found that 110-130 minutes are required at -10 °C, 25 to 45 minutes at -20 °C, and 9 to 11 minutes at -70 °C[169]. Additionally, due to the stationary nature of the vial throughout transportation, supercooling occurs. Handling of these vials results in increased crystallisation due to the agitation that is then induced. These effects lower the potency of the DTP vaccine. It was found that the tetanus toxoid component of the DTP vaccine lost 60% of its potency after three freeze-thaw cycles[169,171].

1.4 Aims and Objectives

The challenges with cold-chain vaccine distribution have created difficulties in maintaining storage and transportation conditions. This exposed vaccines to circumstances beyond the capabilities of added preservatives within the formulation. Ultimately, it affected and still affects millions of people that receive no protection from ineffective vaccines. The routinely used DTP vaccine is sensitive to heating and freezing, therefore a good candidate for thermostabilisation.

This study aims to apply a previously developed methodology, ensilication, to thermostabilise vaccine proteins. Utilising the electrostatic attractions between a positively charged protein and the negative silicic acid, the goal is to coat the protein with a protective layer of silica. The research aims to stabilise TTCF, part of the DTP vaccine, in order to set the precedent for thermostable vaccines via ensilication. The project is focused on understanding protein stability, mechanism of stabilisation and the physiochemical analysis of the material obtained. Future outcomes could remove the need for vaccine continuous refrigeration. This will be achieved by the following objectives:

- Understand and assess the native state of TTCF and its biochemical parameters
- Successfully ensilicate TTCF and analyse the material obtained
- Verify the retention of TTCF protein structure before and after ensilication
- Elucidate the stabilisation mechanism via small-angle x-ray scattering
- Measure the influence of silica on the native and released state using calorimetry
- Confirm the retention of immunogenicity *in vivo*
- Determine the thermal stability of ensilicated TTCF after heating
- Assess the long-term stability of ensilicated TTCF

Chapter 2

TTCF

2.1 Introduction

Described in this chapter is the expression, purification and protein characterisation of recombinant TTCF. These procedures are well-established and shall be utilised to prepare TTCF for ensilication.

TTCF is derived from tetanus neurotoxin, a potent lethal protein that disrupts neuronal signalling[149,150]. This pathogenic effect leads to mortality in humans infected with *C. tetani*. However, the neurotoxin (tetanospasmin, 150 kDa) can be separated into two segments. The light (50 kDa) and heavy chain (100 kDa) individually do not possess the toxic effect[155,156]. This benefited studies investigating the fragments to elucidate each respected function[154,172]. The proportion of heavy chain composed of HC-N and HC-C contains neuron receptor binding regions[157–160,173,174] and these segments combined are labelled the tetanus toxin C fragment. It comprises immunological targets for the immune system to act against.[175] The TTCF protein contains 452 amino acids with a molecular weight of 52 kDa and has a theoretical isoelectric point of 6.83[176] (see Appendix A.1 for more information). The recombinant version has an addition of 10 histidine amino acids for purification[177] on a nickel (Ni^{2+}) column, described in detail later. Structurally, TTCF consists of two large sections, a 25 kDa segment containing 16 β-sheets and 4 α-helices in a jelly roll motif and another 25 kDa segment containing 10 meandering β-sheets in a barrel formation[157–160,173,174]. This information will aid in characterisation using SDS-PAGE[178,179], circular dichroism[119,179,180] and ELISA[119,161] at all structural protein levels. Sizing and electrophoretic mobility in solution will be assessed using dynamic light scattering (DLS). The results gathered from protein characterisation provide a reference control to compare against after ensilication.

2.2 Preparation of recombinant TTCF

To prepare a pure monodisperse solution of TTCF, a number of steps were taken. The preparation comprised of transformation, expression and purification of TTCF. Each step was analysed using biochemical methods to verify the outcome.

The expression of recombinant TTCF is based on the exploitation of internal bacterial machinery (figure 2-1). Usage of the *Lac* operon and multiple cloning site (MCS) allowed researchers to incorporate the DNA sequence for TTCF into a bacterial vector (plasmid) using restriction enzymes[180,181] (figure 2-2). The copied DNA (cDNA) sequence was optimised previously from native *C. tetani* to be expressed in *E. coli*[182]. The modified vector, a double stranded DNA ring, can be then taken up into a susceptible bacterial host. Isopropyl β-D-1-thiogalactopyranoside (IPTG), a lactose analogue, binds to the lac promoter region which induces an enzyme, RNA polymerase, to start expressing TTCF protein internally. Additionally, the TTCF sequence was extended by 10 amino acids situated at the N-termini for purification purposes[183]. The immobilised metal-ion chromatography (IMAC) technology has been widely used for purification of bacterially expressed protein containing a histidine-tag (His-Tag)[177].

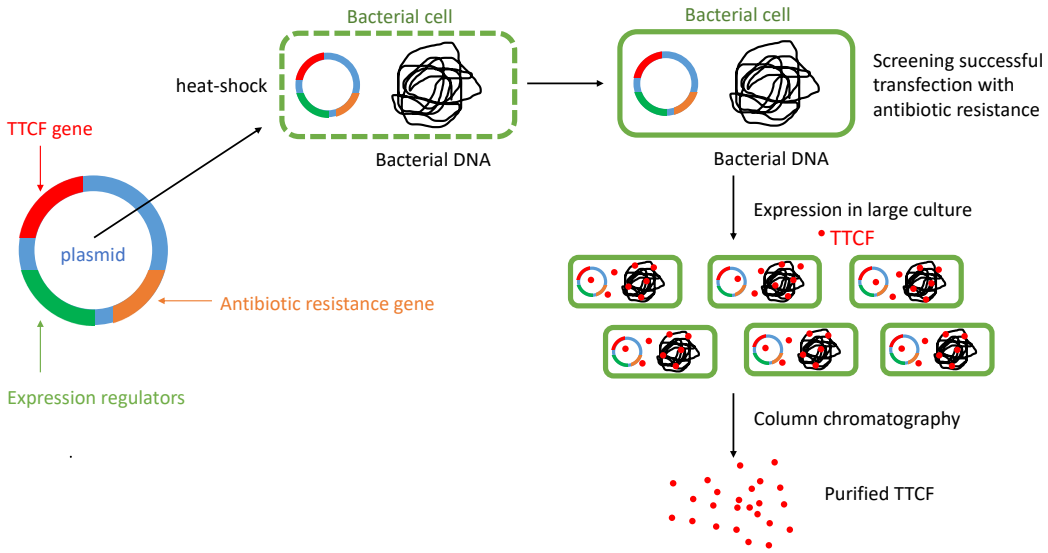

Figure 2-1: Schematic of TTCF production. A plasmid containing TTCF is incorporated in a susceptible *E. coli* host. Antibiotic screening and subsequent growth in large volumes is followed by purification using a his-tag binding nickel column.

2.2.1 Transformation of BL21(DE3) *E.coli*

The plasmid (kindly provided by Dr. K. Marchbank) was transformed into susceptible bacteria via the heat-shock approach. This method temporarily makes the bacterial membrane permeable to favour uptake of the plasmid. Following heat-shock, the bacterial solution was spotted and distributed on a Luria Broth (LB) agar plate containing ampicillin. This is purely intended for screening as the plasmid contains an additional gene that enables ampicillin resistance. After overnight growth at 37 °C, the observed colonies that grew had incorporated the plasmid successfully. From this, a colony was grown in liquid media to make starter stocks for large media preps for expression.

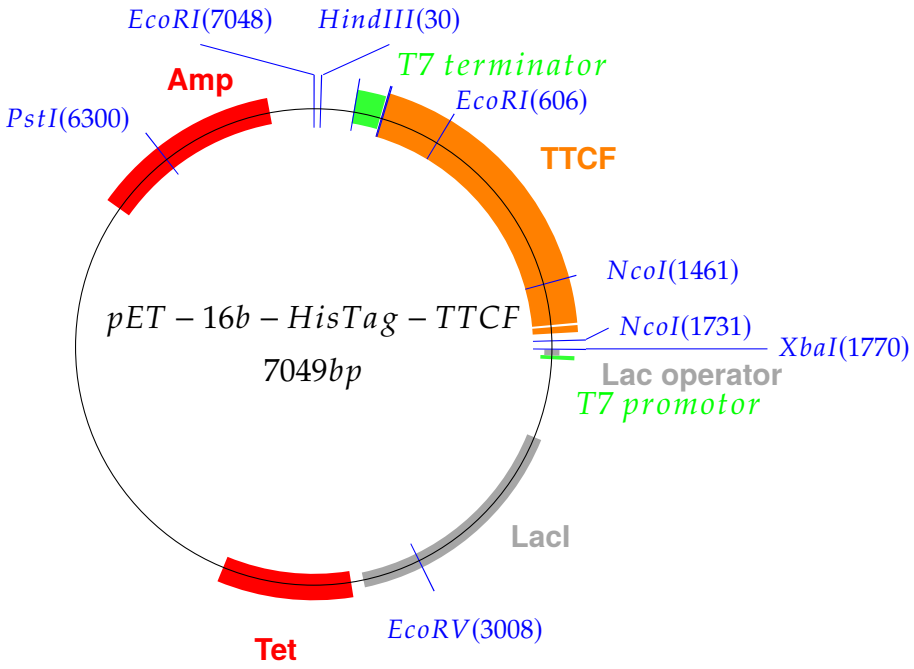

Figure 2-2: TTCF pET-16b-HisTag vector. The commercial pET-16b-HisTag vector was cleaved using BamHI restriction enzyme whereafter the 1446 aa sequence of TTCF was inserted. The plasmid was closed using DNA ligase. Transfection of susceptible E.coli was screened for antibiotic resistance to confirm the successful transfection after overnight incubation.

In more detail, the pET-16b TTCF HisTag plasmid was reconstituted from a filter paper by carefully cutting out the spotted section. This was then incubated with nuclease-free water in an eppendorf for 10 minutes (min) at room temperature (RT) to liberate the plasmid. After centrifugation at 13,000 revolutions per minute (rpm) for 1 min, 5 µl was taken and added to a vial of thawed BL21(DE3, Novagen UK) *E.coli*.

The heat-shock method involved a 45 second (sec) incubation at 42 °C whereafter the vial was placed on ice. Bacterial medium (LB, 10 g/L Tryptone, 5 g/L Yeast Extract, 5 g/L Sodium Chloride, Sigma, in ddH_2O) was added to the vial and this was placed into a 37 °C incubator with shaking at 200 rpm. Agar plates (LB, 10 g/L Tryptone, 5 g/L Yeast Extract, 10 g/L Sodium Chloride, 15 g/L agarose, Sigma, in ddH_2O) containing 10 µl/ml of ampicillin were used to plate out the bacterial solution after a short incubation to solidify the agar . The plates were incubated at 37 °C overnight and screened for bacterial colonies the following day, which indicated successful transformation. One of these colonies was then cultured in 15 ml of LB with ampicillin overnight at 37 °C. Stocks were made by addition of 30 % glycerol and stored at -80 °C until further use.

2.2.2 Expression of TTCF

The production of TTCF in *E.coli* was initiated with an overnight starter culture of transfected *E.coli* in LB medium (+ampicillin) grown at 37 °C with 200 rpm shaking for aeration. The culture was expanded 100-fold in fresh LB media containing ampicillin. This was incubated until optical density (OD) at 600 nm was between 0.4 - 0.6. At this point, isopropyl β-D-1-thiogalactopyranoside (IPTG) was added to start the expression of TTCF. The media was then incubated until the OD reached 2 - 2.5. Thereafter, the dense turbid solution of *E.coli* was centrifuged at 5000 x *g* to collect the bacterial pellets for storage at −80 °C or immediately purified.

2.2.3 Purification of TTCF

Following expression of TTCF, the collected pellets were re-suspended in binding buffer ($IMAC_{25}$, 0.5 M NaCl : 0.1 M Tris : 25 mM Imidazole, pH 8.0) for immobilised metal-ion affinity chromatography (IMAC). Protease inhibitors (Protease Inhibitors Cocktail Set VII, cat:539139, CalBiochem UK) were added, 10x diluted, to prevent protein degradation via enzymatic cleavage. Once homogeneous after re-suspending, the solution was sonicated (Soniprep™ 150) at amplitude of 10 for 15 seconds with 45 seconds rest, repeated 10 times. This disrupts the bacterial cell membranes to release the expressed TTCF into the solution. Centrifugation at 20,000 x *g* separated the cell membranes from the proteins in the solution. The clear supernatant was collected and filtered through a 0.22 µm filter before running IMAC. This method included use of an Akta™ fast protein liquid chromatography (FPLC) machine. It was connected to binding and elution buffer which would run via

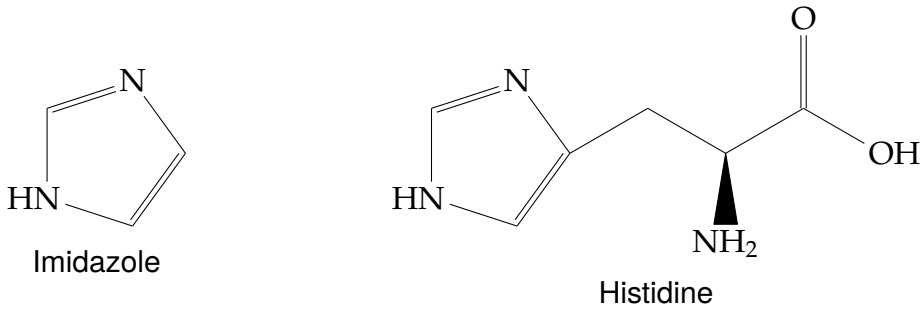

Figure 2-3: Schematic representation of histidine and imidazole. The imidazole ring present in histidine allows for protein separation using his-tags as these bind to a nickel loaded column.

individual pumps trough the system. The sample was connected via a SuperLoop™ injection column with a maximum sample volume of 50 ml. The purification column used was either a FastFlow™ (cat:17531901, GE, Life Sciences, UK) or High Performance™ (cat:17524701 GE, Life Sciences, UK) nickel sepharose column with a column volume (cv) of 1 ml. The principle behind IMAC purification is the use of histidine and imidazole. Histidine contains an imidazole ring (figure 2-3). They both bind the nickel column. The protocol ran at a flow rate of 1 ml/min. First, the column was equilibrated with 10 x cv of $IMAC_{25}$ whereafter the sample was loaded until the loading column was emptied. Before elution, the column was washed with 15 x cv of $IMAC_{25}$. Finally, the elution buffer ($IMAC_{500}$, 0.5 M NaCl : 0.1 M Tris : 500 mM Imidazole, pH 8.0) was added at a gradient of 0 - 100 % over 20 cv's. Fractionation started at sample injection with a fractionation volume of 3.5 ml which changed for elution to 2.5 ml. After elution, the column was washed with binding buffer, ultrapure water and 20% ethanol for storage. The purification was monitored via the attached UV absorbance unit which was situated after the column. It measured absorbance of the solution at 280 nm and confirmed when protein came off the column before the elution buffer reached 100%. Following peak fraction collection of purified TTCF, the solution was buffer-exchanged (dialysed) into tris buffer at neutral pH. The Slide-a-Lyzer™ (cat:87731, G2 Dialysis Cassettes, 10K MWCO, ThermoFisher, UK) cassettes were used to dialyse a maximum of 15 ml purified TTCF per cassette.

2.3 Analysis of TTCF purification

In order to assess and verify the outcome of each step during the preparation of TTCF, the following methods were employed for analysis.

2.3.1 Optical density monitoring of *E.coli* growth

OD 600 nm measurement is a standard approach to estimate at which stage of growth the bacterial population is.[184] Note that a wavelength of 600 nm is in the visible spectrum of electromagnetic radiation, e.g. visible light. This allows measuring turbidity of the bacterial solution. In short, bacterial growth consists of four stages, the lag, log, stationary phase and eventually death. The OD measurement allows monitoring of bacterial growth to identify the right phase for induction of expression and collection of bacterial pellet for further processing.

The spectrophotometer (Biophotometer, Eppendorf) was set to measure absorbance at 600 nm. Blank calibration was done using growth media by adding 0.2 ml in a transparent cuvette (UVette, Epppendorf) with blurry sides. After blanking, 0.25 ml of bacterial solution was added to the rinsed cuvette and measured. Data was output in arbitrary units of absorbance (AU). Absorbance is described in more detail in section 2.3.4.

2.3.2 Bicinchoninic acid assay: protein concentration

Bicinchoninic acid, 2-(4-carboxyquinolin-2-yl) quinoline-4-carboxylic acid, assay (BCA assay) is a colorimetric method to determine protein concentration using UV-vis absorbance of a formed complex[185]. This method utilises the biuret reaction where Cu^{2+} is converted to Cu^{1+} via interaction with peptide bonds in an alkaline environment. The Cu^{1+} ion then forms a stable conjugate complex with BCA. The intensity of this formed complex increases proportionally to a determined range of protein concentration (figure 2-4). Incubation at 37°C increases the sensitivity of the method. Copper-sulphate solution is mixed with BCA reagent and added to standard and sample protein solutions. The absorbance of standardised bovine serum albumin (BSA) at 562 nm can be used to calculate the unknown protein concentration via linear regression and interpolation within the standard.

2.3.2.1 BSA protein standard and sample preparation

To prepare a protein standard for use in the BCA assay, first, 100 µL stock of 2 mg/ml BSA was diluted with 100 µL 0.2 M NaOH. Four separate other solutions were made by taking 40, 30, 20 and 10 µL and topping them up to 50 µL with 0.2 M NaOH. This resulted in a protein standard concentration range of: 1, 0.8 , 0.6 , 0.4 and 0.2 mg/ml of BSA. In duplicate, 10 µL was added to wells for each concentration respectively.

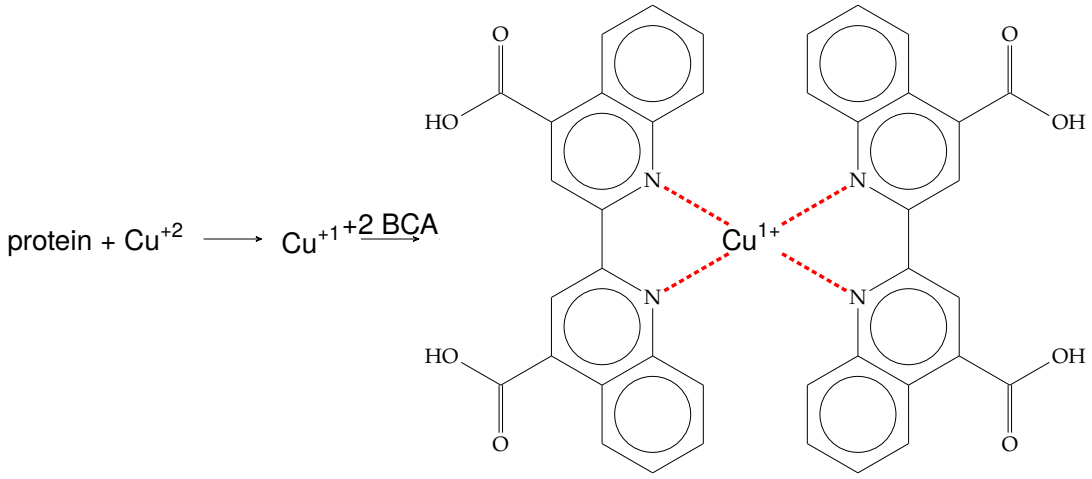

Figure 2-4: BCA reaction scheme. Schematic of reactions involved during the BCA assay. Peptide bonds present in proteins reduce Cu^{2+} to Cu^{1+} (left) which forms a stable complex with two BCA molecules (right). This forms a purple complex which can be read using absorption spectroscopy.

Samples were diluted 2x, 1:1 with 0.2 M NaOH, 10 µL was added in duplicate.

2.3.2.2 Substrate and data acquisition

Pierce BCA Reagent A (8% $Na_2CO_3 \cdot H_2O$, 1.6% NaOH, 1.6% Na_2 tartrate, $NaHCO_3$ to pH: 11.25) and reagent B (4% $CuSO_4 \cdot 5\,H_2O$) were mixed at a 50:1 ratio. The resultant green coloured solution is the combination of Cu^{2+} ions and BCA. 200 µL was added to each well.

Absorbances were read at 565 nm using a microplate reader (Pherastar *FS*, BMG Labtech, UK). The protein standard absorbances were corrected with blank absorbances and fitted with a linear regression $y = ax + b$. Samples were interpolated and adjusted for dilution factors. Results were output in mg/ml.

2.3.3 SDS-PAGE analysis of TTCF molecular weight

Sodium-Dodecyl-Sulphate Poly Acrylamide Gel-Electrophoresis (SDS-PAGE) is a biochemical method that allows for protein molecular weight screening[186]. It is based upon the negative charge SDS provides when mixed with proteins.
SDS is a detergent that unfolds proteins, however disulphide (-S-S-) bonds are not affected by this. Therefore, dithiothreitol (DTT) was used as a reducing agent to completely denature (linearise) the protein. The gel is made out of polymerised acrylamide that contains pores which linearised proteins can move through upon

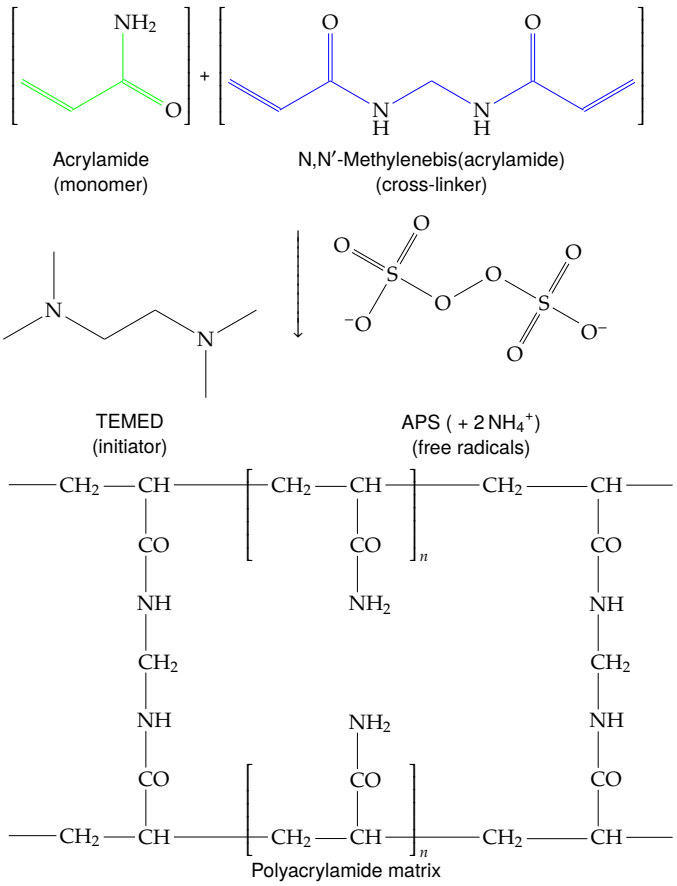

Figure 2-5: SDS-PAGE gel formation schematic. Acrylamide monomers are polymerised using TEMED as initiator with APS providing free radicals for polymerisation. Crosslinking of bisacrylamide molecules creates a porous gel type material. Linearised proteins coated in SDS can move through the gel based on electrophoretic mobility.

conductivity. There are two parts to the gel, a stacking section and a resolving section. The stacking gel allows smaller molecular weight protein to move faster downwards into the resolving gel where, as the name states, molecular weights can be resolved based on electrophoretic mobility. This method allows screening of various protein sizes dependent on the percentage of acrylamide gel. For TTCF, 10 % is used in all screenings. Samples were denatured at 95 °C for a minimum of 5 minutes.

2.3.3.1 Gel preparation

The SDS-PAGE gel was made using a BioRad Mini Protean 3™ cassette assembly unit. One glass plate with notches on either side was assembled with a flush glass plate and sandwiched on a cassette holder.[187] The resolving gel was cast first and

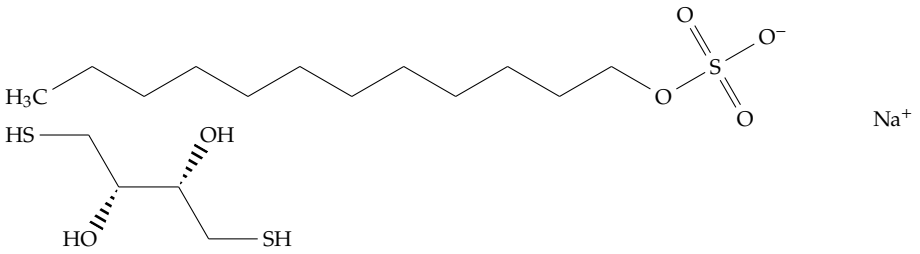

Figure 2-6: Schematic of SDS and DTT chemical structures. SDS (top) and DTT (bottom) used in sample preparation for SDS-PAGE analysis.

prepared using 5 ml of 30% (w/v) acrylamide, 5 ml resolving gel stock (1.5 M Tris-HCl, 0.4% (w/v) SDS, pH 8.8), 5 ml double-distilled (dd)H_2O, 100 µL ammoniumpersulphate (APS) at 100 mg/mL and 8 µL Temed (Sigma, UK).
Iso-propanol was added on top to prevent the gel from drying out during polymerisation. The stacking gel was prepared using 3.4 ml acrylamide, 5 ml stacking gel stock (0.5 M Tris-HCl, 0.4% (w/v) SDS, pH 6.8), 7.5 ml ddH_2O, 100 µL APS at 100 mg/mL and 20 µL Temed and was cast after discarding the iso-propanol and washing with deionised water (figure 2-5).

2.3.3.2 Sample preparation, electrophoresis and staining

A 10-well comb was used to create slots in the gel. These hold up to 30 µL of sample volume. To normalise samples on the gel, 1 - 5 µg (w/v) was added to lanes for molecular weight screening. Each sample consisted of sample, sample buffer (Leamli buffer) and 0.1 M DTT (10% volume). After incubating at 95 °C for 5 - 10 minutes, samples were inserted into sample wells (figure 2-6).

Once the sample and gel were prepared, the assembly was put into a container and filled with running buffer (0.025 M Tris-HCl, 0.1% (w/v) SDS, 0.2 M glycine, pH 8.3). When all samples were loaded, a protein standard containing reference molecular weight proteins was pipetted into a sample well. This is used to identify molecular weights. The gel was run at 200 V for 35-45 min, which was indicated by the sample tracking dye reaching the bottom of the gel. The gel was removed from the cassette and placed into a plastic container before washing several times to remove buffer traces. Thereafter, PageBlue™ a staining solution, was added to the gel and incubated for either 1 hour or overnight at room temperature.

2.3.4 UV-visible spectrum analysis of TTCF

Ultra violet (180-400 nm) - visible spectrum (400-700 nm) spectroscopy is a method based on absorbance (or transmission) of a conjugated compound[188]. This can be in gaseous, liquid, aqueous or solid phase. Light, electromagnetic radiation, has an energy E=*h*·*f* where *h* is Planck's constant, *f* the frequency of light. *f* can be found in the relation c=*f*·λ (c: speed of light, λ: wavelength in nanometre). Combining these formulas gives rise to:

$$E = h \times \frac{c}{\lambda} \tag{2.1}$$

Here, there is a clear correlation between the energy and associated wavelength. Lowering the wavelength results in a higher energetic transition occurring. Aromatic amino acid residues present in proteins such as tryptophan, tyrosine and phenylalanine are conjugate systems with molecular orbitals. The principle behind UV-vis is the molecular electronic shift from highest occupied molecular orbital (HOMO) to the lowest unoccupied molecular orbital (LUMO). These can be indicated as aromatic $\pi - > \pi^*$ transitions. Only transitions between similar types of bonds can take place. The spectrophotometer is able to identify compounds based on their maximum absorption at specific wavelengths. Using the Beer-Lambert law:

$$A = \varepsilon \times c \times l \tag{2.2}$$

where A: absorbance (arbitrary), ε: molar absorption coefficient, c: concentration g/L (or mg/ml), l: path length (in M or cm), accurate measurements can be made depending on purity of the samples. Protein absorbance is normally measured at 280nm.[189]

Sample volume of approx 2-3 ml was pipetted into a UV-vis polystyrene cuvette. Spectrum analysis depended on the type of sample which was either liquid or powder. The spectrophotometer (Lambda 650S, PerkinElmer, USA) was setup to record the spectrum. Data were output in arbitrary units of absorbance.

2.3.5 Circular Dichroism of TTCF secondary structure

CD is a method based on far-UV (180-260nm) or near-UV (260-320 nm) absorption of optically active chiral molecules, such as proteins[190–192]. Chirality is defined by asymmetry of the absorbed polarised rotational light, left and right-handed. The absorbance (Beer-Lambert) from each rotational direction, at a set range of

wavelength, is subtracted CD = $A_r - A_l$ and in combination with the Beer-Lambert law gives rise to $\Delta A = \Delta\varepsilon \cdot c \cdot l$. Another form of output is ellipticity which relates to absorbance by a factor of 32.98, $\theta = 32.98 \cdot \Delta$ Abs. This is commonly associated with reporting CD data. Molar ellipticity [θ] takes protein concentration, path length, and molecular weight into account and allows normalisation.

2.3.5.1 Sample preparation

TTCF was dialysed into 10 mM sodium-phosphate buffer at pH 7.0. The stock solutions: 0.2 M NaH_2PO_4, MW:119.98 g/mol and 0.2 M Na_2HPO_4, MW:141.96 g/L in 100 ml ultra-pure H_2O were combined by adding 57.7 and 42.3 ml of each volume respectively in a bottle and filling up to 1L with ultra-pure water. Protein concentration was adjusted to above and near 0.2 mg/ml. pH adjustments were avoided as chlorine ion interferes at low wavelength.

2.3.5.2 CD measurement and processing

The (Jasco) Chirascan was used to record the far-UV CD spectra for TTCF. The machine was equilibrated for 30 min with nitrogen gas pumping through the system. Following this was initiation of the water bath, temperature controller and switching on the system. Finally, the lamp was ignited and let to warm for 15 min. Using a quartz cuvette (1 mm, Starna Scientific, USA), with a path length of 0.1 cm, 400 µL of sample was inserted into the sample space of the cuvette. This was then placed into the sample holder and a spacer was inserted to hold the cuvette in place. The program output was set to millidegrees with a selected wavelength from 260-185nm. As this method is non-destructive to protein samples, multiple scans were recorded and averaged to increase quality. Bandwidth was set at 2 nm, step at 1 nm with active background subtraction (buffer only). Output files were converted to workable format. CD data in millidegrees were converted to delta epsilon ($\Delta\varepsilon$) values via:

$$\Delta\varepsilon = \theta \times \frac{(0.1 \times MRW)}{(p \times c) \times 3298} \tag{2.3}$$

where θ: measured data in millidegrees, p: path length in cm, c: concentration in mg/ml and MRW: mean residual weight = protein mean weight in atomic mass unit (daltons) divided by the number of residues. This allowed for normalisation and comparison of samples.

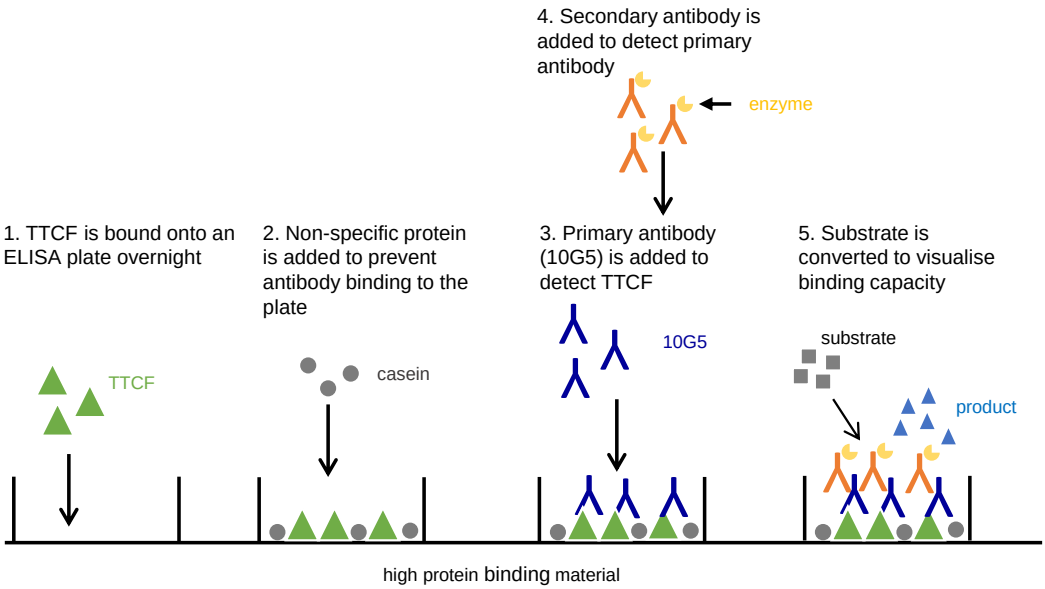

Figure 2-7: Schematic of ELISA for detection of TTCF tertiary structure. Bound TTCF was detected using a specific antibody. Binding of this antibody is measurable by using a secondary antibody conjugated with a reporter enzyme. The substrate conversion is measured using UV-vis absorbance.

2.3.6 ELISA of TTCF immunologic properties

Enzyme Linked ImmunoSorbent Assay (ELISA) is based on the antibody recognition of complementary amino acid sequences (or epitopes) present on the target protein[161,193,194]. In many cases, this can be only detected when the tertiary structure of the protein is in native conformation or near native state. As a result, the ELISA methodology is sensitive to changes in tertiary structure and is an appropriate technique to analyse released protein structure. 96-well high biding microtitre plates (Greiner, USA) were coated with native TTCF, released TTCF, released heated TTCF and denatured TTCF at 1 mg/ml, 100 µl / well and incubated at 4 °C overnight. The following day, the plate is incubated with, in chronological order, blocking agent, specific detecting antibody, secondary antibody conjugated with reporter enzyme and substrate. Substrate conversion is timed and stopped with acid (figure 2-7). This signal can be read using absorbance and plotted versus concentration or dilution.

2.3.6.1 Analysis of TTCF

TTCF at 1 mg/ml was diluted to 10 µg/ml in 50 mM bicarbonate buffer ($NaHCO_3$, Na_2CO_3) at pH 9.6. This solution was added to a high binding 96-wells microtitre

plate, 100 µl/well and incubated overnight at 4 °C. This results in 1 µg of TTCF to be bound to bottom of the well. Following day, the plate was washed 3 times with 1x phosphate buffered saline (PBS) and incubated with 1% casein in PBS + $Tween_{20}$ (0.05%) for 1 hour at room temperature. Washes were repeated and a monoclonal antibody against TTCF binding sites (10G5[161]) was serially diluted two-fold. Starting at 1 µg/ml, 100 µl was added to each well vertically and incubated for 1 hour at RT. Washes were repeated followed by the addition of a goat-anti-mouse IgG horseradish peroxidase (HRP) enzyme conjugated antibody in 1:10,000 x dilution (PBS + 0.05 % $Tween_{20}$) for another hour. Substrate solution was prepared during this incubation. 5'-5' tetra-methyl-benzidine (TMB, Sigma, UK) was dissolved in 1 ml of dimethylsulfoxide (DMSO, Sigma, UK) at 10 µg / ml and 100 µl was added to 10 ml of 0.1M sodium acetate pH 6.0 with addition of 1.5 µl of 30% (v/v) H_2O_2. The plate was washed 4 times after 1 hour incubation and tapped dry. Substrate solution was added to each well, 100 µl/well, and left to develop for approx. 10 minutes while the enzyme converted substrate into a blue colour. 2 M sulphuric acid H_2SO_4 stopped the development. The microtitre plate was read using a plate reader at 450 nm with samples accordingly blanked after measurement.

2.3.7 Dynamic Light Scattering (DLS) of purified TTCF

DLS, also known as Photon Correlation Spectroscopy, was utilised to measure the protein dimension in solution. This is based on the refraction of laser illuminated particles, at particle angle θ, in solution that move according to Brownian motion.[195] It is able to measure as little as 0.1 nm particles. This methodology combines the measured scattering intensity with the electric field equation and allows the Stokes-Einstein equation to be used. The scattering intensity correlation function g^2 measures the intensity, I, of a particle at a time, t, over a period τ. The signal changes in increasing duration of measurement and is displayed as an exponential decay.[196]

$$g^2(q;\tau) = \frac{\langle I(t)I(t+\tau)\rangle}{\langle I(t)\rangle^2} \tag{2.4}$$

This, in an ideal situation, can be a single decay relating to a monodisperse solution containing 1 type of uniform particle. The equation can be correlated to create the Siegert relationship combining the second order function with a first order autocor-

relation function g^1.

$$g^2(q;\tau) = 1 + \beta[g^1(q;\tau)]^2 \tag{2.5}$$

The measured g^1 function can be fitted with an exponential decay. Here, Γ relates to the diffusion coefficient D_t based on the scattering wave vector q. In this equation, λ is the laser (HeNe) wavelength at 632.8 nm, n_0 is the sample refractive index, θ is the angle of detector location oriented from the sample.

$$\begin{aligned} g^1(q;\tau) &= exp\big(-\Gamma\tau\big) \\ \Gamma &= q^2 D_\mathrm{t} \\ q &= \frac{4\pi n_0}{\lambda} * sin\left(\frac{\theta}{2}\right) \end{aligned}$$

Once the diffusion coefficient is calculated, this can be inserted into the Stokes-Einstein equation. Where η: viscosity in cP, κ_B: Boltzmann's constant, T: temperature in Kelvin, r: hydrodynamic radius.

$$D = \frac{\kappa_\mathrm{B} T}{6\pi\eta r} \tag{2.6}$$

It is a very effective method to look at protein size in solution and is sensitive enough to detect buffer effects or protein unfolding. This method was applied to verify a monodisperse solution of column-purified TTCF.
Zeta potential is obtained from measuring the electrophoretic mobility (μ_e) in solution when a charge is applied. Then the following equation is utilised:

$$\mu_e = \frac{V}{E} \tag{2.7}$$

where V = particle velocity (μm/s), E = electric field (Volt/cm). This can be processed further with use of the *Henry* equation to determine the ζ potential.

$$\mu_e = \frac{2\varepsilon_\mathrm{r}\varepsilon_0\zeta f(Ka)}{3\eta} \tag{2.8}$$

where ε_r = relative permittivity/dielectric constant, ε_0 = permittivity of vacuum, ζ = zeta-potential, $f(Ka)$ = Henry's function and η = viscosity at experimental temperature.

2.3.7.1 Sample preparation and measurment

TTCF was analysed for size and zeta potential. Both measurements required specific sample cells. Polystyrene cuvettes (ZEN0040, Malvern Instruments, UK) were used to measure native solution. Zeta potential measurements were carried out in folded capillary cells (DTS1060, Malvern Instruments, UK) with gold-plated electrodes on each side of the channel[196]. These conduct a small charge through the solution and cause particles to move in the direction of neutral charge. This motion was recorded and correlated with a zeta value. The consensus indicates a stable particle to have a zeta potential >+40 mV or <-40 mV. Particles that fall between this range are susceptible to aggregate with the most unstable particle charge to be around 0 mV. TTCF in buffer at 1 mg / ml was centrifuged at 16,000 x *g* for 20 minutes to remove any particles that could interfere with the measurement, such as dust.

The NanoSizer S (Malvern Instruments, UK) was used for measurements. The acquisition protocol is set to measure 10 seconds of counts for 3 repeats. Outputs in size by volume and size by intensity.

2.4 Results & Discussion

2.4.1 OD 600 nm *E.coli* monitoring

A colony of transformed *E. coli* was taken from an ampicillin containing agar plate and incubated overnight in 20 ml of LB media at 37 °C. The next step involved incubating a larger volume of media, 500 ml per flask (total of 3) with the transformed *E.coli* and monitoring the bacterial growth using OD 600 nm measurements. The

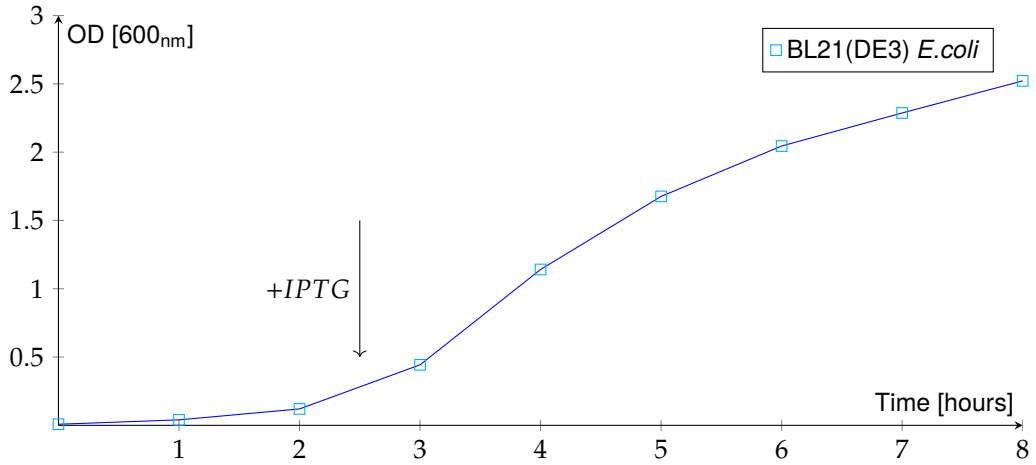

Figure 2-8: OD 600nm measurement growth of BL21(DE3) *E. coli*. Growth curve shows optimal induction stage between 2-3 hours.

optical density monitoring of the initial run (figure 2-8) displayed the time window of induction to be between 2-3 hours. This time was taken from the moment *E.coli* was added to the growth media. Small sample volumes (0.5 ml) were taken at induction and then at hourly intervals following until pelleting and storage. The samples were prepared for molecular screening as described earlier (section 2.3.3.2) and run on an SDS-PAGE gel.

2.4.2 TTCF expression verification

The expression of TTCF was confirmed via SDS-PAGE analysis (figure 2-9). The visible increase in intensity of a protein band at approximately 50 kDa represents the expression of TTCF over time. Each lane corresponds with a time point in hours. All samples were normalised and 10 µg was used for each sample. The concentration was determined using the BCA assay.

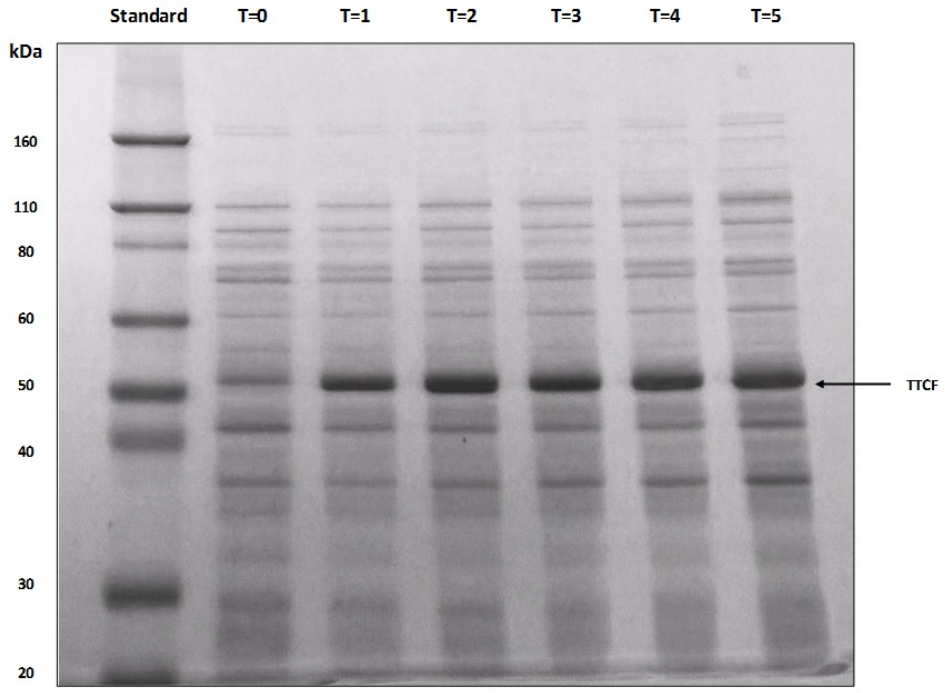

Figure 2-9: SDS-PAGE analysis of TTCF expression. Samples taken during the OD 600 nm monitoring of *E. coli* growth and induction were analysed using SDS-PAGE. At T=0, IPTG was added to induce TTCF expression.

2.4.3 TTCF purification analysis

Subsequently, the collected bacterial pellets were processed to release the TTCF and the supernatant was run over a his-tag binding nickel column. The chromatograph (figure 2-10) displays the several stages of the automated purification protocol. Important features are:

- Increase in absorbance (mAU at 280 nm) during sample injection (in $IMAC_{25}$).
- Returning to baseline (UV 280 signal) after sample injection, ending the column binding phase.
- Single peak elution appearing after the concentration of reservoir B ($IMAC_{500}$) reaches the critical level to out-compete histidine binding.
- Baseline return after full elution and re-equilibration.
- Peak fractions were collected and pooled for dialysis in 50 mM Tris at pH 7.

Samples were collected during each of the purification steps. The protein concentration of these was determined using a BCA assay, interpolating the unknowns using

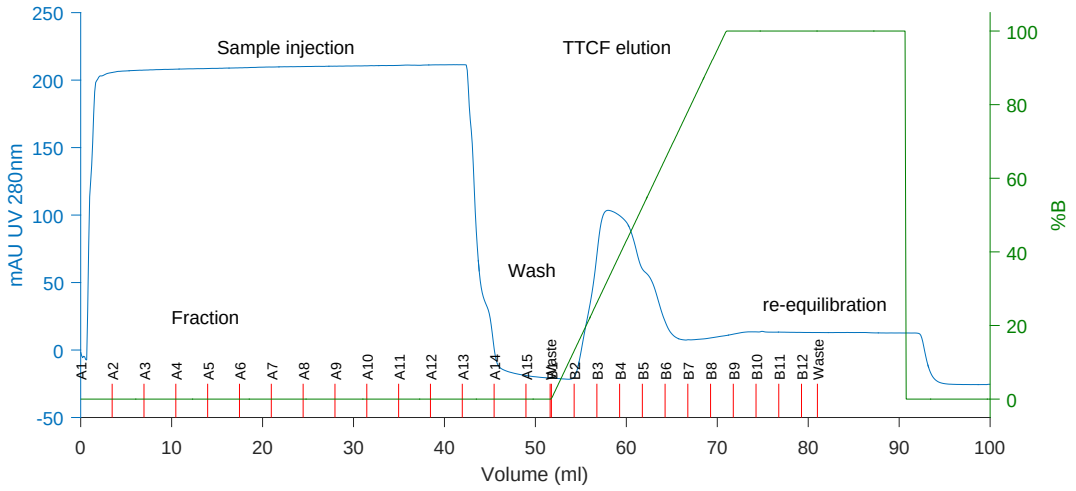

Figure 2-10: AKTA chromatogram of TTCF purification. Signals represent (blue) UV absorbance at 280 nm, (green) % elution buffer, (red) fractions taken. The peak elution seen after the wash contains TTCF protein.

a BSA standard fitted with a linear regression (figure 2-11). Samples were analysed on a SDS-PAGE gel to determine whether optimisation was needed.

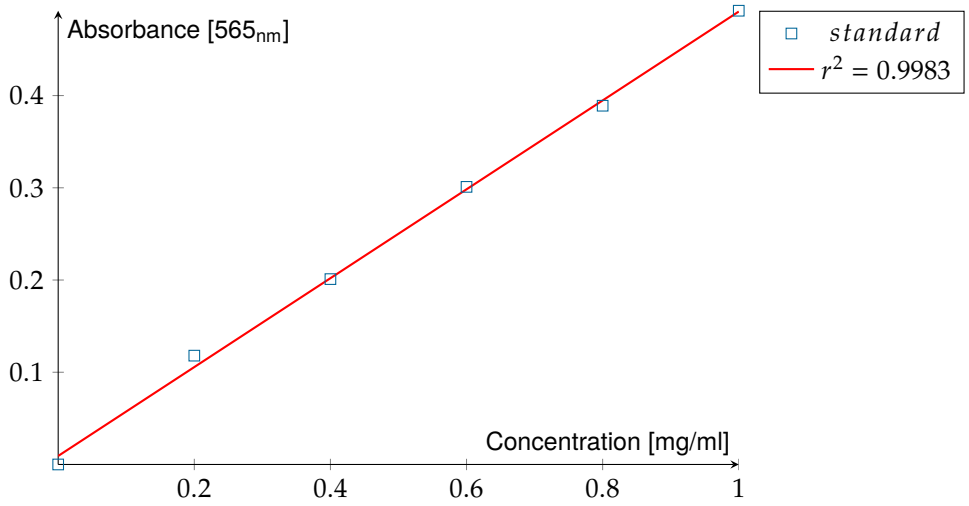

Figure 2-11: BSA standard used in BCA. Bovine serum albumin (BSA) standard with fitted linear regression. This was used for interpolating unknown samples in the BCA assay.

The BCA analysis showed an overall reduction in protein concentration (table 2-1) with detectable levels of purified TTCF protein. There are clear distinctions between different stages visualised in the SDS (figure 2-12). The reduction of bands throughout the purification process indicated the successful removal of unwanted proteins. The purified TTCF showed a thick band at 50 kDa in the peak fraction sample. It

#	sample description	dilution	mg/ml	final conc. (mg/ml)
1	T=0 (hr) IPTG added	-	-	-
2	T=5 (hr) IPTG	4.6	based on OD	-
3	Resuspended sonicated pellets	100	0.29	29.25
4	Supernatant (after sonication)	10	1	10.03
5	TTCF peak fractions A10-14 (Akta)	2	0.43	0.85
6	Flow through (Akta, unbound)	10	0.43	4.29
7	TTCF dialysis / 50 mM Tris pH=7	2	0.48	0.95

Table 2-1: Protein concentration of intermediate purification steps. BCA analysis of samples from protein expression to purified TTCF solution.

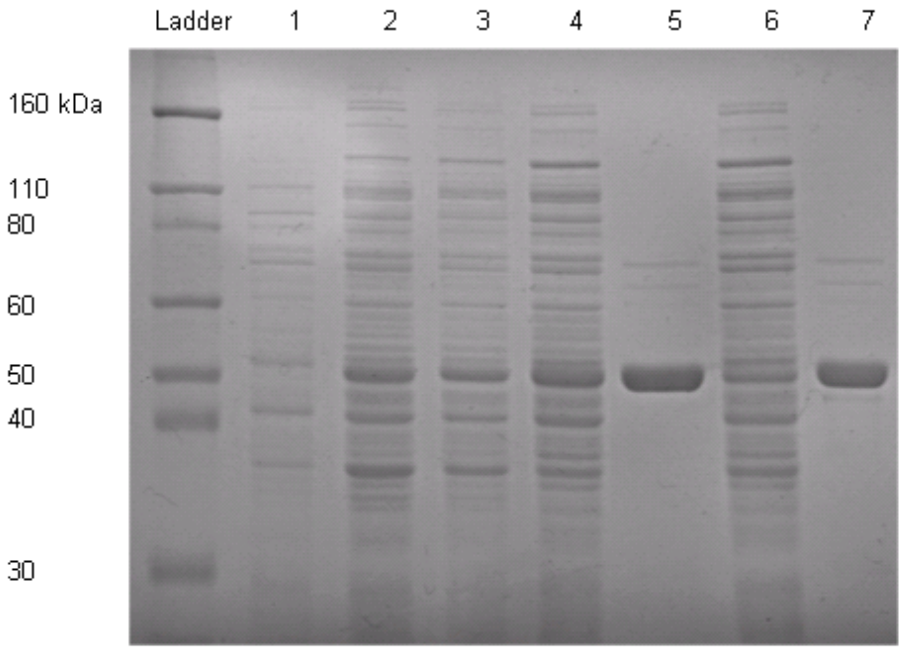

Figure 2-12: SDS-PAGE of TTCF expression and purification. Horizontal numbers represent samples from table 2-1. Vertical numbers represent molecular weights designated by the ladder.

presented some extra faint bands. However, with the small amount of protein loaded on to the gel there was no cause to add another purification step. The results confirmed that the process successfully purified TTCF and removed the majority of non-his tag proteins from the supernatant.

2.4.4 Circular Dichroism of native TTCF

After purification and dialysis, 1 ml of native TTCF was buffer-exchanged into sodium phosphate (10 mM Na_2HPO_4, NaH_2PO_4, pH 7) for CD measurement. Buffer-exchange was achieved using a desalting column (PD-10, ThermoFisher UK). Tris buffer and chlorine ions present interference in CD and were therefore not used as solvent or for adjusting pH. Triplicate CD scans of native TTCF (0.2 mg/ml) from 260-180 nm displayed consistent results (figure 2-13). The averaged TTCF CD pattern

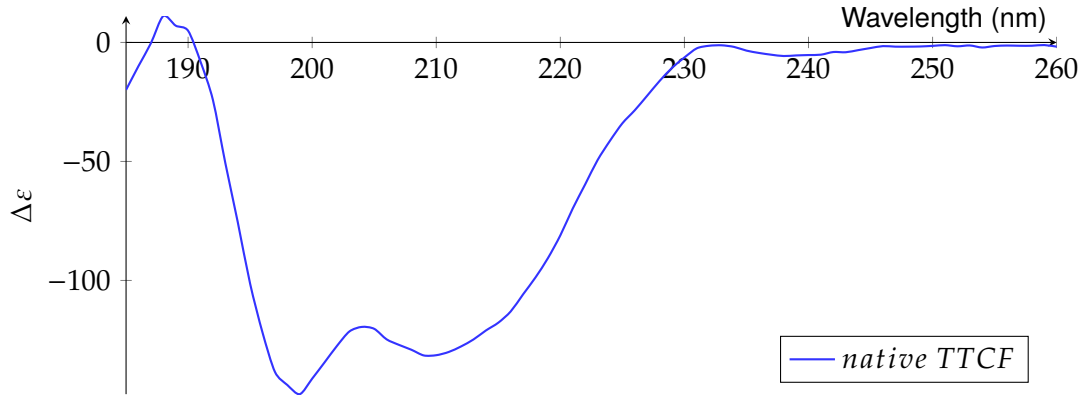

Figure 2-13: Circular Dichroism of native TTCF. Delta epsilon calculated from conversion of measured ellipticity in millidegrees. Conversion variables were the Mean Residual Weight (53545 da / 467 aa), path length of 0.1 cm and concentration of 0.286 mg/ml. Triplicate scans were conducted before conversion.

obtained is a combination of various secondary structural levels. This absorption of polarised rotational light at far UV wavelength was used as a signature reference for native TTCF. The signal is composed of alpha helices, beta sheets and random coil absorbance. More on the deconvolution of TTCF CD patterns described in Chapter 6.

2.4.5 DLS & Zeta of native TTCF

DLS of native TTCF in Tris buffer proved to be challenging. Many adjustments were attempted until a sample was obtained of high purity and dust free. Centrifugation

and filtration were used to obtain an appropriately clean sample. The measured scattering of TTCF in solution (figure 2-14) was a single exponential decay that reached baseline after a short amount of time.The diffusion coefficient was calculated using

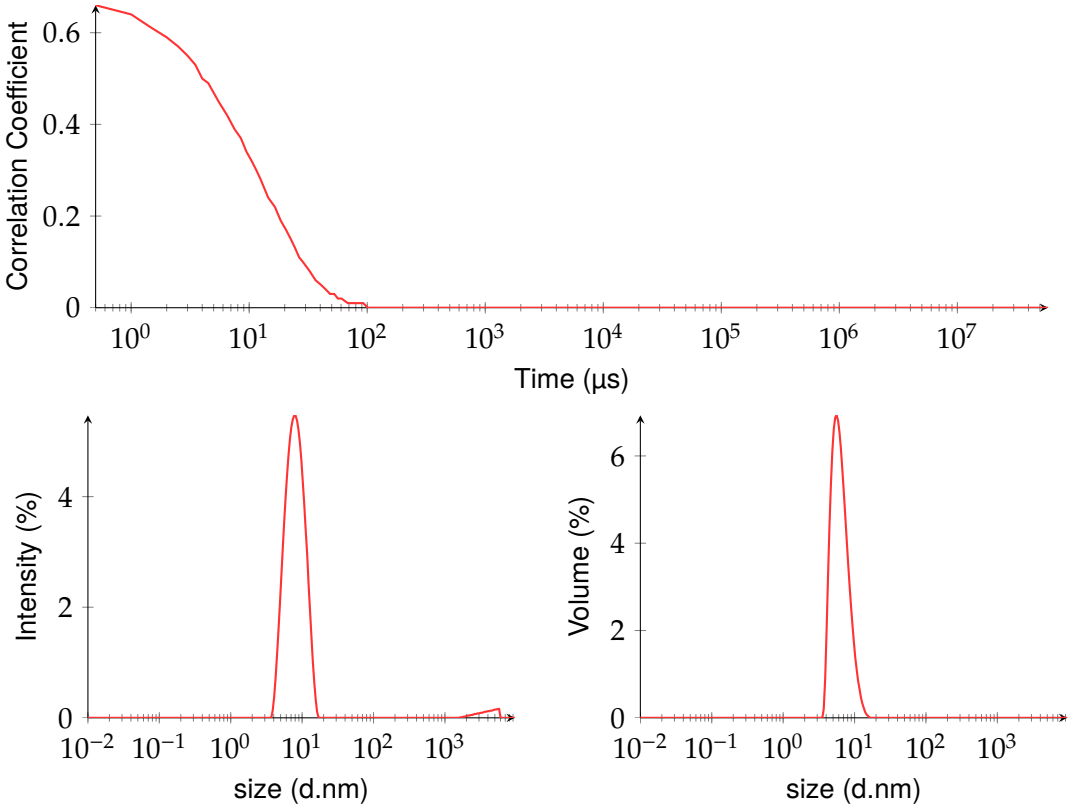

Figure 2-14: Dynamic light scattering of native TTCF. (top) Dynamic light scattering correlogram, (bottom) size by intensity and volume plots. Measured correlation coefficient and processed output for native TTCF. Sizes displayed are 8.235 d.nm (± 2.424 SD) and 6.454 d.nm (± 1.832 SD).

the apex of decay and put through the internal SOP for calculating size by intensity and size by volume. Values obtained indicated the average hydrodynamic diameter (d.nm) for TTCF to be 7.345 ± 2 (d.nm). The hydrodynamic size accounts for the protein and solvent layer present in solution. The difficulty of obtaining a clear clean sample for sizing was explained by the zeta-potential measurement of TTCF. Resulting value for the electro-kinetic mobility of TTCF was 3.54 mV. This indicates TTCF at neutral pH in Tris buffer will flocculate or aggregate over time.

2.4.6 ELISA analysis

Up to this point, native TTCF was analysed based on its molecular weight (primary structure) and chirality (secondary structure). This method allows analysis of con-

formational structure, tertiary level. Here, TTCF was coated on a microtitre plate. Then a detection antibody, 10G5, was used. If the right complementary exposed amino acid residues were present in native conformation, this protein would bind TTCF. Following this, the reporter antibody allowed for substrate conversion. This would relate to the concentration of bound antibody. The graph depicts a dose response curve where a sigmoid trend is visible (figure 2-15). It confirms the presence

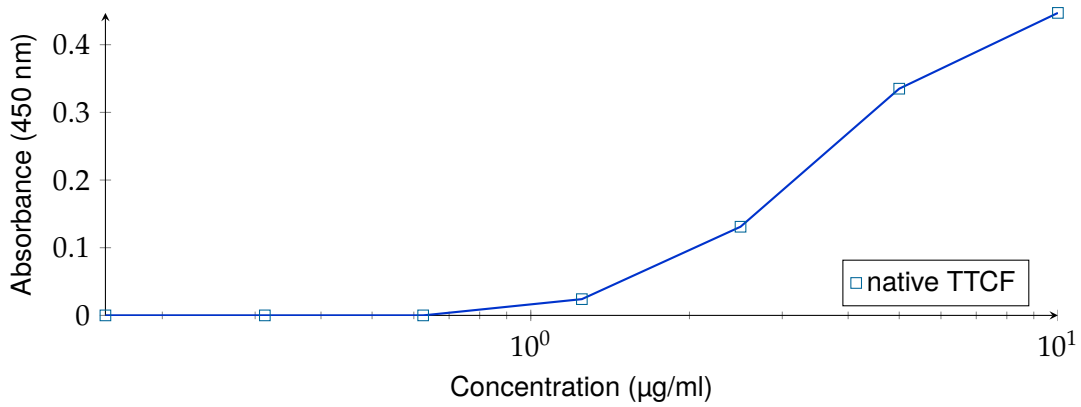

Figure 2-15: ELISA of TTCF. Converted substrate absorbance at 450 nm based on the antibody binding capacity of native TTCF.

of antigenic epitopes necessary for antibody binding. As TTCF is an antigen, this correlates directly to its function. Therefore, it was assumed that TTCF was expressed and purified in native state. Blank wells were used as control. These wells contained TTCF but no primary antibody was added during the analysis. This would help elucidate if any of the secondary antibody would bind. No detectable signal was obtained from these samples. With this evidence it was safe to interpret that the signal displayed was that of specific TTCF binding. Additionally, the 10G5 antibody did not work when the protein was analysed using Western Blot (described in 5.2.2) which requires denatured protein for analysis. It can therefore be inferred that 10G5 recognises epitopes dependent on the conformational integrity of TTCF at tertiary level.

2.5 Summary

TTCF is the heavy chain, 52 kDa, sub-fragment of the full tetanus neurotoxin produced by the bacterium *Clostridium Tetani*. The immunologic epitopes that will interact with the human immune system are found in each of the fragments of TeNT. Fragment A, the light chain, contain epitopes, P12 (amino acids 233–248) and P13 (amino acids 225–243), found in its zinc (Zn) binding domain[197]. These are recognised by T-cells after processing using the MHC type I and II pathways[198]. B-cell recognition was found for epitope P13[198]. Fragment B, the heavy chain (N-terminus region), has seven T-cell epitopes[199–201]. Fragment C, TTCF (HC-N and HC-C), has 3 epitopes which monoclonal antibodies bind, B-cell specific[202]. It was found that antibodies binding fragment A and C were potent neutralizing antibodies compared to fragment specific antibodies as fragment C is responsible for receptor binding and translocation of the light chain[202]. Split into fragments, they do not possess the synaptic properties that make the whole tetanus toxin lethal[180]. Therefore, TTCF is an ideal protein to be studied. Additionally, TeNT is a secreted protein which makes it relatively more stable in solution. Researchers were able to incorporate the gene into a bacterial plasmid. This enabled high yield expression of the protein for structural analysis[181]. The first part of the study was to investigate the structural and functional properties of TTCF in buffered solution before progressing towards stabilisation in silica, ensilication.

Firstly, reporter genes were utilised to verify the transformation of susceptible *E.coli*. Then the expression was verified using SDS-PAGE molecular weight screening and this agreed with published results[178]. This indicated the increasing amount of a protein band at the expected molecular weight. Passing this sample through various purifications steps led to a purified TTCF sample. Usage of column chromatography, BCA assay and SDS-PAGE allowed visualisation of the purification process. After this stage was completed, TTCF was dialysed into tris buffer which is a widely used standard biological buffer. At neutral pH is where most proteins display their mode of action.

Subsequently, progress was made towards analysis of secondary and tertiary protein structure. CD measurement displayed the native conformation of TTCF in agreement with literature[180]. The pattern measured is a convolution of several secondary structures. For the tertiary structure, ELISA analysis was conducted. It revealed good binding of a specific antibody against TTCF and was similar to other studies[161]. Binding of antibodies to an immunogenic protein directly correlates with its structural

integrity and function. Therefore, it was safe to say the immunogenic properties were present. Finally, scattering and absorbance analysis of the purified protein revealed monodispersity and presence of aromatic amino acids. In summary, TTCF was produced, purified and analysed with results that can be used to compare TTCF after ensilication.

Chapter 3

Ensilication of TTCF

3.1 Introduction

Ensilication is a methodology that utilises silica to stabilise proteins[203]. It is based on solution-gelation[139] (sol-gel) where condensation and polymerisation of a monomeric species form particles. These then link and form a gel. Ensilication is performed by adding soluble silica, hydrolysed TEOS to a buffered solution containing protein of interest. Stabilisation is achieved by polymerising silica that attaches electro-statically around these proteins, forming nano-particles. After a specific duration of time, the solution is vacuum filtered and dried at room temperature. The dried nano-particles in powdered form contain the protein. This ensilicated material can then be stored at room temperature and subjected to various thermal fluctuations, established previously[203].

Previous work on ensilication included studies using lysozyme, haemoglobin and insulin[203]. The result of these investigations determined this methodology to be applicable for a range of different proteins. The current "gold standard" in industry of protein preservation is freeze-drying (lyophilisation)[63–65]. This method freezes the sample in solution, then uses vacuum pressure to sublimate water molecules. Material that is lyophilised changes into a powder that can be stored at room temperature[69–71]. However, there are a number of protein based compounds that cannot be lyophilised. Many biopharmaceuticals, such as vaccines containing adjuvants, cannot be freeze-dried as this renders them unusable. Therefore, ensilication is an interesting alternative to employ.

3.2 Ensilication of TTCF

Once a pure mono-disperse solution of TTCF was produced and characterised, the next step was to apply ensilication to this protein. The isoelectric point (pI or IEP) is a key protein parameter in ensilication. TTCF has a theoretical IEP of 6.83 (pH)[176]. TTCF in tris buffer was identified to have a zeta potential (zp) of 3.54 mV[196]. If the zeta potential comes close to zero in difference with the IEP it will cause flocculation or aggregation of particles in solution. The ideal situation is to have the IEP and zeta potential as far apart possible. This is because zeta potential is an important parameter of dispersion stability[196], IEP is the surface charge of a particle at neutral pH[176]. Zeta potential can be influenced by buffer composition. Ensilication requires tris buffer at pH 7.0 with no sodium present (figure 3-1). Sodium ions interfere with ensilication as it is a positive ion[139]. The aim of ensilication is to direct negatively charged silicic acid towards positive residues on the proteins[205,206],

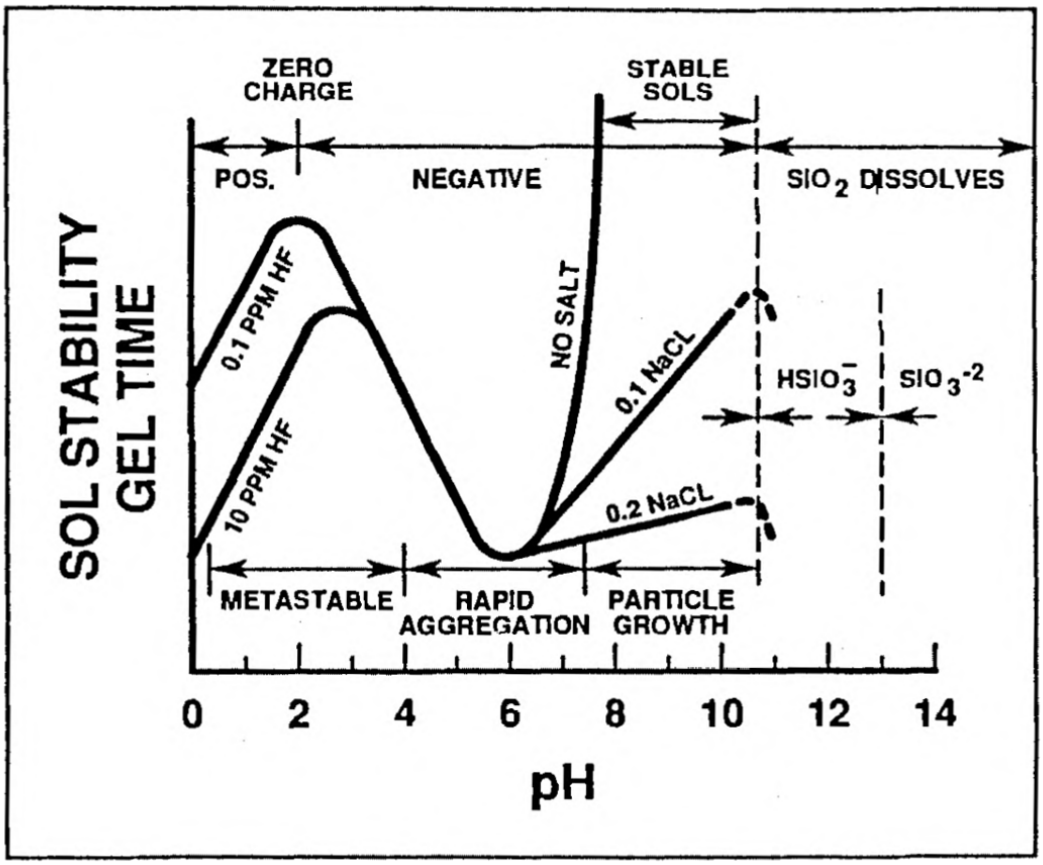

Figure 3-1: Sol gel time and stability. Gel time is relevant to ensilication. At pH 7 there is a boundary between rapid aggregation and particle growth. The particles formed are stable at this pH which also favours native protein state.[204]

these are lysine, arginine and histidine[57]. Analysis of TTCF using bioinformatics indicated the presence of these residues on TTCF[176]. By taking the PDB model, 1A8D[164], of TTCF, calculations[207] were able, using the adaptive Poisson-Boltzmann solver[208,209] (APBS) software, to create and overlay an electrostatic map (figure 3-2) of the protein. Regions positively charged are indicated in blue and negative in red. This visualised whether there were clustered positive or negative charged regions. The simulated model indicated multiple positive regions which aligned to the presence of said amino acid residues. Therefore, it was decided that TTCF is a viable candidate for ensilication. This protein is also a realistic model to use as it can determine whether vaccine proteins could be compatible with this method. It could then be a stepping stone for future projects to build upon.

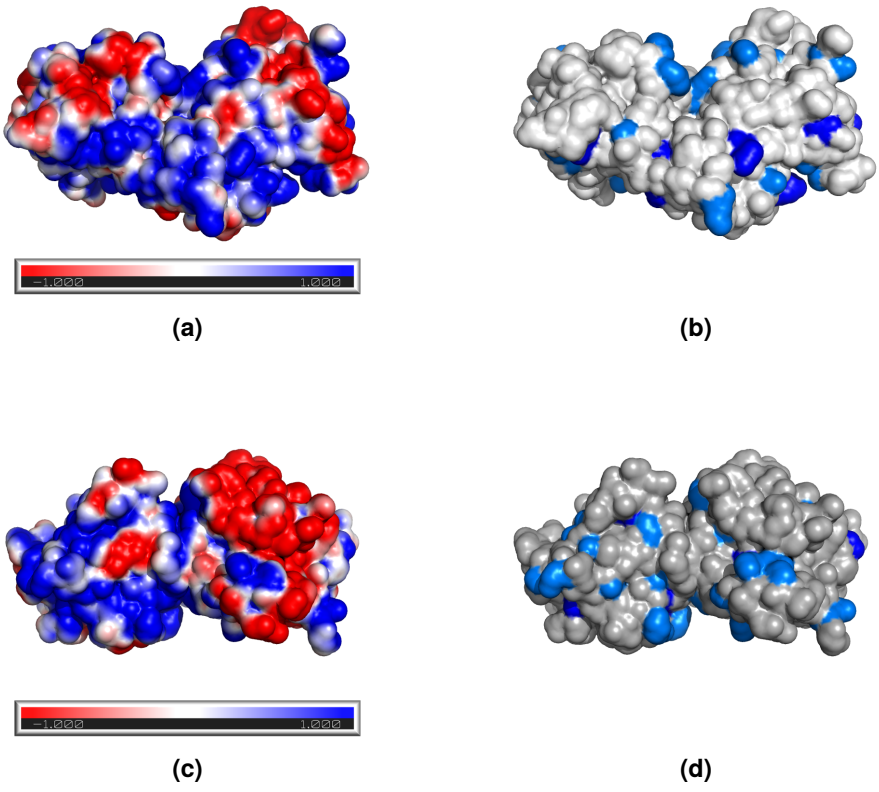

Figure 3-2: APBS simulated electrostatic model of TTCF with amino acid comparison. (a & c) Front and back view of the simulated electrostatic map of TTCF. Blue and red indicate postive or negative charged regions, respectively. (b & d) Blue and light-blue regions indicate the presence of lysine and arginine respectively.

3.2.1 Buffer preparation

The established protocol for ensilication requires 50 mM of Tris buffer at pH 7.0 with no sodium present. Therefore, 3.03 g of Trizma-Base (MW: 121.14 g/mol, cat: T666-1kg, Sigma UK) was weighed out to make 500 ml buffer. In a beaker, 400 ml of ultrapure (MilliQ, MilliPore UK) water was added to the weighed Trizma and using a magnetic stirrer this was dissolved. The pH was set using 32% (v/v) hydrochloric acid. Finally, the solution was filled up to 500 ml final volume with ultrapure water.

3.2.2 Hydrolysation of TEOS

In a glass beaker, 20 ml of TEOS (cat:86578-1L, Sigma UK) was added to 20 ml of ultrapure (MilliQ) water with stirring at 350 rpm at room temperature. Hydrochloric acid 32% (v/v) was added to this solution in a 1:500 ratio to initiate the acid catalysis of TEOS into $Si(OH)_4^-$. Once both components formed a clear homogeneous solution, ethanol was evaporated with slow stirring (60 rpm) for 20 minutes. The solution was then ready to be used within a window of 20 minutes.

3.2.3 TTCF ensilication

Several batches of ensilicated TTCF were made (figure 3-3). On average, a volume of 15 ml TTCF at 1 mg / ml was used. The volume of pre-hydrolysed TEOS added to the protein solution was determined by the volume provided from TTCF expression and purification. Total time of reaction was optimised and set to 15 minutes.

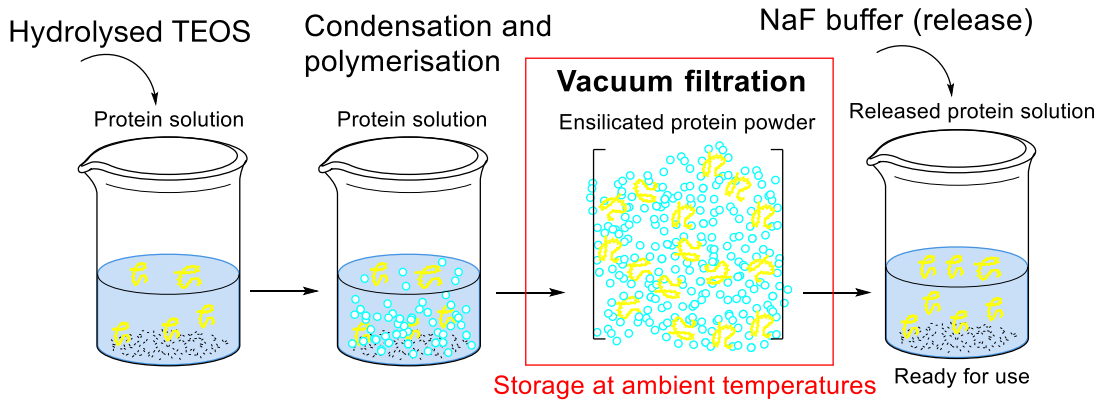

Figure 3-3: Schematic of ensilication. Hydrolysed TEOS is added to a buffered protein solution. Condensation and polymerisation of silica species around the protein grow over time and particles developed. The solution that becomes turbid over time is vacuum filtered and collected. After ambient storage, the samples are released for protein stability testing.

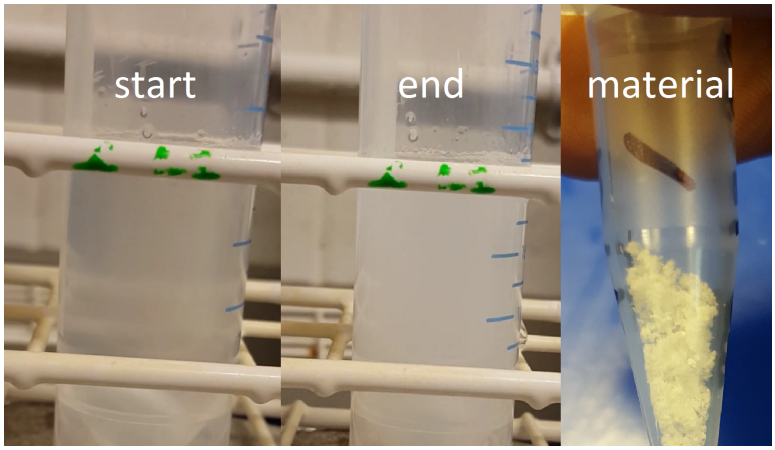

Figure 3-4: Stages of ensilication. Protein solution (translucent) becomes turbid after ensilication.

The sample was collected using a Buchner funnel containing a glass wool fibre pad filter with a size cut-off of 0.03 µm. After drying for 48 hours at room temperature, the material was scraped and collected into an eppendorf tube (figure 3-4). Small sample weights, 1 - 5 mg, were used for further analysis.

3.3 Release of ensilicated TTCF using NaF

Removal of silica from ensilicated TTCF, release, was performed using a previously developed method[203]. Sodium fluoride (NaF) in water acidified with HCl to pH 3.0 forms hydrofluoric acid, HF^-[210]. This compound is highly reactive to oxygen species due to its electron-negativity. In water, it forms an azeotrope with a boiling point of 120 °C. The following scheme displays the dissolution of silica using this method[210].

1. Release buffer: $NaF + HCl \xrightarrow{\text{ultrapure H2O}} Na^+ + Cl^- + HF^-$ (aq, pH 3.0)
2. Added to ensilicated material: $4\,HF^- + SiO_2 \longrightarrow SiF_4 + 2\,H_2O$ (aq)
3. Intermediate I: $SiF_4 + 3\,H_2O \longrightarrow H_2SiO_3 + 4\,HF^-$ (aq)
4. Intermediate II: $2\,SiF_4 + 4\,HF^- \longrightarrow 2\,H_2SiF_6{}^-$ (aq)
5. Total = $3\,SiF_4 + 3\,H_2O \longrightarrow H_2SiO_3{}^- + 2\,H_2SiF_6{}^-$ (aq)

The final products are ortho-silicic acid and hexafluorosilic acid. HF- will be completely converted during this process. The final complexes are stable and therefore allow safe handling of the released sample. Previous investigations using NMR spectroscopy have confirmed no silica to be left after subsequent dialysis of released protein[203].

3.4 Visualization of ensilicated TTCF

Ensilicated TTCF was collected by scraping the filter paper on which it was filtered. Due to the small volume of ensilication, much care was taken to obtain the ensilicated material.

3.4.1 Field Emission - Scanning Electron Microscopy

FE-SEM[211] was used to image the dried final material after vacuum filtration. This technique is based on electron microscopy (EM). Here, a conductive filament (e.g. Tungsten) is put under high current until it emits electrons. These are passed through magnetic coils that redirect it onto the sample. Electrons have elastic and inelastic interactions with the sample. The first describes backscattering electrons at an angle greater than 90° which are deflected by the material off the incident beam[211]. The latter describes excitation of the sample that results in secondary electrons with a lower voltage. These two types of interactions allow FE-SEM to topologically map the sample. In SEM the sample is scanned and the scattered electrons are detected and displayed onto cathode ray tubes. From here, parameters to increase resolution can be adjusted and subsequently an image is captured. FE-SEM is an appropriate method to image the morphology and size distribution of solid silica protein nanoparticles.

Ensilicated material was crushed into a fine powder and distributed across a square of carbon sticky tape. This was fixed onto a metal stub that would fit into the FE-SEM sample holder. The sample required dessication overnight before imaging. The JEOL FESEM6301F was used to take images up to 50,000x magnification.

3.4.2 UV-vis spectroscopy

UV-vis, described 2.3.4 was used to analyse the ensilicated material for presence of protein to examine whether TTCF was incorporated within the material. Native protein and powdered silica were provided as references to compare against.

The spectrum of 3 ml thawed TTCF, 1 mg/ml, from -20°C stock was analysed from 320-240 nm with 50 mM Tris pH 7.0 as buffer background. Silica and ensilicated material were analysed using a powder sample holder with air as background.

3.4.3 FT-IR spectroscopy

Fourier-transform infrared spectroscopy (FT-IR) is a method used to analyse compounds that absorb electromagnetic radiation in the infrared region[212–215]. The absorbance is based on the dipole movement of a diatomic molecule. There are two main events in molecules that indicate infrared absorbance, vibrations and rotations. These movements describe the various quantum states molecules will have when absorbing infrared radiation. The energy difference of these can be measured and plotted either based on absorbance or transmittance. The principle of FT-IR is based on interferometry (figure 3-5). Analysis using FT-IR produces an interferogram which is a complex convolution of signals. Within the IR spectrometer a radiation source emits infrared light which passes a beam splitter, at 45° angle, creating deflected and unaffected beams of infrared light. The beams are directed towards a stationary and movable mirror before being reflected to the detector, passing the sample.

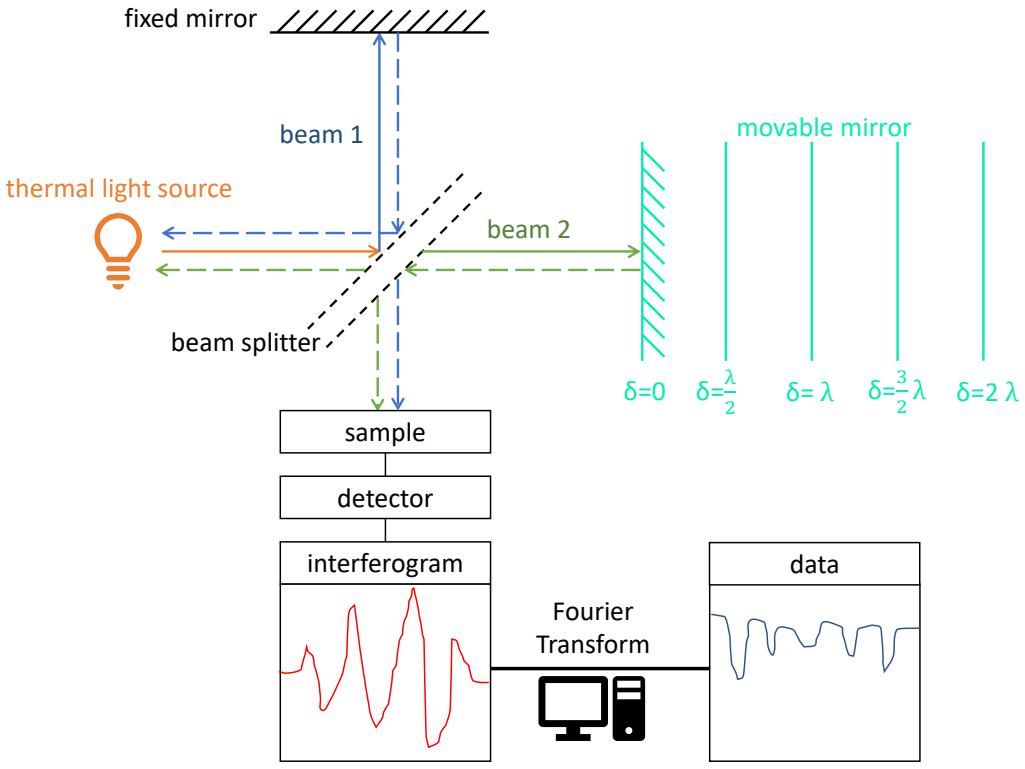

Figure 3-5: Schematic of FT-IR. The FT-IR spectrometer uses a radiation source that passes an angled beam splitter. Two beams of stationary and variable phase interact with a diatomic molecule present in the sample. The interferogram obtained is processed using the Fourier-Transform and produces the FT-IR spectrogram.

The movable mirror allows for constructive or destructive interference by changing the difference in phase between the two beams. The detector passes information via a computer that applies the Fourier Transformation (equation 3.1), producing an FT-IR spectra where transmittance of emitted infrared is plotted against wavenumber in cm^{-1} (frequency).

$$F(v) = \int_{-\infty}^{\infty} f(t) e^{(-2\pi i v t)} dt \tag{3.1}$$

The Fourier Transformation allows conversion of time or space, function $f(t)$, into frequency or spatial frequency, $F(v)$, respectively. As infrared is part of the radiation spectrum with notated wavelength as unit, which is a unit of space, the output is spatial frequency or wave number.

Samples were analysed using a PerkinElmer Spectrum™100, FT-IR attenuated total reflectance (ATR) spectrometer. The background used for powdered samples was air, ultrapure water for liquids. Backgrounds were read before scanning of the sample. The samples were tightly clamped before scanning. Scans were carried out between wave number 4000 and 500. Each measurement was scanned for a minimum of 8 scans. This was to improve the signal-to-noise ratio (SNR). Data were outputted in % transmission versus wave number. Peak analysis was done using a custom MatLab™script. Peak values were identified using literature databases.

3.5 Results & Discussion

3.5.1 Overview of TTCF ensilication attempts

TTCF was ensilicated on several occasions at 1:50 ratio of ensilication based on the previous success with lysozyme[203]. All parameters for ensilication were reported in table 3-1. The important parameter here is the ensilication efficiency, based on release concentration. Ensilication and material efficiency % are calculated using the following equations:

$$\text{ensilication \%} = \frac{\text{release concentration} \times \text{release volume}}{\text{powder weight used for release}} \tag{3.2}$$

$$\text{material \%} = \frac{\text{supernatant concentration} \times \text{supernatant volume}}{\text{protein concentration used for ensilication}} \tag{3.3}$$

Volume (ml)	TEOS (ml)	Conc. (mg/ml)	Time (min)	Powder (mg)	Flow (mg/ml)	Ensilication (%)	Material (%)
25	0.5	1	20	27.2	0.172	66%	83%
25	0.5	1	20	19.4	0.078	12%	92%
24	0.5	1	20	17.2	0.106	1%	89%
20	0.4	1	10	14.7	0.026	44%	97%
25	0.5	1	10	16.1	0.183	39%	82%
15	0.3	1	15	21.0	0.037	71%	94%
15	0.3	1	15	16.1	0.291	64%	62%
15	0.3	1	15	15.4	0.191	54%	62%
15	0.3	1	15	21.5	0.151	73%	85%
15	0.3	1	15	22.6	-	52%	N.D
15	0.3	1	15	16.5	0.060	40%	94%

Table 3-1: Ensilication of several batches. Key parameters are displayed. Volume = the amount of TTCF solution being ensilicated; TEOS = the volume of pre-hydrolysed TEOS used during the ensilication; concentration = concentration of TTCF protein in buffer measured using BCA assay; time = the ensilication time; powder = the yield after subtraction of the weighed filter containing the ensilicated material with the empty start weight of the filter; flow = the supernatant concentration measured using BCA after ensilication; ensilication = released concentration multiplied with the release volume divided with the powder weight used for release; material: supernatant concentration times the supernatant volume divided by the protein concentration used for ensilication.

Ensilication efficiency describes the usable amount of ensilicated material while the material efficiency describes the total amount of ensilicated material produced. The difference between ensilication and material efficiency is due to some of the filtrate being embedded within the filter which cannot be collected. Therefore, using the supernatant protein concentration it is possible to estimate the total incorporation of TTCF within the silica. With an average 64% ensilication efficiency, it appears a reasonable amount of protein is being stabilised within silica.

3.5.2 UV-vis

Protein incorporation was determined using UV-vis spectroscopy. This is verified by measurement of aromatic amino acid residue absorbance such as, tryptophan, tyrosine, phenylalanine and histidine[57]. Analysis of the UV-vis spectra 320-240 nm of native TTCF (in tris buffer), silica (dry powder) and ensilicated material spectra showed the ensilicated TTCF absorbance to be a convolution of both signals (figure 3-6). The broad band of absorption unique to proteins is apparent in native and ensilicated material. Moreover, a powder usually presents sharp absorption peaks, the absence suggests presence of trapped water within the material[189]. This could be due to drying step which is limiting the evaporation of water within cavities present in the material. Another explanation is that the hydration layer around the protein is preserved after ensilication. The increase of absorbance below 240 nm can be directed at the amide absorption relating to the secondary and tertiary protein structures.

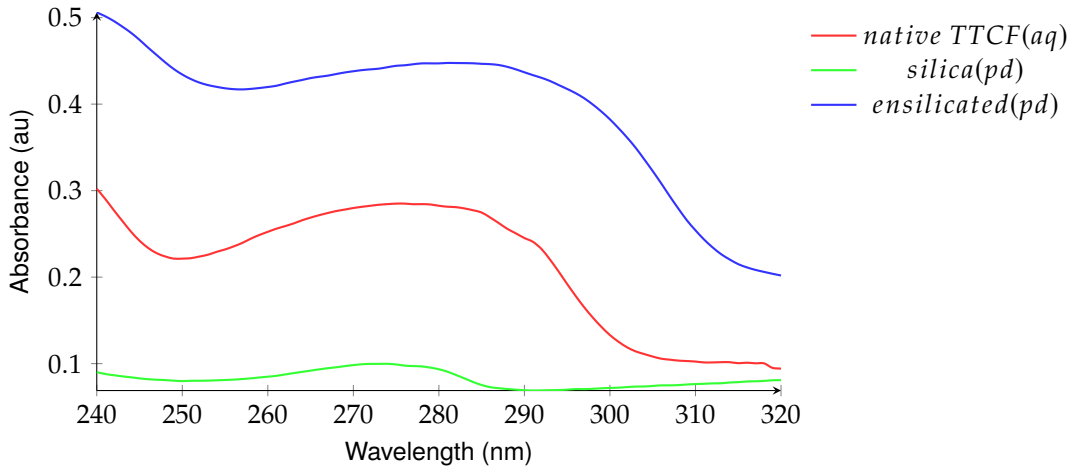

Figure 3-6: UV-vis absorbance spectra of native TTCF, silica and ensilicated TTCF between 320 - 240 nm. Native TTCF in buffer corrected using buffer blank. Silica and ensilicated materials analysed as powder with air as background.

3.5.3 FT-IR of ensilicated TTCF

Ensilicated TTCF was analysed using FTIR and compared to native TTCF (in buffer) and silica (powder) spectra (figure 3-7). The FTIR spectra for ensilicated TTCF displayed several strong peaks in the fingerprint region (1500 and above) and weak signals below that range. From observation of the various spectra, it is evident that the ensilicated material FTIR is a convolution of organic contributions[217] and silica bond absorption[216] (table 3-2). The spectra clearly divide the amide bonds versus the Si-O-Si (1079/1039) and Si-OH (952) signals represented for TTCF protein and silica respectively. Water, used as background for TTCF, removes the strong O-H (3320/3274) signal. Moreover, tris itself has organic bonds contributing to the TTCF spectra. These contributions are represented by amide I C=O, amide II C–N, N–H and C–H bonds. This result indicated the combination of protein and silica bonds within the ensilicated material. Therefore, this method also confirmed the ensilication of TTCF within the material.

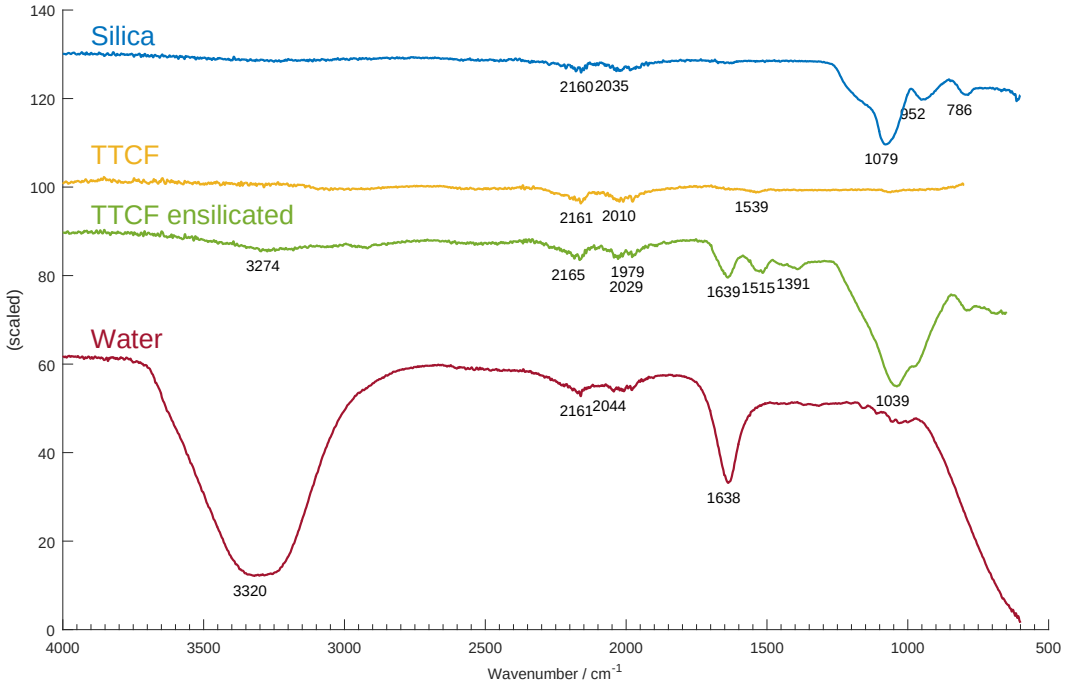

Figure 3-7: FTIR of silica (powder), TTCF (in buffer), ensilicated TTCF and water (background). Percentage transmittance between wavenumber 4000 - 500 cm^{-1} for each sample scaled on y-axis. Labels correspond to index values for specific diatomic molecules listed in table 3-2.

Wavenumber (cm^{-1})	Strength	Bond Type	Mode
3274	weak	O – H	stretching
2165	weak	C ≡ C	(triple bond) stretching
2029	weak	C – H	bending
1979	weak	C – H	bending
1639	strong	C = O	Amide I - stretching
1515	strong	C – N, N – H	Amide II - CN stretching, NH bending
1391	medium	O – H	bending (carboxylic acid)
1039	strong	Si – O – Si	stretching
952	strong	Si – OH	stretching

Table 3-2: FT-IR bond analysis[216,217] of native and ensilicated TTCF. Peak values in wavenumber were extracted from the FT-IR analysis and corresponded to their strength, bond-type and vibrational mode.

3.5.4 FE-SEM of ensilicated material

Several batches of ensilicated TTCF were imaged using FE-SEM (figure 3-8). The images display a fractal structure of sphere-like conglomerated silica particles (figure 3-9). The material itself seems to be very porous. Good consistency was observed

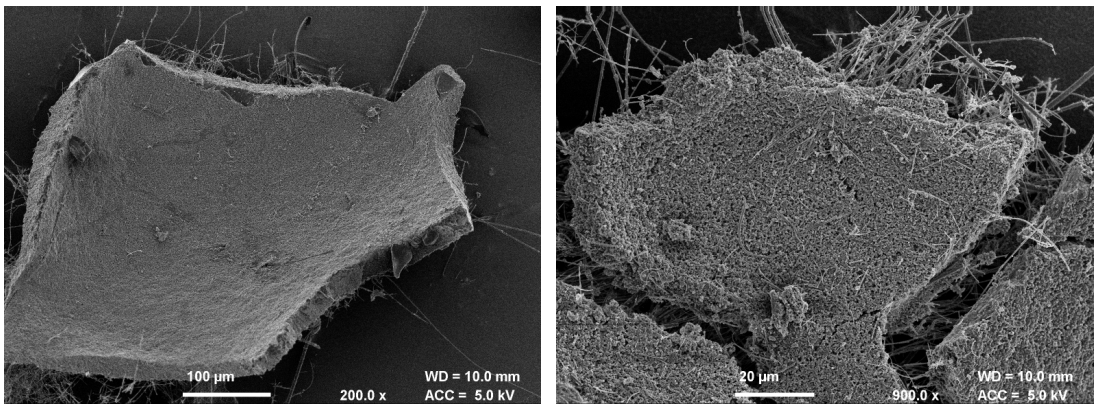

Figure 3-8: FE-SEM of ensilicated TTCF fragments. Images taken at (left) 200x and (right) 900x magnification. Samples were coated with chromium before imaging.

between triplicate batches. The ellipsoidal shape of native TTCF (PDB: 1A8D[164]) contributes to the final shape of the nano-particles formed. This is evidence that ensilication does tailor fit proteins in silica.

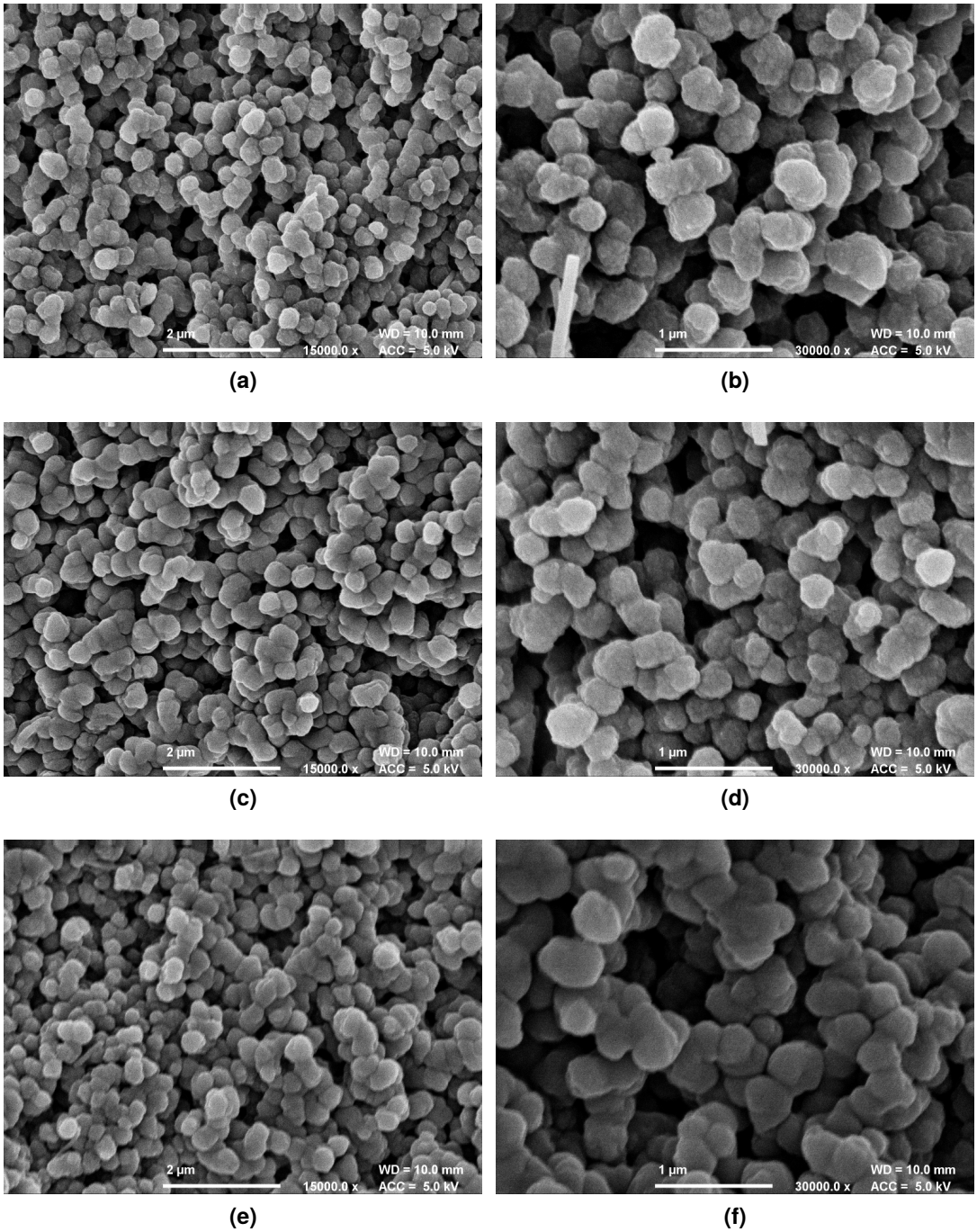

Figure 3-9: FE-SEM triplicate run of ensilicated TTCF. (a-c-e) 15,000 x magnification, (b-d-f) 30,000 x. magnification of ensilicated TTCF.

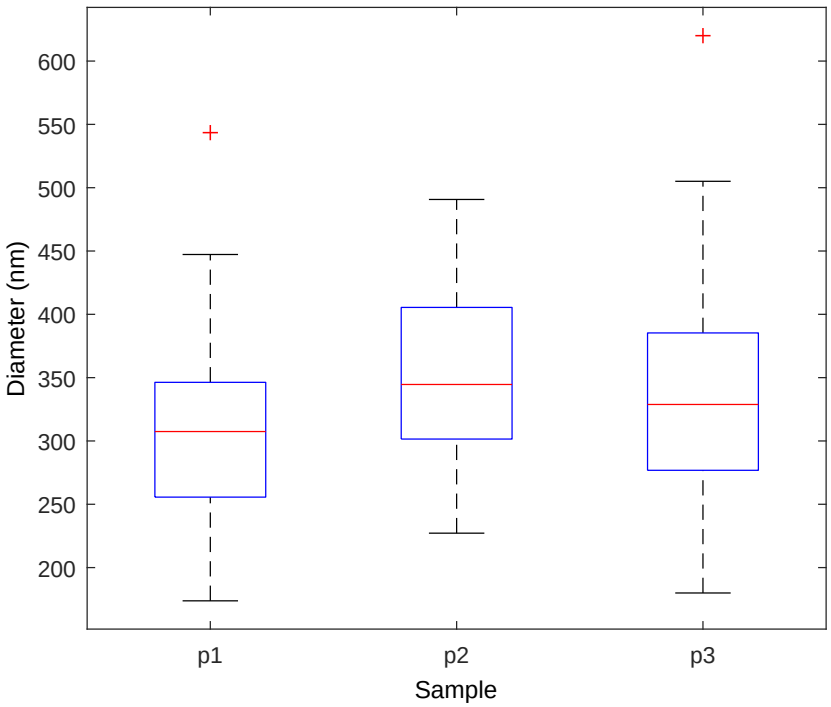

Figure 3-10: ImageJ analysis of ensilicated TTCF. Particles were sized using ImageJ software for batches p1, p2 and p3. Data is visualised in frequency distribution over diameter in nm.

ImageJ[218] was used to measure particle sizes of ensilicated TTCF (figure 3-10). Sizing reveals good consistency between replicate materials. However, there seem to be a large spread within each sample distribution. This can be contributed to the agglomerated state of the nanoparticles.

3.6 Summary

Ensilication is a previously developed method for the purpose of stabilising proteins using silica[203]. It is based on sol-gel technology and yields a dry protein-loaded powder, consisting of nanoparticles. TTCF, the vaccine protein model, was ensilicated. Ensilication was found to have on average 64% efficiency. As large amounts of protein were used for ensilication, this was considered to be an acceptable value. Note, that there were some significant differences between ensilication efficiency and total material yield. This is due to the material occasionally becoming (vitreous) glassy rather than a powder. The impermeability of this glassy material prevents quick release using the NaF buffer. Unfortunately, there is no clear evidence why this occurs. An explanation for this could lie in the preparation of pre-hydrolysed TEOS. The timing of both phases turning homogeneous varies on ambient conditions and this could in effect lead to it to form larger dense silica particles in solution. When the pre-hydrolysed TEOS is added to the protein for ensilication it results in the filtrate progressing towards a glassy material once polymerised and dried. Another explanation is the presence of salt, which has not been sufficiently removed after dialysis. It can also be affected by humidity and temperature when the filtrate is dried.

A possible solution to this problem would be to use a climate chamber with optimised settings for ensilication and drying to provide consistent conditions throughout the ensilication process.

UV-vis and FT-IR analysis revealed the presence of protein within the material. UV-vis showed the absorbance band between 250 - 300 nm with a peak at 280 indicating presence of aromatic amino acids, such as tryptophan. The observed broad absorption band is due to the presence of water (H_2O). FT-IR analysis showed the signal from ensilicated TTCF to be a combination of silica and protein specific bond absorption. These optical methods confirmed successful ensilication of TTCF. The measured protein concentration after release, using BCA, supported these findings. FE-SEM imaging of the material displayed 200 - 400 nm solid silica nano-particles which are in an agglomerated state. Compared to lysozyme[203], these particles were not perfectly spherical and indicated that ensilication does tailor fit proteins. Assessment of protein stability after ensilication will be described in Chapter 5.

Chapter 4

Small Angle X-Ray Scattering of TTCF ensilication

4.1 Introduction

Scattering is deflection of electromagnetic radiation from an incident beam which is focused onto a sample[219]. There are several types of scattering; elastic, inelastic and quasi-elastic[220,221]. These define the interaction of a sample with electromagnetic radiation. Changes in wavelength determine the category of scattering. This chapter describes the utilisation of small angle x-ray scattering (SAXS)[221–226] to elucidate the ensilication mechanism. SAXS was carried out at Diamond Light Source, Didcot (UK) and at the European Synchrotron Research Facility (ESRF) in Grenoble, France. Ensilication was monitored over time *in situ*, and with *ex situ* initiation, at different ratios and pH. This was intended to observe any changes due to the variations of key variables relating to the ensilication process[227]. Analysis led to a proposed ensilication mechanism. The reason for using SAXS is due to the difficulty in visualising ensilication via light scattering because of the inference caused by silica[228].

4.2 SAXS theory

X-ray radiation is part of the electromagnetic spectrum with a wavelength between 0.01 - 10 nm[229]. Synchrotron radiation facilities create x-rays via particle accelerators that increase the speed of electrons towards the speed of light contained within a circular enclosure. Magnetic coils modulate the beam to create a sinusoidal

wave with a specific amplitude and frequency matching the desired wavelength. This can be then selected and bent off the storage ring towards a beam-line. X-ray radiation interacts with electrons in the atomic shell which start oscillating[223]. This event causes elastic x-ray scattering at the site where an incident x-ray beam hits the sample (figure 4-1). The angle of deflection can be limited at the detector to set a range of sizes and is visualised for x-rays by Bragg's Law[230].

$$n\lambda = 2d\ sin\ \theta \tag{4.1}$$

Where λ is the wavelength of x-rays (Å), d is the atomic spacing (Å) and θ is the angle (°). Small angle x-ray scattering is able to detect 0.1 - 100 nm sized particles at a typical angle of 2θ between 0.3 - 5°. In principle, the incident beam k_0 is scattered k_s upon interaction with a sample. The elastic scattering[220,221], no energy loss between incident and scattered photon, is then measured at the detector $q = k_s - k_0$. As $k_0 = \frac{2\pi}{\lambda}$ and $|k_0| = |k_s|$ the scattering is resolved by trigonometric calculation. Here, the sine of angle $\theta = k_s$ divided by q, $sin\theta = \frac{2\pi}{q}$ which can

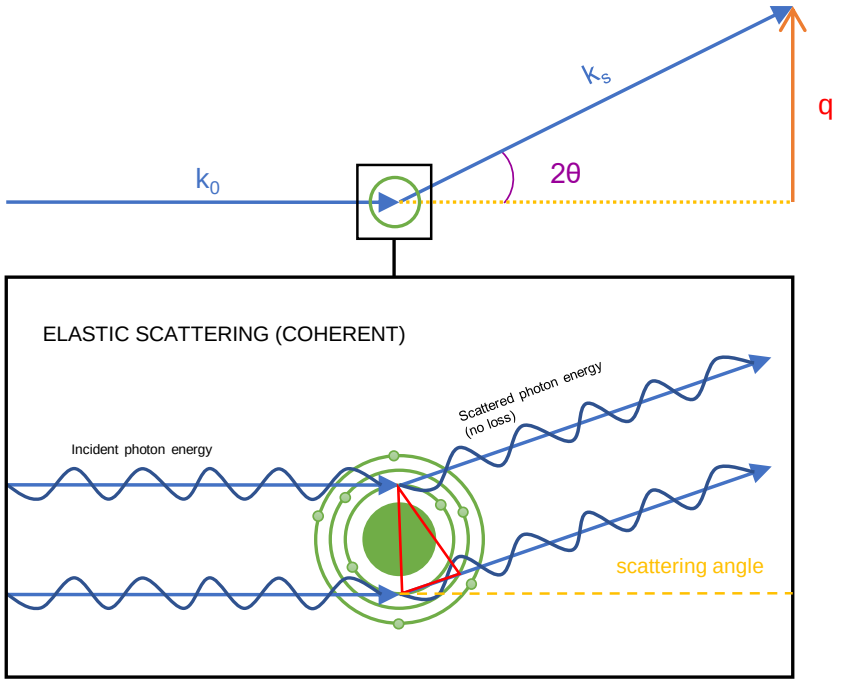

Figure 4-1: SAXS scattering basics. The incident beam of x-rays hits the target molecule. Interaction with the sample causes electrons to oscillate. The oscillation is an energy (momentum) transfer with no loss, elastic scattering. Intensity can be measured over the wave vector q which is expressed as = $\frac{4\pi \cdot sin\theta}{\lambda}$

be adjusted into $\frac{q}{2} = \frac{2\pi}{\lambda} sin\theta$. The momentum transfer (or wave-vector) s is then expressed as:

$$q = \frac{4\pi \sin\theta}{\lambda} \tag{4.2}$$

This does not record the amplitude, however does allow the measurement of scattering intensity. The collected 2D data is then, after instrumental correction, averaging and background subtraction, plotted as 1-dimensional (1D) $I(q)$ versus q. For a dilute (mono)disperse system the intensity, $\Delta\, I(q)$ is:

$$\Delta I(q) = N \cdot I_0 \cdot \Delta\rho^2 \cdot V^2_{particle} \cdot P(q) \cdot S(q) \tag{4.3}$$

Here, intensity ($I(q)$) is the number of particles (N) multiplied by I_0 which is the scattered intensity of the incident beam. The contrast between particle and solvent ($\Delta\rho = \rho_{particle} - \rho_{solvent}$) is accounted for as well as structure factor (S), typically S = 1, and volume (V_1). The equation involves form factor (P) to indicate the geometrical shape of said particle, e.g. sphere, ellipsoid or cubic etc. which contribute to the overall scattering pattern in their own way[226]. More on the use of form factors and fitting of experimental data described in the results section.

The 1D SAXS plot, $I(q)$ versus q, displays three regions of interest (figure 4-2). Low-q is the range at higher size and can indicate inter-particle effects and structure factors. Intermediary zone can be fitted to elucidate the particle shape and size, form factors. High-q region displays the interface between particles and solute. This is high resolution and therefore contains great variation. Experimental data allows for simple mathematical fitting that provide a start for data interpretation. The distance distribution function p(r), Guinier, Porod and Kratky analysis allow estimations of the particle dimension probability, radius of gyration (R_g), surface analysis and protein folding assumptions[222,224–226,231]. The p(r) function[224] calculates, in real-space, the distance distribution between pairs of electrons in a macromolecule. This is visualised with the probability on the y-axis and distance in Å on the x-axis. This method is able to distinguish slight changes in protein conformation and also provides an R_g value. The Guinier equation[222] is fitted directly to the data in the form of:

$$I(q) = scale \cdot exp[\frac{(-Q^2 {R_g}^2)}{3}] + background \tag{4.4}$$

From this, the radius of gyration (R_g) provides average radii of a particle based on its density and total size estimated from a particular axis, xyz. Porod analysis[226,232] determines the exponential decay of the signal based on its slope, Porod slopes

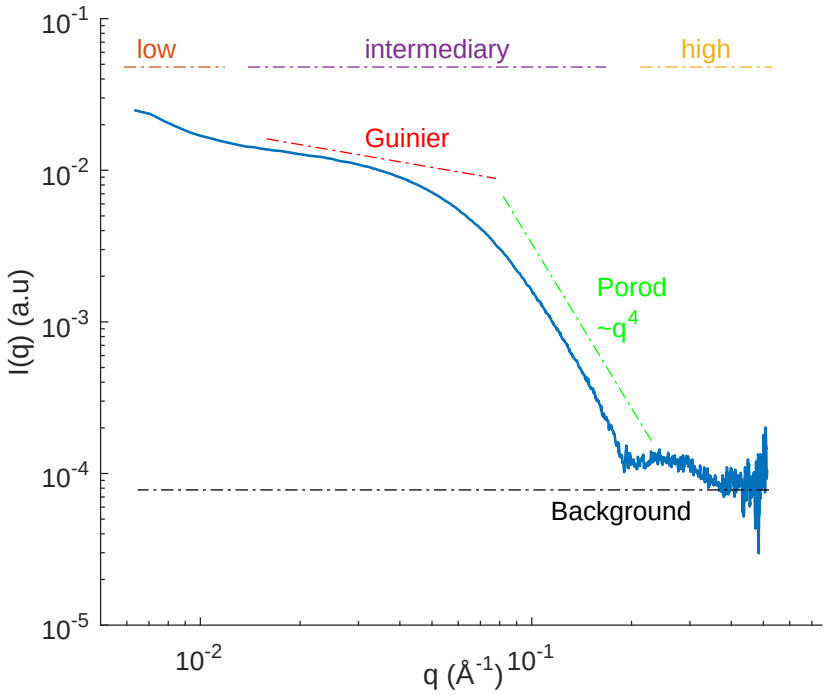

Figure 4-2: SAXS 1D plot regions of interest. SAXS scattering of native TTCF above shows regions where initial fitting can be performed. The apex of the exponential decay allows for fitting of the Guinier function. The slope afterwards is indicative of a Porod slope. High q region displays greater variability in the measured scattering. The decrease in scattering at low q is due to the increase of scattering angle proportional to the scattered energy.

range from 0 to 4 where the highest number indicates that the surface is too dense to be resolved in any basic geometrical structure. The Kratky plot,[222] visualised by $I(q) * q^2$ plotted against q, can suggest protein flexibility and derivative type shapes such as globular or ellipsoidal. Overall, these initial assessments will guide towards a representation of the actual process occurring and will allow fitting of mathematical functions that other researchers have established for various types of reactions.

4.3 SAXS method: Diamond Light Source

4.3.1 *in situ* TTCF ensilication

TTCF at 1 mg/ml in 50 mM Tris pH 7.0 buffer, 25 ml volume, was circulated using a peristaltic pump at 2 ml/min through Teflon tubing with an internal diameter of 1.6 mm. The sample solution passed through a 1.5 mm capillary flow cell in a loop before addition of hydrolysed TEOS (figure 4-3). Both pump and injector were remotely controlled. SAXS frames were taken at 1 frame/sec for 120 seconds whereafter the

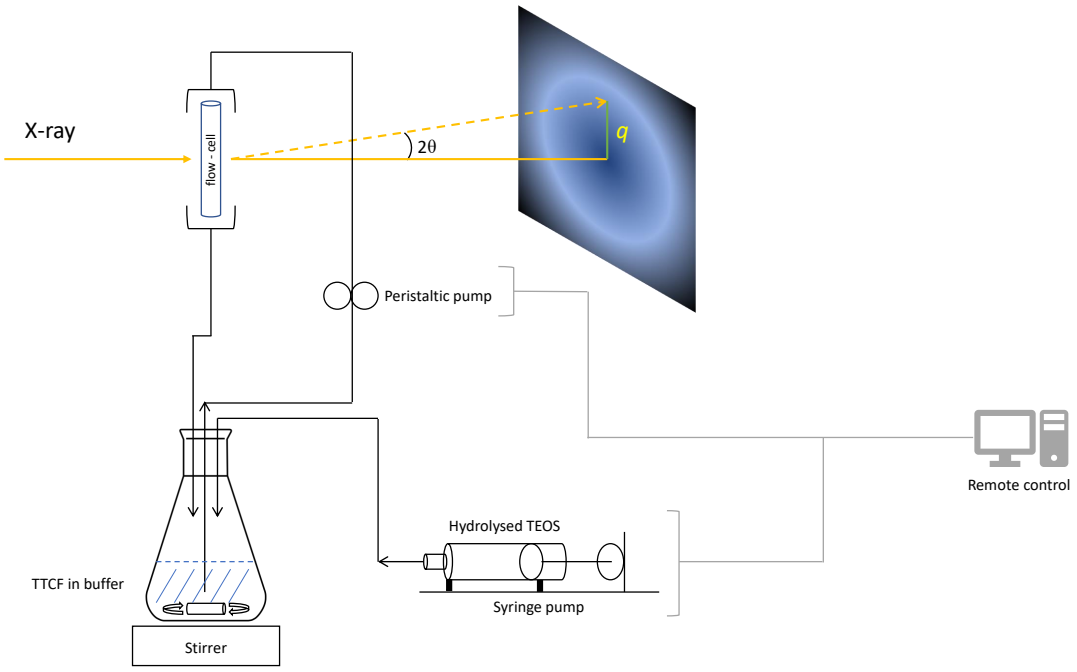

Figure 4-3: SAXS set-up at i22, Diamond. Continuous flow path of circulating protein in buffer was set up. Using remotely controlled pump and injector, the speed of circulation was set and the injection of hydrolysed silica was timed to additionally obtain pre-ensilication scattering.

frequency was altered to 1 frame/sec for 5 seconds every 20 sec interval. Total time of acquisition was 900 seconds. Pre-hydrolysed TEOS was added to the sample at 1:50 ratio after 3 seconds of measurement start. The incident X-ray energy was 12.4 keV. SAXS data were acquired using the Pilatus P3-2M detector at 2.2 m sample distance. This resulted in a SAXS range of $0.008<q<0.75$ Å^{-1}. The experiment was performed at room temperature. Native TTCF scattering was measured before addition of hydrolysed TEOS. Empty capillary and buffer scattering were measured and used for background correction.

4.3.2 2D data processing

Measured 2D SAXS data was processed into 1D data using the Data Analysis WorkbeNch (DAWN) software.[233] Figure 4-4 is an example of sample correction using lysozyme. Lysozyme is a standard model protein used in many studies as a reference. The SAXS mask and detector calibration files, provided by the instrument scientist, were loaded into a pipeline. Then the Poisson error was set and azimuthal integration added. The pipeline was completed by adding division steps that divided the data internally and with a scalar value (1.5) to compensate for the capillary width. The above was done for empty capillary scattering. The sample scattering was pro-

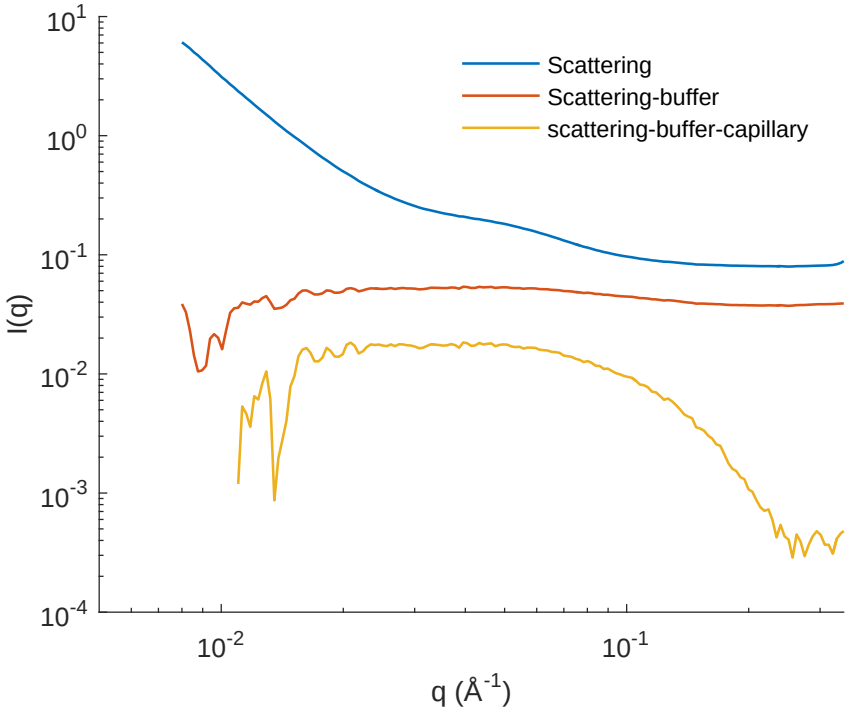

Figure 4-4: SAXS subtraction for lysozyme. Measured scattering was subtracted with buffer and then empty capillary scattering. This removed the solvent and container effects.

cessed via:

$$sample = sample(\text{+buffer +capillary}) - buffer(\text{-capillary}) - capillary \quad (4.5)$$

Before the final step, all data was multiplied with a scalar (1e9) and was averaged before output into a *.dat file. The processing yielded files containing a q-range of 0.008 - 0.75 Å^{-1}.

4.4 SAXS method: ESRF

4.4.1 *ex situ* TTCF ensilication

Pre-hydrolysed TEOS was prepared as previously described (section 3.2.2). This was added to 10 ml of 1 mg/ml TTCF solution at 1:50 ratio at pH 7 in a glass beaker. Using a sterile syringe, 1 ml of sample was taken and injected into a quartz capillary (figure 4-5). SAXS measurements were performed on the Time-Resolved Ultra Small-Angle Scattering beam-line ID02 at the ESRF, Grenoble, France[234]. The incident X-ray energy was 12.46 keV and two sample-detector distances were employed at 1.5 and 10 m. SAXS data were acquired using the Rayonix MX-170HS

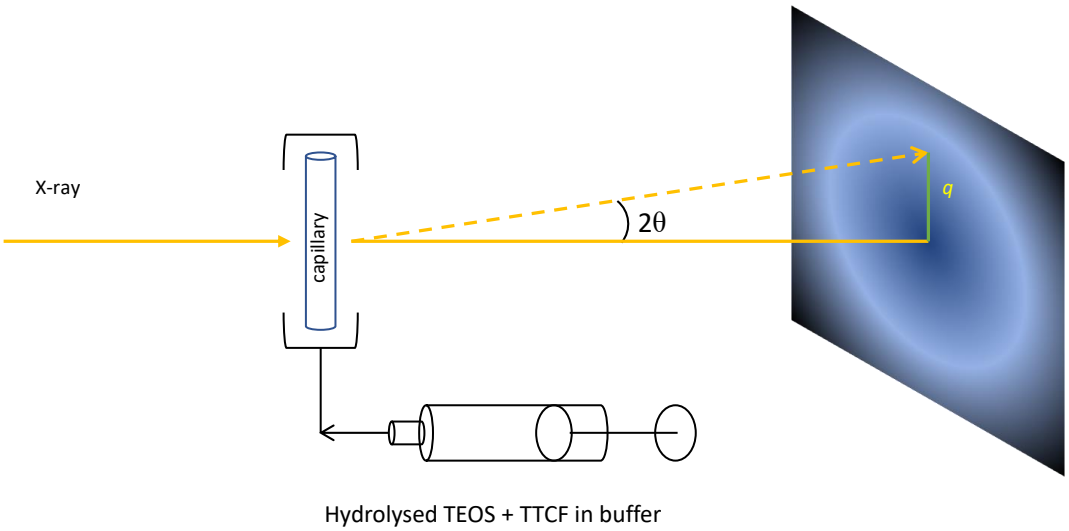

Figure 4-5: SAXS set-up at ID02, ESRF. Hydrolysed TEOS was added to TTCF in buffer and this solution was then taken up using a syringe and subsequently injected into a quartz capillary for SAXS measurement.

detector with exposure times between 0.01 and 0.03 sec. The measured 2D patterns after normalization by incident flux, sample transmission, and the solid angle were azimuthally averaged to obtain the 1D static scattering profiles as a function of the magnitude of scattering vector, q. Where q is given by, $q = \frac{4\pi \sin\theta}{\lambda}$, with λ the incident X-ray wavelength (=0.0996 nm) and θ the scattering angle. This gave two overlapping q-ranges of 0.0001<q<0.03 and 0.006<q<0.5 Å^{-1}. The scattering background in each case was measured using buffer and the normalized background subtracted data is represented by $I(q)$.

4.4.2 TTCF ensilication ratios

Ensilication of TTCF at 1:50 ratio occurs rapidly in standard conditions, therefore additional ratios of ensilication were measured to investigate any difference in particle morphology and size. 1:20 and 1:100 silica to protein ratios were chosen to assess as they will have significantly different amounts of silica present in the solution. The procedure of measurement was equal to the 1:50 ratio, once the hydrolysed silica was added to the TTCF solution, a sample was injected in the capillary and the experiment initiated. Other implications could be the increased resolution of ensilication at 1:100 or the depletion of $SiOH_4$ at 1:20 and the subsequent effects on the ensilication process.

4.4.3 TTCF ensilication pH

Ensilication is heavily influenced by pH[139]. As with 1:50 ratio, the condensation and polymerisation occurs rapidly at 1:100 ratio. pH 8 and 6, at this ratio, were chosen to investigate whether these changes would influence ensilication speed, particle morphology and size.

4.5 Results & Discussion

4.5.1 Initial data assessment

The morphology of native and released TTCF was obtained by using real-space inversion P(r)[224] function and Guinier[222] approximation. The acquired SAXS signal pattern between 0.006<q<0.51 Å^{-1} (ID02) and 0.008<q<0.35 Å^{-1} (i22) (figure 4-6, A) where R_g is calculated via slope analysis at low q. The R_g (figure 4-6, D) obtained

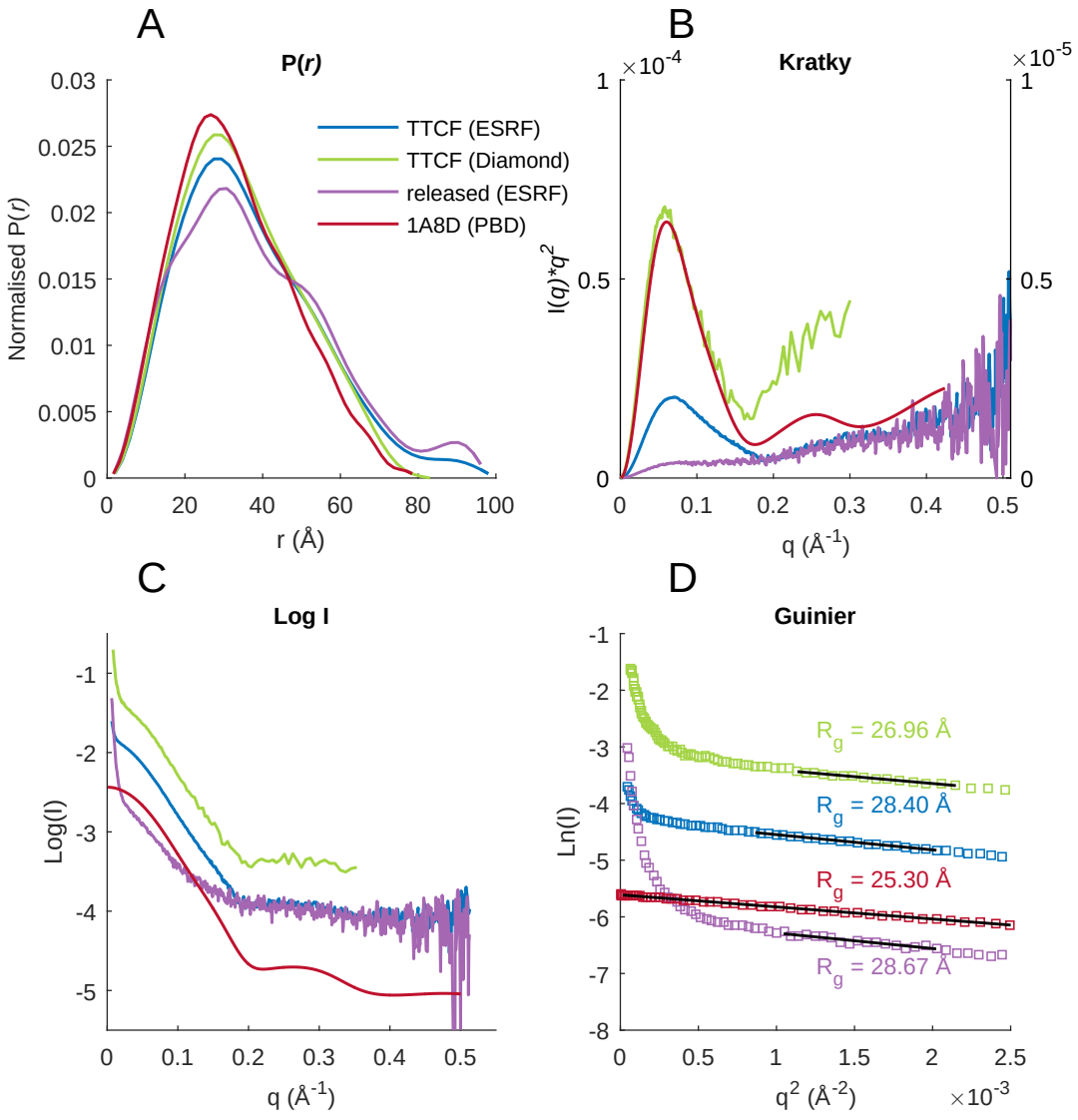

Figure 4-6: SAXS TTCF data p(r), Kratky, Log view and Guinier plot. (a) Real-space function displaying probability of radii (b) Kratky plot displaying intrinsic flexibility for TTCF (c) Log view for SAXS data (d) Guinier analysis, slope fit and R_g values display similar sizes.

SAXS MW analysis	1A8D	Native (ESRF)	Native (Diamond)	Released (ESRF)
Sequence weight (kDa):	52.22036	53.5455	53.5455	53.5455
Found molecular weight: (kDa)	45.594	48.598	41.918	39.014
Discrepancy (%):	14.53	10.18	27.74	37.25
Oligomeric state:	monomer	monomer	monomer	monomer

Table 4-1: Molecular weight analysis for TTCF scattering. Approximations using SAXS reveals monomeric protein species of TTCF in solution.

for native TTCF (ID02) is 28.40 Å, (i22) 26.96 and released TTCF is 28.67 Å. The observed sizes are in agreement with the homologous (96.7% sequence overlap) published crystal structure of TTCF (PDB: 1A8D[164,235,236]) with an R_g of 25.30 Å. This is obtained via simulated SAXS scattering of the crystal model and confirms the P (r) function derived shape of an ellipsoidal particle (figure 4-6, A). Differences in scattering intensity observed are either due to environmental differences (beamline setup) or concentration variations. Observed r ($Å^{-1}$) reveals consistency in particle radius at 30 Å. However, at higher size there are interparticle effects or polydispersity influences visible. It is also apparent that the protein does not present a Gaussian distribution and the Kratky plot (figure 4-6, B) reveals intrinsic flexibility. The lower signal for released protein in the Kratky plot is due to the reduced concentration after release (figure 4-6, C). Additionally, the signal is affected by the presence of (soluble) silica particulates in solution. However, our published study gives detailed analysis of protein after release, described in the next Chapter[227]. Molecular weight analysis of TTCF SAXS scattering[237] revealed monomeric states (table 4-1) and agreed with the linearity of the Guinier approximation with the integration limit defined as: $q_m = \frac{8}{R_g}$.

4.5.2 Native TTCF

Native TTCF at 1 mg/ml in Tris pH 7 buffer was measured at both (i22 & ID02) beamlines. Fitting was done using an ellipsoidal model[226] with power law added (figure 4-7). Calculations were done using the sum of:

$$I(q) = scale \cdot q^{-power} + P(q,\alpha)(\frac{scale}{V}F^2(q,\alpha)) + background \tag{4.6}$$

The ellipsoidal form factor includes the Fourier transform:

$$F(q,\alpha) = \frac{3\Delta\rho V(\sin[qr(R_p,R_e,\alpha)] - \cos[qr(R_p,R_e,\alpha)])}{[qr(R_p,R_e,\alpha)]^3} \tag{4.7}$$

where R_p: polar radius, R_e: equatorial radius, $\Delta\rho$: scattering length density (SLD) difference between particle and solvent, α: axis angle, V: ellipsoid volume;

$$V = (4/3)\pi R_p R_e^2 \tag{4.8}$$

The ellipsoid volume is calculated via multiplication of the polar R_p and equatorial radius R_e.

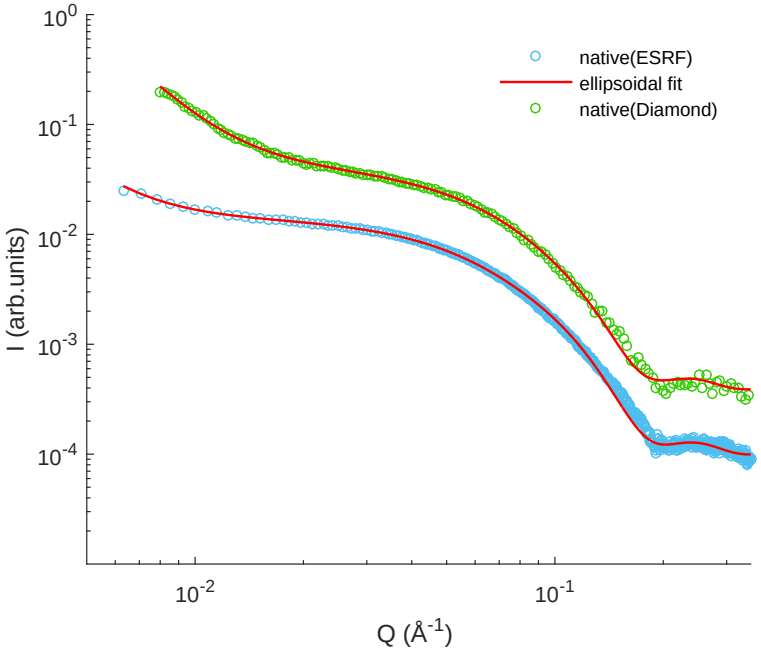

Figure 4-7: SAXS of native TTCF in 50 mM Tris pH 7.0 at Diamond and ESRF. Fitting carried out using an ellipsoidal model with power law added.

Parameters	TTCF (ESRF)	TTCF (Diamond)
scale	$13.10e^{-5}$	$42.12e^{-5}$
background	$9.50e^{-5}$	$3.30e^{-4}$
scattering length density (protein)	12.47	12.47
scattering length density (solvent)	9.44	9.44
radius (polar) Å	61.24 ± 0.11	57.68 ± 0.37
radius (equatorial) Å	21.54 ± 0.02	21.85 ± 0.06

Table 4-2: SAXS TTCF native fit parameters. Scale used as multiplication factor for fitting. Background represents residual scattering near zero. SLD accounts for component scattering. Polar and equatorial radii provide structural information about the ellipsoidal particle.

The scattering length density (SLD) for TTCF was calculated using the molecular density (1.37 g/ml) and its formula which provided an SLD of 12.4681 x 10^{-6} Å^2. The fit provides structural information about the length of the polar and equatorial radii (table 4-2). Comparison of both reveal non significant differences between native TTCF measured independently at both beamlines.

4.5.3 TTCF ensilication 1:50

Ensilication of TTCF *in situ* was measured at Diamond. The pump flow system circulated TTCF and, after 3 seconds, hydrolysed TEOS was added. Initial protein scattering was measured after which the ensilication measurement was started. Frames were taken each second up to 120 seconds. After which frames were taken every 15 seconds, 5 frames in 5 seconds up to a total time of 900 seconds. The subtracted SAXS scattering is displayed in figure 4-8. Observed is the jump in scattering at high-q after silica has been injected into the loop. This increase in scattering continues with the protein apex shifting towards the lower q-range, suggesting particle growth. At high q, silica particle scattering is increasing over time. The bump at low-q disappears over time and reduces to a broad peak.
Ensilication of TTCF *ex situ*, where hydrolysed TEOS was added to a solution of buffer TTCF before measurement, disabled observation of onset ensilication. However, it allowed monitoring of longer evolution (figure 4-9). Observed was the same broad peak and silica scattering seen in the Diamond data. The signal evolved to a smooth surface due to the extension of the high-q signal towards the low q region. Good residual fits were found using a combination of power law, ellipsoid, broad peak

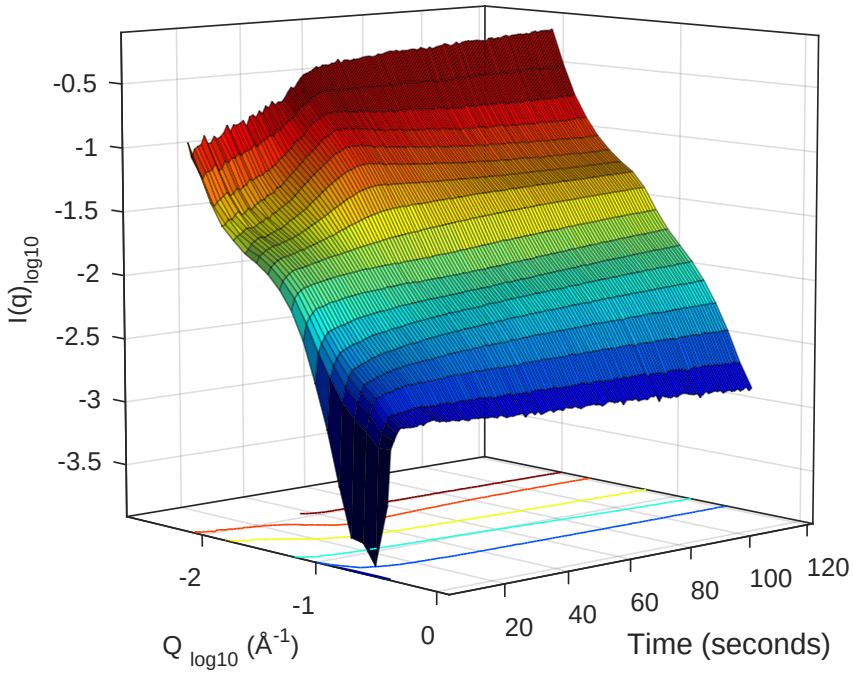

Figure 4-8: SAXS 3D perspective *in situ* ensilication of TTCF. Continuous measurement of the ensilication onset and up to 120 seconds after. Various transitions can be observed. Particle growth and broad peak formation are key identifiers in this process.

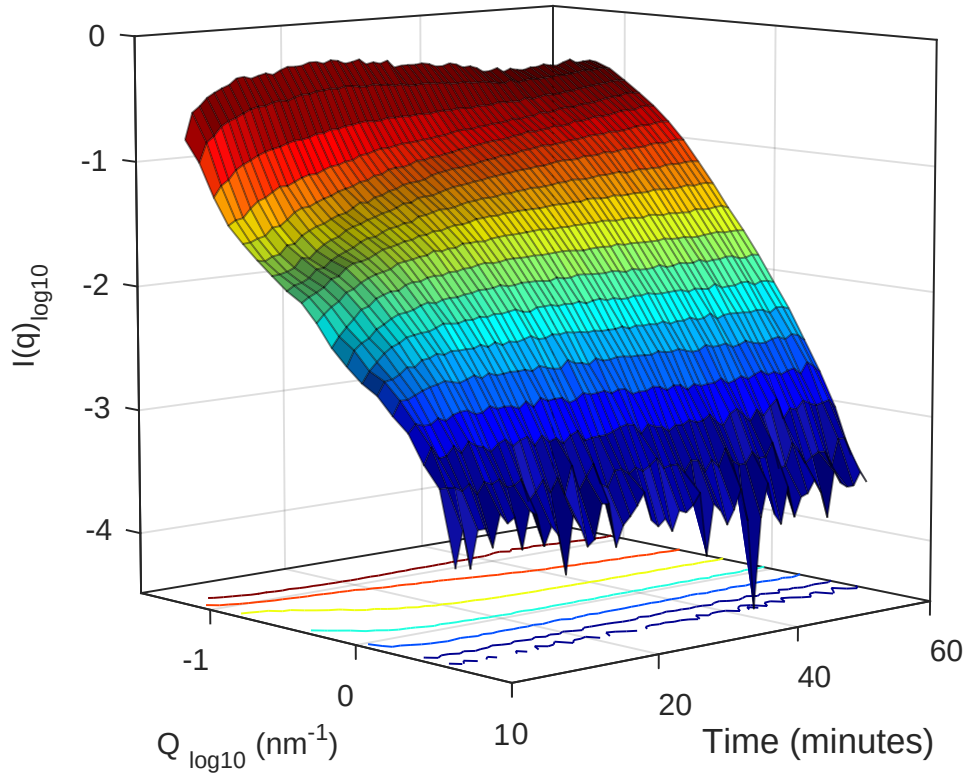

Figure 4-9: 3D perspective *in situ* ensilication of TTCF (ID02). SAXS of TTCF ensilication with a longer duration of time. Fractal growth is indicated by the extension from high to low q over time.

and mass fractal models for TTCF ensilication. The fractal model is of interest as it describes the attachment of colloidal particles (silica species) to protein/ each other. It provides a fractal dimension, D_f, which is dependent on the ability of particles to aggregate/ stick and is a function of the spatial dimension. This value is of importance as it will suggest what type of reaction is occurring during ensilication[238].
Fractals are defined as a geometric structure consisting of many individual units that possess the same geometrical shape[239]. There are many examples of fractals found in nature with trees being prominent.

4.5.3.1 Modelling of ensilication

Modelling of ensilication during onset and longer evolution involved the use of mathematical models that represented several structures present in the solution during ensilication. The models have their own parameters and were combined to find an agreeable complete fit of the SAXS scattering recorded. The models have been designated model parameter keys, P, relating to SASview output tables A.2, A.3, A.4 and A.5 described in the Appendix.

Stage I

i22, *in situ* 0 - 60 seconds X-ray scattering measured *in situ* after addition of silica, and up to 60 seconds, was fitted with several models combined into one. Combination of these respective models, visualised below (figure 4-10) , indicated a reasonable fit with a χ^2 below 10. The power law model was intended to indicate any large surfaces or instrumental scattering. The ellipsoidal model was used to display the protein as a particle, where a fractal structure of the silica polymerising and attaching to the protein is represented with a fractal model[225].

(P1) power law + (P2) ellipsoid + (P3) mass fractal (**stage I**)

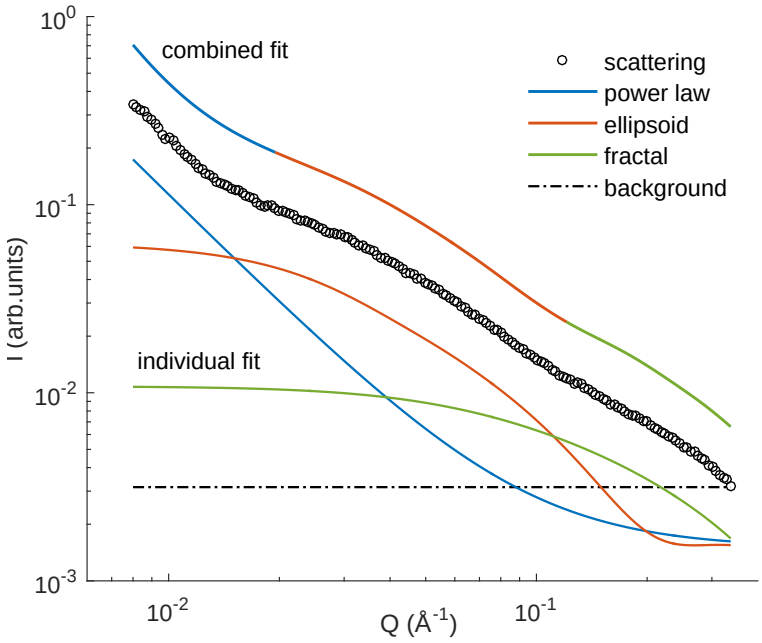

Figure 4-10: Stage I fit model applied to scattering data. Individual fits highlight regions of interest while the combined fit is used to follow transitions during the *in situ* measurement.

$$I(q) = scale \cdot q^{-power} + P(q,\alpha) = \left(\frac{scale}{V} F^2(q,\alpha)\right) + scale \cdot P(q)S(q) + background$$

where: $P(q) = F(qR)^2$ and $S(q) = \frac{(\Gamma(D_m-1)\zeta^{(}D_m^{-}1))}{[1+(q\zeta)^2]^{(Dm-1)/2}} \cdot \frac{(\sin[(D_m-1)\tan^{-1}(q\zeta)])}{q}$

with R: radius building block, D_m: fractal dimension, ζ(zeta): cut-off length. Where:

$$F(q,\alpha) = \frac{3\Delta\rho V(\sin[qr(R_p,R_e,\alpha)] - \cos[qr(R_p,R_e,\alpha)])}{[qr(R_p,R_e,\alpha)]^3} \tag{4.9}$$

with R_p: polar radius, R_e: equatorial radius, $\Delta\rho$: scattering length density (SLD) difference between particle and solvent, α: axis angle, V: ellipsoid volume;

$$V = (4/3)\pi R_p R_e^2 \tag{4.10}$$

Stage II

i22, *in situ* 60 - 120 seconds After 60 seconds, during the ensilication, scattering underwent a transition. This change required a new approach to fit these data (figure 4-11). The broad peak model was utilised because the data presented a broad peak. The model represents scattering of various structures, in this case protein and silica, at a specific size in the q range. It also included a Porod exponent, therefore making the power law model redundant. The fractal portion of scattering remained.

(P1) broad peak + (P2) mass fractal (**stage II**)

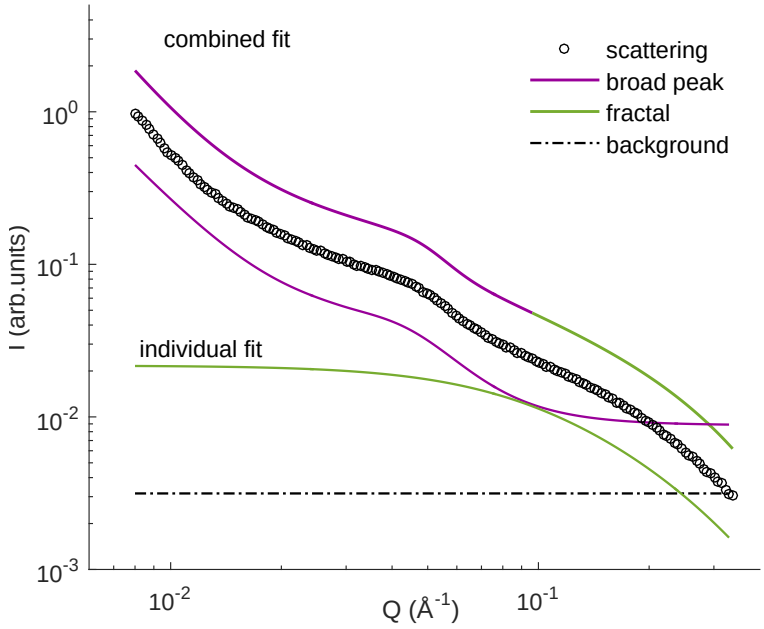

Figure 4-11: Stage II fit model applied to scattering data. Individual fits highlight regions of interest while the combined fit is used to follow transitions during the *in situ* measurement.

$$I(q) = \frac{A}{q^n} + \frac{C}{1+(|q-q_0|\zeta)^m} + scale \cdot P2(q)S2(q) + background$$

Where: A: Porod law scale factor, n: the Porod exponent, C: Lorentzian scale factor, m the exponent of q, ζ: the screening length.

Stage III

ID02 *in situ, ex situ* initiation, 2 - 60 mins The scattering measured over longer duration of time initially displayed the same scattering fitted with the broad peak and mass fractal combined fit. After several minutes, this signal changed and a new model was required to address this transition (figure 4-12). Observed was the broad peak reduction and increase in mass fractal scattering. Therefore, the power law model and mass fractal were combined which obtained a good fit.

(P1) broad peak + P2) mass fractal (stage II) (same as before)

(P1) power law + (P2) mass fractal (**stage III**)

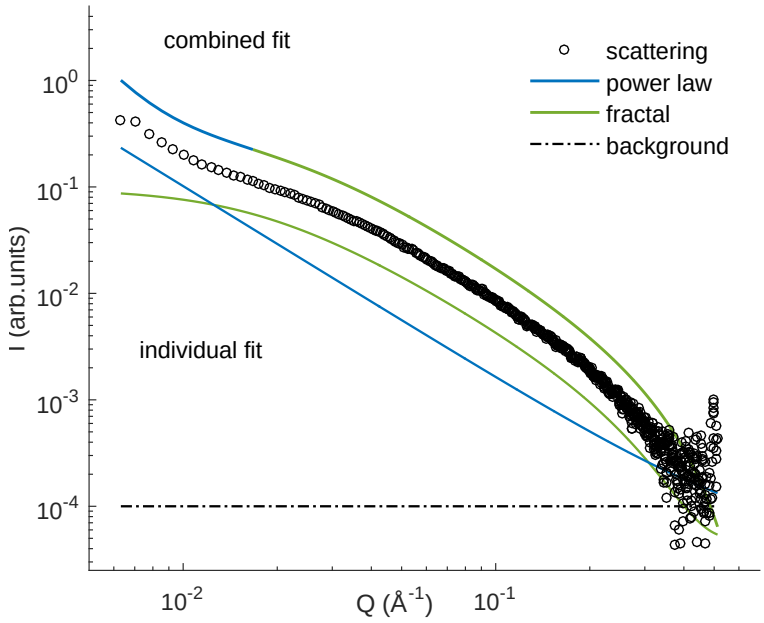

Figure 4-12: Stage III fit model applied to scattering data. Individual fits highlight regions of interest while the combined fit is used to follow transitions during the *in situ* measurement.

$$I(q) = scale \cdot q^{-power} + scale \cdot P2(q)S2(q) + background$$

Note that each model and combined models in SASview have a scalar and background value. These are accounted for when fitting 1D SAXS data.

4.5.3.2 Parameter output of SAXS fitting

Fitting of (1:50) ensilication scattering was done using three mathematical models that indicated various stages during TTCF ensilication. The fittings were based on biomolecular SAXS and silica scattering derived from sol-gel chemistry[139]. Combined, they provided a good fit for this process. This is displayed below (figure 4-13) where the three stages are clearly indicated. The red fit has been described earlier for native TTCF (section 4.5.2). After silica is added to the buffer with protein, a clear shift is seen at high q[240]. This then follows with the apex of the protein signal moving

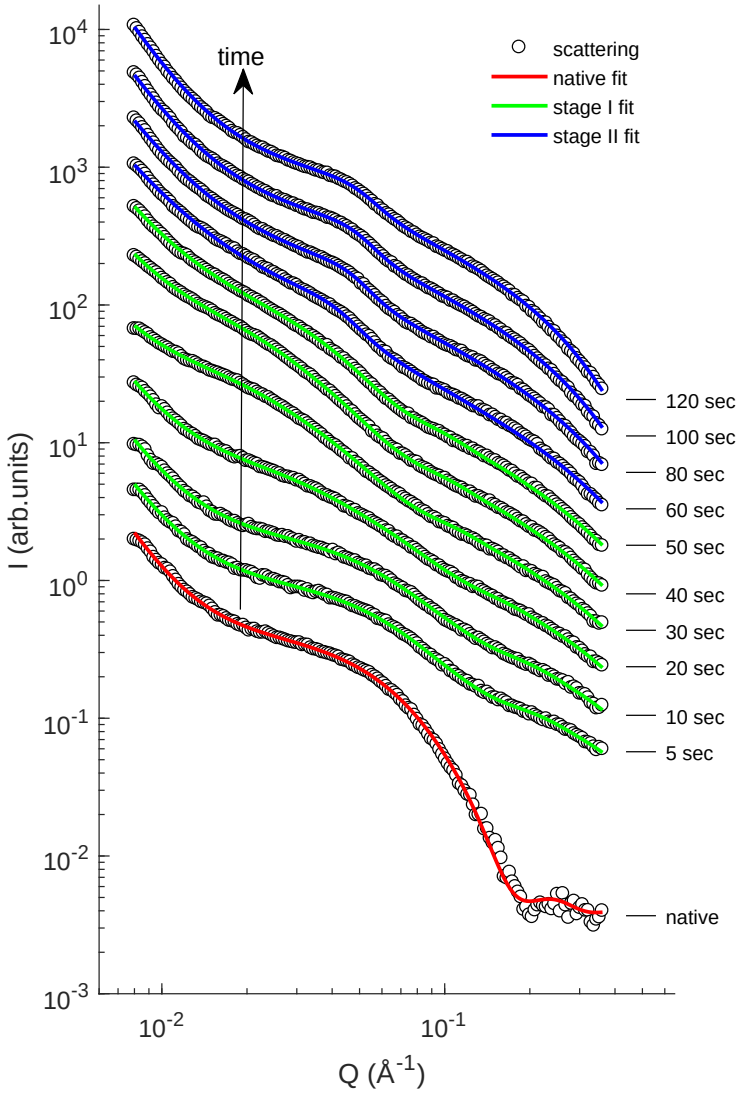

Figure 4-13: Scaled TTCF *in situ* TTCF SAXS data. Sliced SAXS data for clarity with fits based on three staged models to depict transitions occurring during ensilication. Red displays the native fit for TTCF. Green (stage I) and blue (stage II).

towards low-q and a broad peak appearing shortly after. This is also found in the ESRF data (figure 4-14) and this suggests that the silica grows to a larger structure. The parameters used in these fits were derived from native modelling and literature values[241]. If there were multiple backgrounds within the formula, only one would be set. This also applied to the scaling factor for each individual function because of the shift in intensity and transitions occurring. Only the power law and ellipsoidal model were allowed to have an implicit scale factor, where the fractal and overall scale factor were ignored and fixed in place. These changes were necessary for the fitting

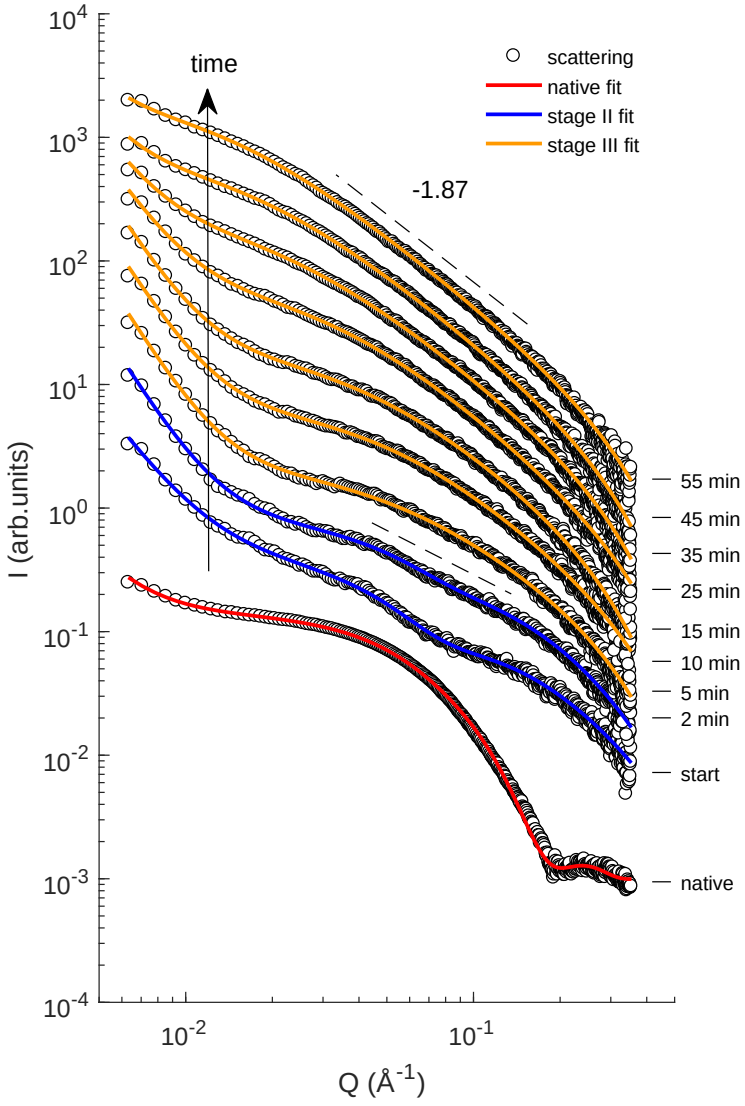

Figure 4-14: Scaled TTCF *in situ* TTCF SAXS data. Sliced data for clarity with fits based on three staged models to depict transitions occurring during ensilication. Red displays the native fit for TTCF. Blue (stage II) and orange (stage II).

algorithm to calculate variables that would be in align with real-world observations. Limitations on sizes of radii and fractal particles were also based on this approach. For more detail see the Appendix A.2. Outputs of all the fittings were gathered and the most prominent parameters visualised (figure 4-15). Some interesting transitions were taking place rapidly during the 1:50 ensilication. Important parameters in fitting were the polar and equatorial radii, the cut-off length, fractal dimension and χ^2 good-

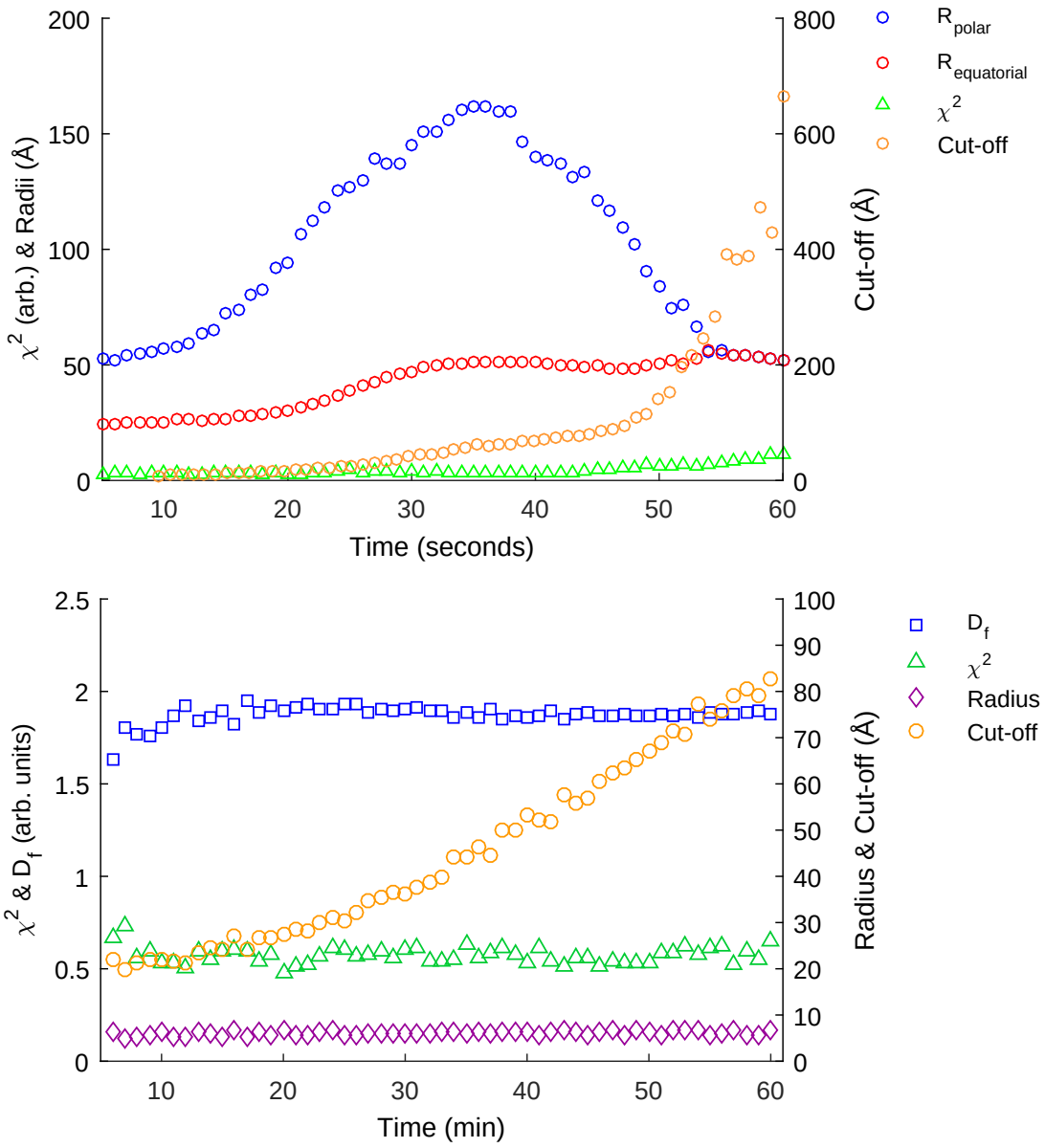

Figure 4-15: Parameter output for SAXS fits. (top) Data for the flow *in situ* measurement. Radial parameters show the growth of TTCF-silica nanoparticles. Cut-off length is the polymer attaching to the protein. (bottom) Data for the longer evolution of ensilication. Important parameters, D_f, cut-off and radius (Å) show the growth of a larger fractal structure.

ness of fit (gof). The first two parameters describe the protein particle sizes. Cut-off length describes the static silica polymer accumulations and the fractal size. Fractal dimension indicates the type of process taking place with gof being approximately 1. The gof supports representation of the fitting to the actual process taking place. The better the fit, the more likely the data visualises real events. From the visualisation of parameter output it was apparent that the polar radius of the ellipsoidal protein particle increases dramatically over a short period. The equatorial radius seemed to increase as well but remained static after 30 seconds. The cut-off length which rapidly increased in size, suggests the adhesion of silica polymer to the protein. The radius of fractal particles remains static (figure 4-15, bottom) and is in line with the fractal dimension (1.87) that indicates diffusion-limited (controlled) cluster aggregation (DLCA)[139,238,242,243]. The cut-off length is the minimum resolvable fractal size measured using the fit model.

The DLCA process describes the aggregation of colloidal particles in solution[243], i.e. silica species large enough for electrostatic attachment to the protein. Once a cluster is formed, growth occurs by other particles attaching to the external branches of this entity. Diffusion is the rate-limiting step in this scenario and can be influenced via temperature or viscosity. Agitation has an effect on the maximum size of large fractal structures of protein and silica. The force created by the solute movement will be greater once the fractal particles accumulate and invariably shear. With the absence of agitation, sedimentation was observed.

4.5.3.3 Convolution of SAXS ensilication data

There are visible differences in scattering between agitated and non-agitated sample that suggest this reaction to be diffusion controlled (figure A-1, Appendix A.6). Fitting revealed three stages during ensilication (figure 4-16):

Stage I: Formation and growth of low q particle radii initiated at the onset of ensilication (figure 4-8, A, until 40 sec). Here, ensilication is observed via the increase in ellipsoidal radii (polar, equatorial) over time, indicating silica forming around the protein.

Stage II: Broad amorphous peak formation due to aggregation of silica.

Stage III: Fractal growth of silica particles associated with aggregation which relates to increase in fractal dimension and cut-off length (figure 4-13, A). This is confirmed by the mass fractal dimension (D_f) during the longer evolution (figure 4-14, B) which provides an increase to D_f = 1.87 and has been shown to be indicative of fast silica growth and defines the mechanism of ensilication as a diffusion limited cluster aggregation (DLCA) type process[139,238,242,243].

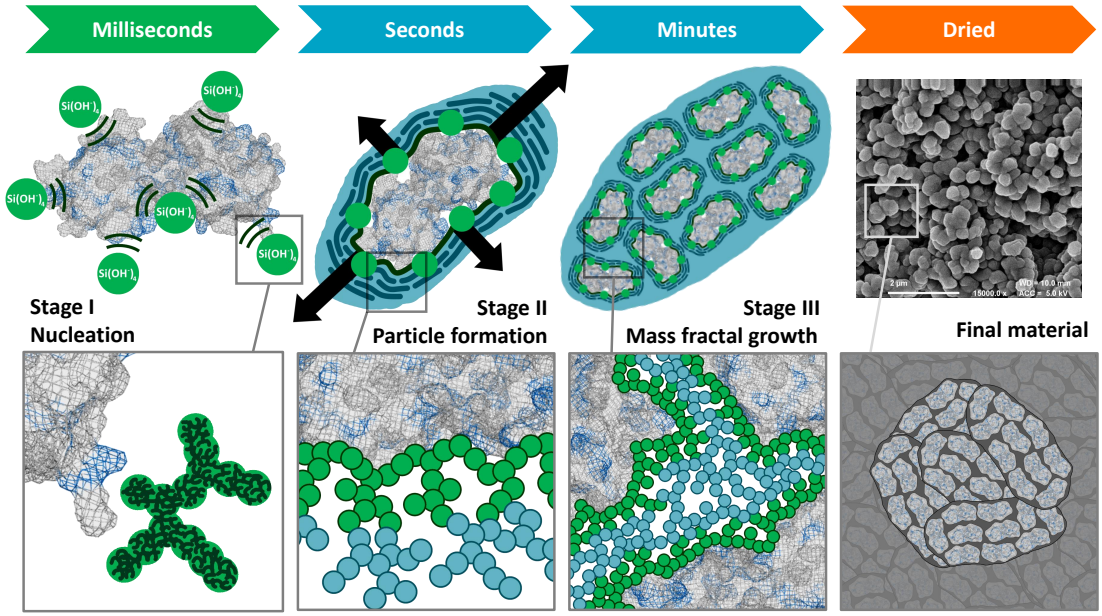

Figure 4-16: Graphical representation of TTCF ensilication. Nucleation, induced via electrostatics, initiates ensilication at positive external residues (lysine, arginine, blue) present on the protein. Poly-condensation of $SiOH_4$ results in silica coating of individual proteins (stage I, green) which triggers aggregation (stage II, blue). Vacuum filtration of the then turbid solution results in dried powder material containing protein loaded silica nanoparticles (FE-SEM at 15,000x magnification).

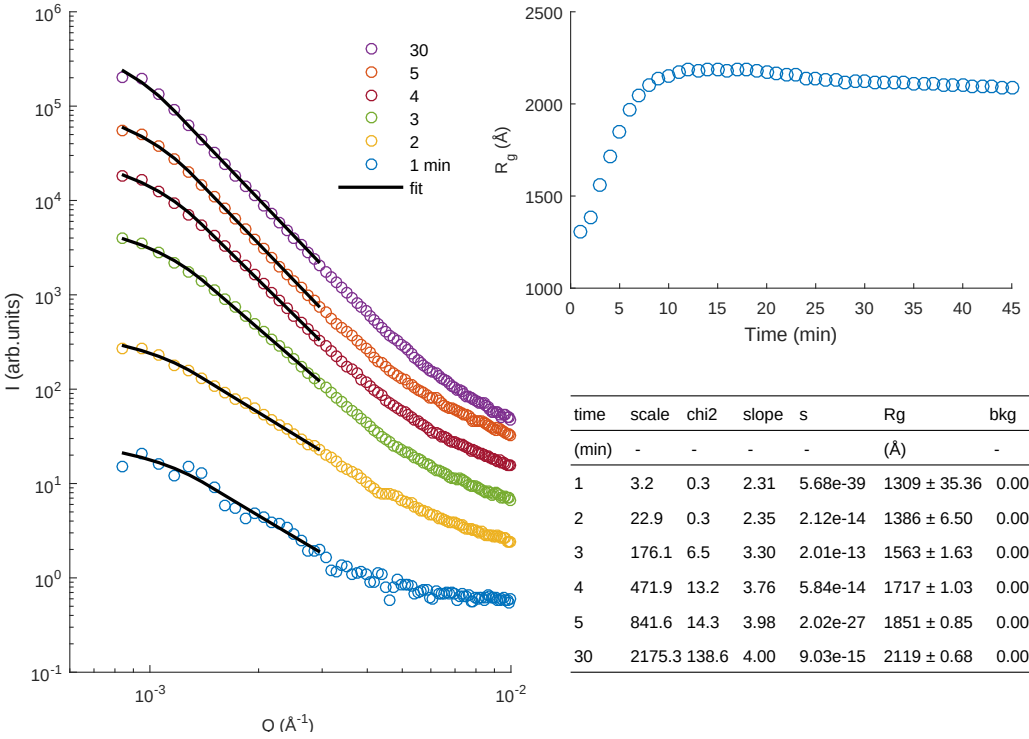

time	scale	chi2	slope	s	Rg	bkg
(min)	-	-	-	-	(Å)	-
1	3.2	0.3	2.31	5.68e-39	1309 ± 35.36	0.005
2	22.9	0.3	2.35	2.12e-14	1386 ± 6.50	0.005
3	176.1	6.5	3.30	2.01e-13	1563 ± 1.63	0.005
4	471.9	13.2	3.76	5.84e-14	1717 ± 1.03	0.005
5	841.6	14.3	3.98	2.02e-27	1851 ± 0.85	0.005
30	2175.3	138.6	4.00	9.03e-15	2119 ± 0.68	0.005

Figure 4-17: ultra-SAXS supplementary data supporting the graphical representation. Guinier-Porod slope and R_g analysis show the formation of large: nano-particles short after initiation of ensilication process.

The findings are further supported by SAXS carried out a lower q-range (0.0008 to 0.05 Å^{-1}) displaying large particle formation after silica addition (figure 4-17). Particle sizes increasing to a stable range of 2000 - 2200 Å (200-220 nm) are observed. These data suggest that once TTCF is coated with silica, it is prone to aggregate and form a stable complex. FE-SEM imaging of the final dried material confirms these sizes (figure 4-16). Overall, the SAXS data elucidated the ensilication mechanism by providing evidence of a fast DLCA process where, once TTCF is coated, on average 2000 Å aggregates of protein-silica particles will form.

4.5.4 TTCF ensilication 1:20 and 1:100

SAXS experiments on different ratios of silica were intended to provide more evidence on the influence of these conditions during ensilication. The expected observations were based on difference in rates of ensilication. From earlier experiments, it was shown that more silica increased the polymerisation and therefore speeds up ensilication. When there is less silica, it takes more times for the polymer fragments to find each other and connect.

Looking at the time-resolved scattering data (figure 4-18), there is a smoother interface to be seen in the higher silica ratio experiment. The opposite is the case when using a significantly lower ratio of silica. There is a broad peak formation and some increase in scattering at low q. However, the transitions were slow and there was not much visually occurring. Buffer with added silica did turn turbid, however the process was relatively slower than 1:50. After observing SAXS data of the 1:20 run, the stage III (power law + mass fractal, figure 4-20, a) fit was applied to this higher silica ratio. A similar trend comparable to the 1:50 data was observed. The fractal dimension and cut-off length seem to behave similarly (figure 4-21). The sample-to-silica ratio here evidently presented the rapid evolution of the ensilication process. It

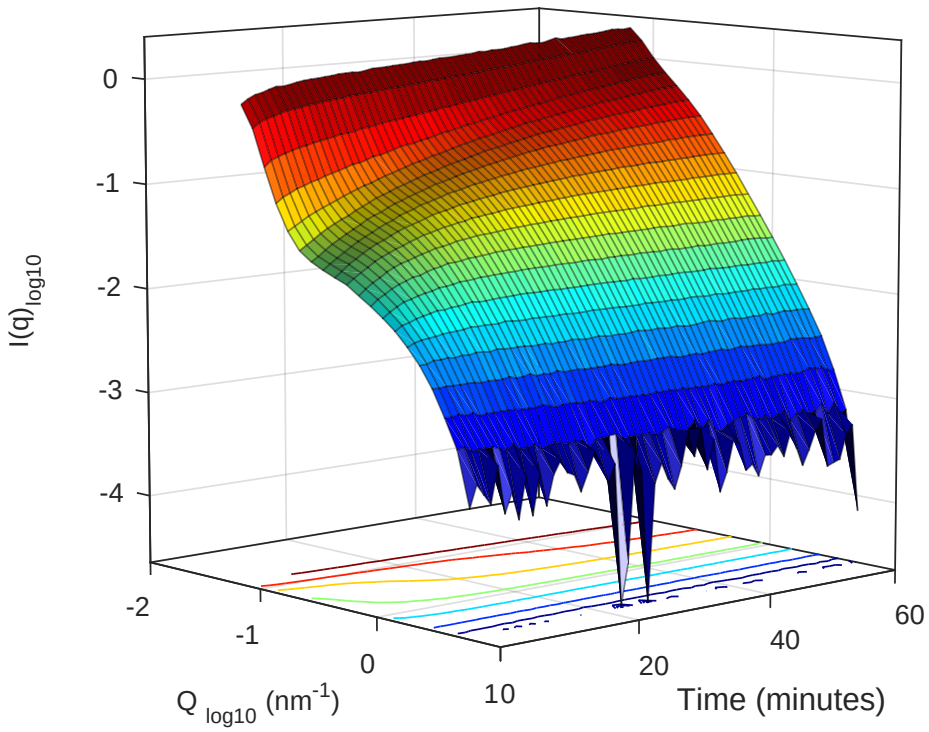

Figure 4-18: SAXS of TTCF ensilication experiment at 1:20 ratio. Observed is the smooth transition with a fractal structure growing at low q.

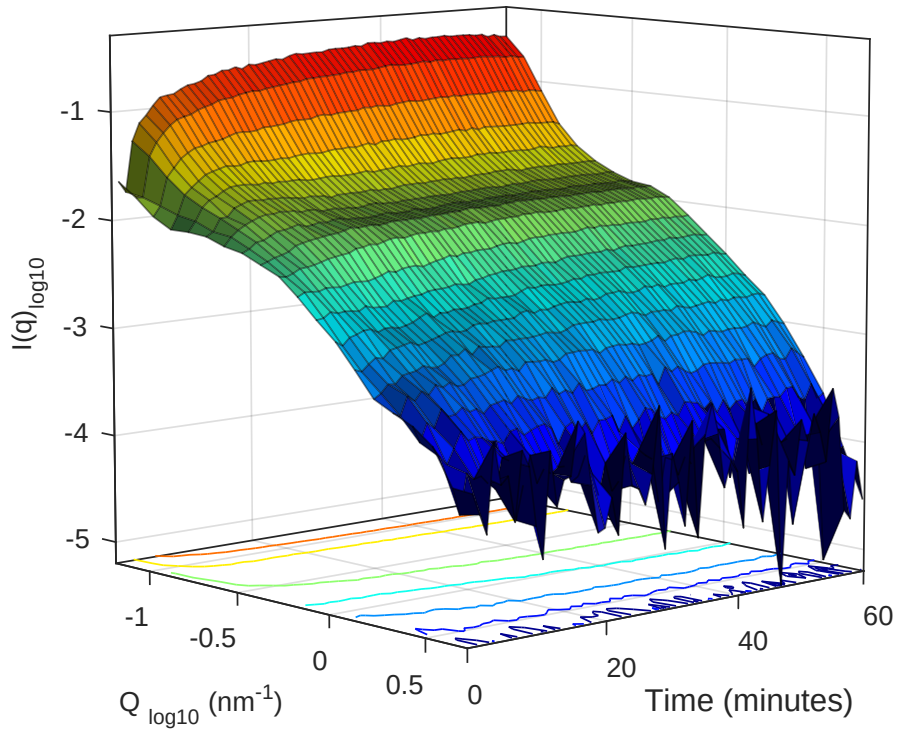

Figure 4-19: SAXS of TTCF ensilication experiment at 1:100 ratio. Observed is the slow transition with a fractal structure growing at high q and broad peak forming.

was not possible to capture any of the first two stages. The reaction here proceeded directly to the final stage (III) once the measurement was started. For the 1:100 ratio, the opposite is the case (figure 4-19). Here, there is a slow transition (after 10 minutes) from the first stage of the ensilication process towards the second stage. This is supported by the overall good fit (χ^2) for the models at each stage (figure 4-20, B). The parameter output showed a similar trend to the 1:50 data in the first two stages. The increase in polar and equatorial radii, the subsequent dip in these radii and the following formation of an amorphous broad peak (Lorentz length, figure 4-22) are identical to the transitions occurring in the 1:50 ratio (figure 4-15). There is a difference in fractal dimension. However, after experimenting with different values for the D_f there was no significant change in any of the associated parameters. Both fit models have good agreement on the radius of fractal building blocks at 10 Å. Overall, the SAXS experiments on adjusting the ratio of hydrolysed TEOS:protein show an increase of the ensilication speed at higher amounts of silica added. When lower amounts are used the opposite is seen with both experiments at neutral pH.

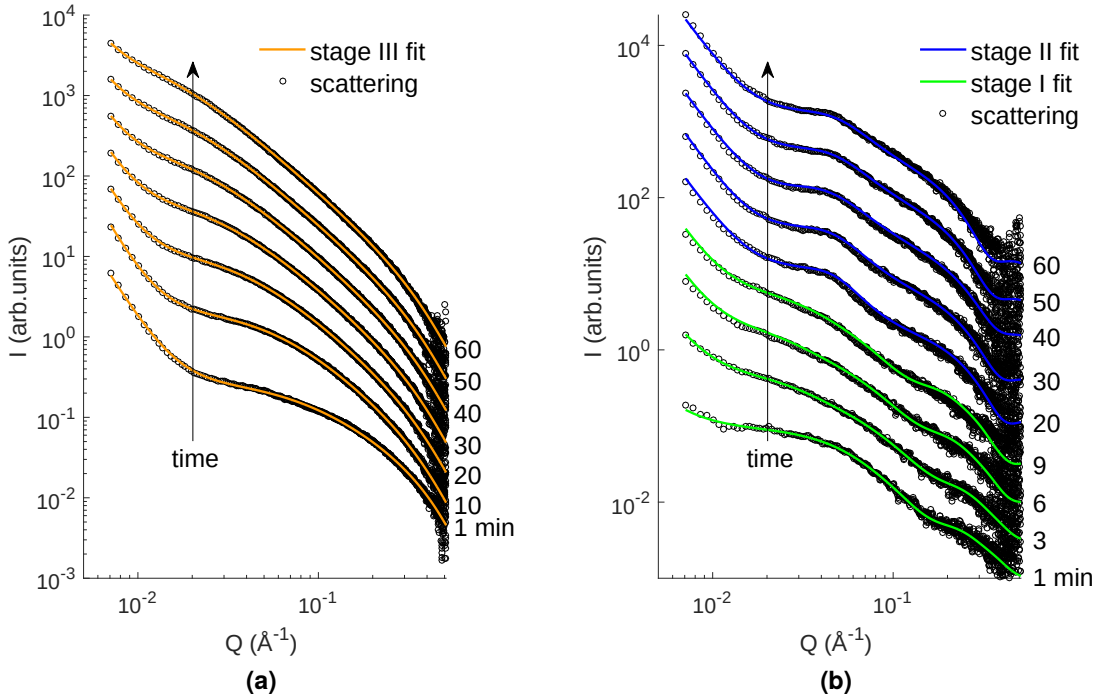

Figure 4-20: SAXS scattering with model fits for 1:20 and 1:100 data. (a) stage III fit for the fast ensilication at 1:20. (b) stage I and II fits for the slower progression of ensilication at 1:100.

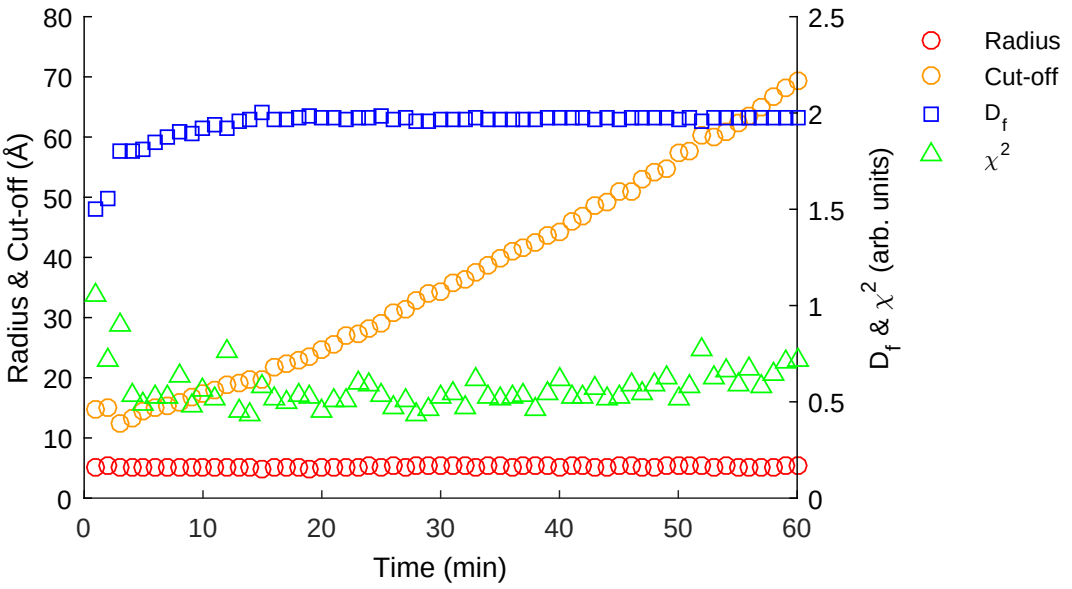

Figure 4-21: Parameter output for SAXS fitting of 1:20. Stage III fit shows a similar trend in output compared to 1:50 ensilication

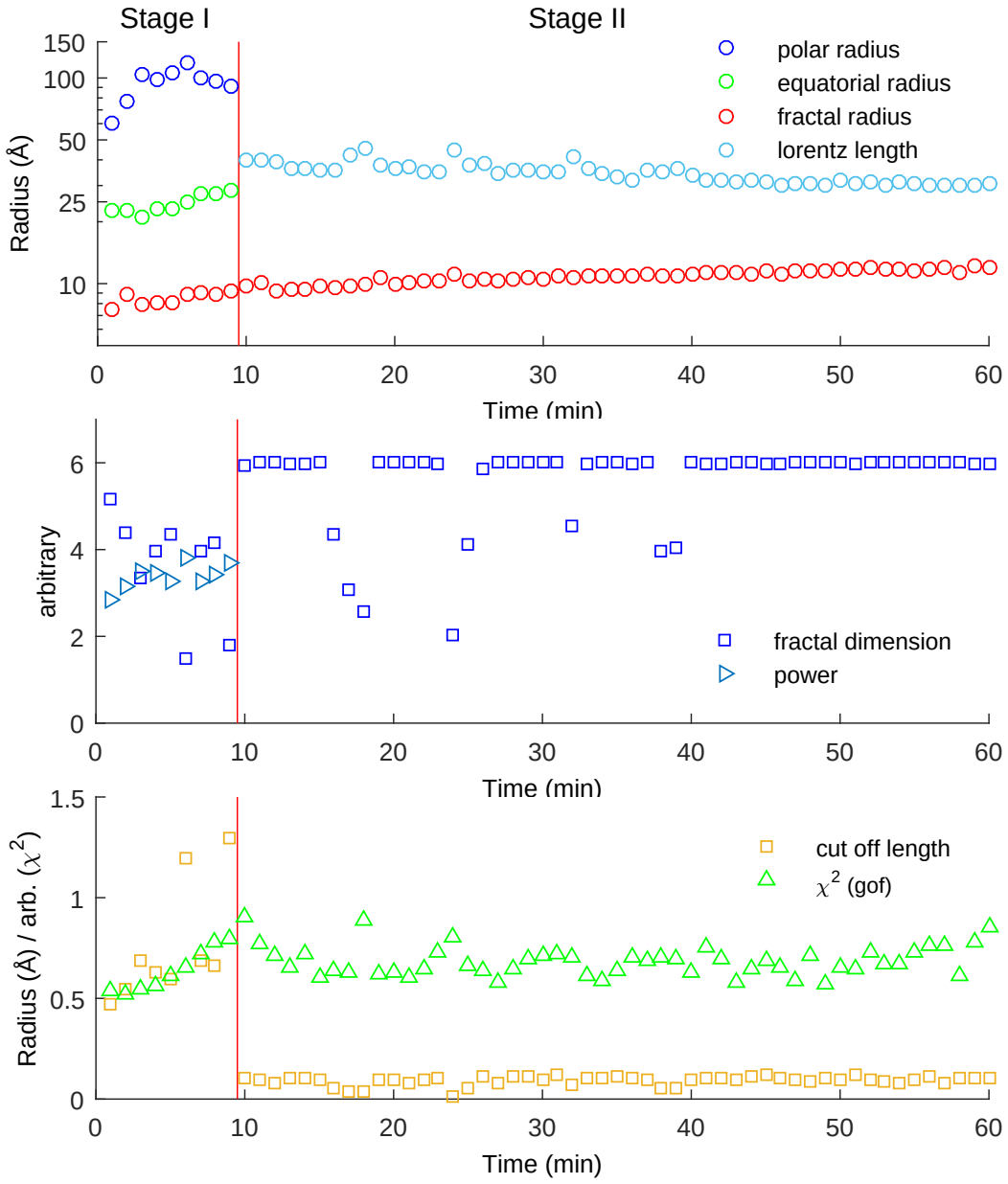

Figure 4-22: Parameter output for SAXS fitting of 1:100. Stage I & II fit shows a similar trend in output compared to 1:50 ensilication. (top) Output radii of the fit models for polar, equatorial, fractal building blocks and amorphous peak Lorentz length. (bottom left) cut-off length and χ^2 goodness-of-fit. (bottom right) Output fractal dimension and power (Porod) slope.

4.5.4.1 DLS of TTCF ensilication at 1:100

Ensilication was additionally monitored using DLS. The results show similarities with the SAXS data, however there is increased variability. During the measurements, it was apparent that the ensilication occurred too rapidly for the DLS ZetaSizer to capture. Therefore, the reaction was initiated as it would be in normal conditions. After initiation the volume was increased tenfold to allow for greater resolution during measurements. The DLS output provided the mean intensity hydrodynamic diameter (d.nm). The Z-average was not used for comparison as this would be the average of all peaks and does not represent the data gathered. Experimental data from the ultra-SAXS experiments was used to compare against the DLS data (figure 4-23). It was found that there was a high level of polydispersity which prevents comparison to small range particles.

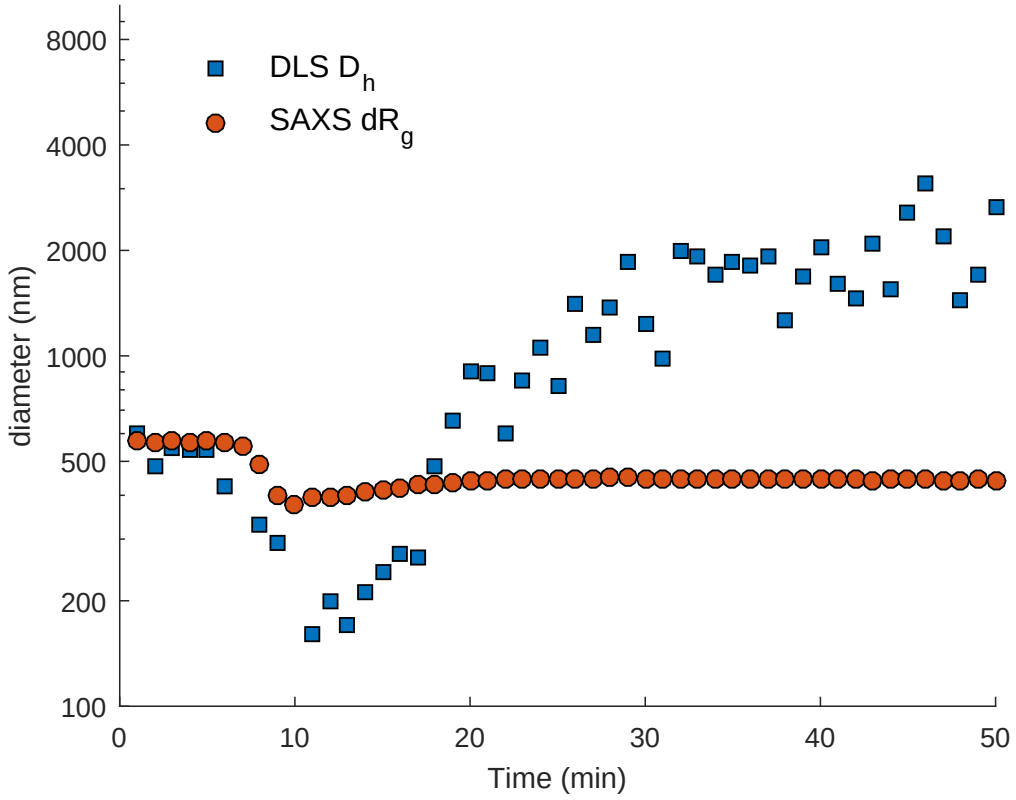

Figure 4-23: SAXS and DLS at 1:100 ratio. Scattering data using similar techniques with different wavelengths. DLS shows large aggregates forming. Particle sizes from SAXS were calculated directly from applying the Guinier function and display consistent values.

4.5.5 TTCF ensilication 1:100 ratio, pH 6 and 8

After establishing that varying ratios of silica influence the rate of ensilication, the following was to performed to examine the effect of pH. As 1:100 ratio significantly slowed the ensilication process, this was utilised to provide more resolution. This decision was based on the fast transition occurring during the 1:50 *in situ* flow experiment. From the time-resolved scattering, it is apparent that there are no obvious transitions happening (figure 4-24) at pH 6. However, there are two scattering populations visible at pH 8. The visualised data (figure 4-24 and 4-25) showed scattering for both data sets over time, 60 minutes pH 6 and 120 minutes at pH 8. For the latter, there is an increase in signal present during the initial moments of this run due to the introduction of silica to the system. These data were subsequently fitted with the stage I model (figure 4-26). The sliced view of the fitted data showed a transition during the first 10 minutes of ensilication after which the solution stabilised. The signal showed no transition towards the stage II or III as observed in the other experiments. This suggested that the particles that are formed are sta-

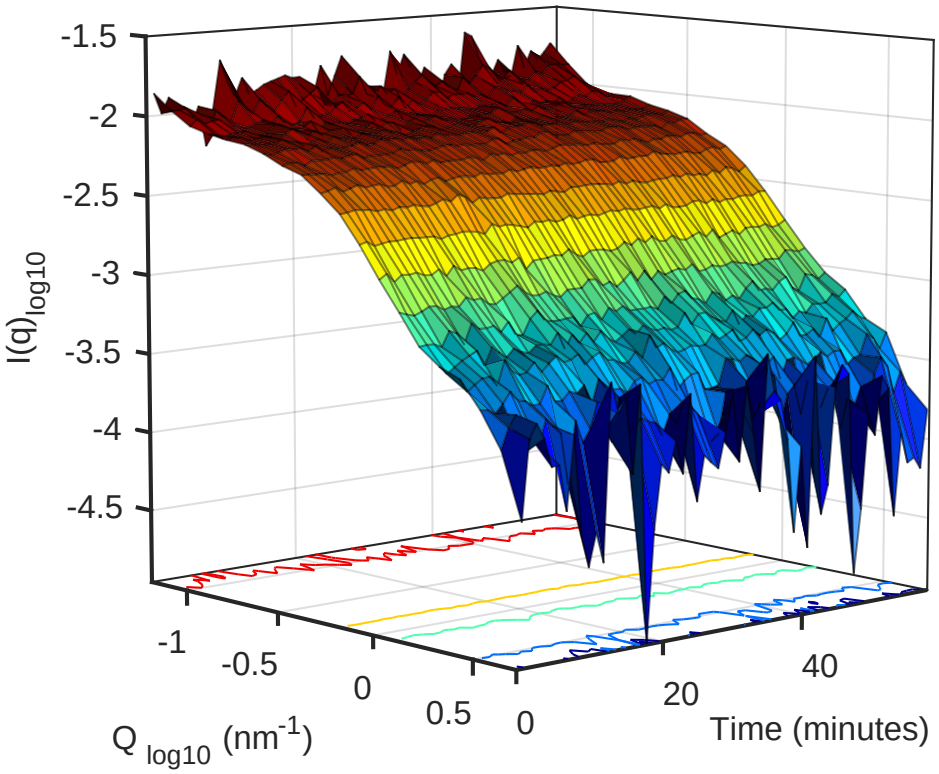

Figure 4-24: SAXS scattering of TTCF ensilication 1:100 at pH 6. 3D plot of intensity vs q over time. pH 6 scattering of TTCF ensilication does not present any transitions occurring over 60 minutes.

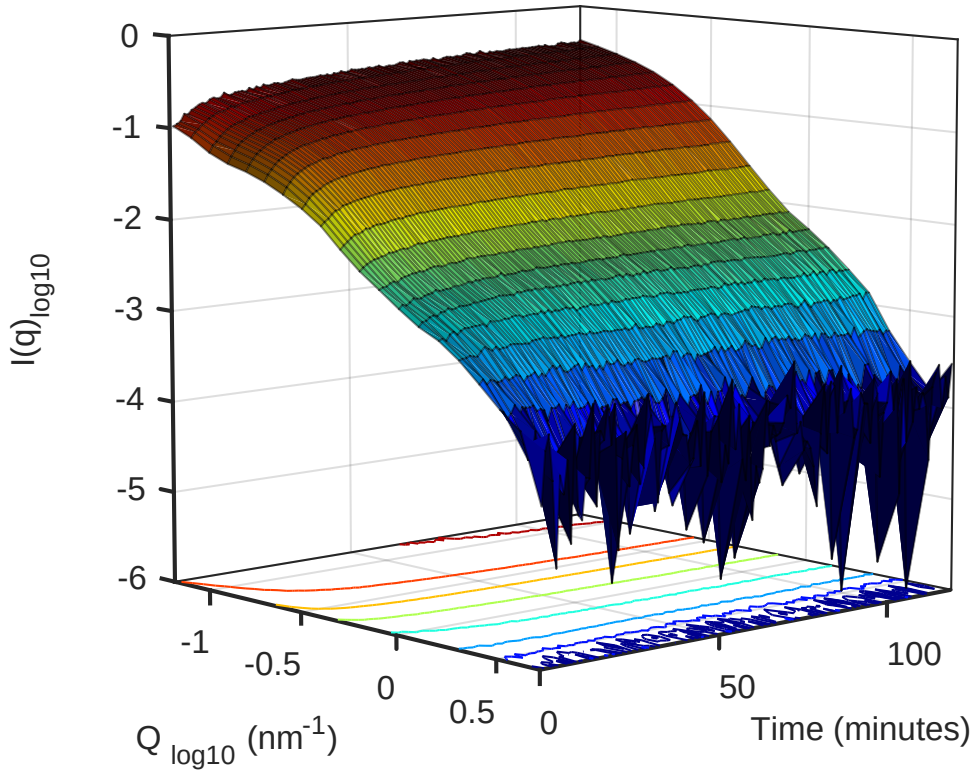

Figure 4-25: SAXS scattering of TTCF ensilication 1:100 at pH 8. 3D plot of intensity vs q over time. pH 8 scattering of TTCF ensilication does present a modest transition at early stages. There seem to be two populations of scattering present.

bilised in solution after adding the hydrolysed TEOS. This stabilisation occurs after 10 minutes. The fit model provides several outputted parameters which can help elucidate the effect of pH 8 on the ensilication of TTCF. The model distinguishes the two populations where the low-mid q population is an ellipsoidal particle, representing the growing TTCF ensilicated particle, and the high-q population is the fractal scattering caused by the polymeric silica particles. Parameters were calculated for the ensilication of TTCF 1:100 at pH 8. The radii for the ellipsoidal particle, polar and equatorial displayed an increase in size. Especially, the polar radius increased from 120 Å to 175 Å over time. The equatorial had a lower margin of growth, but was still visible. The radius associated with the building blocks of the fractal structure displayed growth, however the growth was only minimal. These parameters suggest that TTCF grows over its polar radius, similar to the 1:50 experiment. However, the signal of the particle does not disappear in the scattering signal and points towards the effect of pH. It was previously understood that once TTCF-silica particles reach a particular size, aggregation is initiated (section 4.5.3.3). However, this was not observed at pH 8. This absence of aggregation is also supported by the calculated

cut-off length for the polymer-protein particle (figure 4-27). The scattering has large fluctuations present during the initial stages but does settle over time with particles having an approximate length of 200-300 Å. This trend is also visible in the fractal dimension (D_f) as this parameter can identify the kind of polymerisation process occurring. With a D_f of 1.45 stabilising towards the end, this indicates a slow sol-gel process. Note that this solution turned visibly turbid, therefore confirming ensilication was taking place. It also does present particles large enough to refract visible light and make the solution cloudy, therefore there is some aggregation or gelation taking place. This experiment displayed the stabilisation of TTCF-silica particles at small sizes without the creation of large aggregates. The idea of individual stabilised TTCF-silica particles with a lower amount of silica is not only beneficial to increase surface area for release, it is also cost-effective. More attempts towards increasing

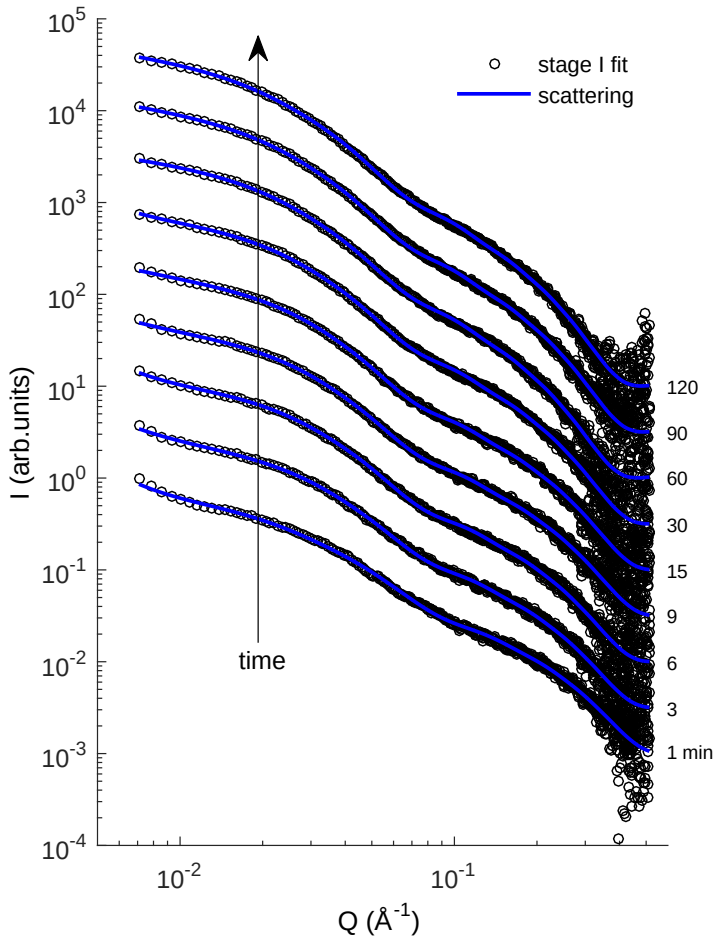

Figure 4-26: Stage I fitting of SAXS data for TTCF ensilication 1:100 ratio at pH 8. The first 10 minutes display modest transitions in scattering. After this period the signal stabilised as has a good fit with the fitting model. There are no transitions into stage II or III observed.

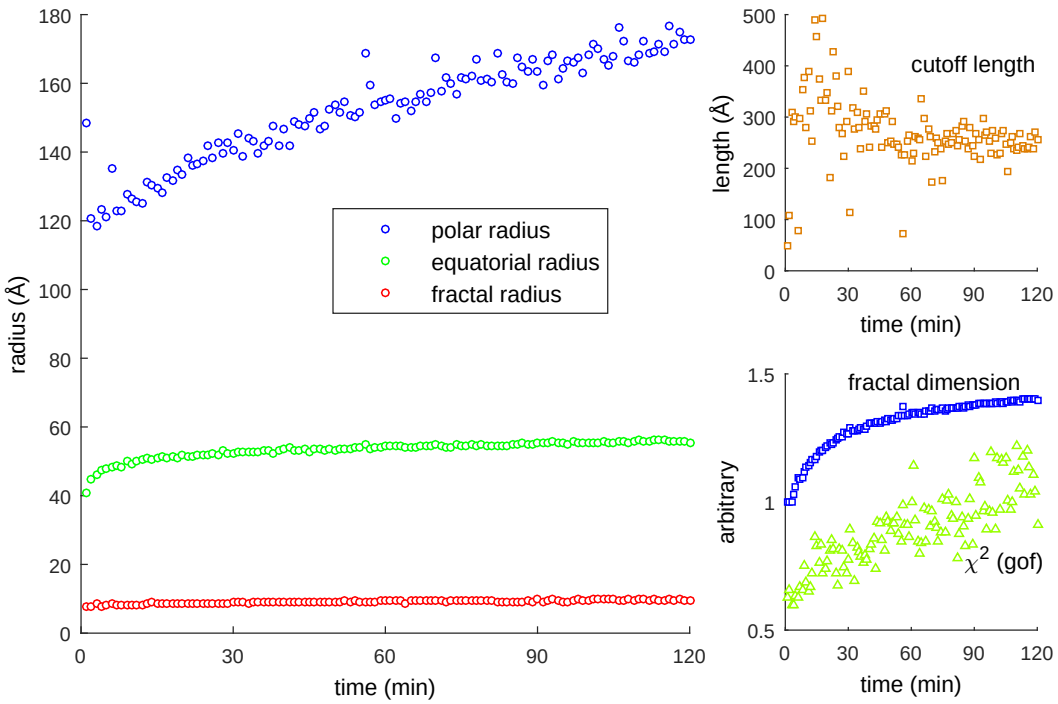

Figure 4-27: Parameter output of stage I fitting for SAXS scattering of TTCF ensilication 1:100 at pH 8. The parameters for ellipsoidal radii and the fractal radius display an increase in size. In particular, the polar radius displays the largest growth. Correlation length, of polymer and protein, stabilises over time. The fractal dimension displays an initial rapid increase and does also stabilise later on. The χ^2, gof, displays a good agreement between the experimental and fitted data.

the silica-protein ration can identify the minimum concentration necessary to ensilicate all proteins in solution and optimise the time needed for this. Fluctuating the pH does add a layer of additional control in a diffusion based system.

4.6 Summary

Small angle x-ray scattering is a powerful tool to find a representative image of processes occurring at nanometre scale[226]. The utilisation of high resolution beam-line x-ray scattering allows for greater in-depth analysis. The elastic scattering analysed in this setting was used to understand which events were occurring during ensilication[223]. Observation of scattering at various ratios and wave vectors provided understanding of the different phases of ensilication.

Initial assessment of protein scattering data provided the reference parameters. As a protein is technically a polymer (polypeptide) it could cause confusion in understanding as the silica here acts as a polymer[225]. Therefore, TTCF was modelled as an ellipsoid structure rather than a flexible object. Once TTCF was characterised using the p(r), Guinier, Kratky and Porod analysis the subsequent aim was to understand the transitions to the protein during ensilication. Based on previous evidence, the hypothesis was to observe particle growth by addition of silica. The formed structures would aggregate which would cause the turbidity seen during ensilication.

The findings under standard protocol conditions displayed a three staged process where, during stage I, small silica particulates adhere to the protein positive residues. These particulates are not large enough to nucleate, however once clustered via electrostatics nucleation is induced[244]. This then proceeds to the growth of the TTCF-silica nano-particles. During this growth, a silica shell forms which is represented in the data as an amorphous broad peak (stage II). Once the polar and equatorial radii reach a critical mass point, aggregation is induced. This was observed during ultra-SAXS measurement which supports the statement. During the final stage (stage III), the fractal scattering provided by the silica overtakes the intensity in the measured q-range. This growth is characterised using the fractal dimension, D_f, parameter and indicates fast silica growth with a value of -1.87[139]. Earlier studies using SAXS on the condensation and polymerisation confirm this finding[240,241]. The drying of the particles solidifies them between 200-400 nm.

The investigations on the influence of silica ratios supported the findings under standard conditions (table 4-3). By changing the ratios of silica introduced to the protein solution, it was possible to understand whether ensilication occurs or another kind of reaction takes place. From the fitted data, it was evident that increasing or decreasing the silica ratio would either push the reaction to stage III or slow it down to visualise transitions between stage I and II. When adjusting the pH, it was found that below pH 6.5 ensilication does not occur or is significantly reduced with the time

	ID02	i22		ID02		ID02		
Ratio	1:20	1:50		1:50		1:100		
pH	7	7	7	7	7	7	7	8
Stage	III	I	II	II	III	I	II	I
D_f (arb.)	1.5 - 2.0	1.1	1.1	1.1	1.6 - 1.9	-	-	1.0 - 1.5
R_{equat} (Å)	-	25 - 50	-	-	-	22 - 28	-	40 - 55
R_{polar} (Å)	-	50 - 165 -50	-	-	-	60 - 120 - 90	-	120 - 175
Cut-off (Å)	14- 69	10 - 600	165 - 20	12	20 - 80	> 1	> 1	50 - 300
χ^2 (arb.)	> 1	3.0 - 12	5.0 - 12	> 1	> 1	> 1	> 1	> 1
Lorentz (Å)	-	-	54 - 48	42 - 33	-	-	40 - 30	-
R_{frac} (Å)	5.0	4.4 - 4.9	5.1 - 7.4	7.1 - 10	5.5 - 7.1	7.5 - 9.3	9.5 - 12	7.6 - 9.5

Table 4-3: SAXS ensilication parameter overview. Key parameters displayed are grouped according to ratio, pH and stages. D_f: fractal dimension; R_{equat}; equatorial radius; R_{polar}: polar radius; Cut-off: static protein and silica aggregates; Lorentz length: average particle radius: R_{frac}: radius fractal particles: χ^2: goodness-of-fit.

for nucleation being increased to a matter of days.

Another explanation could be the protonation of the protein, resulting in a change of affinity between the silica and the protein. As the 1:50 ratio is already relatively dilute, it is possible that some silica spheres can form over a longer course of time. At pH 8, it seemed that the silica and protein particles reach an equilibrium early on during stage I of the ensilication process. There is evidence of stable complexes around 300 Å after 2 hours with no clear sign of increasing size. The data do present an initial burst in growth, however this is followed with the parameters stabilising quickly after. In summary, good evidence has been found to hypothesise a multi-staged process during ensilication. To further improve the resolution, small angle neutron scattering (SANS) might complement this study. SANS has the benefit of contrast matching that would probe the silica protein formation even further.

Chapter 5

TTCF protein stability after ensilication

5.1 Introduction

Ensilication aims to stabilise vaccine proteins that are unsuitable for freeze-drying[227]. These vaccines are therefore stored in liquid formulations which require excipients to improve shelf-life[79] and metal salts to enhance efficacy. These are the modulators that affect vaccines detrimentally when exposed to fluctuating temperatures.[79] During such an event, proteins unfold, aggregate or precipitate. This results in the loss of potency and does not infer protection against infectious disease. Up to this point, the described results displayed successful ensilication of TTCF within the silica and elucidated the mechanism of stabilisation via SAXS.

Here, the stability of TTCF before and after release was assessed. The material was additionally stored for long term duration and tested at several time points. Experiments *in vivo* allowed assessment of the immunogenicity retained after ensilication. Calorimetric and physical analysis during stress testing provided evidence as to whether the material is thermally resilient. The combination of various protein analysis methods determined the feasibility of ensilication to thermally stabilise vaccine proteins.

5.2 Methods of protein stability

5.2.1 Initial release, thermal stability and long term storage

To test whether ensilication protects against heat, ensilicated powders (n=3) were heated at 80 °C for 2 hours. TTCF is rapidly inactivated above 60 °C[5], therefore for TTCF a treatment temperature of 80 °C[166] was employed. Triplicate ensilication of TTCF was performed and released to be analysed using previously described methods of SDS-PAGE, Circular Dichroism and ELISA (Chapter 2).

5.2.2 Western Blot

His-tag presence of purified and released TTCF was detected by Western Blotting[245]. An SDS-PAGE was prepared with proteins separated based on molecular weight. These were then transferred to a protein binding nitrocellulose membrane. Filter pads and membrane were cut to size (8 x 6 cm) and soaked in transfer buffer (1x Tris Buffered Saline). The SDS-PAGE gel was washed in transfer buffer and the transfer set-up was stacked as follows; filter pad, membrane, gel, filter pad. This sandwiched stack was then placed in a semi-dry blotting machine and a current was run at 0.8 mA / cm^2 for 1 hour 50 minutes to transfer the proteins from gel to membrane. Protein transfer was verified using Poncheau S[246] staining added to the membrane for 1 min.

The stain was removed after confirming protein presence on the membrane. This was done by several washes with ddH_2O and TBS + Tween 20 (0.05 %) (T-BST). The membrane was then incubated in 20 ml of TBST with 5 % casein (milk protein) for 35 mins at room temperature. An antibody (anti-His IgG + HRP) with specificity to histidine residues and a conjugated reporter enzyme were added to the solution (at 1000x dilution) and incubated for 1 hour at room temperature. Several washes in TBST and addition of luminol substrate mixture of reagent A+B initiated the substrate conversion. Immediately after this, luminescent imaging was performed by an imager equipped with the ClearLive program software.

5.2.3 *in vivo* animal titration study

Native TTCF at 1 mg/ml in 50 mM Tris-HCL pH 7.0 was used for an animal study, performed at Newcastle University by Dr Yi Yang and Dr Kevin Marchbank. Five mice (Charles River laboratories), 1 mice/group, were used in a 21 day' immunisation pro-

tocol. Groups were assigned based on native TTCF dosage as follows: 1/2.5/5 and 10 µg with a PBS only group as negative control. Following pre-immunisation bleed (day 0), mice received an intra-peritoneal injection of the specified TTCF amounts. Mice were bled weekly by tail venesection and a terminal bleed collected at day 21. Serum was sent to the University of Bath and analysed using ELISA[161].

5.2.4 *in vivo* animal study

Ensilicated TTCF was heated at 80 °C for 2 hours. After release from ensilication, protein was dialysed in 50 mM Tris-HCL pH 7.0 using a 10k MWCO Slide-A-Lyzer™ dialysis cassette (ThermoFisher, UK), with Triton-X 100 lipopolysaccharide (LPS) extraction before injection. Twenty BALB/C mice (Charles River lab.), 5 mice/group, were used in a 48 day' immunisation protocol performed at Newcastle University by Dr Yi Yang and Dr Kevin Marchbank. Groups were assigned as follows:

- native TTCF (+ve control)
- heated TTCF (-ve control, denatured protein)
- ensilicated TTCF then released
- ensilicated TTCF + heated at 80°C then released

Following pre-immunisation bleed (day 0), mice received an intra-peritoneal injection 5 µg per dose of treated TTCF. A PBS only group was also included as a further negative control. Mice were bled weekly by tail venesection; a booster dose (5 µg TTCF) was given at day 28 and a terminal bleed collected at day 42. Gathered serum was sent to the University of Bath and analysed using ELISA.

5.2.4.1 ELISA analysis of serum samples

Purified recombinant TTCF was coated at 10 µg/ml, 100 µl/well onto high-binding 96-wells ELISA microtitre plates (Greiner, UK) in Na_2CO_3 buffer, pH 9.6 overnight at 4°C. Plates were washed three times with PBS and then blocked for 1 hour in PBS-Tween 0.05% (PBS-T) containing 1% Casein (Sigma, UK). Plates were washed 3 x 150 µl/well with PBS-T. Anti-TTCF mouse monoclonal antibody (clone 10G5) at a concentration of 1 µg/ml was added to act as a positive control and allow normalisation across ELISA plates. Fifty times pre-diluted samples (in PBS-T) and 10G5 were serially two-fold diluted before transfer to the ELISA plates and incubated for 1 hour. These were then washed again 3 times. Horse-radish peroxidase (HRP) conjugated goat-anti-mouse IgG (Sigma UK), at 1:10,000 dilution in PBS-T was then

added for 1 hour incubation. Plates were washed 4x and freshly prepared tetramethyl-benzidine (TMB) substrate solution (0.1 M Sodium Acetate pH 6.0, 10 µg/ml TMB, 0.015% H_2O_2) added, followed by 10% H_2SO_4 to stop the reaction. Absorbances were read at 450 nm and corrected by subtraction of the reference read at 650 nm and normalised to the positive control (10G5 monoclonal antibody) absorption[161]. Statistical analysis was performed using SPSS v13 (IBM, USA), one-way ANOVA with post-hoc Tukey HSD test.

5.2.5 Calorimetry of TTCF

Calorimetry is a physiochemical principle that can measure physical transition of materials. It is commonly used to monitor protein unfolding (T_m) or for identifying glass transition temperatures (T_g)[247–250]. This method is based on the change of temperature in exothermic or endothermic reactions that materials undergo once they are heated. Protein unfolding is an endothermic change, where conformational changes lead to uptake of energy from its environment. To establish the thermal resilience of ensilicated material, micro-calorimetry (a more sensitive form) was applied to identify the T_m of native TTCF. Following this, powder DSC was utilised to screen ensilicated material for transitions that could indicate protein unfolding.

5.2.6 DSC

Weighed ensilicated TTCF powder (5.6 mg) was added to an aluminium calorimetry pan. The apparatus (DSC Q20, TA instruments) was set to run a temperature range from -10 to 100 °C for 3 cycles at 5 °C/min followed by a hold at each extremity (figure 5-9) for 5 min. After cycles were completed, material was held at 100 °C for 5 hours to assess thermal resilience.

The Setaram µDSC was used to measure native and released TTCF melting temperatures. This machine is a heat-flux DSC. It indicates that the reference and sample cells, nickel alloy, are contained within the same environment. Energy needed to keep the reference cell at the same level as the sample cell is denoted as heat-flow. This variable can have various units, however mW were used. The minimum required sample concentration was 2 mg protein weight.

5.2.7 TGA-DTA-MS

Thermogravimetric[251] (TGA) differential thermal analysis (DTA) coupled with a mass spectrometer[229] (MS) was performed on lyophilised and ensilicated TTCF material. It is a similar technique to DSC, with the temperature difference between the sample and reference being measured instead of the heat flow. A Setsys Evolution 16/18 (Setaram) was used with alumina pans as sample holders; the reference pan was left empty. The analysis of 0.95 ensilicated and 3.09 mg lyophilised TTCF was run from 30 to 200 °C at 10 °C/min under argon flow at 20 ml/min. Alongside with the DTA signal, the mass evolution of the sample was measured by thermogravimetry (TGA) and evolved gases were detected using a mass spectrometer (MS) attached to the instrument (Omnistar GSD 320, Pfeiffer Vacuum, equipped with a quadrupole mass analyser and a SEM detector) through a stainless steel capillary. The MS was set to record atomic mass units (amu) from 1-200 for duration of the run. Known decomposition elements for proteins were investigated for (increasing) presence during the analysis.

5.2.8 CD

Circular dichroism, used for determining the proportion of specific secondary structures,[190–192,252] is also capable of studying protein unfolding. The CD spectrometer can perform thermal ramps. Monitoring the ellipticity of a protein change over a limited range of temperatures can elucidate the thermal transition midpoint, T_m. Using a modified Gibbs-Helmholtz equation, the absorbance data can be processed and fitted with an equation which describes a two-state transition which is applicable for the majority of protein[253]. Depending on which secondary structure is abundant, the wavelength of analysis can be chosen. For most proteins this will be 222 nm. For TTCF, absorbance at 200 nm represented the aborbances of major contributing secondary structures present within this protein.

Native and released TTCF at a minimum of 50 µg/ml concentration was analysed. The protein was dialysed beforehand into 10 mM Na_2HPO_4, NaH_2PO_4 buffer at pH 7.0 and CD was measured between 185 — 260 nm. The temperature ramp initially consisted from 20 to 70 °C at 5 °C intervals. Each measurement was set to 2 seconds per wavelength with a bandwidth of 2 nm. The second ramp was set from 50 — 70 °C at 1 °C interval. Both ramps were incremental at 1 °C/min. Acquired data was converted to delta epsilon and fitted using the custom equation in the MatLab™software package. The data was processed using:

Parameters

h=-20000 ; starting enthalpy in cal/mol = -6.0643

tm=60 ; starting TM (observed) in deg. C.

u=-10; delta epsilon of 100% folded helical protein

l=-1; delta epsilon of unfolded protein

Variables

v=col(1) ; temperature in deg. C

w=col(2) ; delta epsilon

Equations

m=tm+273.15; convert Centigrade to Kelvin

t=v+273.15; convert Centigrade to Kelvin

k=exp((h/(1.987*t))*((t/m)-1)); calculate folding constant at any given temperature

y=k/(1+k); calculate fraction folded at any given temperature

f=((u-l)*y)+ l ; calculate ellipticity at any given temperature

fit f to w; fit the calculated ellipticity to the observed ellipticity

5.3 Results & Discussion

5.3.1 Initial release

TTCF was ensilicated, released and analysed using SDS-PAGE, Western Blot, CD and ELISA. Native TTCF was used as a control. Various samples during ensilication were taken and visualised on a gel. There is protein present in the flow through which has not been incorporated as shown on the SDS-PAGE and WB images (figure 5-1) where a bright band is visible in the respective lane. Subsequent washes do

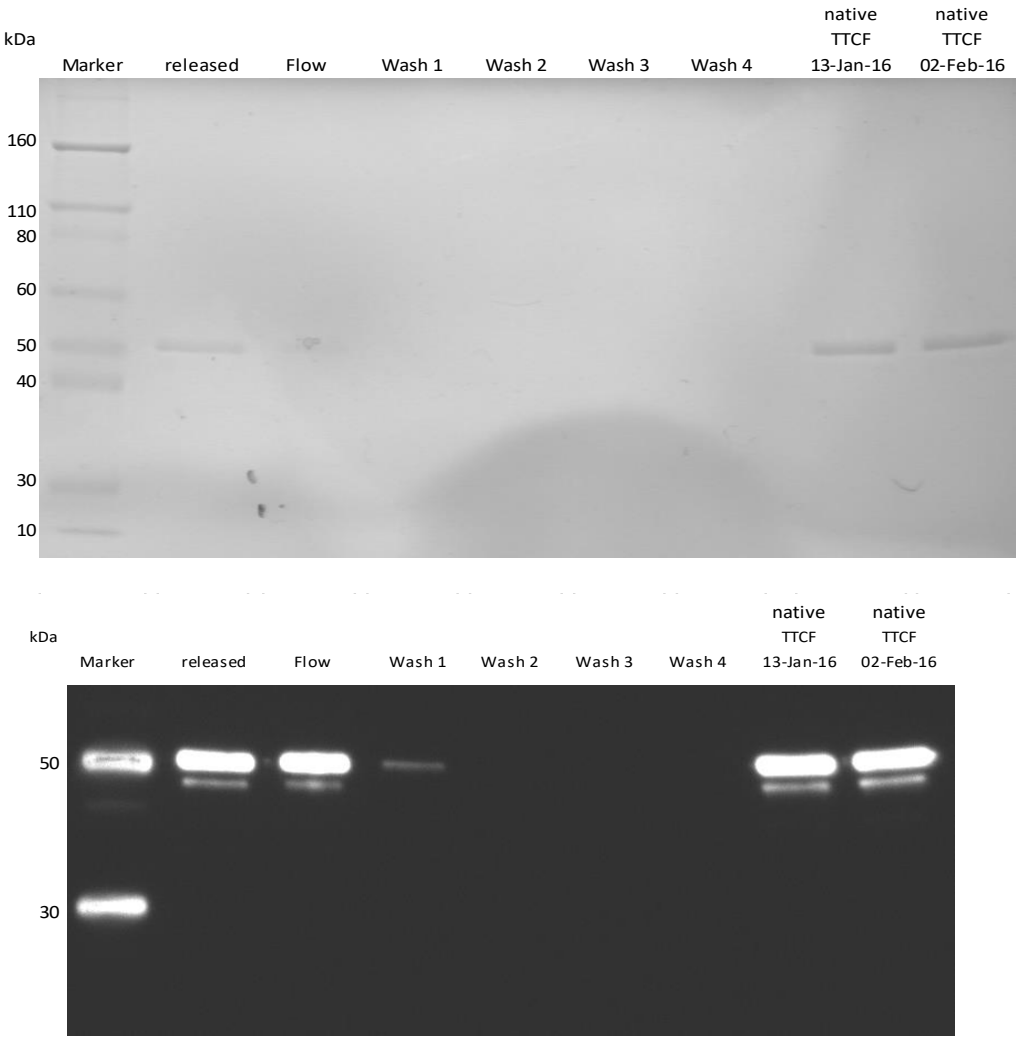

Figure 5-1: Initial SDS and WB of TTCF ensilication. (top) SDS-PAGE of native, released and washing steps after ensilication. Amount (w/v) was normalised before loading on the gel. Visualisation achieved using Coomassie stain. (bottom) Western blot of the same gel using an anti-histidine antibody. Bands visualised by measured chemiluminescence.

present a slight band in the first wash on the WB. This displays the sensitivity of using an antibody detection method compared to the same gel stained using Coomassie. Newly purified TTCF was added to verify consistency between batches (outermost

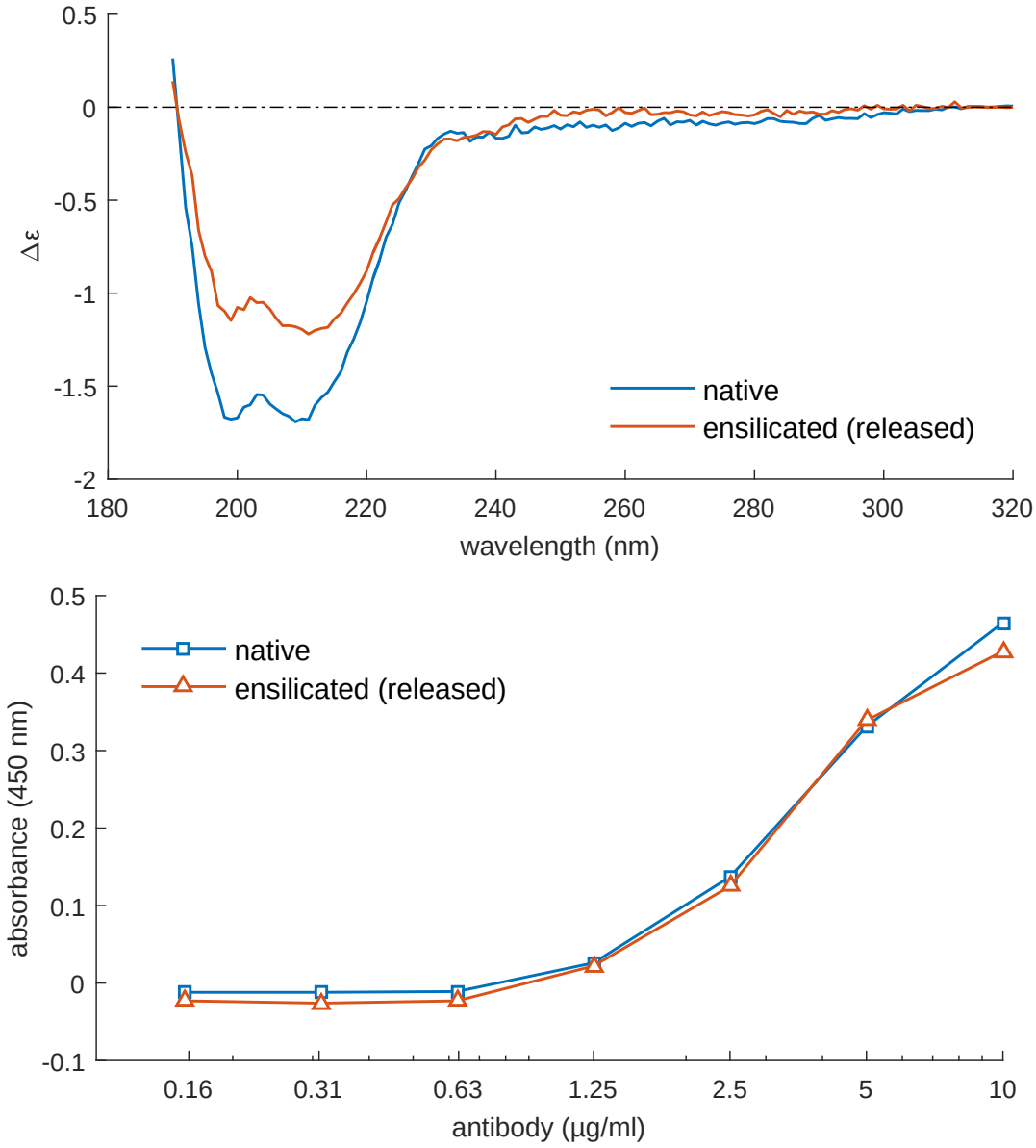

Figure 5-2: Initial assessment of released TTCF from silica using CD (top) and ELISA (bottom). CD spectra obtained between 320 - 185 nm for native and released TTCF. Data were converted from millidegrees to $\Delta\varepsilon$ and normalised according to concentration. ELISA absorbance was obtained from detection of bound native and released TTCF using 10G5 and secondary antibody conjugated with HRP. Substrate conversion was read at 450 nm and subsequently plotted as antibody concentration over absorbance.

lanes). The anti-histidine IgG antibody with HRP enzyme conjugate allowed assessment of any N-terminal shearing of the protein during ensilication. There was

no evidence found for this. The apparent bands at 44 and 52 kDa represents TTCF with bound and free sulfhydryl groups. Following the analysis using SDS-PAGE and WB, released TTCF was dialysed overnight into 10 mM sodium phosphate buffer (pH 7 adjusted with HCl) to remove any interference from the silica present in the release buffer during CD. The spectra from 320 to 195 nm showed a similar pattern between released and native TTCF (figure 5-2). This is promising as CD provides structural information about the state of secondary structures present in the protein. Differences in delta epsilons values between native and released were due to background subtraction differences. This technicality does not change the outcome of this result. CD is sensitive to changes in secondary structures. Alterations in these would shift the peak position left or right-hand, as this was not observed it confirms the retention of native structure.

Finally, native TTCF and released were coated onto a high-binding microtitre plate to assess antigenic (functional) conformation. The monoclonal antibody detected no differences between native and released protein. Therefore, it was safe to say that it was possible to stabilise TTCF within the silica and retrieve its native state afterwards, in ambient conditions.

5.3.2 Thermal stability

To asses the thermal stability of TTCF, three batches of purified TTCF protein were ensilicated. From each batch, 5 mg was heated at 80 °C for 2 hours with native TTCF in solution as a negative control. Heated and untreated material were released subsequently and analysed using SDS-PAGE in triplicate (figure 5-3). The native and untreated released protein did not show an increase in shear, which would result in additional bands. Heat treated released acted accordingly with these results. In contrast, the heated unprotected protein seemed to have completely sheared due to the heating of protein which is visualised as a smear on the gel.
To verify the secondary structure integrity, released samples from one batch were dialysed into 10 mM phosphate buffer. The circular dichroism of these samples was measured from 260 — 185 nm, far UV. The machine output in millidegrees was converted to delta epsilon which allowed normalisation of concentration variances. Results displayed an overall similar pattern (figure 5-4). The heat treated and untreated released material possessed very similar patterns compared to native absorbance

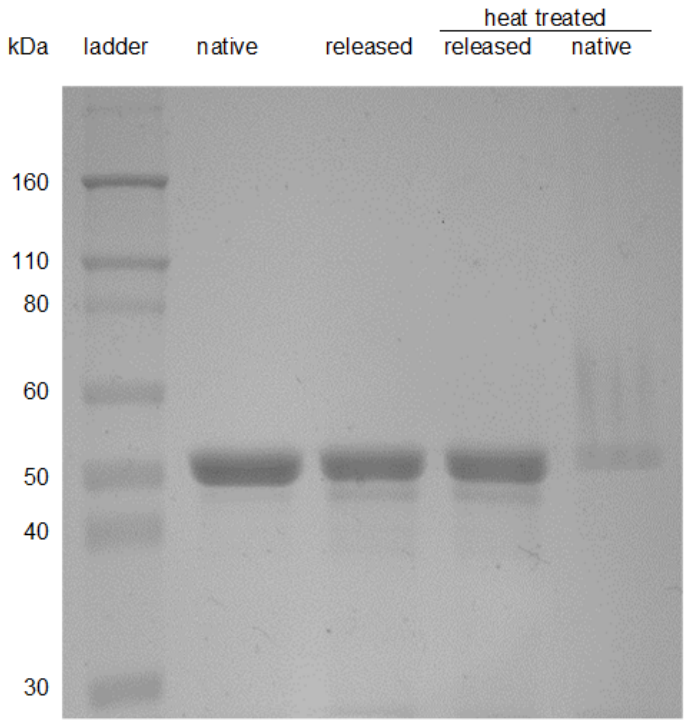

Figure 5-3: SDS-PAGE of native TTCF, untreated released, heat-treated released and heat-treated native[227]. Samples were normalised and 5 µg of protein was loaded in each respective lane. Heat-treated samples were exposed to 80 °C for 2 hours before analysis.

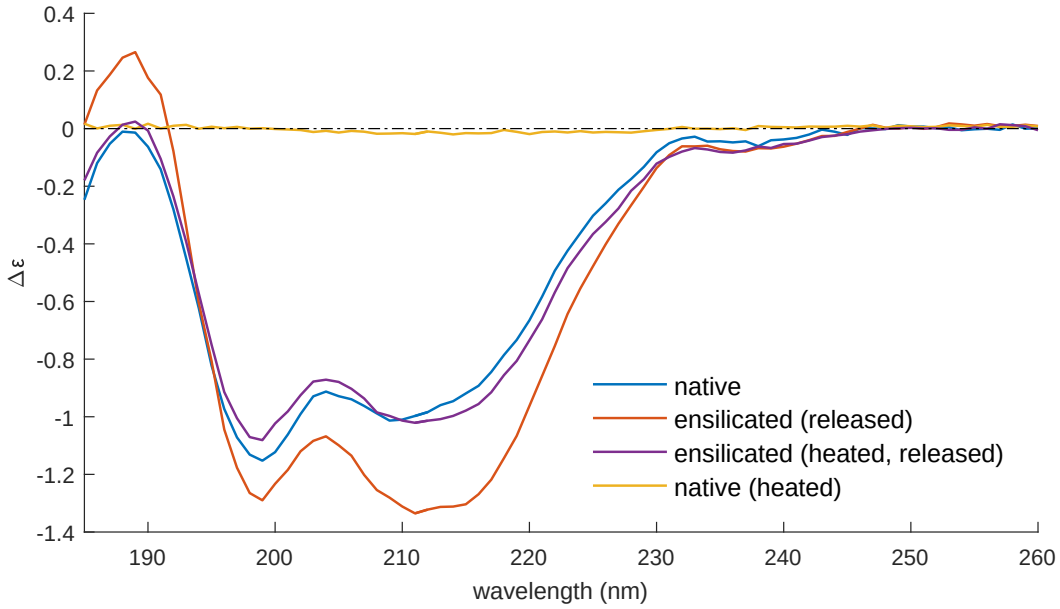

Figure 5-4: CD spectra of TTCF thermal stability. CD spectra between 260 - 185 nm of native, released and heat treated (native & released) TTCF samples were obtained. Sample data were converted from millidegrees to $\Delta\varepsilon$ and normalised according to concentration. Deconvolution of each spectra was subsequently performed using DichroWeb.

suggesting no loss of or very small loss secondary structure. There is a difference observed in the released material where there is increased chirality between 205 and 222nm. This could likely be due to background subtraction errors.

Unprotected native which was heated did not show chirality as its absorbance of both rotational polarised lights was effectively zero. This meant the protein had completely unfolded and lost its tertiary and secondary structure. The CD spectra of these samples were deconvoluted using the CDSSTR (reference set 6) algorithm[254–256] to define the individual contributions of major secondary structures (table 5-1). It was found that the overall contributions of α-helices, β-sheets and random coils did not significantly differ between native, released and heat treated

Sample	Helix[1]	Helix[2]	Strand[1]	Strand[2]	Turns	Unordered	Total	Resi
native	-0.01	0.03	0.22	0.12	0.2	0.43	0.99	0.044
released	-0.01	0.03	0.24	0.13	0.2	0.39	0.98	0.043
heated rel	-0.01	0.03	0.22	0.12	0.19	0.42	0.97	0.047

Table 5-1: Deconvolution of secondary structures TTCF circular dichroism. Individual contributions to the overall CD spectrum. Observed is the similarity of distribution across all samples excluding heated native. Helix 1: α-helix, regular; Helix 2: α-helix, distorted; Sheet 1: β-sheet, regular; Sheet 2: β-sheet, distorted; Turns: β-turns; Unordered: random coils.

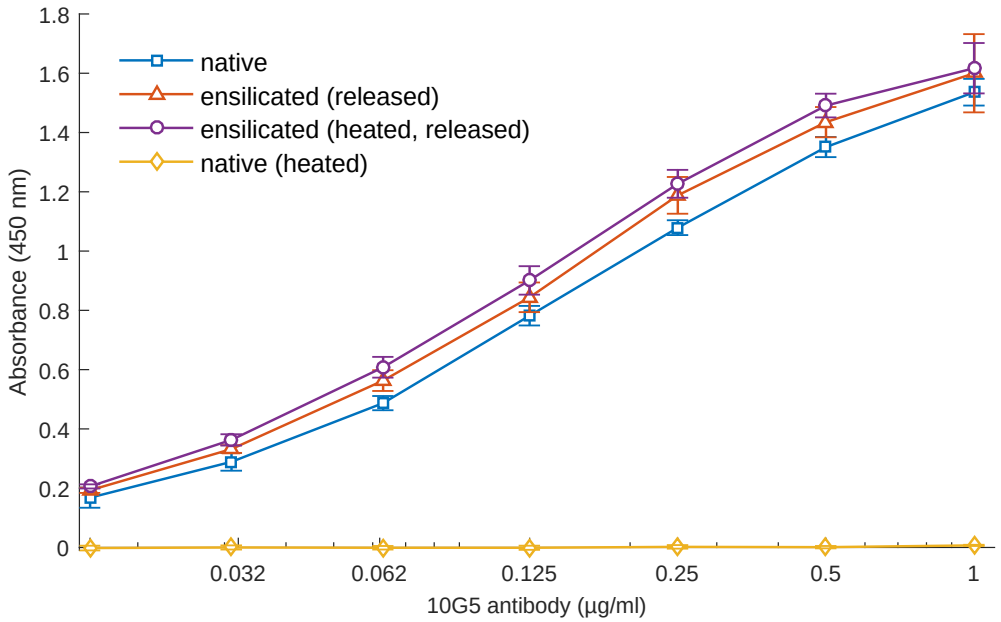

Figure 5-5: TTCF antibody binding capacity before and after ensilication[227]. ELISA assay was performed on native TTCF (blue), native TTCF heated for 2 h at 80 °C (purple), TTCF released from ensilication (orange) and ensilicated TTCF heated for 2 h at 80 °C and released (yellow). Data are visualised as antibody concentration over absorbance with standard error of the mean (SEM), n = 3.

released. The normalized root-mean-square deviation[257] (NRMSD) shows that the fitting across the samples is equal, therefore allowing good confidence in the assumption that the TTCF protein in various stages has retained its secondary structural integrity. ELISA was then performed after confirming the retention of primary and secondary structure of TTCF heat treated material. The protein was bound to a microtitre plate and detected using a monoclonal antibody, 10G5, specific to TTCF. The result from this analysis displayed the preservation of antigenic epitopes present on the protein (figure 5-5). An antigen requires structural integrity and specific conformation to be bound by an antibody, therefore it was safe to say that the protected material, either heat treated and untreated retained its native conformation. This was observed from the non-significant absorbance difference between the native and ensilicated groups calculated using the non-parametric Kruskal-Wallis test. Unprotected heated material had lost all of its antigenicity as it lacked the ability to be bound by the monoclonal antibody.

TTCF was also lyophilised to provide a comparison between lyophilisation and ensilication. Freeze-drying is a widely used method to stabilise proteins. Both ensilicated and lyophilised material were exposed to the same conditions described

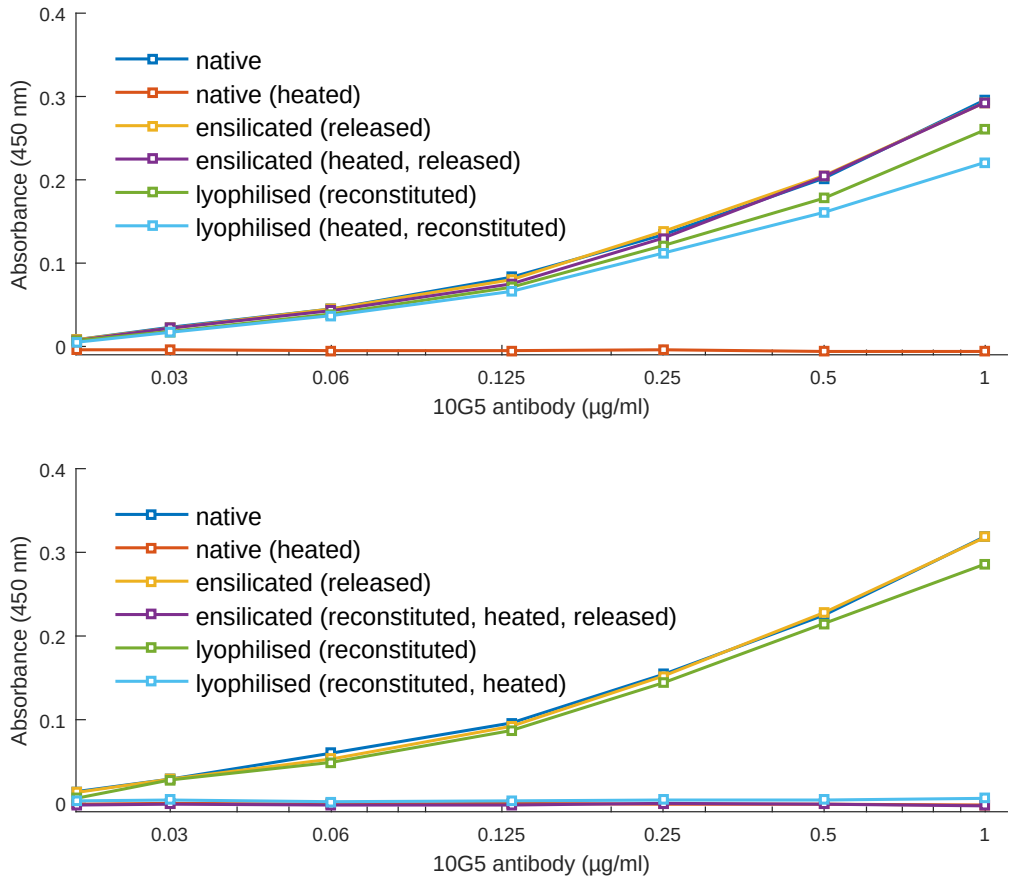

Figure 5-6: ELISA on lyophilised TTCF[227]. (top) Lyophilised and ensilicated material were heated, then reconstituted and released respectively. Bound TTCF was detected using 10G5 antibody and secondary antibody against IgG conjugated with HRP. Data were plotted antibody concentration over measured absorbance at 450 nm. (bottom) Same experiment as above, however buffer was added to lyophilised and ensilicated material before heating. Ensilicated material was released thereafter. TTCF was then bound onto the microtitre plate for detection.

earlier. The reconstituted and heated materials were analysed using ELISA to assess whether the antigenic properties were retained in comparison to freeze-drying. The results (figure 5-6) display binding capacity of native versus both methods. There is no difference between the three samples, with the native heated serving as a negative control. Note that these materials were exposed in dry state. The same figure (figure 5-6, bottom) indicates that hydration before heating completely removes any binding capacity of both methods. This suggests that both materials would be susceptible to increased humidity and temperature combined. The overall result indicates ensilication to be as protective as freeze-drying.

5.3.3 *in vivo*

Confirming the retention of TTCF at all relevant protein levels, the logical way forward was to verify its functionality *in vivo*. Before the *in vivo* study on TTCF was performed, optimal dosage needed was to be determined. Five mice were injected with increasing dosage of native TTCF. Their serum was collected every 7 days up to 21 in total. The serum was analysed using ELISA (see Appendix A.7 for plate responses). The results were convoluted and visualised. Data presented (figure 5-7) clearly show an optimal immune response at 5 µg/dose. The 10 µg/dose displays a lower overall response which is an indication of immunological threshold whereafter an antigen starts to be tolerated by the immune system. Therefore, 5 µg/dose was chosen as the effective concentration in the following *in vivo* study. This preliminary data increased the confidence that released TTCF would induce an immune response based on biochemical data.

Ensilicated TTCF, made for this study, was tested directly after release with no dialysis to exclude that this was a critical step during release. Dialysis is normally performed overnight at 4°C in a large volume of target buffer. This helps to refold proteins that are slightly unfolded. The ELISA analysis found good binding capacity of various released samples compared to native TTCF. These were analysed using the mouse serum obtained from the titration study. This implicates some binding due to linear epitopes which do not require the protein to possess a specific conformation. However, the signal from these samples were in decent alignment with native TTCF. It may be that dialysis partially refolds the protein after incubation as the released

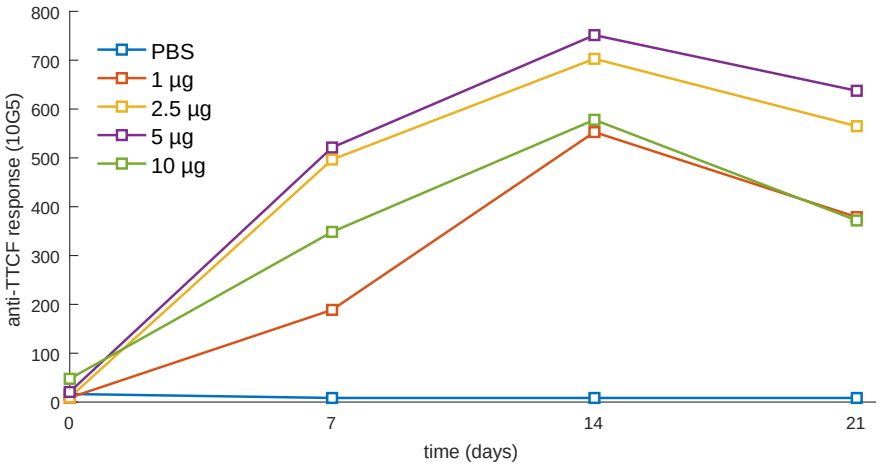

Figure 5-7: Serum ELISA TTCF titration. Serum IgG responses to various doses of native TTCF injected in mice. Overview of combined results where absorbance data is normalised to 10G5 standard.

samples were diluted in high pH sodium bicarbonate buffer before overnight binding on the microtitre plate (figure A-3, Appendix A.8).

The protective capacity of ensilication on TTCF was then confirmed *in vivo*. This experiment included 4 groups of mice consisting of 5 mice per group. Each group was assigned as described in methods section 5.2.4. Observed was an early stage immune response in the mice injected with native TTCF and this immune response was matched when the mice were injected with TTCF which had been stored as ensilicated powder and released prior to immunisation (figure 5-8).The results confirmed the protective capacity of ensilication to maintain normal protein/epitope conformation at ambient temperature, as well as when the ensilicated material was heated at 80 °C for 2 hours (responses per day, see Appendix A.9). The ensilicated material

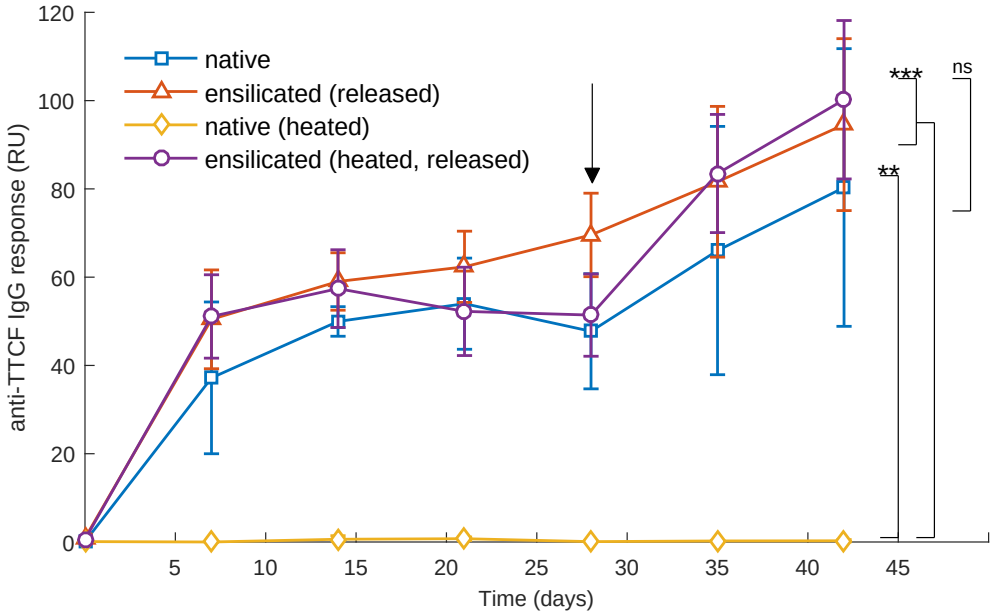

Figure 5-8: Serum IgG responses from mice immunised with TTCF after ensilication. Normalised absorbance values against monoclonal 10G5 (RU: relative units) with secondary anti-IgG antibody for detection of class-switched antibodies. Sample groups consisted of 5 mice which were immunised with 5 µg of TTCF at the start of experiment and boosted at 28 days (arrow). Data are expressed as mean +/- SD (n=5). Statistical analysis was performed applying one-way ANOVA with post-hoc Tukey HSD test. Comparison vs native TCCF (ns = non-significant) or vs native TTCF heated to 80 °C to denature and inactivate ((* $p < 0.05$, ** 0.01 and *** 0.001,)

used during this study was stored in powdered form for 1 month at room temperature and then transported using commercially available means without any specialised equipment. The ensilicated TTCF was protected from elevated temperature denaturation, as demonstrated by the lack of specific immune response when unprotected and heat-denatured TTCF was injected into mice. After 28 days, the booster shot

was given which is reflected by the immune response. Statistics revealed no significant differences between the responding groups and a significant difference between the groups and denatured protein.

5.3.4 Calorimetry

DSC was employed to probe the thermal resilience of ensilicated TTCF (figure 5-9). The run, which included several ramps between -10 to 100°C showed no endothermic transitions that could indicate protein unfolding. The first cycle displayed a large downwards slope which could be associated with bound H_2O being liberated from this material. This slope does not present itself in subsequent cycles. After 5 repeats, the hold at 100°C does not indicate any noticeable changes in this material.

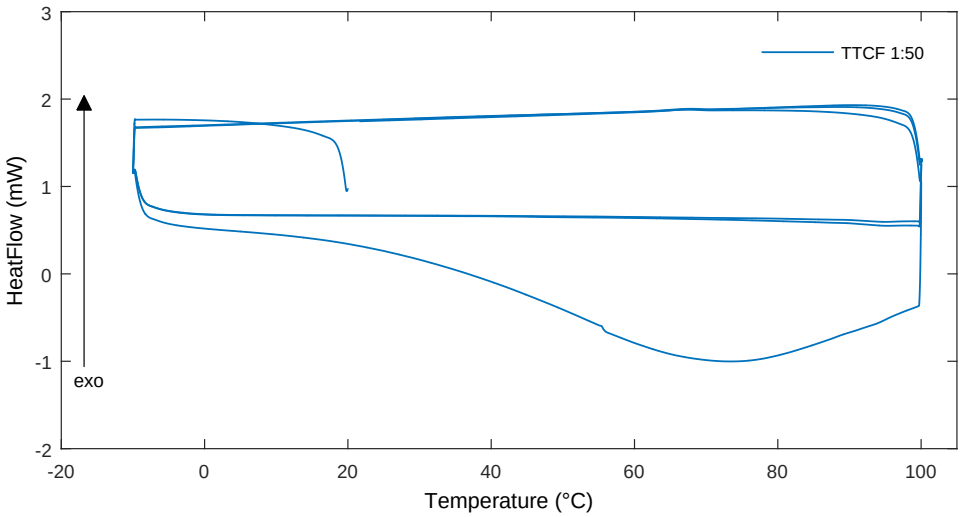

Figure 5-9: DSC calorimetry experiment of ensilicated TTCF. Three cycles of -10 to 100 °C with a hold of 100°C for three hours does not present a sharp endothermic peak.

The DSC experiment was repeated for 1 cycle from 20 to 200°C using a TG-DTA-MS (figure 5-10). TGA signal reported a weight loss of 11% for ensilicated and 3% for lyophilised TTCF. This loss of mass for ensilicated TTCF material is in line with previous data reported on ensilicated lysozyme where it was found to lose 10% of mass during the TGA[203,227]. Mass spectrometer signal reported the loss of weight associated with water loss at atomic mass unit (amu) of 18. Interestingly, the unprotected TTCF showed an endothermic transition at 150 °C. This is not observed in the protected TTCF and displays the protective capacity of ensilication. Temperatures

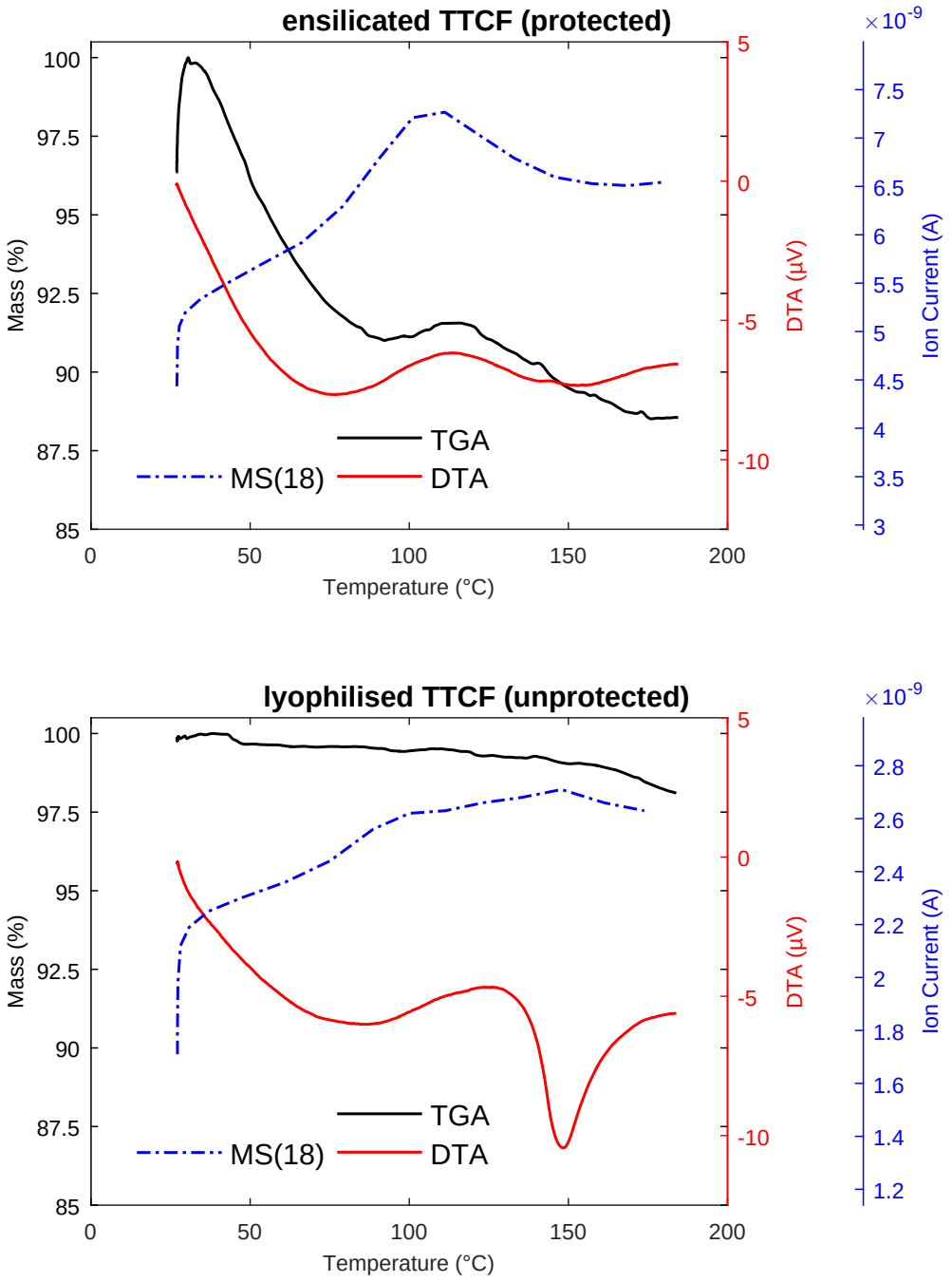

Figure 5-10: TGA-DTA-MS of ensilicated TTCF. (top) Ensilicated TTCF displays a weight reduction of 10 % during heating. The DTA shows an endothermic transition associated with liberation of water supported by the MS peak. (bottom) Unprotected TTCF shows a small weight loss with associated water signal increasing. At 149 °C there is a sharp endothermic peak present, indicating a transition taking place.

above 50°C are highly unlikely to occur during vaccine transportation. However, this data is reassuring of ensilication stabilising capacity.

Circular dichroism was employed to assess protein unfolding under thermal stress. TTCF native, released and heat treated were measured between 260 - 185 nm from 50 to 70 °C. An initial global run was performed from 5 to 85 °C to probe the nature of TTCF unfolding. The CD data were converted into delta epsilon (thermal ramp data, see Appendix A.10). This value at 200 nm for all measurements was plotted versus temperature and fitted using the Gibbs-Helmholtz equation (figure 5-11). Good fits were observed for each data set. There were some differences in the unfolding pattern between the native and ensilicated samples. However, an additional repeat displayed this to be a concentration dependent occurrence as this unfolding pattern was similar to released and heat-treated released measured at identical protein concentration.

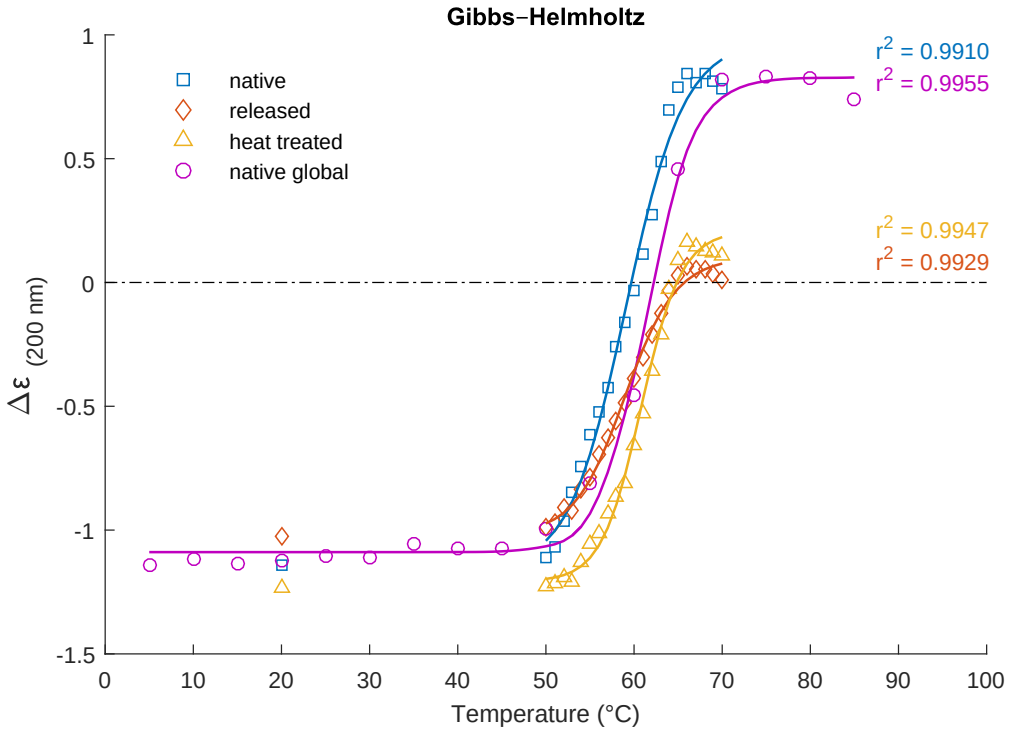

Figure 5-11: TTCF Gibbs-Helmholtz fitted CD data. Delta epsilon values measured at 200 nm were plotted versus temperature. The Gibbs-Helmholtz fit was applied to this data with set starting points. Good fits were obtained and calculated parameters were deconvoluted further to obtain calorimetric identifiers of protein stability. Native, release and heat-treated TTCF were run at 1 °C increment between 50 - 70 °C. Native TTCF global was run at 5 °C increment between 5 - 90 °C

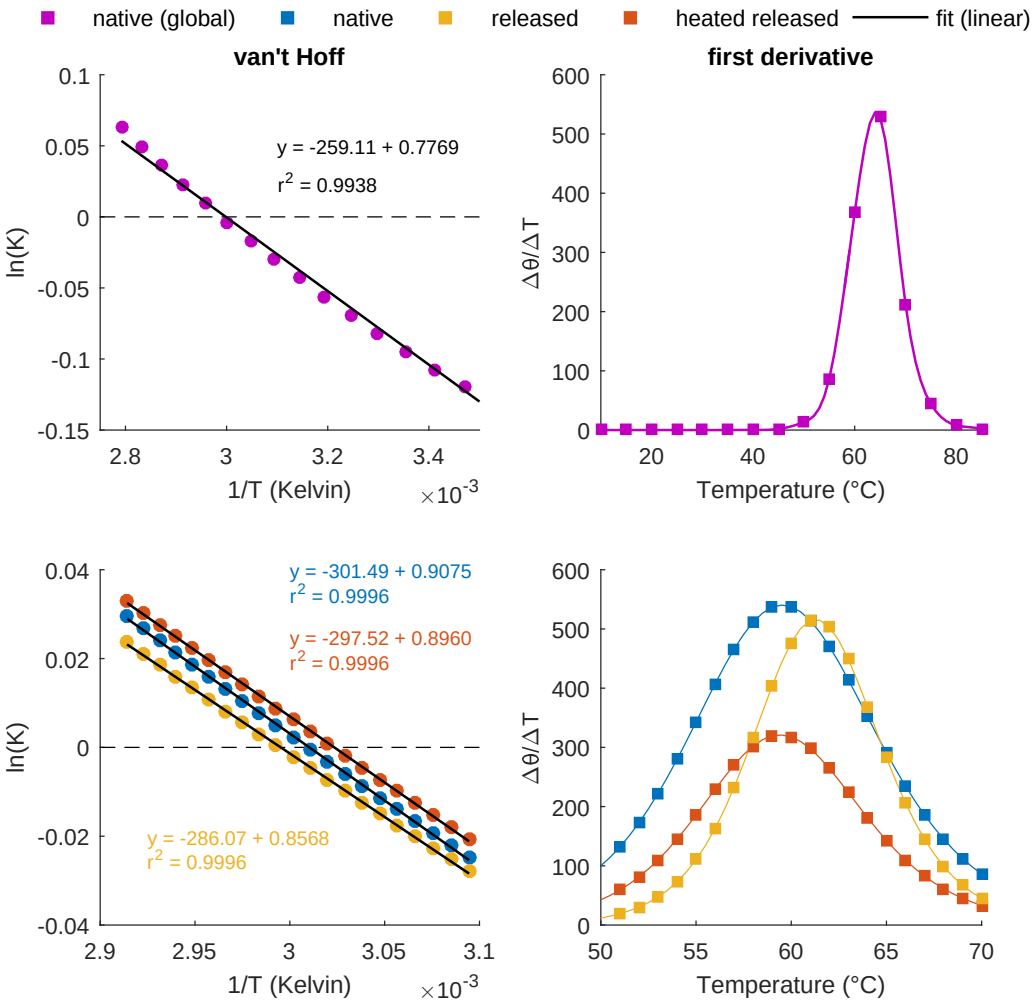

Figure 5-12: TTCF fitted CD data van'T Hoff plots and first derivatives. (top and bottom left) Data fitted with linear regression to the global and limited range runs. (top and bottom right) First derivatives of fitted CD spectra. Peaks correlate with thermal unfolding of TTCF.

Processed calculated data were visualised in van 'T Hoff plots and first derivatives of unfolding (figure 5-12). The fitting showed that all varieties of TTCF were structurally unaffected with no significant differences in thermal transition midpoints observed between native (global) 61.41 °C, native (local) 59.16°C, released 60.84°C and heat-treated released 59.01°C.

5.3.5 Long term storage

Ensilicated TTCF was released and analysed after 2 weeks, 1 month, 3 months, 1 year and 2 years of storage at room temperature (20 - 22 °C) to assess long term storage. The material was released using the standard protocol and analysed using the experiments described for all three protein levels. The initial triple batch (R1-3) used for the thermal stability experiment was used until the third month of storage. Limited amounts of material were available for testing, therefore additional batches were made for storage at longer durations.

The SDS-PAGE and ELISA analysis for the first three months showed the material retaining its primary and tertiary structural integrity (figure 5-13). The CD data acquired for these samples showed increased background errors due to technicalities. Therefore, these data could not provide any reliable information about the secondary structures (Appendix A.11). However, since analysis of tertiary structure showed good antibody binding this was not of concern.

The 1 and 2 year samples were difficult to release using NaF buffer. This material displayed signs of vitrification and meant the filtrate had changed from a powder-like state towards a glassy dense state. The reason for this has not yet been identified. To resolve this, 0.1 M of NaOH was used to dissolve the glass like material. Once this was dissolved, solution pH was quickly adjusted using HCl to neutralise any free hydroxyl radicals. Analysis of the material did confirm incorporation of TTCF.

SDS-PAGE analysis of vitrified samples stored over long term showed presence of TTCF polypeptide molecular weight (figure 5-14). This confirms the retention of TTCF at primary level.

The ELISA analysis of these samples was done with use of mouse serum obtained from the *in vivo* experiment (figure 5-15). Resultant response in absorbance is a convolution of linear and conformational epitopes present. It is promising to have found protein after release from ensilicated material which does not dissolve when using NaF buffer. Ensilicated lysozyme was used as a release buffer control. This material did dissolve in the standard protocol buffer.

Overall, TTCF can be stored using ensilication up to two years. However, vitrification renders the material unusable for release in standard conditions. NaOH is a powerful denaturant and would not be a suitable replacement for NaF. Therefore, more control on the ambient conditions of ensilication is required to prevent vitrification.

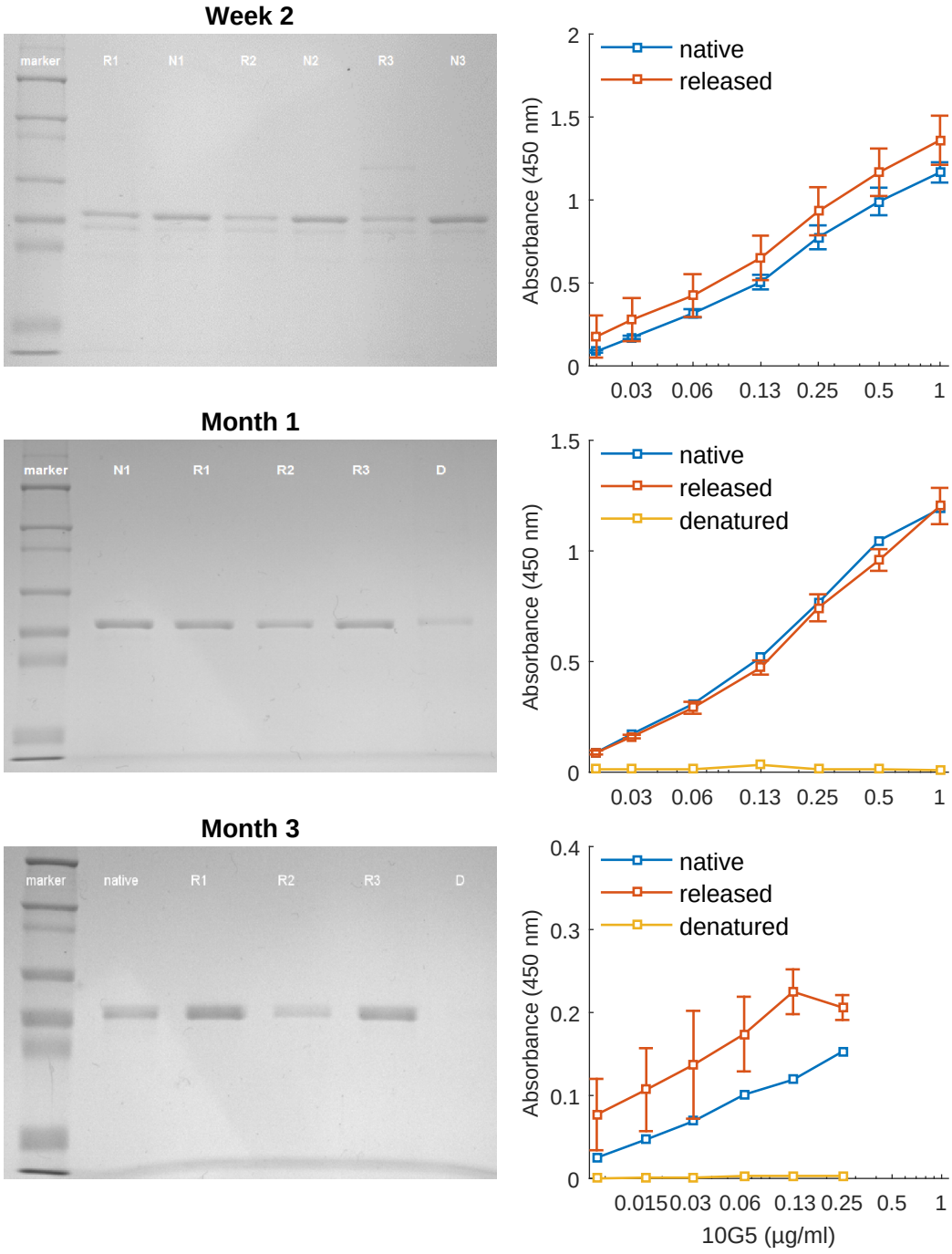

Figure 5-13: SDS-PAGE and ELISA of released TTCF after storage up to 3 months at room temperature. (left) SDS-PAGE analysis of TTCF polypeptide weight after release from storage. R1-3 represent triplicate ensilicated batches and N1-3 are the native purified TTCF solutions used for ensilication. D = denatured TTCF, native TTCF heated at 80 °C for 2 h. (right) ELISA analysis for N1-3 and R-3. TTCF was bound and detected using 10G5 with secondary anti-IgG conjugated with HRP. Data were plotted as antibody concentration over averaged absorbance at 450 nm. Error bars display SEM (n=3).

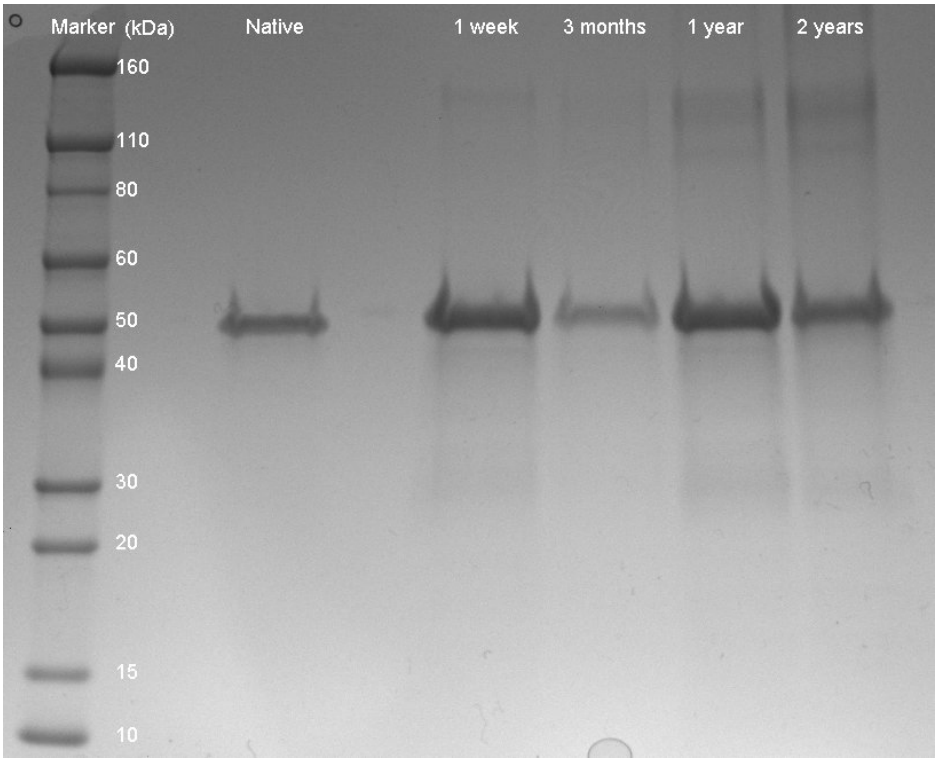

Figure 5-14: SDS-PAGE of released TTCF after storage up to 2 years. A gradient gel (4 - 20 %) was used to run native TTCF and released TTCF from ensilicated material that was stored at room temperature for 1 week, 3 months, 1 year and 2 years. The latter two samples were released using 0.1 M NaOH for 1 hour rotating at room temperature with pH to 7 afterwards.

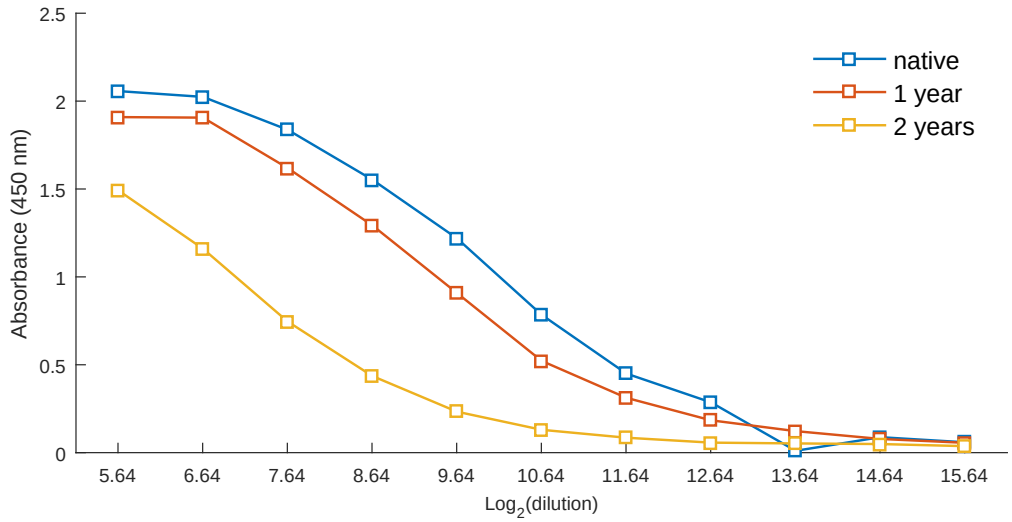

Figure 5-15: ELISA of released TTCF after storage up to 2 years. Ensilicated TTCF was released using NaOH and pH to 7. Protein was bound and detected using serum from the *in vivo*experiment. Secondary antibody was targeted at IgG response. Data were plotted as $\log_2$-dilution over absorbance. Serial dilution started at 50x.

5.4 Summary

After establishing that TTCF could be successfully ensilicated, it was necessary to determine whether the protein could be released from the silica shell and retain its structural integrity. Initial release experiments were performed to analyse the three levels of TTCF protein structure after dissolving the silica shell. Primary structure was investigated by SDS-PAGE which showed retention of the polypeptide length (52 kDa). Western blot confirmed that there was no shearing indicating that the protein's primary structure was unaffected by release. Secondary structure was examined by CD which displayed similar structural patterns between native and released. More importantly, the analysis of tertiary structure by ELISA showed identical responses from native and released TTCF. This confirmed retention of the 10G5 recognised conformational epitope[161]. Since all structural levels appeared to have been maintained, the study was progressed towards the examination of the thermal resilience of ensilicated TTCF.

Ensilicated material was heated together with native TTCF and examined with the methodologies described above to assess the protective capacity of ensilication. The data showed no difference between native, released and heat-treated released material while heated non-ensilicated TTCF had lost its structure at all levels. Deconvolution of the CD pattern confirmed retention of secondary structures with the overall contributions of -helices, -sheets and random coils not significantly differing between native, released and heat treated released. The binding capacity measured in the ELISA displayed no significant difference again with the aforementioned groups.

The immunogenic capability of the released and heat treated material was analysed in an *in vivo* experiment. The initial titration experiment suggested 5 µg of TTCF would produce an optimal dose response. Serum analysis showed no significant differences in response between native, released and heat treated released material. This supported the evidence from the thermal stability experiment and showed that ensilication is a viable method for vaccine stabilisation.

The biophysical properties of ensilicated, native and released TTCF were probed using calorimetry. The aim of this was to identify whether the energetic value required for denaturation was affected by ensilication. Ensilicated material was subjected to repetitive thermal ramps using a DSC apparatus. A broad endothermic peak was observed which was associated with water coming off the material. This was duplicated in an experiment using TGA-DTA-MS. The sample mass loss showed cor-

relation with the mass spectrometer peak for water. Lyophilised TTCF showed an endothermic peak in the DTA which was not observed in ensilicated material. This demonstrated the protective capacity of ensilication.

Calorimetric analysis of native and released protein was done using CD. Fitting of CD spectra at specific wavelengths with samples heated over time showed a two state transition between folded and unfolded state. Comparison of the fitted parameters showed no difference in thermal transition temperatures and therefore indicated that TTCF was not physically affected by ensilication and release.

The long term storage study showed retention of TTCF for up to two years. Producing a large batch to be examined throughout the two year study was a challenge as the production of large amounts of recombinant antigen (>1 gram) was expensive and time consuming. Therefore, the study had to be done in using three separate batches of ensilicated TTCF. This exposed a major challenge in protein ensilication as the method does not always provide powder-like material. Instead, the dried sample may vitrify into a dense glassy state. There are several possible parameters that may cause this: TEOS starting material, humidity, temperature, presence of salt ions, duration of ensilication or buffer preparations. Investigation into these was beyond the scope of this study, however it needs to be addressed for future studies. In all, ensilication protects and stabilises TTCF over time and against thermal stress with immunogenic capacity retained. It is therefore suitable for the development of thermostable vaccines.

Chapter 6

Lysozyme

6.1 Introduction

The ensilication methodology was initially developed with use of hen egg-white lysozyme[203]. This ubiquitous 14 kDa protein plays a significant role in protection against bacterial pathogens. It is able to break down the cell-walls of Gram$^-$ bacteria. This protein has been well studied and characterised on many occasions. Other proteins such as insulin and horse haemoglobin were also evaluated in the ensilication project. In this Chapter, an account is made of the additional studies that supplemented the lysozyme project. The aim was to complement the findings of TTCF ensilication and show the versatility of protein ensilication.

6.2 Methods

6.2.1 Released lysozyme crystal structure

The crystal structure of released lysozyme was examined and compared to the native hen egg-white lysozyme to confirm structural retention on a fundamental level. Ensilicated lysozyme was released and crystallised. This crystal was then analysed using x-ray diffraction (XRD) and a 3D-model refined.

6.2.1.1 Lysozyme crystallography

Crystallisation of lysozyme released from silica was achieved with use of the 'hanging drop' vapour diffusion technique. Pure lysozyme has been crystallised on many occasions before and the conditions mentioned here have been adapted from

literature for use within this procedure. Released lysozyme was dialysed in 0.1 M sodium acetate pH 4.6 and concentrated to 25 mg/ml. In a 24-well crystallisation plate, 700 µl of 1.5 M NaCl in 0.1 M sodium acetate pH 4.6 was added to each reservoir. The lysozyme solution was mixed 1:1 on a siliconised coverslip with reservoir solution creating a 2 µl droplet. Diffusion within the covered well provided changes in the precipitant causing the reservoir solution to retain more water, thus resulting in the formation of crystals within the droplet as the protein concentration increased, until equilibrium was obtained. Crystals were formed after approximately 5 days incubation at 18°C.

6.2.1.2 Lysozyme X-ray diffraction

Crystals were flash frozen in a loop (reservoir solution + 25% glycerol) under a continuous nitrogen cryo stream (Oxford Cryosystems Cobra) and full data set was collected on an in-house rotating anode X-ray source (Rigaku MicroMax-007HF) with a Saturn 944 + CCD detector. The structure of released lysozyme was resolved using molecular replacement (using Balbes) and refined (using Phenix) with model building in COOT. This work was performed by a collaborator (see Acknowledgements).

6.2.2 Lysozyme *in vivo*

To conduct the lysozyme *in vivo* experiment, several samples were prepared and analysed before continuing with the animal study.

6.2.2.1 Material preparation and analysis

Lyophilised lysozyme (native control) was dissolved, 27 mg, in 10 ml of 50 mM Tris-HCl pH 7 buffer. Two millilitres were heat-treated separately. Previously made ensilicated lysozyme, under standard protocol conditions (section 3.2), was split in two with half being heat-treated prior to release. Heat-treatment was performed for 5 hours at 95°C in a thermal heating block. Samples were contained in 1.5 ml eppendorfs. Enzyme kinetic analysis (EnzCheck™ lysozyme assay kit, ThermoFisher, UK), normalised using protein concentration determined by BCA assay, validated the samples for use in the animal study. The analysis was performed according to manufacturers instruction.

6.2.2.2 Sample preparation before intra-peritoneal injection

Ensilicated samples were released in 1:1 ratio of 190 mM NaF pH 2.65 and Tris-HCl pH 7 buffer. Ensilicated lysozyme (7.5 mg), ensilicated heated treated lysozyme (7.8 mg) and ensilicated lysozyme (5.8 mg, Master sample for comparison) were dissolved in 10 ml of release buffer. After 1 hour incubation on a roller bank, 3 ml of each sample was added to a Slide-A-Lyzer™10k MWCO dialysis cassette to be buffer-exchange into Tris-HCl overnight at 4°C. The following day, samples were extracted from their cassettes. Quick UV-absorbance analysis using a NanoDrop™ One Microvolume UV-Vis Spectrophotometer (Thermo Scientific) analyser verified protein presence. Samples were filtered using a 0.22 µm spin column. Samples were sterile filtered for 1 min at 16,000 x *g*. Final concentrations were checked using the NanoDrop system. 50 µg of lysozyme was used per dosage with 10 µg of LPS added for each mouse to boost the immune response.

6.2.2.3 Animal mouse study

The lysozyme *in vivo* study include 25 mice with 5 mice designated per group under the following conditions:

- Native lysozyme (+ve)
- Native heat-treated, denatured (-ve)
- Ensilicated, released
- Ensilicated, heat-treated, released
- Ensilicated master sample (long term storage > 3 years, provided by Dr Y-C. Chen), released

Each mouse received an intra peritoneal injection. Blood was collected by tail venesection on days 0, 7, 14, 21, 28, 35 with a final bleed on day 42. At day 28, mice were given a booster dose of stored sample of the same condition.

6.2.2.4 ELISA serum analysis

Native lysozyme was coated on a 96-well microtitre plate (10 µg / ml, 100 µl / well) at 4°C overnight in PBS pH 7.4. Plates washed 3x with PBS and blocked with 1% Casein in PBS-T (0.05%) for 2 hours. After four washes serum was added. This was diluted in a two-fold titration starting at 50 times dilution and corrected for serum volume before being transferred to the ELISA plate. Monoclonal, Hyhel-10[258], antibody was added to two wells in each plate and diluted accordingly with the samples.

This was used to normalise the plates. After 1-hour incubation, goat-anti-mouse IgG + HRP was added in 1:5000 dilution to PBS-T (0.05%) and added to each plate for another 1-hour incubation at room temperature. Finally, after extensive washing, TMB substrate was added and the reaction ended after addition of 10% H_2SO_4. Absorbances were read at 450 nm with a reference at 650 nm and subtracted subsequently.

6.2.2.5 ELISA data processing

Serum absorbances collected for all conditions were normalised using the HyHel-10 monoclonal antibody responses. These values were output in relative units (RU) and allowed comparison between all ELISA plates. Samples were plotted in RU responses at 200x dilution over the experiment duration. An overview of all responses per day is visualised in the Appendix A.13. Samples that showed deviating responses with a blood sample volume below 10 µl were masked. Minimum replicates were n=3 up to n=5.

6.2.3 Calorimetric analysis of lysozyme using CD

Ensilicated lysozyme was released, in triplicate, and dialysed according as previously described (section 5.2.8). The measurement settings were identical to the TTCF experiments. Triplicate batches of native lysozyme, reconstituted in sodium phosphate buffer, were analysed using the thermal CD ramp[253]. Data recorded data in millidegrees was normalised to delta epsilon. Spectral data at 222 nm was fitted using the same equation as for TTCF. Thermal transition temperatures and van 'T Hoff plots were visualised using MatLab™.

6.3 Results & Discussion

6.3.1 Lysozyme crystal structure

Lysozyme crystals were formed after several days of incubation at ambient temperature. One of these crystals was placed into the sample holder for the XRD (see

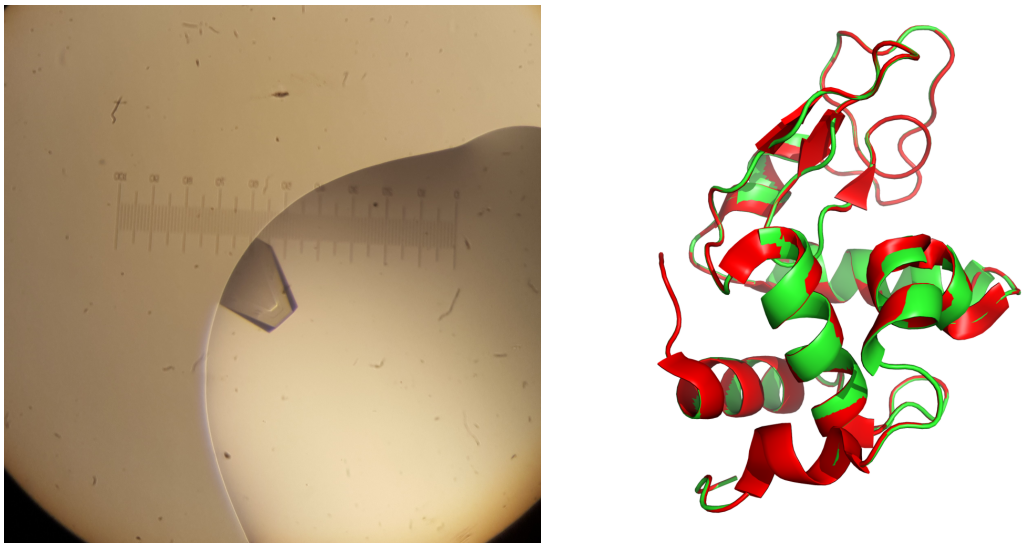

Figure 6-1: Released lysozyme crystal and refined 3D structure. (left) released lysozyme crystal grown after 5 days incubation. (right) refined 3D structure of released lysozyme overlayed with the hen-egg white lysozyme PDB 2w1x[259] structure used for molecular replacement.

collection and refinement details, Appendix A.12). After alignment and additional checks, the diffraction patterns were collected and the model was refined using the PDB 2w1x[259] protein sequence for molecular replacement (figure 6-1). The compiled protein structure from released lysozyme was overlayed with 2w1x. The results found a 100% match between both crystal structures. This confirmed complete structural retention of hen egg-white lysozyme after ensilication.

6.3.2 Lysozyme *in vivo*

Protein concentrations of prepared material were quantified using BCA (table 6-1). Based on these values, the enzyme kinetics were assessed using the Enzcheck™ analysis. Results showed good consistency between native and ensilicated treated material. Following dialysis and sterile filtration, LPS was added and this solution was subsequently injected into the animals. Serum samples were shipped after

Sample	BCA	Enzcheck™	
	mg/ml	IU	IU/ml
native	2.70	85719	31747
released	0.48	16576	34533
released (heated)	0.53	6110	11528
denatured	1.11	73	66

Table 6-1: Lysozyme, ensilicated sample preparation for *in vivo* study. Proteins concentrations for each sample was quantified using BCA and subsequently checked for enzyme activity in IU/ml.

completion of the experiment and analysed using ELISA (overview per day, Appendix A.13). The responses were compared to internal HyHEL-10 standard and visualised (figure 6-2). Master sample represented ensilicated lysozyme produced (and released here for *in vivo*) during the proof-of-concept study for this protein[227], which had been stored for over 3 years. Other samples were made 1 month before the *in vivo* study.

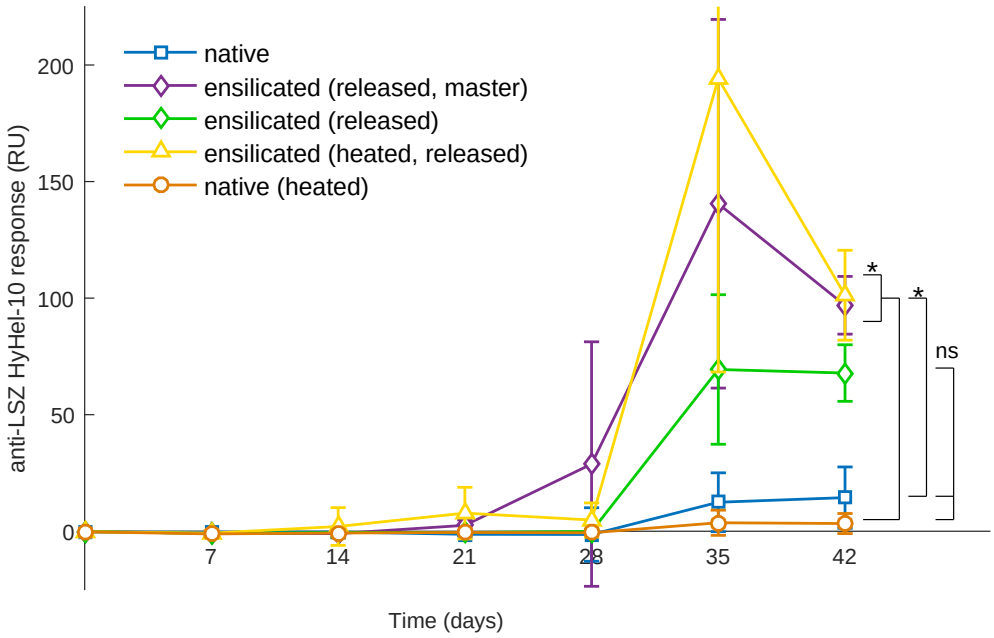

Figure 6-2: Lysozyme *in vivo* serum responses measured by ELISA. 5 mice per group were injected, intra-peritioneally, with native, released (including master sample), heat treated released and heated native lysozyme. Serum was collected each week and analysed using ELISA. Master sample stored > 3 years at room temperature was used for long term stability assessment. Average responses, normalised using HyHel-10 monocolonal, at 200x dilution are visualised. Statistical analysis was carried out using a one-way ANOVA with post-hoc Tukey HSD where *P <0.05, ns = non-significant.

Lysozyme is an antigen to mice and the *in vivo* experiment showed an increased response for released and heated treated released material compared to others. The latter presented the highest responses with great variation in each time point. A possible explanation for the could be the increased adhesion of LPS to a partially unfolded protein that exposed its hydrophobic region. Adhesion of LPS to lysozyme has been utilised before[260]. In this study, the binding of lysozyme to LPS prevented a normal immune response to LPS which includes septic shock. The suggestion of a partially unfolded protein can be deduced from the enzymatic activity of this sample which was a third compared to released. This could have then enhanced the immunological response to the lysozyme which was seen in the serum responses.
It is apparent that there was no initial response in all groups after injection. This could be because of tolerance. When a foreign protein is introduced in the body, there is a threshold presence after which the immune system will tolerate such an entity[261]. It is unclear why native lysozyme with added LPS did not respond and therefore this experiment should be repeated.

6.3.3 Calorimetric analysis of lysozyme using CD

Spectrophotometric measurements of lysozyme while heating allowed assessment of protein thermal stability using circular dichroism (Appendix A.14). Thermodynamic analysis of lysozyme unfolding showed no significant difference in thermal transition temperatures between native and released lysozyme (figure 6-3). These were 73.47 °C ± 0.12 °C for native and agreed with literature values[262–264]. Released lysozyme showed a T_m of 72.10 °C ± 0.99 °C. Statistics using *t*-test calculated $P > 0.05$ therefore retaining the null hypothesis. This aligned with findings, which were seen in the TTCF experiments and confirms the thermal resilience of ensilicated protein.

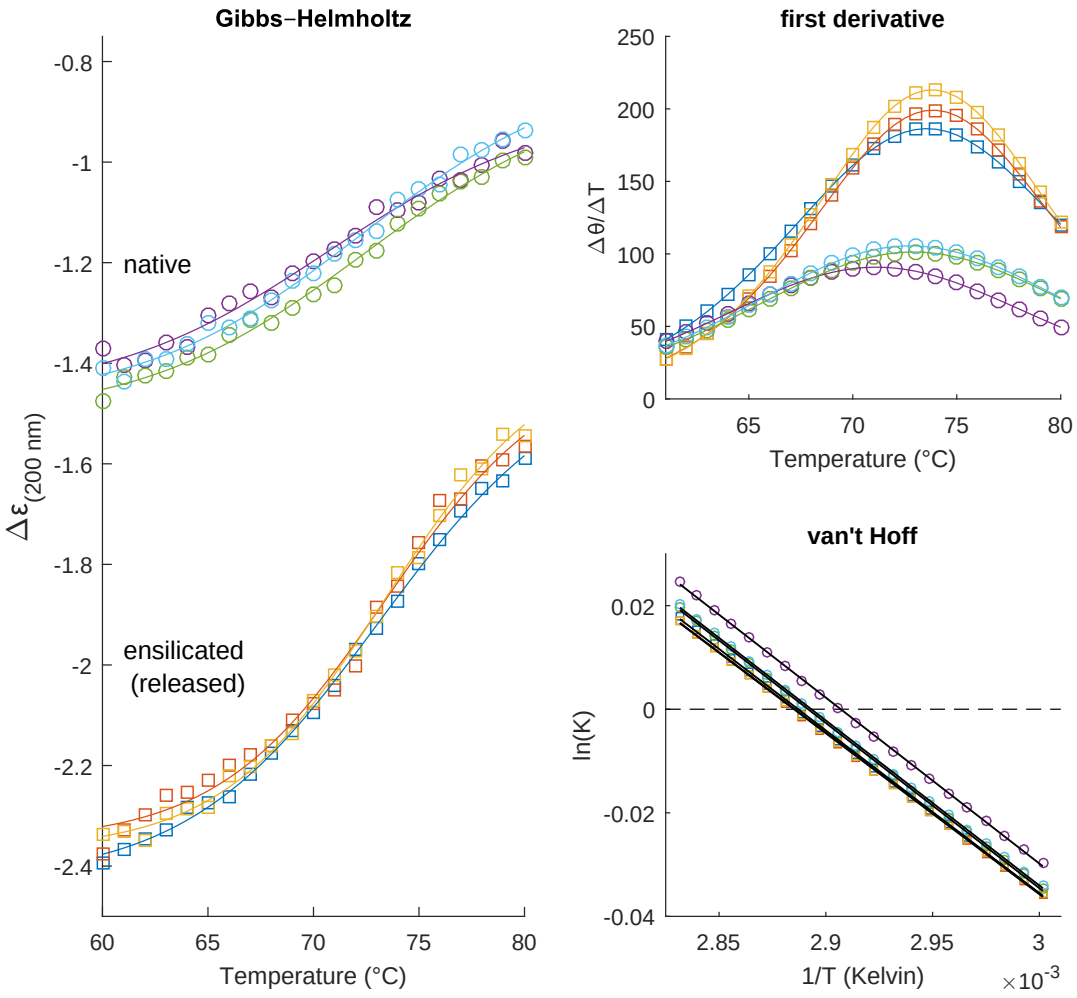

Figure 6-3: Lysozyme fitted CD data van'T Hoff plots and first derivatives. (left) Non-linear least squares regression fits to native and released lysozyme. (top right) First derivatives of fitted CD spectra. Peaks correlate with thermal unfolding of lysozyme. (bottom right) van 't Hoff plot of lysozyme unfolding. Statistical analysis performed using Student's *t* test.

6.4 Summary

The capability of ensilication to retain native structure was examined using XRD. The crystallisation of released lysozyme and subsequent analysis by XRD showed an exact match with PDB 2w1x crystal model of native hen egg-white lysozyme[259]. This showed that protein folding was unaffected by ensilication and release.

The *in vivo* lysozyme experiment showed no significant differences observed between the released, native and denatured lysozyme. This may be due to the high variability seen within each group. The released heated sample induced the overall highest immune response and can be related to a partially unfolded protein. This was deduced from the enzymatic analysis. Additionally, there were no immediate responses after immunisation suggesting a possible dosage threshold. These observations are in contrast with the TTCF experiment and suggest further optimisation required in the experimental design.

Calorimetric analysis of native and released lysozyme showed no significant difference in thermal midpoint transitions. Using circular dichroism and application of the thermodynamic fit, the data (n=3) strongly suggest no apparent influence of silica on the reconstituted protein conformation. This is in alignment with the biochemical and enzymatic data gathered in previous studies[203].

The evidence presented here shows that ensilication retains the protein structure of lysozyme after release. The calorimetric results confirm this finding and strengthen the applicability of ensilication to vaccines.

Chapter 7

Discussion

7.1 Aims of the project

Ensilication is a stabilising method for proteins that renders them immobilised within a silica matrix[203,227]. This physically prevents protein unfolding following exposure to thermal fluctuations, an event that is frequently seen during the shipment of vaccines[19,29–31,33,265,266]. The cold-chain logistics network, specifically built for this purpose, ensures refrigeration temperatures through distribution[15]. However, technical and handling errors plague this system[15,32,34,35]. Over half the vaccines are exposed to freezing and or heating[11]. As these valuable biological mixtures contain proteins, the exposure renders them ineffective resulting in a large proportion of people not vaccinated. Ensilication has been proven effective using a proxy protein, lysozyme[203,227]. Here, the native structure and functionality was retained even after stress testing the material. Ensilication is a sol-gel based process using TEOS as a precursor metal alkoxide. The hydrolysation yields polymeric species that encapsulates the protein within a silica shell[139]. Ensilicated protein is then converted in to a dried powder to be stored and used when required. This study intended to build on this previous success and expand it towards its ultimate use: developing thermostable vaccines.

7.2 Properties of TTCF

Several methodologies were utilised to understand and assess the native state of TTCF and its biochemical parameters before progressing towards ensilication.
SDS-PAGE showed a band at 52 kDa which was the reported molecular weight

of this protein[181]. TTCF occasionally showed an additional band at 44 kDa and this was likely due to the presence of bound cysteine residues which were not fully reduced[178]. The addition of DTT should have prevented this but could be improved with increased duration of the sample incubation.
Far-UV CD data showed the presence α-helices with equal proportions of β-sheets and random coils in line with an earlier study on TTCF[180]. Near-UV data were not measured as the tertiary structure was assessed using another sensitive methodology.
ELISA, using a monoclonal antibody raised against TTCF, showed a sigmoidal dose response as expected[161]. A histidine antibody was utilised as a capture antibody but presented cross binding with the detection antibody (10G5). This situation was resolved by coating the protein directly onto the microtitre plate well surface. However, this resulted in the protein being partially disguised from the detection antibody. In future studies, this method could be improved with the utilisation of a capture antibody without cross-binding.
DLS, after several attempts, provided the hydrodynamic diameter of 7.345 $\pm$ 2 d.nm and zeta-potential, +3.54 mV, in Tris buffer. The former was in line with sizes reported in the crystal structure[164]. The latter indicated an unstable solution of TTCF at pH 7 in Tris buffer with, more importantly, an overall positive charge. This was assumed from the results with lysozyme[227].
Bioinformatics using the PDB:1A8D TTCF structure proved useful in mapping positive and negatively charged regions which confirmed the suitability of this protein for ensilication[227].

7.3 Ensilication of TTCF

TTCF was successfully ensilicated with an average incorporation of 64%. We believed this was an acceptable level of incorporation as at least half of the protein used for ensilication is stabilised. However, recombinant proteins are an expensive source material and therefore improving the ensilication efficiency is imperative. One way of doing so could be the introduction of electrostatic effectors or balancing the ionic strength. Achieving this would shift the overall outer charge of the protein exposed to the aqueous environment and make it more favourable for silica species, undergoing condensation and polymerisation, to improve attachment. Lysozyme is a positively charged protein with a pI $>$ 11 and has 95% ensilication efficiency[227], which makes a good argument for altering the surface charges as the zeta-potential

for TTCF was identified to be in the unstable region. DLS could measure the stabilising charge effects of added solutes, which would have to be compatible with the ensilication process.

The material was analysed using FE-SEM and showed angled ellipsoidal particles with sizes ranging from 200 - 400 nm. This was due to the apparent aggregation and agglomeration that occurs during ensilication and drying of the material. At present, this is not an issue as we are setting a precedent for vaccine thermostabilisation via ensilication. For future uses it is necessary to optimise and control particle size of protein-silica conglomerates and implement uniformity to create a consistent material. Another study done within our group found a possible way[267]. The study focused on the ensilication of lysozyme using flow-chemistry and showed control over particle size by using either glycine or lysine instead of tris in combination with the removal of chloride ions[267]. This was a promising find and needs further exploration.

It would also help to add an easier way of extracting small amounts of filtrate. This, however, renders a new possible issue that might come to pass if this method is taken to larger quantities: scalability.

FT-IR and UV-vis confirmed the incorporation of protein within silica. The absorbances of amide peaks and convolution of both SiO_2 and protein were evident. Comparison between triplicate batches revealed no differences in morphology. This, however, does not indicate whether the material can be released, to check if it has been vitrified. Using release buffer and testing the material for release with use of ensilicated reference material as a control is, at time of writing, the only option. Investigation into the parameters that affect vitrification would reduce time and efforts spent on preparation of recombinant proteins and the subsequent waste of these.

Additionally, the addition of BCA reagent to ensilicated powder resulted in a dark purple colour developing. This indicated that there are peptide bonds available for the reduction of copper. This suggests exposure of protein partially incorporated within the material or that the material possesses enough porosity for the buffer to penetrate through the material. The latter would explain why it releases quickly.

The assessment of porosity for the aggregated conglomerates would be an interesting addition. The Brunauer–Emmett–Teller (BET) method is able to measure the surface area of a solid material[268]. However, if the pores are present they might be packed with protein and provide no additional information on the distribution of silica, whether this is vitrified or not. Initial experiments would elucidate if this occurs.

Due to the interference of silica in many methodologies, the conformation of protein

within the ensilicated matrix has not been addressed. An approach to this could be UV resonance Raman spectroscopy (UVRR). Based on the difference in relaxation energies of vibrational molecules it is sensitive to conformational changes of protein structures and other small molecules including polymers[269]. This was seen in a study where the conformation of sol-gel entrapped ligand-bound haemoglobin was studied[269,270]. Researchers were able to understand the conformational changes this protein underwent when incorporated within the silica matrix[270,271]. It would be an appropriate strategy to pursue and complete the analysis of ensilicated material.

7.4 Mechanism of TTCF ensilication

To probe the stabilisation mechanism of ensilication, SAXS was employed. This methodology provides an averaged representable image of processes occurring at nanometre scale[221–226]. TTCF was ensilicated while being monitored *in situ* and for a longer duration at two independent beamlines[234]. Data gathered from these experiments provided comparable images. It was found that TTCF has an ellipsoidal shape using the distance distribution function and fitting using an ellipsoidal model with a goodness of fit (χ^2) close to 1. Other types of analysis such as the Kratky plot confirmed this observation.

The shape and morphology of TTCF were calculated based on one concentration. To strengthen our observations, additional concentrations should have been employed as these can influence protein morphology or aggregation[272]. Unfortunately, there were limited amounts of material available. For future experiments, it would be advised to include 0.5 mg/ml up to 5 mg/ml protein concentrations.

Ensilication under standard conditions proceeded rapidly within the first two minutes. Analysis of the data gathered in this window showed a three staged transition. First, ångström sized silica particulates attached to the protein therefore increasing its scattering intensity. Second, the apex of the ellipsoidal particle shifted towards the low-q region of the SAXS plot which indicated particle growth. Finally, it was apparent a fractal-like object was forming.

Additionally, TTCF was ensilicated at different ratios and pH. The analysed data displayed the effect of these parameters on the ensilication process. Changing the ratios increased or decreased the speed of the ensilication process with 1:20 progressing faster towards a fractal stage and 1:100 slowing down to provide increased resolution between stage I and II. Adjusting both parameters led to a interesting effect seen in the pH 8 and 1:100 ratio. The particles formed seem to stabilise early

on without aggregation occurring. This process did not progress towards the latter stage which might be indicative of a limiting factor such as the depletion of silicate polymeric species[139].

The initial observations, on the onset of ensilication, were made based on data from the *in situ* experiment (i22) which were gathered from one session. The experiments where ensilication was initiated *ex situ* (ID02) had multiple repeats on several parameters and displayed a consistent image. Therefore, an argument could be made for repeating the initial experiment to show reproducibility. Another argument could be made for repeating the *ex situ* experiments with agitation. This would confirm the DLCA process as agitation improves particle collision in solution, thereby affecting diffusion.

Fitting of the SAXS data was initially focussed on the basis of a core-shell ellipsoid[241]. This model was assumed on the hypothesis that TTCF was the central core and silica would form an even shell around, using TTCF protein as a template. This would lead to a monodisperse solution of TTCF-silica nanoparticles that would sediment and stick together. The reality did not differ much from this assumption. Fitting elucidated a DLCA type process where TTCF acted as a nucleation centre. This was deduced based on the slope of the SAXS plots which provided a fractal dimension, D_f. Our hypothesis assumed a perfect uniform particle, which would have a slope $D_f > 3$ indicating a surface fractal. The findings led to a D_f between 1.5 - 2 over several experiments which provided the understanding of the ensilication process. It would be interesting to run these SAXS experiments by adding other moieties to influence the fractal dimension.

7.5 Protein stability of TTCF and Lysozyme

Verifying protein stability of TTCF before and after release was carried out using the same methods for analysing primary, secondary and tertiary protein levels of native TTCF. Additional methods such as calorimetry aided in providing biophysical data.

Initial release of ensilicated TTCF showed retention of structure and antibody binding capacity of the protein. This set the basis for proceeding towards the thermal stability experiment. Heated ensilicated material withstood 2 hours of extreme temperatures showing ensilication to possess an exceptional level of thermal resilience. There were slight differences in CD spectra, representing secondary structures, however these were found not to be significant as confirmed using ELISA which indicated no difference in tertiary structure.

In a study where tetanus toxoid (TT), i.e. the full inactivated protein, was encapsulated in PGLA micro-spheres, researchers found similar observations using CD and ELISA[119]. Additionally, they performed a long term thermal stability experiment at elevated temperature, 37°C, for >6 - 30 days and determined the functional level of the protein. It was shown that the addition of amino acid excipients improved the stability of PGLA encapsulated TT[119].

The final test of protein stability was to conduct an *in vivo* study. This would help to show immunogenic retention of heat treated and released TTCF ensilicated material. The study showed no significant difference between the native,released and heat treated released material. There was a significant difference between these groups and the denatured native antibody responses which supported the findings. The secondary immunisation showed an increase in the measure serum immune response, however we expected a higher increase as seen in *in vivo* data for tetanus toxoid[273]. This could have been due to the lack of alum adjuvant which is commonly utilised.

Future projects will have to investigate the incorporation of adjuvants within the silica matrix. The current understanding is that metal ions (specifically aiming at alum) will influence the sol-gel process, therefore there might be some difficulty with alum[139]. The worst case scenario is where aluminosilicates are formed, zeolites. Possible solution to this problem would be to ship ensilicated vaccines with vials of adjuvants which can be kept at room temperature due to the absence of protein. After reconstitution and release of ensilicated material, this could be mixed with the adjuvant. Syringe filter injection needles could then prevent any undissolved silica from passing into the patient. Protein based adjuvants would not pose a problem as these could be incorporated together with the antigenic protein.

The preparation of samples during the *in vivo* experiment involved release and dialysis. Therefore, further studies will be required to investigate the toxicology of TTCF-silica nanoparticles (in buffer) if injected directly. Moreover, there has been a study that uses protein-silica nanoparticles coated in combination with polyethyleneimine (PEI) which successfully demonstrated this as a viable injectable vaccine delivery carrier for the Japanese encaphelitis virus (JEV)[274].

Calorimetric experiments were carried out to understand the biophysics of protein folding. Powder DSC and TGA-DTA-MS showed no endothermic transitions in ensilicated material that could indicate protein unfolding. Calorimetric analysis of a CD temperature ramp elucidated the equilibrium constant and T_m value (60°C) at which the TTCF protein unfolded. There were no significant differences found between the

T_m of native, released and heat treated released TTCF. This confirmed that silica did not structurally affect the TTCF protein. Native and released lysozyme were also assessed using the method above and showed no difference in T_m values. This was confirmed in another study where lysozyme was ensilicated at various ratios, 1:20, 1:50 and 1:100[275]. The calorimetric analysis using µDSC of native and released lysozyme were in alignment with the findings here.

Ensilicated, released lysozyme was crystallised and analysed using x-ray diffraction and showed full retention of native structure. The refined model matched the crystal model of native lysozyme[259] and confirmed that ensilication works with other proteins. Crystallisation of released TTCF was attempted, however no crystals formed during this project.

The *in vivo* experiment of lysozyme showed immune responses to released, heat treated but not native lysozyme. The results from this experiment indicated experimental optimisation to be required.

Long term storage of ensilicated TTCF is possible. The analysis of released TTCF uncovered the main problem with the ensilication methodology. Vitrification of ensilicated material resulted in a situation where the protein could not be released by the standard NaF buffer. The reason why the ensilicated material vitrified is thought to be due to environmental conditions when ensilication occurs. Temperature, humidity and drying speed can affect the end material. The only way to establish that TTCF was present in the ensilicated material was to dissolve the silica with NaOH. This is a highly denaturing condition, however allowed the measurement of polypeptide length and serum polyclonal antibody binding. These showed retention of the material up to two years at ambient temperatures. This sets a precedent for sustainability of ensilicated vaccine storage compared to conventional around the clock refrigeration.

7.6 Other work

Enzymatic digestion, using trypsin, of ensilicated TTCF was performed to understand which parts of TTCF were ensilicated and exposed. The attempts in visualising this were not successful, however are still of interest. The reason could be because of steric hindrance, where the enzyme catalytic site is sterically hindered from catalysing exposed amino acid residues. If a solution could be found, these short polypeptides could then be visualised using Western Blot for specificity or SDS-PAGE for molecular weight. Additionally, mass-spectrometry could be utilised to support

the findings.
Manduca Sexta caterpillars were also used to test the release of ensilicated proteins. These insects do no possesses a mammalian immune system and were used to verify whether ensilicated material could be ingested, digested and measured in their blood. The ELISAs performed on the collected blood did not show a measurable signal compared to control. Oral delivery is still of interest and could be explored and optimised in the future. A preliminary study done in our group showed the release of lysozyme when passed through an artificial digestive system[203].
Another project within our group involved the use of a monoclonal antibody against breast cancer, Rituximab™. Here, we ensilicated the antibody and verified its molecular integrity using a method designed in the Pudney group at the University of Bath[276]. It was based on the fluorescence spectroscopy of tryptophan residues. By measuring the area under the curve and integrated this with a mathematical model which would calculate its central spectral mass (CSM)[277]. The model provided additional parameters that could elucidate whether the protein was unfolded, aggregated (the main problem with antibodies which reduces their functionality) or was moving towards either direction. We found released Rituximab™ to have a similar CSM to that of native, thereby confirming it could be successfully stabilised using ensilication[278].

7.7 Future perspectives

Ensilication has been shown to perform excellently for stabilising TTCF and does not affect the structural integrity of the protein after release. The successful response *in vivo* shows the feasibility of ensilication to thermally stabilise vaccines. As TTCF is part of the DTP vaccine, a logic path forward is to work towards a thermostable DTP vaccine. Each of the additional bacterial antigens could be ensilicated. The approach towards assessment of these would be in line with the approach for TTCF. The main parameter that would need extensive investigation is the use of metal salts for boosting the immune response and ensuring longevity of protection[79]. Metal salts, however, influence the ensilication procedure[139]. Positively charged ions could have an impact on the soluble silica species, which are negatively charged, preventing them from adhering to and polymerising around the protein of interest. An argument could be made for adding metal salts after release, which could simplify storage and avoid drastic changes to the ensilication process.
There is an argument for the addition of rotary evaporation during the preparation of

hydrolysed TEOS as it would eliminate ethanol which is protein denaturing.
Buffer optimisation is another field in which ensilication could benefit. Short experiments showed glycine to be an effective replacement for tris buffer. This has a lower pKa which could improve electrostatic control and preferential hydration[84]. A study where additives were used to stabilise adenovirus vectors showed an improvement in thermal stability from hours to months[279]. The researchers employed simple chemical moieties such as poly-ethylene-glycol and sucrose to enhance the stability of these viruses and showed the importance of simple rational design.
The release method involves the formation of hydrofluoric acid (HF^-), which is able to chelate proteins, for the dissolution of silica. This acid affects protein tertiary structure and would be unsuitable for ultimate use. Therefore, alternatives will need to be investigated.
Finally, the process will have to be made scalable. Vaccine manufacturers produce antigens in batches that will create tens of thousands of doses. The ability to stabilise this high amount of purified protein is essential for ensilication and requires more investigation.

7.8 Conclusion

This project utilised biochemical and physical methodologies to understand and assess the native state of TTCF. TTCF was successfully ensilicated with the analysis showing incorporation of protein within the silica shell. The retention of TTCF protein structure before and after ensilication was verified and showed no significant differences. SAXS experiments at two different locations provided an aligned view on the stabilisation mechanism of ensilication. This was classed as a staged diffusion limited cluster aggregation type reaction. Protein immobilisation in silica was shown to have no influence on TTCF and lysozyme protein state after release measured by calorimetry. Immunogenicity of released and heat treated TTCF was maintained and shown in the *in vivo* study. Ensilicated material showed retention of TTCF after long term storage, up to two years. These observations confirm that ensilication can be utilised for the development of thermostable vaccines which could lead to the end of the road for cold chain vaccine transportation.

Appendix A

A.1 ExPasy ProtParam analysis

FASTA sequence of recombinant TTCF:

10	20	30	40	50
MGHHHHHHHH	HHSSGHIEGR	HMLDNEEDID	VILKKSTILN	LDINNDIISD
60	70	80	90	100
ISGFNSSVIT	YPDAQLVPGI	NGKAIHLVNN	ESSEVIVHKA	MDIEYNDMFN
110	120	130	140	150
NFTVSFWLRV	PKVSASHLEQ	YGTNEYSIIS	SMKKHSLSIG	SGWSVSLKGN
160	170	180	190	200
NLIWTLKDSA	GEVRQITFRD	LPDKFNAYLA	NKWVFITITN	DRLSSANLYI
210	220	230	240	250
NGVLMGSAEI	TGLGAIREDN	NITLKLDRCN	NNNQYVSIDK	FRIFCKALNP
260	270	280	290	300
KEIEKLYTSY	LSITFLRDFW	GNPLRYDTEY	YLIPVASSSK	DVQLKNITDY
310	320	330	340	350
MYLTNAPSYT	NGKLNIYYRR	LYNGLKFIIK	RYTPNNEIDS	FVKSGDFIKL
360	370	380	390	400
YVSYNNNEHI	VGYPKDGNAF	NNLDRILRVG	YNAPGIPLYK	KMEAVKLRDL
410	420	430	440	450
KTYSVQLKLY	DDKNASLGLV	GTHNGQIGND	PNRDILIASN	WYFNHLKDKI
460				
LGCDWYFVPT				

Amino acid composition:

Ala (A)	18	3.90%	Lys (K)	32	6.90%
Arg (R)	17	3.60%	Met (M)	8	1.70%
Asn (N)	48	10.30%	Phe (F)	17	3.60%
Asp (D)	33	7.10%	Pro (P)	14	3.00%
Cys (C)	3	0.60%	Ser (S)	37	7.90%
Gln (Q)	7	1.50%	Thr (T)	21	4.50%
Glu (E)	18	3.90%	Trp (W)	8	1.70%
Gly (G)	29	6.20%	Tyr (Y)	28	6.00%
His (H)	19	4.10%	Val (V)	24	5.10%
Ile (I)	42	9.00%	Pyl (O)	0	0.00%
Leu (L)	44	9.40%	Sec (U)	0	0.00%

A.1.1 TTCF descriptors

Number of amino acids: 467
Molecular weight: 53545.50
Theoretical pI: 6.83

Total number of negatively charged residues (Asp + Glu): 51
Total number of positively charged residues (Arg + Lys): 49

Atomic composition:

Carbon	C	2412
Hydrogen	H	3699
Nitrogen	N	651
Oxygen	O	711
Sulfur	S	11

Formula: $C_{2412}H_{3699}N_{651}O_{711}S_{11}$
Total number of atoms: 7484

Extinction coefficients:
Extinction coefficients are in units of M^{-1} cm^{-1} at 280 nm measured in water.
Ext. coefficient 85845
Abs 0.1% (=1 g/l) 1.603, assuming all pairs of Cys residues form cystines
Ext. coefficient 85720
Abs 0.1% (=1 g/l) 1.601, assuming all Cys residues are reduced

A.2 1:50 SAXS data tables

Diamond Data Fit - Parameter Output (Stage I)

= fixed values

= key variables

		min	max	unit
Limits	p2_radius (equatorial)	45	200	Å
	p2_radius (polar)	15	150	Å
	p3_cut-off length	0	inf	Å
	p3_radius (fractal)	1	10	Å

	Time	p1_background	p1_power	p1_scale	p2_background	p2_radius (equatorial)	p2_radius (polar)	p2_scale	p2_sld	p2_sld_solvent	p3_background	p3_cut-off length	p3_fractal_dim_mass	p3_radius (fractal)	p3_scale	scale_factor	χ^2
unit	(seconds)	(mm^{-1})	-	-	(mm^{-1})	Å	Å	-	$*10^6/Å^2$	$*10^6/Å^2$	(mm^{-1})	Å	-	Å	-	-	
	5	0.0006	3.1	6.35E-08	0	24.23	52.61	4.78E-05	17.5	9.44	0	8.14	1.1	4.24	0.001	1	2.72
	6	0.0006	3.1	7.17E-08	0	24.72	52.34	4.56E-05	17.5	9.44	0	8.92	1.1	4.36	0.001	1	3.17
	7	0.0006	3.1	5.82E-08	0	24.73	53.94	4.47E-05	17.5	9.44	0	9.58	1.1	4.41	0.001	1	3.28
	8	0.0006	3.1	6.12E-08	0	25.13	54.56	4.28E-05	17.5	9.44	0	10.32	1.1	4.39	0.001	1	2.73
	9	0.0006	3.1	7.14E-08	0	25.34	55.34	4.17E-05	17.5	9.44	0	11.05	1.1	4.44	0.001	1	2.97
	10	0.0006	3.1	6.61E-08	0	25.21	57.25	4.14E-05	17.5	9.44	0	11.54	1.1	4.44	0.001	1	3.01
	11	0.0006	3.1	7.41E-08	0	26.54	57.92	3.78E-05	17.5	9.44	0	12.71	1.1	4.38	0.001	1	3.06
	12	0.0006	3.1	7.34E-08	0	26.29	59.32	3.74E-05	17.5	9.44	0	13.33	1.1	4.42	0.001	1	2.49
	13	0.0006	3.1	8.09E-08	0	25.94	63.40	3.81E-05	17.5	9.44	0	13.82	1.1	4.34	0.001	1	2.46
	14	0.0006	3.1	7.65E-08	0	26.51	65.38	3.58E-05	17.5	9.44	0	15.05	1.1	4.40	0.001	1	3.03
	15	0.0006	3.1	7.99E-08	0	26.75	72.14	3.50E-05	17.5	9.44	0	15.91	1.1	4.33	0.001	1	2.92
	16	0.0006	3.1	7.98E-08	0	27.68	73.78	3.25E-05	17.5	9.44	0	17.43	1.1	4.54	0.001	1	3.16
	17	0.0006	3.1	7.93E-08	0	27.64	80.14	3.27E-05	17.5	9.44	0	17.92	1.1	4.56	0.001	1	2.93
	18	0.0006	3.1	8.43E-08	0	28.89	82.84	3.04E-05	17.5	9.44	0	19.35	1.1	4.55	0.001	1	2.66
	19	0.0006	3.1	7.53E-08	0	29.37	92.14	2.94E-05	17.5	9.44	0	20.61	1.1	4.67	0.001	1	2.91
	20	0.0006	3.1	8.25E-08	0	30.23	94.13	2.86E-05	17.5	9.44	0	21.70	1.1	4.65	0.001	1	2.47
	21	0.0006	3.1	8.15E-08	0	31.68	106.40	2.64E-05	17.5	9.44	0	24.03	1.1	4.61	0.001	1	2.83
	22	0.0006	3.1	7.92E-08	0	33.18	112.18	2.53E-05	17.5	9.44	0	25.61	1.1	4.74	0.001	1	3.13
	23	0.0006	3.1	8.10E-08	0	34.75	117.92	2.40E-05	17.5	9.44	0	27.75	1.1	4.72	0.001	1	3.24
	24	0.0006	3.1	7.42E-08	0	36.79	125.13	2.27E-05	17.5	9.44	0	30.74	1.1	4.83	0.001	1	4.15
	25	0.0006	3.1	8.16E-08	0	38.67	126.78	2.15E-05	17.5	9.44	0	33.32	1.1	4.95	0.001	1	4.40
	26	0.0006	3.1	7.40E-08	0	40.79	129.80	2.05E-05	17.5	9.44	0	36.82	1.1	4.88	0.001	1	3.47
	27	0.0006	3.1	7.94E-08	0	42.78	139.26	1.97E-05	17.5	9.44	0	40.82	1.1	4.80	0.001	1	4.25
	28	0.0006	3.1	7.77E-08	0	44.41	137.23	1.94E-05	17.5	9.44	0	43.77	1.1	4.78	0.001	1	4.01
	29	0.0006	3.1	7.36E-08	0	46.33	137.26	1.95E-05	17.5	9.44	0	45.99	1.1	4.83	0.001	1	3.46
	30	0.0006	3.1	7.11E-08	0	46.89	145.21	2.02E-05	17.5	9.44	0	48.03	1.1	4.83	0.001	1	4.28
	31	0.0006	3.1	7.22E-08	0	48.87	150.95	1.94E-05	17.5	9.44	0	55.05	1.1	4.89	0.001	1	3.33
	32	0.0006	3.1	8.58E-08	0	49.96	151.17	1.97E-05	17.5	9.44	0	56.85	1.1	4.90	0.001	1	3.88
	33	0.0006	3.1	9.06E-08	0	50.38	155.97	2.01E-05	17.5	9.44	0	61.49	1.1	4.87	0.001	1	3.40
	34	0.0006	3.1	8.87E-08	0	50.30	160.57	2.11E-05	17.5	9.44	0	58.77	1.1	4.91	0.001	1	3.56
	35	0.0006	3.1	9.30E-08	0	51.00	161.80	2.12E-05	17.5	9.44	0	63.27	1.1	4.89	0.001	1	3.04
	36	0.0006	3.1	9.30E-08	0	51.00	161.80	2.12E-05	17.5	9.44	0	63.28	1.1	4.89	0.001	1	3.04
	37	0.0006	3.1	1.10E-07	0	51.41	159.72	2.12E-05	17.5	9.44	0	67.14	1.1	4.87	0.001	1	3.63
	38	0.0006	3.1	1.17E-07	0	51.29	159.91	2.12E-05	17.5	9.44	0	68.02	1.1	4.90	0.001	1	2.95
	39	0.0006	3.1	1.33E-07	0	51.40	146.45	2.08E-05	17.5	9.44	0	70.68	1.1	5.03	0.001	1	3.30
	40	0.0006	3.1	1.40E-07	0	51.38	139.79	2.03E-05	17.5	9.44	0	75.34	1.1	4.91	0.001	1	3.10
	41	0.0006	3.1	1.46E-07	0	50.84	138.78	2.04E-05	17.5	9.44	0	76.98	1.1	4.93	0.001	1	3.50
	42	0.0006	3.1	1.57E-07	0	49.80	137.01	2.06E-05	17.5	9.44	0	77.05	1.1	4.94	0.001	1	3.63
	43	0.0006	3.1	1.59E-07	0	49.63	131.53	2.00E-05	17.5	9.44	0	80.38	1.1	4.90	0.001	1	3.51
	44	0.0006	3.1	1.64E-07	0	48.95	133.12	1.99E-05	17.5	9.44	0	84.48	1.1	4.83	0.001	1	3.84
	45	0.0006	3.1	1.65E-07	0	49.52	121.27	1.90E-05	17.5	9.44	0	89.18	1.1	5.06	0.001	1	4.66
	46	0.0006	3.1	1.67E-07	0	48.59	116.87	1.87E-05	17.5	9.44	0	94.07	1.1	4.91	0.001	1	5.06
	47	0.0006	3.1	1.74E-07	0	48.61	109.20	1.80E-05	17.5	9.44	0	108.49	1.1	4.95	0.001	1	5.49
	48	0.0006	3.1	1.76E-07	0	48.63	102.22	1.75E-05	17.5	9.44	0	115.89	1.1	5.03	0.001	1	5.48
	49	0.0006	3.1	1.81E-07	0	49.88	90.25	1.64E-05	17.5	9.44	0	140.21	1.1	4.95	0.001	1	6.55
	50	0.0006	3.1	1.71E-07	0	50.27	83.66	1.58E-05	17.5	9.44	0	152.86	1.1	5.14	0.001	1	6.32
	51	0.0006	3.1	1.75E-07	0	51.90	74.35	1.50E-05	17.5	9.44	0	196.13	1.1	5.04	0.001	1	5.98
	52	0.0006	3.1	1.67E-07	0	50.52	75.96	1.50E-05	17.5	9.44	0	216.70	1.1	4.89	0.001	1	6.99
	53	0.0006	3.1	1.65E-07	0	52.66	66.65	1.46E-05	17.5	9.44	0	246.66	1.1	4.93	0.001	1	6.14
	54	0.0006	3.1	1.63E-07	0	56.03	55.96	1.45E-05	17.5	9.44	0	282.53	1.1	4.96	0.001	1	7.06
	55	0.0006	3.1	1.59E-07	0	55.14	56.10	1.41E-05	17.5	9.44	0	392.48	1.1	4.96	0.001	1	7.60
	56	0.0006	3.1	1.59E-07	0	54.43	54.41	1.43E-05	17.5	9.44	0	383.83	1.1	4.91	0.001	1	8.07
	57	0.0006	3.1	1.59E-07	0	53.93	53.84	1.44E-05	17.5	9.44	0	389.66	1.1	4.97	0.001	1	8.94
	58	0.0006	3.1	1.61E-07	0	53.12	53.18	1.46E-05	17.5	9.44	0	472.24	1.1	4.81	0.001	1	9.18
	59	0.0006	3.1	1.62E-07	0	52.56	52.52	1.48E-05	17.5	9.44	0	428.91	1.1	4.90	0.001	1	11.09
	60	0.0006	3.1	1.49E-07	0	52.21	52.20	1.44E-05	17.5	9.44	0	665.88	1.1	4.90	0.001	1	11.20

Diamond Data Fit - Parameter Output (Stage II)

= fixed values

= key variables

Limits		min	max	unit
	p1_lorentz_exp	0	5	-
	p1_lorentz_length	47	100	Å
	p1_peak_pos	0.025	0.05	Å
	p2_cutoff_length	0	inf	Å
	p2_radius	0	10	Å

	Time	p1_background	p1_lorentz_exp	p1_lorentz_length	p1_lorentz_scale	p1_peak_pos	p1_porod_exp	p1_porod_scale	p1_scale	p2_background	p2_cutoff_length	p2_fractal_dim_mass	p2_radius	p2_scale	scale_factor	χ^2
unit	seconds	mm^{-1}	-	Å	-	q	-	-	-	mm^{-1}	Å	-	Å	-		
	60	0.0006	4.49	54.88	80	0.030	2.65	0.006	2.9E-04	0	164.71	1.1	5.05	1.0E-03	1	11.8
	61	0.0006	4.29	53.74	80	0.029	2.65	0.006	3.1E-04	0	138.07	1.1	5.05	1.1E-03	1	11.9
	62	0.0006	4.57	53.88	80	0.030	2.65	0.006	3.0E-04	0	143.40	1.1	5.16	1.1E-03	1	12.0
	63	0.0006	4.26	52.82	80	0.030	2.65	0.006	3.1E-04	0	112.76	1.1	5.13	1.1E-03	1	11.8
	64	0.0006	4.31	49.30	80	0.028	2.65	0.006	3.3E-04	0	92.94	1.1	5.13	1.1E-03	1	10.6
	65	0.0006	4.14	51.66	80	0.029	2.65	0.006	3.3E-04	0	87.81	1.1	5.26	1.1E-03	1	11.0
	66	0.0006	4.44	47.56	80	0.028	2.65	0.006	3.3E-04	0	87.52	1.1	5.19	1.1E-03	1	10.2
	67	0.0006	4.23	49.86	80	0.029	2.65	0.006	3.4E-04	0	78.49	1.1	5.31	1.1E-03	1	10.1
	68	0.0006	4.13	48.45	80	0.029	2.65	0.006	3.4E-04	0	72.45	1.1	5.41	1.1E-03	1	8.5
	69	0.0006	4.19	50.03	80	0.029	2.65	0.006	3.4E-04	0	69.92	1.1	5.47	1.1E-03	1	9.3
	70	0.0006	4.28	49.44	80	0.029	2.65	0.006	3.4E-04	0	66.50	1.1	5.46	1.2E-03	1	10.1
	71	0.0006	4.41	47.03	80	0.028	2.65	0.006	3.4E-04	0	64.56	1.1	5.50	1.2E-03	1	8.4
	72	0.0006	4.18	48.48	80	0.029	2.65	0.006	3.5E-04	0	56.40	1.1	5.57	1.2E-03	1	8.5
	73	0.0006	4.29	48.29	80	0.029	2.65	0.006	3.5E-04	0	53.94	1.1	5.68	1.2E-03	1	7.7
	74	0.0006	4.21	47.60	80	0.029	2.65	0.006	3.5E-04	0	52.67	1.1	5.69	1.2E-03	1	8.2
	75	0.0006	4.01	48.16	80	0.029	2.65	0.006	3.6E-04	0	48.29	1.1	5.74	1.2E-03	1	7.8
	76	0.0006	4.14	49.29	80	0.030	2.65	0.006	3.5E-04	0	51.58	1.1	5.84	1.2E-03	1	7.6
	77	0.0006	4.15	48.68	80	0.030	2.65	0.006	3.4E-04	0	52.61	1.1	5.72	1.2E-03	1	7.1
	78	0.0006	4.06	48.59	80	0.030	2.65	0.006	3.7E-04	0	43.72	1.1	5.90	1.3E-03	1	7.2
	79	0.0006	4.26	47.93	80	0.030	2.65	0.006	3.6E-04	0	44.78	1.1	5.95	1.3E-03	1	7.7
	80	0.0006	4.11	48.22	80	0.030	2.65	0.006	3.6E-04	0	43.95	1.1	5.95	1.3E-03	1	6.2
	81	0.0006	3.99	48.63	80	0.030	2.65	0.006	3.6E-04	0	41.67	1.1	6.05	1.3E-03	1	6.7
	82	0.0006	3.93	48.68	80	0.030	2.65	0.006	3.7E-04	0	40.36	1.1	6.10	1.3E-03	1	7.3
	83	0.0006	3.95	47.00	80	0.030	2.65	0.006	3.8E-04	0	36.25	1.1	6.18	1.4E-03	1	6.3
	84	0.0006	4.06	47.00	80	0.030	2.65	0.006	3.7E-04	0	37.00	1.1	6.17	1.4E-03	1	6.3
	85	0.0006	4.02	47.35	80	0.030	2.65	0.006	3.7E-04	0	37.76	1.1	6.16	1.4E-03	1	5.5
	86	0.0006	3.92	49.66	80	0.031	2.65	0.006	3.7E-04	0	37.14	1.1	6.20	1.4E-03	1	5.6
	87	0.0006	3.78	48.59	80	0.031	2.65	0.006	3.9E-04	0	33.18	1.1	6.30	1.4E-03	1	6.1
	88	0.0006	4.04	47.57	80	0.031	2.65	0.006	3.7E-04	0	35.07	1.1	6.47	1.4E-03	1	5.7
	89	0.0006	3.77	47.49	80	0.031	2.65	0.006	3.8E-04	0	33.76	1.1	6.36	1.4E-03	1	4.9
	90	0.0006	3.83	47.00	80	0.031	2.65	0.006	3.8E-04	0	32.53	1.1	6.43	1.5E-03	1	6.2
	91	0.0006	3.78	47.81	80	0.031	2.65	0.006	3.9E-04	0	31.51	1.1	6.46	1.5E-03	1	5.2
	92	0.0006	3.68	48.61	80	0.032	2.65	0.006	3.9E-04	0	30.73	1.1	6.52	1.5E-03	1	5.8
	93	0.0006	3.74	47.68	80	0.031	2.65	0.006	3.9E-04	0	30.08	1.1	6.62	1.5E-03	1	5.2
	94	0.0006	3.73	47.97	80	0.031	2.65	0.006	3.9E-04	0	30.17	1.1	6.71	1.5E-03	1	4.9
	95	0.0006	3.68	48.39	80	0.032	2.65	0.006	3.9E-04	0	28.85	1.1	6.61	1.5E-03	1	4.7
	96	0.0006	3.68	49.26	80	0.032	2.65	0.006	3.8E-04	0	29.86	1.1	6.61	1.5E-03	1	5.4
	97	0.0006	3.65	47.25	80	0.032	2.65	0.006	3.8E-04	0	29.96	1.1	6.62	1.5E-03	1	5.0
	98	0.0006	3.59	48.67	80	0.032	2.65	0.006	4.0E-04	0	27.86	1.1	6.70	1.6E-03	1	5.6
	99	0.0006	3.64	47.96	80	0.032	2.65	0.006	4.0E-04	0	27.25	1.1	6.77	1.6E-03	1	5.5
	100	0.0006	3.59	48.32	80	0.032	2.65	0.006	3.9E-04	0	28.43	1.1	6.79	1.6E-03	1	4.8
	101	0.0006	3.59	47.92	80	0.032	2.65	0.006	3.9E-04	0	27.69	1.1	6.86	1.6E-03	1	5.6
	102	0.0006	3.55	48.29	80	0.032	2.65	0.006	3.9E-04	0	27.21	1.1	6.98	1.6E-03	1	5.6
	103	0.0006	3.43	48.23	80	0.033	2.65	0.006	4.0E-04	0	26.93	1.1	6.91	1.6E-03	1	5.0
	104	0.0006	3.40	48.28	80	0.033	2.65	0.006	4.1E-04	0	25.05	1.1	6.90	1.7E-03	1	5.8
	105	0.0006	3.45	48.37	80	0.033	2.65	0.006	4.0E-04	0	26.01	1.1	7.00	1.6E-03	1	5.1
	106	0.0006	3.34	48.49	80	0.033	2.65	0.006	4.0E-04	0	24.87	1.1	7.00	1.7E-03	1	5.9
	107	0.0006	3.33	48.53	80	0.033	2.65	0.006	4.0E-04	0	25.69	1.1	6.97	1.7E-03	1	5.0
	108	0.0006	3.28	48.61	80	0.033	2.65	0.006	4.0E-04	0	25.05	1.1	7.00	1.7E-03	1	5.4
	109	0.0006	3.23	48.99	80	0.033	2.65	0.006	4.1E-04	0	23.87	1.1	7.07	1.7E-03	1	6.0
	110	0.0006	3.30	48.40	80	0.033	2.65	0.006	4.0E-04	0	24.47	1.1	7.14	1.7E-03	1	6.1
	111	0.0006	3.24	48.89	80	0.033	2.65	0.006	4.1E-04	0	24.15	1.1	7.12	1.7E-03	1	5.7
	112	0.0006	3.40	48.79	80	0.033	2.65	0.006	4.0E-04	0	24.55	1.1	7.13	1.7E-03	1	5.7
	113	0.0006	3.16	48.96	80	0.034	2.65	0.006	4.1E-04	0	23.93	1.1	7.18	1.7E-03	1	6.2
	114	0.0006	3.17	49.19	80	0.034	2.65	0.006	4.1E-04	0	23.32	1.1	7.24	1.8E-03	1	5.1
	115	0.0006	3.13	48.73	80	0.034	2.65	0.006	4.1E-04	0	22.96	1.1	7.23	1.8E-03	1	4.9
	116	0.0006	3.18	48.97	80	0.034	2.65	0.006	4.1E-04	0	22.90	1.1	7.28	1.8E-03	1	6.3
	117	0.0006	3.09	48.07	80	0.034	2.65	0.006	4.2E-04	0	22.31	1.1	7.33	1.8E-03	1	5.6
	118	0.0006	3.08	48.21	80	0.034	2.65	0.006	4.1E-04	0	22.98	1.1	7.20	1.8E-03	1	7.4
	119	0.0006	3.06	48.41	80	0.034	2.65	0.006	4.2E-04	0	22.28	1.1	7.38	1.8E-03	1	5.8
	120	0.0006	3.00	48.61	80	0.033836	2.65	0.006	4.2E-04	0	21.44	1.1	7.41	0.001843	1	6.4

ESRF Data Fit - Parameter Output (Stage II)

= fixed values

= key variables

Limits		min	max	unit
	p1_lorentz_exp	0	5	-
	p1_lorentz_length	10	100	Å
	p1_peak_pos	0.025	0.05	Å
	p2_cutoff_length	0	inf	Å
	p2_radius	0	10	Å

	Time	p1_background	p1_lorentz_exp	p1_lorentz_length	p1_lorentz_scale	p1_peak_pos	p1_porod_exp	p1_porod_scale	p1_scale	p2_background	p2_cutoff_length	p2_fractal_dim_mass	p2_radius	p2_scale	scale_factor	χ^2
unit	seconds	mm^{-1}	-	Å	-	q	-	-	-	mm^{-1}	Å	-	Å	-		
	1	0.0001	2.97	42.74	80	0.025	2.65	2.62E-03	9.8E-05	0	11.37	1.1	7.13	3.3E-04	1	0.6
	2	0.0001	2.85	57.47	80	0.035	2.65	5.65E-03	5.7E-05	0	19.23	1.1	6.56	3.4E-04	1	0.7
	3	0.0001	1.95	38.99	80	0.034	2.65	3.95E-03	8.9E-05	0	10.96	1.1	8.06	4.1E-04	1	0.6
	4	0.0001	1.54	35.93	80	0.037	2.65	3.99E-03	1.0E-04	0	10.82	1.1	9.21	4.0E-04	1	0.7
	5	0.0001	1.57	30.97	80	0.035	2.65	3.46E-03	1.3E-04	0	11.26	1.1	9.19	3.7E-04	1	0.7
	6	0.0001	1.63	33.92	80	0.038	2.65	4.02E-03	1.2E-04	0	11.64	1.1	10.00	4.5E-04	1	0.8

ESRF Data Fit - Parameter Output (Stage III)

= fixed values

= key variables

Limits		min	max	unit
	p1_power	0	4	-
	p2_cutoff_length	0	inf	Å
	p2_fractal_dim_mass	1	6	Å
	p2_radius	0	15	Å

	Time	p1_background	p1_power	p1_scale	p2_background	p2_cutoff_length	p2_fractal dim_mass	p2_radius	p2_scale	scale_factor	χ^2
unit	min	(mm^{-1})	-	-	(mm^{-1})	Å	Å	Å	-	-	-
	6	0	3.79	1.15E-05	0.0001	21.94	1.64	6.29	1	1.77E-04	0.67
	7	0	3.74	2.04E-05	0.0001	19.84	1.80	4.82	1	1.38E-04	0.73
	8	0	3.71	2.28E-05	0.0001	21.54	1.76	5.32	1	1.51E-04	0.56
	9	0	3.69	2.48E-05	0.0001	21.82	1.77	5.62	1	1.55E-04	0.59
	10	0	3.70	2.58E-05	0.0001	22.01	1.81	6.21	1	1.43E-04	0.53
	11	0	3.70	2.97E-05	0.0001	21.47	1.87	5.39	1	1.30E-04	0.53
	12	0	3.72	3.07E-05	0.0001	21.16	1.93	5.10	1	1.20E-04	0.50
	13	0	4.00	5.98E-06	0.0001	25.55	1.79	6.70	1	1.51E-04	0.64
	14	0	3.73	2.49E-05	0.0001	24.38	1.86	6.06	1	1.36E-04	0.55
	15	0	3.69	3.45E-05	0.0001	24.30	1.90	5.41	1	1.26E-04	0.59
	16	0	3.71	2.72E-05	0.0001	26.63	1.83	6.81	1	1.42E-04	0.61
	17	0	3.66	4.47E-05	0.0001	24.26	1.95	5.37	1	1.16E-04	0.60
	18	0	3.72	2.98E-05	0.0001	26.69	1.88	6.50	1	1.29E-04	0.54
	19	0	3.59	5.90E-05	0.0001	26.68	1.92	5.64	1	1.22E-04	0.58
	20	0	3.62	4.72E-05	0.0001	28.17	1.88	6.62	1	1.31E-04	0.48
	21	0	3.60	5.69E-05	0.0001	28.80	1.91	5.79	1	1.24E-04	0.51
	22	0	3.49	9.77E-05	0.0001	28.52	1.93	5.57	1	1.20E-04	0.52
	23	0	3.58	5.95E-05	0.0001	30.40	1.90	6.55	1	1.24E-04	0.57
	24	0	3.51	7.90E-05	0.0001	31.44	1.90	6.59	1	1.24E-04	0.62
	25	0	3.51	8.57E-05	0.0001	30.95	1.93	5.65	1	1.18E-04	0.60
	26	0	3.49	9.17E-05	0.0001	31.86	1.93	5.57	1	1.16E-04	0.57
	27	0	3.59	5.04E-05	0.0001	35.07	1.88	6.17	1	1.29E-04	0.57
	28	0	3.51	7.25E-05	0.0001	35.40	1.90	5.82	1	1.21E-04	0.60
	29	0	3.61	4.41E-05	0.0001	36.84	1.89	6.06	1	1.25E-04	0.56
	30	0	3.52	6.80E-05	0.0001	37.61	1.89	5.96	1	1.22E-04	0.61
	31	0	3.54	5.94E-05	0.0001	38.25	1.91	5.90	1	1.19E-04	0.62
	32	0	3.53	6.06E-05	0.0001	39.72	1.89	6.13	1	1.24E-04	0.54
	33	0	3.44	9.41E-05	0.0001	40.50	1.88	6.23	1	1.24E-04	0.54
	34	0	3.46	7.53E-05	0.0001	43.60	1.86	6.26	1	1.27E-04	0.55
	35	0	3.58	4.52E-05	0.0001	43.83	1.89	6.01	1	1.19E-04	0.63
	36	0	3.54	4.53E-05	0.0001	46.91	1.86	6.43	1	1.28E-04	0.56
	37	0	3.52	5.45E-05	0.0001	44.96	1.90	6.00	1	1.17E-04	0.59
	38	0	3.81	1.11E-05	0.0001	50.80	1.85	6.47	1	1.30E-04	0.61
	39	0	3.44	6.99E-05	0.0001	48.76	1.88	6.26	1	1.22E-04	0.58
	40	0	3.82	9.50E-06	0.0001	53.29	1.86	6.47	1	1.25E-04	0.53
	41	0	4.00	3.77E-06	0.0001	55.04	1.86	5.77	1	1.26E-04	0.62
	42	0	3.48	5.18E-05	0.0001	50.99	1.90	6.27	1	1.15E-04	0.55
	43	0	3.36	7.58E-05	0.0001	56.32	1.85	6.72	1	1.27E-04	0.51
	44	0	3.46	4.65E-05	0.0001	54.75	1.88	6.30	1	1.17E-04	0.56
	45	0	3.51	3.76E-05	0.0001	56.72	1.88	5.56	1	1.17E-04	0.56
	46	0	3.80	6.98E-06	0.0001	60.17	1.87	6.46	1	1.18E-04	0.51
	47	0	3.63	1.72E-05	0.0001	60.43	1.88	6.52	1	1.17E-04	0.54
	48	0	4.00	2.42E-06	0.0001	63.46	1.88	5.62	1	1.17E-04	0.53
	49	0	4.00	4.40E-08	0.0001	65.31	1.82	7.01	1	1.31E-04	0.53
	50	0	3.86	4.44E-06	0.0001	64.90	1.88	6.42	1	1.15E-04	0.54
	51	0	3.57	1.63E-05	0.0001	65.97	1.88	5.75	1	1.16E-04	0.59
	52	0	3.74	7.34E-06	0.0001	68.32	1.87	6.64	1	1.17E-04	0.59
	53	0	3.48	2.51E-05	0.0001	68.41	1.88	6.54	1	1.15E-04	0.63
	54	0	3.48	1.96E-05	0.0001	74.17	1.86	6.83	1	1.19E-04	0.58
	55	0	3.22	7.92E-05	0.0001	69.97	1.89	5.63	1	1.12E-04	0.62
	56	0	4.00	1.60E-06	0.0001	73.47	1.88	5.96	1	1.15E-04	0.62
	57	0	3.62	8.26E-06	0.0001	76.50	1.88	6.67	1	1.13E-04	0.53
	58	0	3.90	1.44E-06	0.0001	78.61	1.89	5.67	1	1.12E-04	0.60
	59	0	3.66	5.15E-06	0.0001	76.80	1.90	5.64	1	1.10E-04	0.55
	60	0	4.00	5.03E-07	0.0001	81.46	1.88	6.81	1	1.13E-04	0.65

A.3 1:20 SAXS data table

ESRF Data Fit - Parameter Output (1:20)

= fixed values

= key variables

		min	max	unit
Limits	p1_power	0	4	-
	p2_cutoff_length	10	150	Å
	p2_radius	0	20	Å
	p2_fractal_dim_mass	1	6	Å

q = 0.08<*q* <0.51 Å^{-1}

	Time	p1_background	p1_scale	p1_power	p2_background	p2_scale	p2_cutoff_length	p2_radius	p2_fractal _dim_mas	χ2	scale_factor
unit	minutes	mm^{-1}	-	-	mm^{-1}	-	Å	Å	-	-	-
	1	0.0001	8.97E-09	3.62	0	5.31E-04	14.82	5.16	1.50	1.05	1
	2	0.0001	2.19E-09	3.95	0	5.29E-04	15.05	5.41	1.55	0.72	1
	3	0.0001	7.41E-09	3.71	0	3.91E-04	12.33	5.00	1.81	0.90	1
	4	0.0001	3.87E-09	3.85	0	3.93E-04	13.43	5.15	1.81	0.54	1
	5	0.0001	2.06E-09	3.99	0	3.90E-04	14.57	5.15	1.81	0.49	1
	6	0.0001	2.08E-09	4.00	0	3.71E-04	14.89	5.18	1.85	0.53	1
	7	0.0001	2.12E-09	4.00	0	3.59E-04	15.44	5.21	1.87	0.52	1
	8	0.0001	2.17E-09	4.00	0	3.38E-04	15.83	5.24	1.90	0.64	1
	9	0.0001	2.29E-09	3.99	0	3.45E-04	16.81	5.23	1.90	0.48	1
	10	0.0001	2.22E-09	4.00	0	3.30E-04	17.25	5.17	1.92	0.56	1
	11	0.0001	2.24E-09	4.00	0	3.22E-04	17.86	5.19	1.94	0.51	1
	12	0.0001	4.16E-09	3.87	0	3.38E-04	18.97	5.19	1.92	0.76	1
	13	0.0001	2.90E-09	3.95	0	3.10E-04	19.05	5.17	1.96	0.45	1
	14	0.0001	3.74E-09	3.90	0	3.03E-04	19.76	5.13	1.97	0.44	1
	15	0.0001	5.83E-09	3.81	0	2.88E-04	19.85	4.80	2.00	0.58	1
	16	0.0001	2.36E-09	4.00	0	3.02E-04	21.65	5.16	1.97	0.52	1
	17	0.0001	2.40E-09	4.00	0	3.00E-04	22.38	5.17	1.97	0.50	1
	18	0.0001	2.88E-09	3.96	0	2.94E-04	23.06	5.14	1.98	0.54	1
	19	0.0001	4.14E-09	3.89	0	2.90E-04	23.64	4.93	1.99	0.52	1
	20	0.0001	4.50E-09	3.87	0	2.93E-04	24.59	5.19	1.98	0.45	1
	21	0.0001	3.44E-09	3.92	0	2.90E-04	25.50	5.18	1.98	0.51	1
	22	0.0001	2.40E-09	4.00	0	2.94E-04	26.94	5.20	1.97	0.51	1
	23	0.0001	3.34E-09	3.93	0	2.91E-04	27.43	5.25	1.97	0.60	1
	24	0.0001	4.32E-09	3.88	0	2.92E-04	28.19	5.28	1.97	0.59	1
	25	0.0001	4.20E-09	3.88	0	2.85E-04	28.99	5.18	1.98	0.54	1
	26	0.0001	2.86E-09	3.96	0	2.93E-04	30.70	5.31	1.96	0.47	1
	27	0.0001	2.47E-09	4.00	0	2.89E-04	31.45	5.25	1.97	0.50	1
	28	0.0001	2.66E-09	3.97	0	2.95E-04	32.95	5.33	1.96	0.44	1
	29	0.0001	2.47E-09	3.99	0	2.95E-04	33.95	5.38	1.96	0.46	1
	30	0.0001	2.44E-09	4.00	0	2.88E-04	34.21	5.29	1.97	0.53	1
	31	0.0001	2.39E-09	4.00	0	2.91E-04	35.69	5.33	1.96	0.54	1
	32	0.0001	3.19E-09	3.94	0	2.87E-04	36.37	5.29	1.97	0.47	1
	33	0.0001	2.39E-09	4.00	0	2.85E-04	37.46	5.24	1.97	0.62	1
	34	0.0001	2.42E-09	4.00	0	2.87E-04	38.63	5.27	1.97	0.53	1
	35	0.0001	2.38E-09	4.00	0	2.87E-04	39.71	5.32	1.97	0.52	1
	36	0.0001	2.40E-09	4.00	0	2.91E-04	41.12	5.19	1.96	0.52	1
	37	0.0001	2.55E-09	3.99	0	2.84E-04	41.53	5.29	1.97	0.53	1
	38	0.0001	2.70E-09	3.97	0	2.84E-04	42.53	5.32	1.97	0.46	1
	39	0.0001	2.35E-09	4.00	0	2.82E-04	43.73	5.27	1.97	0.55	1
	40	0.0001	6.48E-09	3.79	0	2.81E-04	44.16	5.25	1.97	0.61	1
	41	0.0001	2.33E-09	4.00	0	2.80E-04	45.89	5.28	1.97	0.53	1
	42	0.0001	2.36E-09	4.00	0	2.82E-04	46.94	5.31	1.97	0.52	1
	43	0.0001	2.32E-09	4.00	0	2.83E-04	48.54	5.19	1.97	0.57	1
	44	0.0001	2.32E-09	4.00	0	2.81E-04	49.33	5.15	1.97	0.51	1
	45	0.0001	2.30E-09	4.00	0	2.80E-04	50.95	5.33	1.97	0.52	1
	46	0.0001	4.21E-09	3.87	0	2.79E-04	51.06	5.29	1.97	0.59	1
	47	0.0001	2.29E-09	4.00	0	2.81E-04	53.08	5.15	1.97	0.54	1
	48	0.0001	2.29E-09	4.00	0	2.82E-04	54.19	5.13	1.97	0.59	1
	49	0.0001	5.05E-09	3.83	0	2.79E-04	54.63	5.32	1.97	0.62	1
	50	0.0001	2.18E-09	4.00	0	2.81E-04	57.29	5.32	1.97	0.52	1
	51	0.0001	2.83E-09	3.95	0	2.78E-04	57.53	5.30	1.97	0.58	1
	52	0.0001	2.19E-09	4.00	0	2.85E-04	60.37	5.40	1.96	0.77	1
	53	0.0001	2.21E-09	4.00	0	2.76E-04	60.09	5.14	1.98	0.63	1
	54	0.0001	5.23E-09	3.82	0	2.76E-04	60.75	5.30	1.97	0.66	1
	55	0.0001	2.87E-09	3.94	0	2.76E-04	62.42	5.11	1.98	0.58	1
	56	0.0001	2.91E-09	3.94	0	2.76E-04	63.57	5.13	1.98	0.67	1
	57	0.0001	2.20E-09	4.00	0	2.74E-04	65.06	5.13	1.98	0.58	1
	58	0.0001	2.16E-09	4.00	0	2.76E-04	66.69	5.15	1.97	0.65	1
	59	0.0001	2.09E-09	4.00	0	2.76E-04	68.24	5.35	1.97	0.70	1
	60	0.0001	2.09E-09	4.00	0	2.74E-04	69.27	5.29	1.97	0.71	1

A.4 1:100 pH 7 SAXS data table

ESRF TTCF 1:100 pH 7 Data Fit - Parameter Output (Stage I)

= fixed values

= key variables

		min	max	unit
Limits	p2_radius (equatorial)	20	75	Å
	p2_radius (polar)	40	200	Å
	p3_cut-off length	0	inf	Å
	p3_radius (fractal)	1	15	Å
	p1_power	0	4	arb.
	p3_fractal dim mass	1	6	arb.

	Time	p1_background	p1_power	p1_scale	p2_background	p2_radius (equatorial)	p2_radius (polar)	p2_scale	p2_sld	p2_sld_solvent	p3_background	p3_cut-off length	p3_fractal_dim_mass	p3_radius (fractal)	p3_scale	scale_factor	χ^2
unit	(minutes)	(mm^{-1})	-	-	(mm^{-1})	Å	Å	-	$*10^6/Å^2$	$*10^6/Å^2$	(mm^{-1})	Å	-	Å	-	-	
	1	0.0001	2.83	5.72E-09	0	22.56	60.51	1.06E-05	17.5	9.44	0	0.47	5.17	7.55	0.001	1	0.54
	2	0.0001	3.15	1.51E-09	0	22.49	77.05	1.05E-05	17.5	9.44	0	0.55	4.39	8.87	0.001	1	0.52
	3	0.0001	3.49	1.08E-09	0	21.23	103.52	1.20E-05	17.5	9.44	0	0.68	3.33	7.89	0.001	1	0.55
	4	0.0001	3.46	1.88E-09	0	22.97	97.96	1.08E-05	17.5	9.44	0	0.63	3.95	8.11	0.001	1	0.56
	5	0.0001	3.25	6.45E-09	0	22.93	106.23	1.10E-05	17.5	9.44	0	0.59	4.36	8.13	0.001	1	0.62
	6	0.0001	3.81	4.93E-10	0	25.10	119.18	1.01E-05	17.5	9.44	0	1.20	1.50	8.84	0.001	1	0.66
	7	0.0001	3.26	8.09E-09	0	27.18	99.88	8.88E-06	17.5	9.44	0	0.69	3.98	9.09	0.001	1	0.72
	8	0.0001	3.42	4.11E-09	0	27.14	96.83	9.30E-06	17.5	9.44	0	0.66	4.17	8.86	0.001	1	0.78
	9	0.0001	3.68	1.31E-09	0	28.69	90.49	8.89E-06	17.5	9.44	0	1.29	1.79	9.25	0.001	1	0.80

ESRF TTCF 1:100 pH 7 Data Fit - Parameter Output (Stage II)

= fixed values

= key variables

		min	max	unit
Limits	p1_lorentz_exp	0	5	-
	p1_lorentz_length	30	100	Å
	p1_peak_pos	0.025	0.05	Å
	p2_cutoff_length	0	inf	Å
	p2_radius	1	15	Å

	Time	p1_background	p1_lorentz_exp	p1_lorentz_length	p1_lorentz_scale	p1_peak_pos	p1_porod_exp	p1_porod_scale	p1_scale	p2_background	p2_cutoff_length	p2_fractal_dim_mass	p2_radius	p2_scale	scale_factor	χ^2
unit	(minutes)	mm^{-1}	-	Å	-	q	-	-	-	mm^{-1}	Å	-	Å	-		
	10	0.0001	2.17	40.10	2.44E+04	0.028	3.1	7.12E-02	4.0E-07	0	0.11	5.92	9.77	5.9E+00	1	0.9
	11	0.0001	2.31	39.67	2.78E+04	0.028	3.1	7.19E-02	3.4E-07	0	0.09	6.00	10.10	1.6E+01	1	0.8
	12	0.0001	2.19	39.14	3.92E+04	0.028	3.0	1.57E-01	2.5E-07	0	0.08	6.00	9.15	4.6E+01	1	0.7
	13	0.0001	2.45	36.62	3.50E+04	0.028	3.2	6.98E-02	2.8E-07	0	0.10	5.99	9.37	9.4E+00	1	0.7
	14	0.0001	2.45	36.48	3.89E+04	0.028	3.2	6.05E-02	2.6E-07	0	0.10	5.99	9.44	1.1E+01	1	0.7
	15	0.0001	2.62	35.85	4.23E+04	0.028	3.2	7.37E-02	2.2E-07	0	0.09	6.00	9.77	1.9E+01	1	0.6
	16	0.0001	2.69	35.34	4.23E+04	0.028	3.1	1.28E-01	2.2E-07	0	0.06	4.35	9.65	4.9E+01	1	0.6
	17	0.0001	2.25	42.18	2.13E+04	0.035	2.7	5.87E-01	3.9E-07	0	0.04	3.08	9.75	1.3E+01	1	0.6
	18	0.0001	2.10	45.19	1.20E+04	0.038	2.4	1.15E+00	6.3E-07	0	0.04	2.57	9.88	5.1E+00	1	0.9
	19	0.0001	2.39	37.96	2.41E+04	0.032	3.2	6.23E-02	3.7E-07	0	0.10	6.00	10.62	1.8E+01	1	0.6
	20	0.0001	2.61	36.12	3.69E+04	0.031	3.3	6.20E-02	2.5E-07	0	0.10	6.00	9.99	1.9E+01	1	0.6
	21	0.0001	2.40	36.69	4.14E+04	0.032	3.2	8.98E-02	2.2E-07	0	0.08	6.00	10.03	6.7E+01	1	0.6
	22	0.0001	2.60	34.79	4.30E+04	0.029	3.4	4.22E-02	2.2E-07	0	0.09	6.00	10.25	2.3E+01	1	0.6
	23	0.0001	2.45	34.85	4.58E+04	0.031	3.4	5.13E-02	2.0E-07	0	0.11	5.99	10.26	9.2E+00	1	0.7
	24	0.0001	2.24	44.91	1.59E+04	0.038	2.7	6.44E-01	4.8E-07	0	0.01	2.03	11.05	1.3E+01	1	0.8
	25	0.0001	2.14	37.76	3.92E+04	0.034	3.2	1.14E-01	2.4E-07	0	0.05	4.13	10.25	4.0E+01	1	0.7
	26	0.0001	2.12	38.73	2.78E+04	0.035	3.2	7.25E-02	3.4E-07	0	0.12	5.87	10.54	5.4E+00	1	0.6
	27	0.0001	2.40	34.22	4.91E+04	0.032	3.3	7.90E-02	1.9E-07	0	0.08	6.00	10.29	6.3E+01	1	0.6
	28	0.0001	2.23	35.45	4.74E+04	0.033	3.4	4.37E-02	2.0E-07	0	0.11	6.00	10.55	7.9E+00	1	0.6
	29	0.0001	2.26	35.52	3.66E+04	0.033	3.4	4.43E-02	2.6E-07	0	0.12	6.00	10.68	6.3E+00	1	0.7
	30	0.0001	2.26	34.65	3.74E+04	0.032	3.4	4.04E-02	2.7E-07	0	0.10	6.00	10.56	2.0E+01	1	0.7
	31	0.0001	2.28	34.66	3.76E+04	0.032	3.4	3.47E-02	2.6E-07	0	0.12	6.00	10.86	5.4E+00	1	0.7
	32	0.0001	1.73	41.31	2.42E+04	0.038	2.9	3.13E-01	4.0E-07	0	0.07	4.54	10.78	2.2E+01	1	0.7
	33	0.0001	2.28	36.04	3.83E+04	0.033	3.4	4.22E-02	2.5E-07	0	0.10	5.98	10.89	1.4E+01	1	0.6
	34	0.0001	2.21	34.33	4.16E+04	0.033	3.4	5.15E-02	2.3E-07	0	0.10	6.00	10.86	1.4E+01	1	0.6
	35	0.0001	2.31	33.03	4.73E+04	0.032	3.4	4.21E-02	2.1E-07	0	0.11	6.00	10.99	8.3E+00	1	0.6
	36	0.0001	2.38	32.06	4.20E+04	0.031	3.4	4.65E-02	2.3E-07	0	0.10	5.99	10.93	1.6E+01	1	0.7
	37	0.0001	2.11	35.60	4.07E+04	0.034	3.4	5.45E-02	2.5E-07	0	0.10	6.00	11.09	1.8E+01	1	0.7
	38	0.0001	1.92	35.09	4.03E+04	0.035	3.2	1.05E-01	2.6E-07	0	0.05	3.95	10.84	4.1E+01	1	0.7
	39	0.0001	1.87	36.39	5.32E+04	0.036	3.2	1.50E-01	2.0E-07	0	0.05	4.02	10.86	4.4E+01	1	0.7
	40	0.0001	1.99	33.76	4.24E+04	0.034	3.3	6.27E-02	2.5E-07	0	0.10	6.00	11.01	2.1E+01	1	0.6
	41	0.0001	2.25	32.09	3.46E+04	0.032	3.4	4.46E-02	2.9E-07	0	0.10	5.99	11.31	1.8E+01	1	0.8
	42	0.0001	2.25	31.57	4.27E+04	0.031	3.5	3.26E-02	2.4E-07	0	0.10	5.99	11.27	1.8E+01	1	0.7
	43	0.0001	2.31	31.43	4.68E+04	0.031	3.5	3.70E-02	2.2E-07	0	0.09	6.00	11.30	2.5E+01	1	0.6
	44	0.0001	2.05	31.91	3.86E+04	0.032	3.4	4.76E-02	2.8E-07	0	0.12	6.00	11.04	6.8E+00	1	0.6
	45	0.0001	2.26	31.09	3.78E+04	0.031	3.4	4.33E-02	2.7E-07	0	0.12	5.99	11.46	6.0E+00	1	0.7
	46	0.0001	2.11	30.08	4.26E+04	0.032	3.4	4.71E-02	2.5E-07	0	0.10	5.99	11.05	1.5E+01	1	0.7
	47	0.0001	2.22	30.52	4.28E+04	0.031	3.5	3.17E-02	2.5E-07	0	0.10	6.00	11.50	2.2E+01	1	0.6
	48	0.0001	2.25	30.88	4.02E+04	0.032	3.3	5.94E-02	2.6E-07	0	0.08	6.00	11.45	5.1E+01	1	0.7
	49	0.0001	2.27	30.01	3.60E+04	0.031	3.4	4.32E-02	2.8E-07	0	0.10	6.00	11.57	1.9E+01	1	0.6
	50	0.0001	2.21	31.59	4.16E+04	0.032	3.4	5.13E-02	2.5E-07	0	0.10	6.00	11.66	2.3E+01	1	0.7
	51	0.0001	2.23	30.53	4.16E+04	0.031	3.4	5.37E-02	2.5E-07	0	0.12	5.99	11.72	6.4E+00	1	0.6
	52	0.0001	2.16	31.03	2.68E+04	0.033	3.3	4.37E-02	3.8E-07	0	0.10	6.00	11.94	2.2E+01	1	0.7
	53	0.0001	2.23	30.01	5.46E+04	0.031	3.5	3.98E-02	2.0E-07	0	0.09	6.00	11.72	3.3E+01	1	0.7
	54	0.0001	1.99	31.12	4.50E+04	0.034	3.3	9.39E-02	2.4E-07	0	0.08	6.00	11.71	5.8E+01	1	0.7
	55	0.0001	2.03	30.82	3.99E+04	0.033	3.3	6.43E-02	2.7E-07	0	0.10	6.00	11.63	1.8E+01	1	0.7
	56	0.0001	2.32	30.00	4.74E+04	0.031	3.4	4.11E-02	2.2E-07	0	0.12	6.00	11.83	8.2E+00	1	0.8
	57	0.0001	2.29	30.36	4.44E+04	0.032	3.2	1.02E-01	2.2E-07	0	0.08	6.00	11.97	7.3E+01	1	0.8
	58	0.0001	2.14	30.01	4.48E+04	0.032	3.4	5.42E-02	2.4E-07	0	0.10	6.00	11.42	1.5E+01	1	0.6
	59	0.0001	2.31	30.00	3.80E+04	0.030	3.4	4.42E-02	2.7E-07	0	0.10	5.99	12.10	2.1E+01	1	0.8
	60	0.0001	2.29	30.37	3.47E+04	0.032	3.3	6.01E-02	2.9E-07	0	0.10	5.99	12.09	1.9E+01	1	0.9

A.5 1:100 pH 8 SAXS data table

ESRF TTCF 1:100 pH 8 Data Fit - Parameter Output (Stage I)

= fixed values

= key variables

		min	max	unit
Limits	p2_radius (equatorial)	1	75	Å
	p2_radius (polar)	75	200	Å
	p3_cut-off length	0	inf	Å
	p3_radius (fractal)	1	15	Å
	p1_power	0	4	arb.
	p3_fractal dim mass	1	6	arb.

	Time	p1_background	p1_power	p1_scale	p2_background	p2_radius (equatorial)	p2_radius (polar)	p2_scale	p2_sld	p2_sld_solvent	p3_background	p3_cut-off length	p3_fractal_ dim_mass	p3_radius (fractal)	p3_scale	scale_factor	χ^2
unit	(minutes)	(mm^{-1})	-	-	(mm^{-1})	Å	Å	-	$*10^6/Å^2$	$*10^6/Å^2$	(mm^{-1})	Å	-	Å	-	-	
1		0.0001	2.97	1.40E-08	0	41.01	148.30	6.84E-06	17.5	9.44	0	47.75	1.00	7.67	0.0002	1	0.63
2		0.0001	3.05	1.26E-08	0	44.85	120.52	6.73E-06	17.5	9.44	0	108.07	1.00	7.88	0.0002	1	0.66
3		0.0001	2.94	1.41E-08	0	46.31	118.26	7.20E-06	17.5	9.44	0	308.77	1.00	8.44	0.0002	1	0.60
4		0.0001	2.92	1.41E-08	0	47.32	123.27	7.81E-06	17.5	9.44	0	290.95	1.03	7.93	0.0002	1	0.60
5		0.0001	2.92	1.41E-08	0	47.82	121.23	8.32E-06	17.5	9.44	0	299.31	1.06	8.09	0.0002	1	0.64
6		0.0001	3.03	1.41E-08	0	48.17	135.18	9.34E-06	17.5	9.44	0	78.72	1.09	8.59	0.0002	1	0.62
7		0.0001	2.95	1.41E-08	0	48.62	122.66	9.28E-06	17.5	9.44	0	297.69	1.09	8.12	0.0002	1	0.67
8		0.0001	2.96	1.41E-08	0	48.43	122.86	9.73E-06	17.5	9.44	0	353.62	1.10	8.03	0.0002	1	0.65
9		0.0001	2.86	1.41E-08	0	49.86	127.60	9.61E-06	17.5	9.44	0	375.98	1.12	8.20	0.0002	1	0.75
10		0.0001	2.89	1.41E-08	0	49.33	126.34	1.01E-05	17.5	9.44	0	279.02	1.13	8.21	0.0002	1	0.69
11		0.0001	2.84	1.41E-08	0	50.09	125.45	1.02E-05	17.5	9.44	0	390.38	1.14	8.30	0.0002	1	0.65
12		0.0001	2.91	1.41E-08	0	50.67	125.26	1.04E-05	17.5	9.44	0	311.92	1.16	8.19	0.0002	1	0.67
13		0.0001	2.85	1.41E-08	0	50.74	131.27	1.05E-05	17.5	9.44	0	254.06	1.17	8.78	0.0002	1	0.72
14		0.0001	2.74	1.41E-08	0	50.39	130.31	1.07E-05	17.5	9.44	0	489.07	1.16	8.88	0.0002	1	0.87
15		0.0001	2.73	1.41E-08	0	51.13	129.35	1.07E-05	17.5	9.44	0	458.13	1.18	8.42	0.0002	1	0.83
16		0.0001	2.76	1.41E-08	0	51.56	128.09	1.08E-05	17.5	9.44	0	375.25	1.19	8.45	0.0002	1	0.76
17		0.0001	2.71	1.41E-08	0	50.98	132.46	1.12E-05	17.5	9.44	0	334.31	1.20	8.44	0.0002	1	0.83
18		0.0001	2.05	1.41E-08	0	51.38	131.69	1.12E-05	17.5	9.44	0	493.18	1.20	8.60	0.0002	1	0.72
19		0.0001	2.52	1.41E-08	0	51.13	134.89	1.15E-05	17.5	9.44	0	333.26	1.21	8.47	0.0002	1	0.74
20		0.0001	2.73	1.41E-08	0	51.62	133.58	1.16E-05	17.5	9.44	0	349.07	1.22	8.52	0.0002	1	0.77
21		0.0001	2.90	1.41E-08	0	51.57	138.47	1.18E-05	17.5	9.44	0	182.67	1.23	8.48	0.0002	1	0.81
22		0.0001	2.74	1.41E-08	0	51.57	135.89	1.19E-05	17.5	9.44	0	311.52	1.23	8.60	0.0002	1	0.85
23		0.0001	0.27	1.41E-08	0	51.69	136.76	1.20E-05	17.5	9.44	0	426.97	1.23	8.53	0.0002	1	0.82
24		0.0001	1.81	1.41E-08	0	52.03	137.46	1.19E-05	17.5	9.44	0	381.50	1.24	8.59	0.0002	1	0.72
25		0.0001	2.42	1.41E-08	0	51.82	141.77	1.19E-05	17.5	9.44	0	320.22	1.25	8.76	0.0002	1	0.67
26		0.0001	2.54	1.41E-08	0	52.28	138.11	1.21E-05	17.5	9.44	0	279.10	1.25	8.71	0.0002	1	0.82
27		0.0001	2.69	1.41E-08	0	51.74	142.92	1.24E-05	17.5	9.44	0	266.41	1.25	8.66	0.0002	1	0.81
28		0.0001	2.70	1.41E-08	0	52.96	139.69	1.21E-05	17.5	9.44	0	223.41	1.27	8.81	0.0002	1	0.75
29		0.0001	2.66	1.41E-08	0	52.38	142.56	1.23E-05	17.5	9.44	0	290.71	1.27	8.70	0.0002	1	0.72
30		0.0001	1.47	1.41E-08	0	52.17	140.65	1.24E-05	17.5	9.44	0	388.87	1.26	8.83	0.0002	1	0.78
31		0.0001	3.04	1.41E-08	0	52.79	145.28	1.28E-05	17.5	9.44	0	114.11	1.29	8.88	0.0002	1	0.89
32		0.0001	2.61	1.41E-08	0	52.69	138.70	1.24E-05	17.5	9.44	0	316.88	1.28	8.87	0.0002	1	0.84
33		0.0001	2.14	1.41E-08	0	52.78	144.07	1.26E-05	17.5	9.44	0	276.56	1.28	8.77	0.0002	1	0.69
34		0.0001	2.56	1.41E-08	0	52.65	143.01	1.28E-05	17.5	9.44	0	309.34	1.28	8.90	0.0002	1	0.82
35		0.0001	2.66	1.41E-08	0	52.84	139.52	1.27E-05	17.5	9.44	0	278.78	1.29	8.89	0.0002	1	0.80
36		0.0001	2.77	1.41E-08	0	53.05	141.88	1.27E-05	17.5	9.44	0	237.51	1.29	8.90	0.0002	1	0.79
37		0.0001	2.17	1.41E-08	0	53.00	143.38	1.28E-05	17.5	9.44	0	351.96	1.29	8.88	0.0002	1	0.76
38		0.0001	2.67	1.41E-08	0	52.26	147.78	1.32E-05	17.5	9.44	0	291.35	1.29	8.90	0.0002	1	0.79
39		0.0001	2.28	1.41E-08	0	53.33	141.72	1.28E-05	17.5	9.44	0	306.20	1.30	8.99	0.0002	1	0.78
40		0.0001	2.73	1.41E-08	0	53.48	146.89	1.28E-05	17.5	9.44	0	241.95	1.31	9.03	0.0002	1	0.82
41		0.0001	1.96	1.41E-08	0	53.90	142.03	1.27E-05	17.5	9.44	0	281.75	1.31	9.11	0.0002	1	0.83
42		0.0001	2.49	1.41E-08	0	52.94	148.70	1.31E-05	17.5	9.44	0	281.45	1.31	9.10	0.0002	1	0.86
43		0.0001	2.35	1.41E-08	0	53.00	148.04	1.33E-05	17.5	9.44	0	276.48	1.31	9.03	0.0002	1	0.74
44		0.0001	2.43	1.41E-08	0	53.42	147.70	1.31E-05	17.5	9.44	0	294.07	1.31	9.08	0.0002	1	0.92
45		0.0001	2.27	1.41E-08	0	52.90	149.60	1.34E-05	17.5	9.44	0	307.44	1.31	9.05	0.0002	1	0.91
46		0.0001	2.37	1.41E-08	0	53.81	151.44	1.33E-05	17.5	9.44	0	242.27	1.32	9.13	0.0002	1	0.85
47		0.0001	2.25	1.41E-08	0	53.69	146.72	1.31E-05	17.5	9.44	0	307.44	1.32	9.17	0.0002	1	0.81
48		0.0001	2.50	1.41E-08	0	53.30	147.42	1.34E-05	17.5	9.44	0	312.17	1.31	9.13	0.0002	1	0.94
49		0.0001	2.24	1.41E-08	0	53.73	152.40	1.33E-05	17.5	9.44	0	249.63	1.32	9.06	0.0002	1	0.92
50		0.0001	2.52	1.41E-08	0	53.01	153.86	1.38E-05	17.5	9.44	0	253.10	1.32	9.14	0.0002	1	0.88
51		0.0001	2.28	1.41E-08	0	53.49	151.49	1.37E-05	17.5	9.44	0	290.53	1.32	9.12	0.0002	1	0.91
52		0.0001	2.17	8.27E-09	0	53.54	154.57	1.37E-05	17.5	9.44	0	248.48	1.33	9.28	0.0002	1	0.92
53		0.0001	2.62	1.41E-08	0	53.67	150.79	1.37E-05	17.5	9.44	0	247.26	1.33	9.12	0.0002	1	0.94
54		0.0001	2.48	1.41E-08	0	53.96	150.19	1.36E-05	17.5	9.44	0	241.72	1.33	9.27	0.0002	1	0.88
55		0.0001	2.55	1.41E-08	0	54.17	151.51	1.37E-05	17.5	9.44	0	227.73	1.34	9.18	0.0002	1	0.85
56		0.0001	3.32	3.93E-09	0	54.73	168.70	1.48E-05	17.5	9.44	0	72.79	1.37	9.24	0.0002	1	0.99
57		0.0001	1.48	1.41E-08	0	53.69	159.51	1.40E-05	17.5	9.44	0	226.52	1.34	9.24	0.0002	1	0.91
58		0.0001	2.18	1.41E-08	0	53.92	153.75	1.39E-05	17.5	9.44	0	251.65	1.34	9.23	0.0002	1	0.91
59		0.0001	1.89	1.41E-08	0	53.84	154.62	1.38E-05	17.5	9.44	0	263.75	1.34	9.27	0.0002	1	0.86
60		0.0001	2.67	1.41E-08	0	54.27	155.01	1.39E-05	17.5	9.44	0	213.11	1.35	9.34	0.0002	1	1.00
61		0.0001	1.30	1.41E-08	0	54.68	155.68	1.35E-05	17.5	9.44	0	229.88	1.35	9.69	0.0002	1	1.14
62		0.0001	2.12	1.41E-08	0	54.60	149.87	1.38E-05	17.5	9.44	0	260.51	1.35	9.33	0.0002	1	0.93
63		0.0001	2.19	1.41E-08	0	54.51	154.09	1.39E-05	17.5	9.44	0	257.77	1.35	9.27	0.0002	1	0.84
64		0.0001	1.81	1.41E-08	0	54.12	154.53	1.44E-05	17.5	9.44	0	256.32	1.35	8.80	0.0002	1	0.80
65		0.0001	1.53	1.41E-08	0	54.21	152.19	1.40E-05	17.5	9.44	0	335.75	1.35	9.28	0.0002	1	0.84

66	0.0001	2.14	1.41E-08	0	53.95	154.61	1.44E-05	17.5	9.44	0	296.79	1.35	9.27	0.0002	1	0.98
67	0.0001	2.13	3.07E-09	0	54.58	156.73	1.42E-05	17.5	9.44	0	222.83	1.35	9.27	0.0002	1	0.84
68	0.0001	2.21	1.41E-08	0	54.51	154.68	1.40E-05	17.5	9.44	0	275.55	1.36	9.43	0.0002	1	0.97
69	0.0001	1.70	1.41E-08	0	54.39	157.34	1.42E-05	17.5	9.44	0	261.54	1.36	9.43	0.0002	1	0.91
70	0.0001	3.08	2.25E-09	0	54.87	167.49	1.42E-05	17.5	9.44	0	173.70	1.37	9.46	0.0002	1	0.96
71	0.0001	2.26	1.41E-08	0	54.64	157.67	1.43E-05	17.5	9.44	0	231.21	1.36	9.42	0.0002	1	0.92
72	0.0001	1.57	1.41E-08	0	54.25	161.75	1.46E-05	17.5	9.44	0	258.77	1.36	8.96	0.0002	1	0.90
73	0.0001	2.17	1.41E-08	0	54.24	159.97	1.45E-05	17.5	9.44	0	249.66	1.36	9.43	0.0002	1	0.85
74	0.0001	2.40	1.41E-08	0	55.06	156.96	1.43E-05	17.5	9.44	0	238.49	1.36	9.42	0.0002	1	0.88
75	0.0001	2.79	1.36E-08	0	54.69	161.77	1.47E-05	17.5	9.44	0	175.29	1.37	9.49	0.0002	1	1.01
76	0.0001	2.27	1.41E-08	0	54.67	161.11	1.46E-05	17.5	9.44	0	254.37	1.36	9.38	0.0002	1	0.88
77	0.0001	2.05	1.41E-08	0	54.77	161.99	1.46E-05	17.5	9.44	0	266.78	1.36	9.39	0.0002	1	1.01
78	0.0001	2.09	1.41E-08	0	54.53	167.13	1.44E-05	17.5	9.44	0	247.78	1.37	9.44	0.0002	1	1.03
79	0.0001	2.64	1.41E-08	0	54.96	160.60	1.44E-05	17.5	9.44	0	250.02	1.37	9.38	0.0002	1	0.95
80	0.0001	2.10	1.41E-08	0	54.63	161.20	1.44E-05	17.5	9.44	0	267.38	1.37	9.51	0.0002	1	0.94
81	0.0001	2.41	1.41E-08	0	54.54	160.19	1.46E-05	17.5	9.44	0	272.46	1.37	9.46	0.0002	1	1.00
82	0.0001	1.27	1.41E-08	0	54.44	168.80	1.52E-05	17.5	9.44	0	242.90	1.37	9.08	0.0002	1	0.78
83	0.0001	2.04	1.41E-08	0	54.61	162.71	1.48E-05	17.5	9.44	0	254.88	1.37	9.14	0.0002	1	0.88
84	0.0001	2.04	1.41E-08	0	54.69	160.20	1.47E-05	17.5	9.44	0	283.45	1.38	9.21	0.0002	1	0.94
85	0.0001	2.52	1.41E-08	0	54.72	159.78	1.50E-05	17.5	9.44	0	290.22	1.37	9.02	0.0002	1	0.90
86	0.0001	2.22	1.41E-08	0	54.78	167.29	1.50E-05	17.5	9.44	0	252.73	1.37	9.15	0.0002	1	0.83
87	0.0001	2.43	1.41E-08	0	55.17	164.78	1.49E-05	17.5	9.44	0	239.37	1.38	9.24	0.0002	1	0.93
88	0.0001	2.13	1.41E-08	0	54.81	163.29	1.49E-05	17.5	9.44	0	280.34	1.37	9.55	0.0002	1	1.01
89	0.0001	1.97	1.41E-08	0	55.12	166.82	1.49E-05	17.5	9.44	0	244.60	1.38	9.21	0.0002	1	0.83
90	0.0001	1.99	1.41E-08	0	55.29	163.44	1.49E-05	17.5	9.44	0	222.55	1.38	9.71	0.0002	1	1.17
91	0.0001	2.28	1.41E-08	0	55.45	159.35	1.50E-05	17.5	9.44	0	267.44	1.38	9.20	0.0002	1	0.95
92	0.0001	2.06	1.41E-08	0	55.45	166.52	1.48E-05	17.5	9.44	0	256.74	1.38	9.36	0.0002	1	1.09
93	0.0001	1.88	1.41E-08	0	55.83	168.36	1.47E-05	17.5	9.44	0	217.11	1.38	9.74	0.0002	1	1.07
94	0.0001	1.93	1.41E-08	0	55.15	161.14	1.50E-05	17.5	9.44	0	296.60	1.38	9.35	0.0002	1	0.96
95	0.0001	2.04	1.41E-08	0	55.46	164.36	1.49E-05	17.5	9.44	0	264.72	1.38	9.26	0.0002	1	0.98
96	0.0001	2.20	1.41E-08	0	54.87	166.35	1.52E-05	17.5	9.44	0	270.51	1.38	9.22	0.0002	1	0.89
97	0.0001	2.11	1.41E-08	0	55.93	166.14	1.49E-05	17.5	9.44	0	253.67	1.39	9.39	0.0002	1	0.97
98	0.0001	2.12	1.41E-08	0	55.34	167.59	1.51E-05	17.5	9.44	0	228.23	1.38	9.77	0.0002	1	1.20
99	0.0001	2.58	1.41E-08	0	55.49	163.03	1.51E-05	17.5	9.44	0	272.79	1.39	9.38	0.0002	1	0.96
100	0.0001	2.38	1.41E-08	0	55.32	168.22	1.51E-05	17.5	9.44	0	258.81	1.39	9.39	0.0002	1	0.89
101	0.0001	2.08	1.41E-08	0	55.52	171.22	1.51E-05	17.5	9.44	0	226.85	1.39	9.84	0.0002	1	1.17
102	0.0001	2.29	1.37E-08	0	55.57	170.17	1.51E-05	17.5	9.44	0	229.48	1.39	9.85	0.0002	1	0.97
103	0.0001	1.87	1.41E-08	0	55.94	166.95	1.48E-05	17.5	9.44	0	269.11	1.39	9.84	0.0002	1	1.17
104	0.0001	2.08	1.41E-08	0	55.41	165.28	1.52E-05	17.5	9.44	0	273.56	1.39	9.80	0.0002	1	1.15
105	0.0001	1.92	1.41E-08	0	55.51	167.93	1.52E-05	17.5	9.44	0	248.19	1.39	9.76	0.0002	1	1.17
106	0.0001	2.68	1.41E-08	0	55.61	176.06	1.56E-05	17.5	9.44	0	193.79	1.39	9.41	0.0002	1	1.01
107	0.0001	1.91	1.41E-08	0	55.90	172.33	1.53E-05	17.5	9.44	0	251.34	1.39	9.35	0.0002	1	0.97
108	0.0001	2.19	1.41E-08	0	55.54	166.53	1.52E-05	17.5	9.44	0	261.01	1.39	9.88	0.0002	1	1.00
109	0.0001	2.03	1.41E-08	0	56.03	166.15	1.53E-05	17.5	9.44	0	236.99	1.40	9.41	0.0002	1	1.12
110	0.0001	1.20	1.41E-08	0	56.15	168.39	1.51E-05	17.5	9.44	0	234.22	1.40	10.03	0.0002	1	1.22
111	0.0001	2.11	1.41E-08	0	55.64	172.14	1.53E-05	17.5	9.44	0	241.37	1.40	9.77	0.0002	1	1.13
112	0.0001	2.12	1.41E-08	0	55.69	168.84	1.55E-05	17.5	9.44	0	268.68	1.39	9.37	0.0002	1	1.05
113	0.0001	0.39	1.41E-08	0	56.46	169.06	1.51E-05	17.5	9.44	0	243.17	1.40	9.92	0.0002	1	1.18
114	0.0001	0.97	1.41E-08	0	56.12	171.50	1.54E-05	17.5	9.44	0	239.29	1.40	9.45	0.0002	1	1.03
115	0.0001	1.97	1.41E-08	0	56.21	169.08	1.54E-05	17.5	9.44	0	236.79	1.40	9.55	0.0002	1	1.20
116	0.0001	2.06	1.41E-08	0	56.03	176.69	1.52E-05	17.5	9.44	0	240.74	1.40	9.87	0.0002	1	1.13
117	0.0001	2.09	1.41E-08	0	56.01	171.29	1.55E-05	17.5	9.44	0	262.80	1.40	9.43	0.0002	1	1.03
118	0.0001	2.42	1.41E-08	0	55.67	174.95	1.55E-05	17.5	9.44	0	237.88	1.40	9.93	0.0002	1	1.10
119	0.0001	2.09	5.06E-09	0	55.87	172.60	1.56E-05	17.5	9.44	0	271.08	1.40	9.48	0.0002	1	1.04
120	0.0001	2.31	1.41E-08	0	55.55	172.90	1.60E-05	17.5	9.44	0	255.54	1.40	9.38	0.0002	1	0.91

A.6 Kratky plots of TTCF ensilication

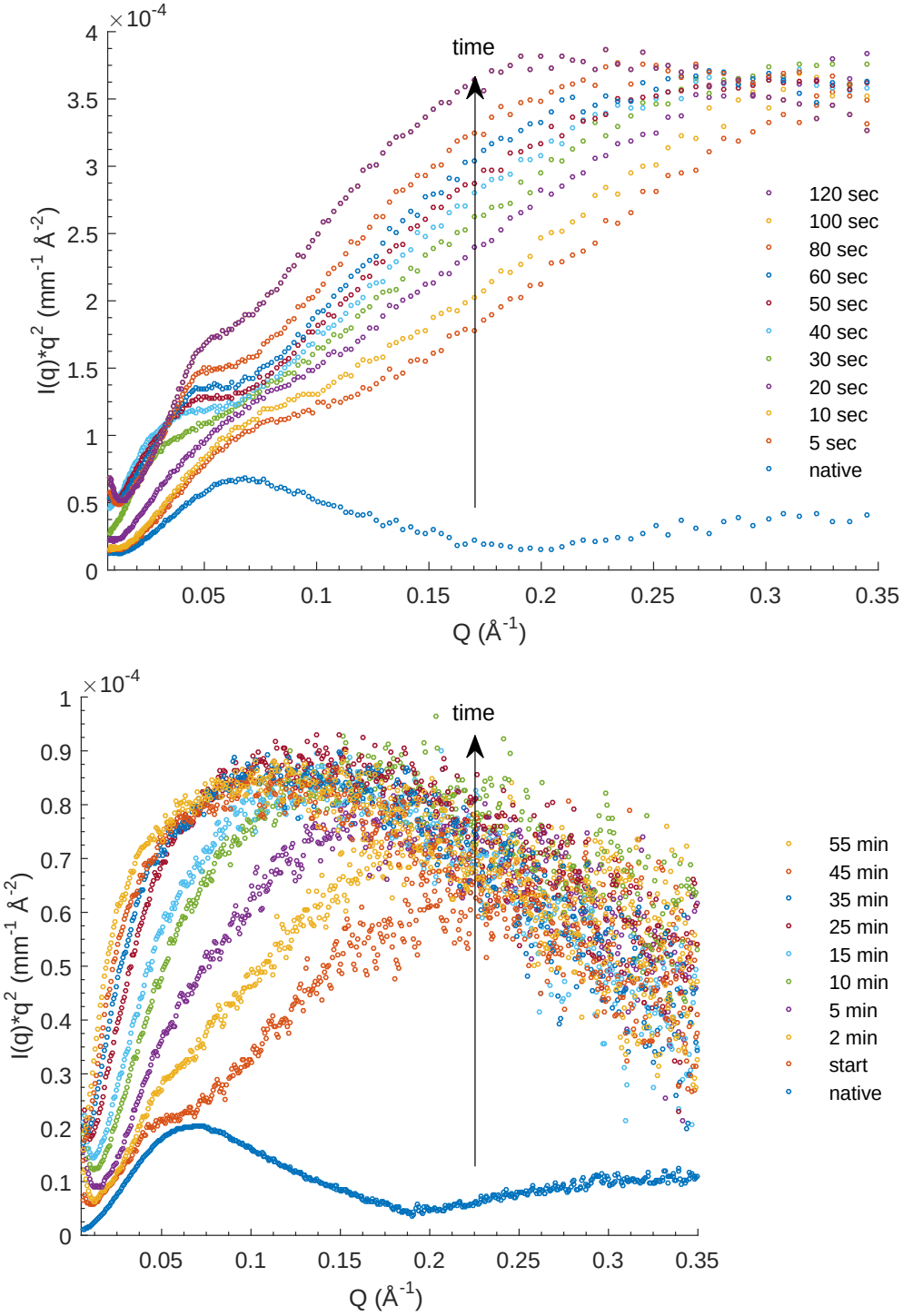

Figure A-1: Kratky plots of TTCF ensilication. (top) The agitated sample setup measurement at Diamond (Bottom) The static sample measurement at ESRF (bottom)

A.7 ELISA titration

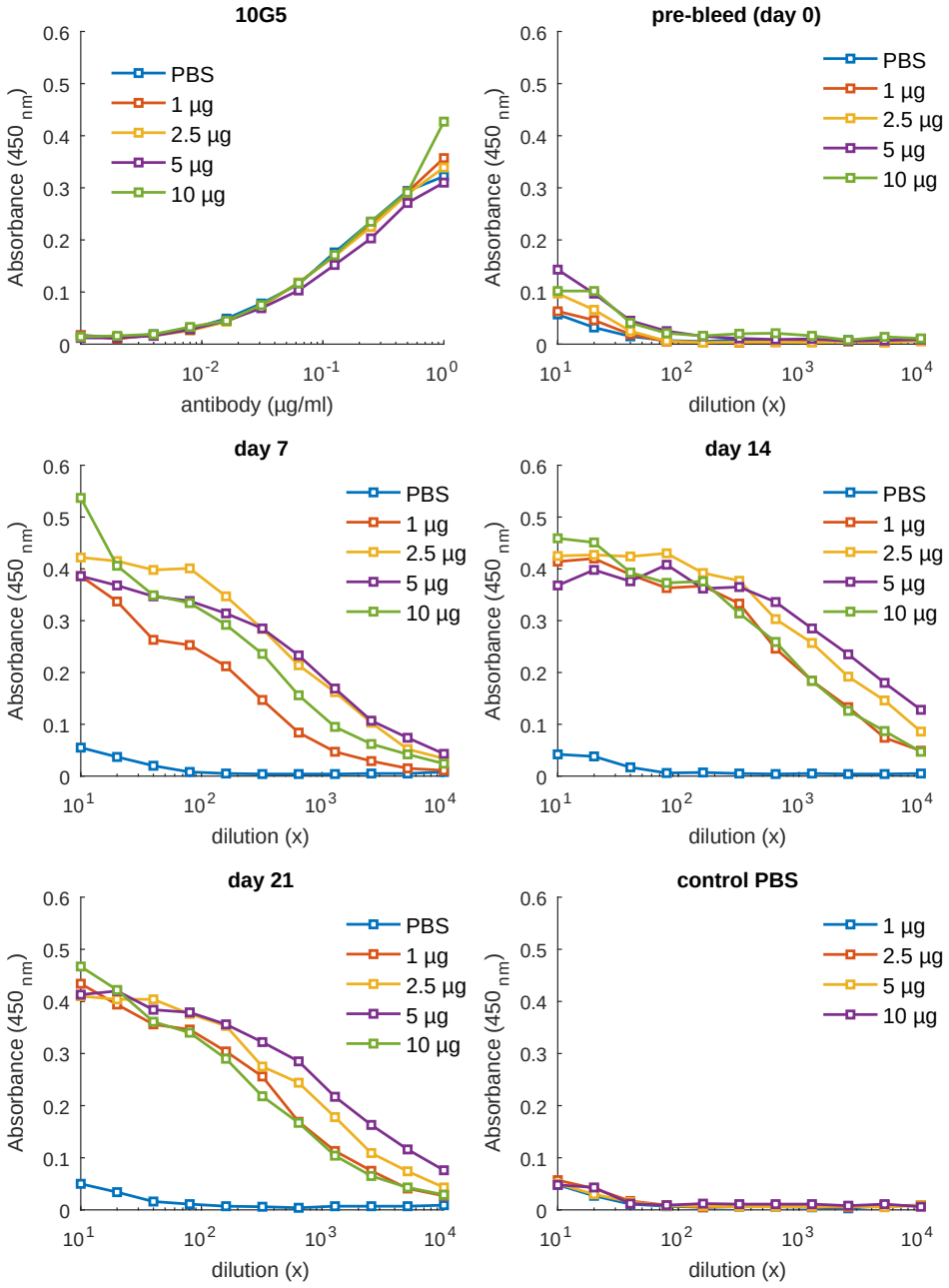

Figure A-2: ELISA serum TTCF titration overview. Serum responses of mice injected with various doses of TTCF over a 6 week time period. 10G5 used as inter plate control for normalisation.

A.8 ELISA release without dialysis

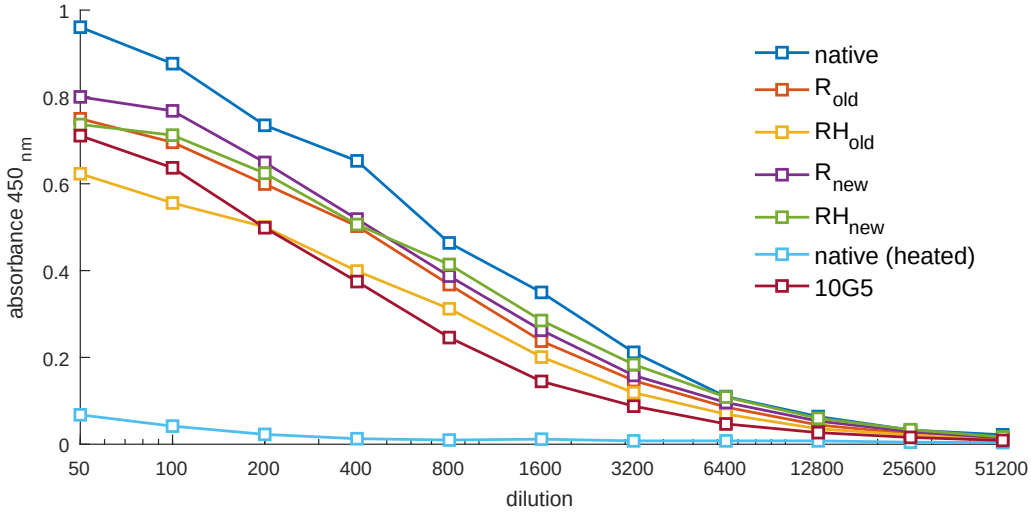

Figure A-3: ELISA binding assay of native and released ensilicated material without dialysis. Non-dialysed released TTCF was diluted in bicarbonate buffer and bound onto an ELISA plate. Mouse polyclonal serum was used to measure released TTCF binding capacity. R = released, RH = heat treated released, old = 1 month, new = 1 week after ensilication.

A.9 ELISA TTCF in vivo

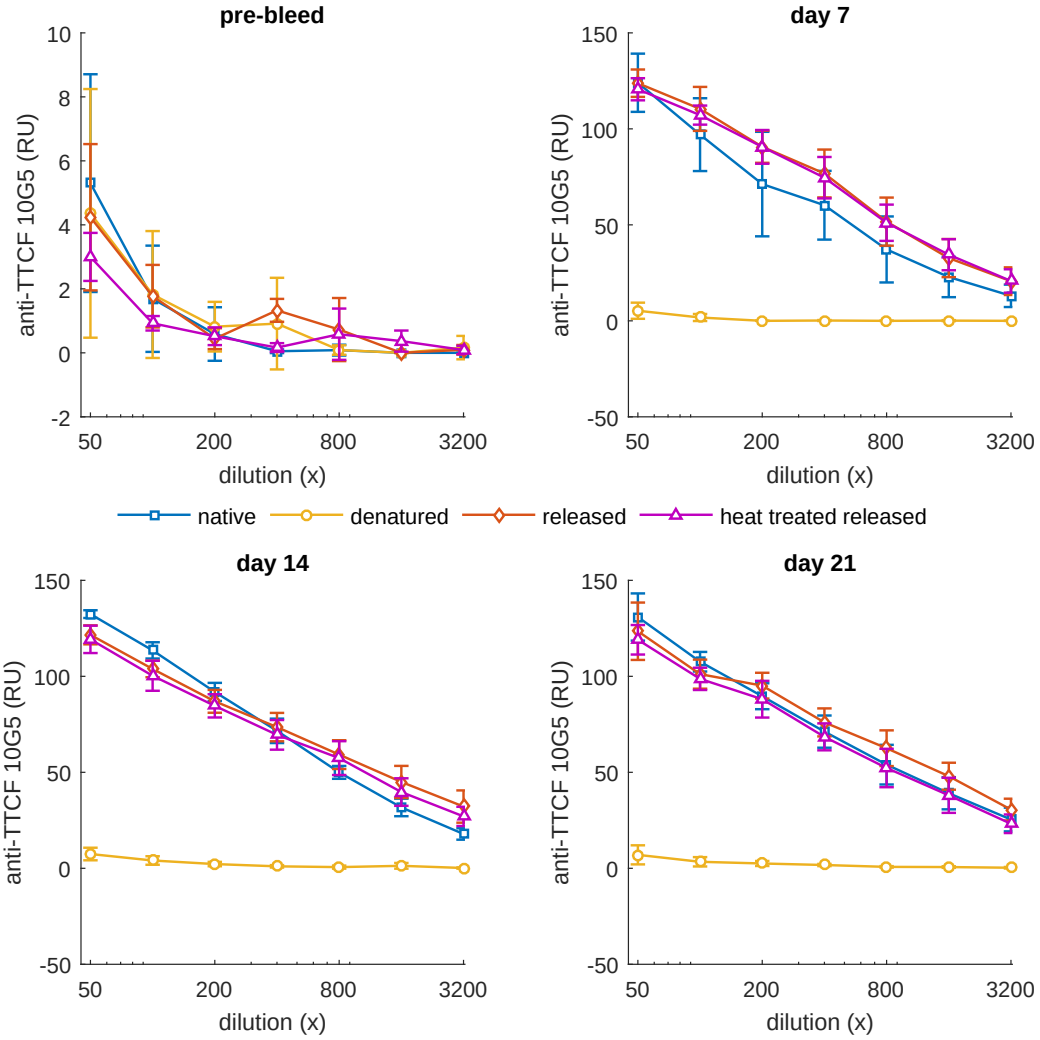

Figure A-4: ELISA serum TTCF *in vivo* overview Serum responses of 5 mice/group injected with various samples of TTCF over a 6 week time period. 10G5 used as inter plate control for normalisation.

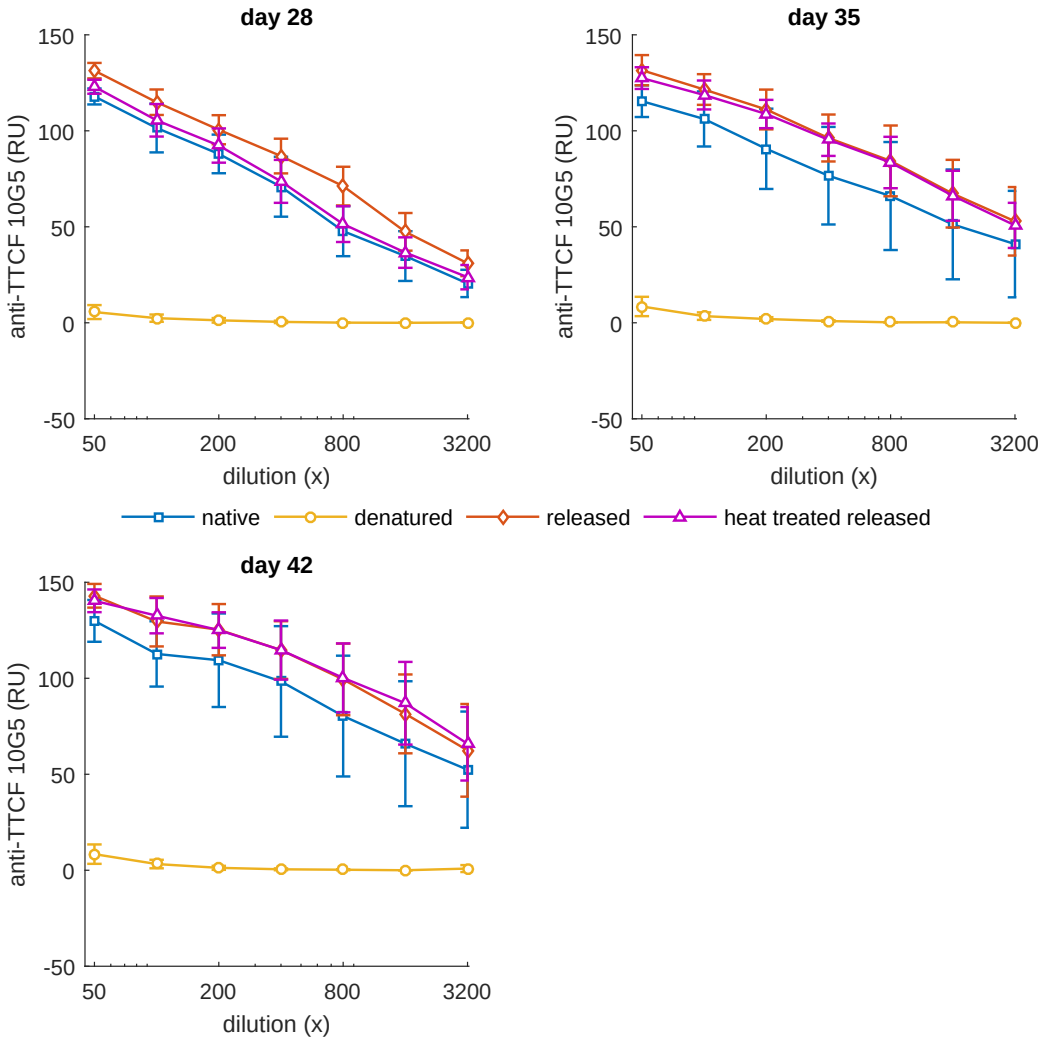

Figure A-5: ELISA serum TTCF *in vivo* overview Serum responses of 5 mice/group injected with various samples of TTCF over a 6 week time period. 10G5 used as inter plate control for normalisation.

A.10 CD thermal ramp TTCF

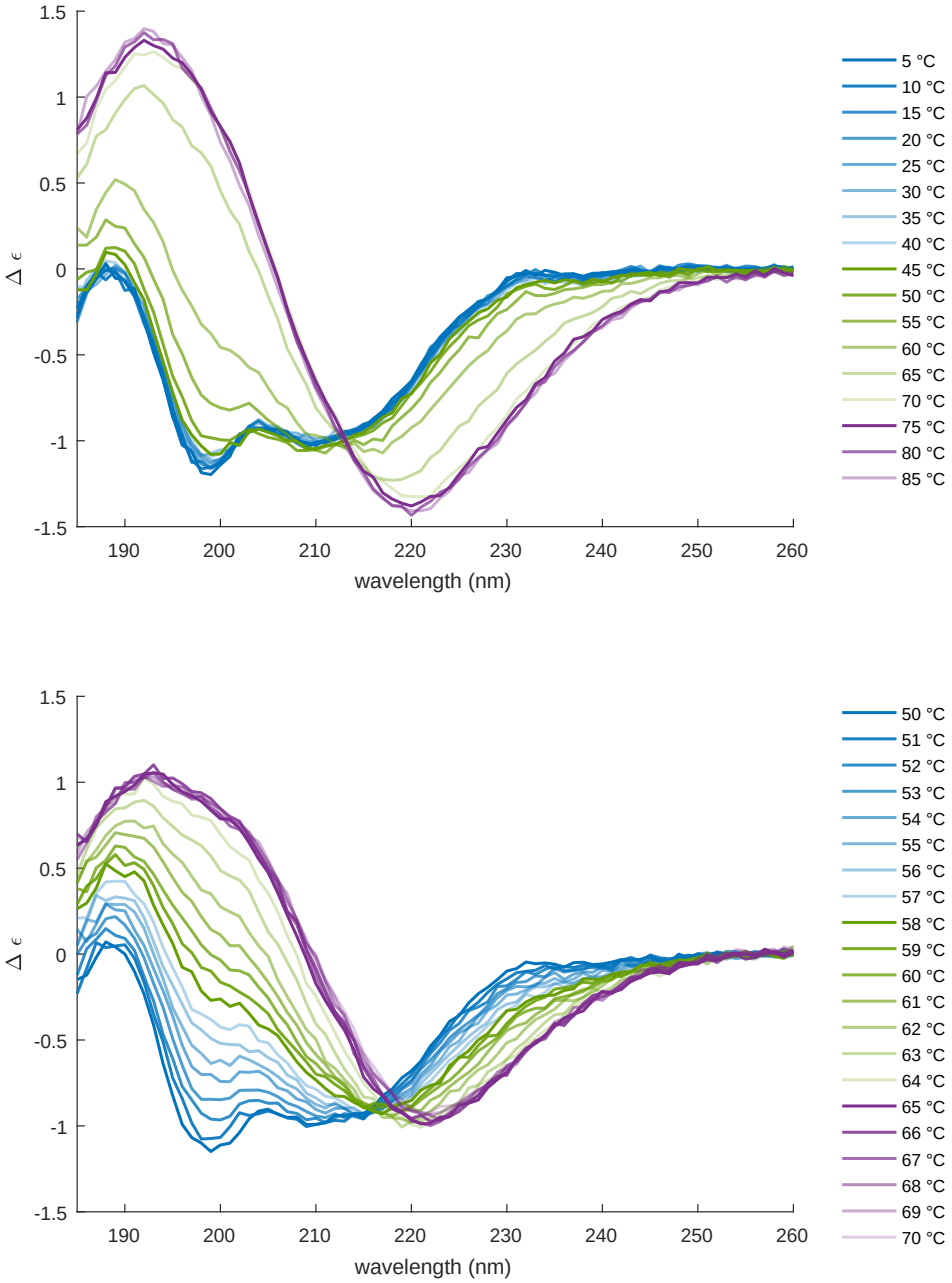

Figure A-6: CD thermal ramp native TTCF within a limited range. CD spectra between 260—185 nm were acquired for each temperature interval starting at 50°C up to 70°C with 1°C increments. Range was based on the global run to provide accurate unfolding temperatures, T_m.

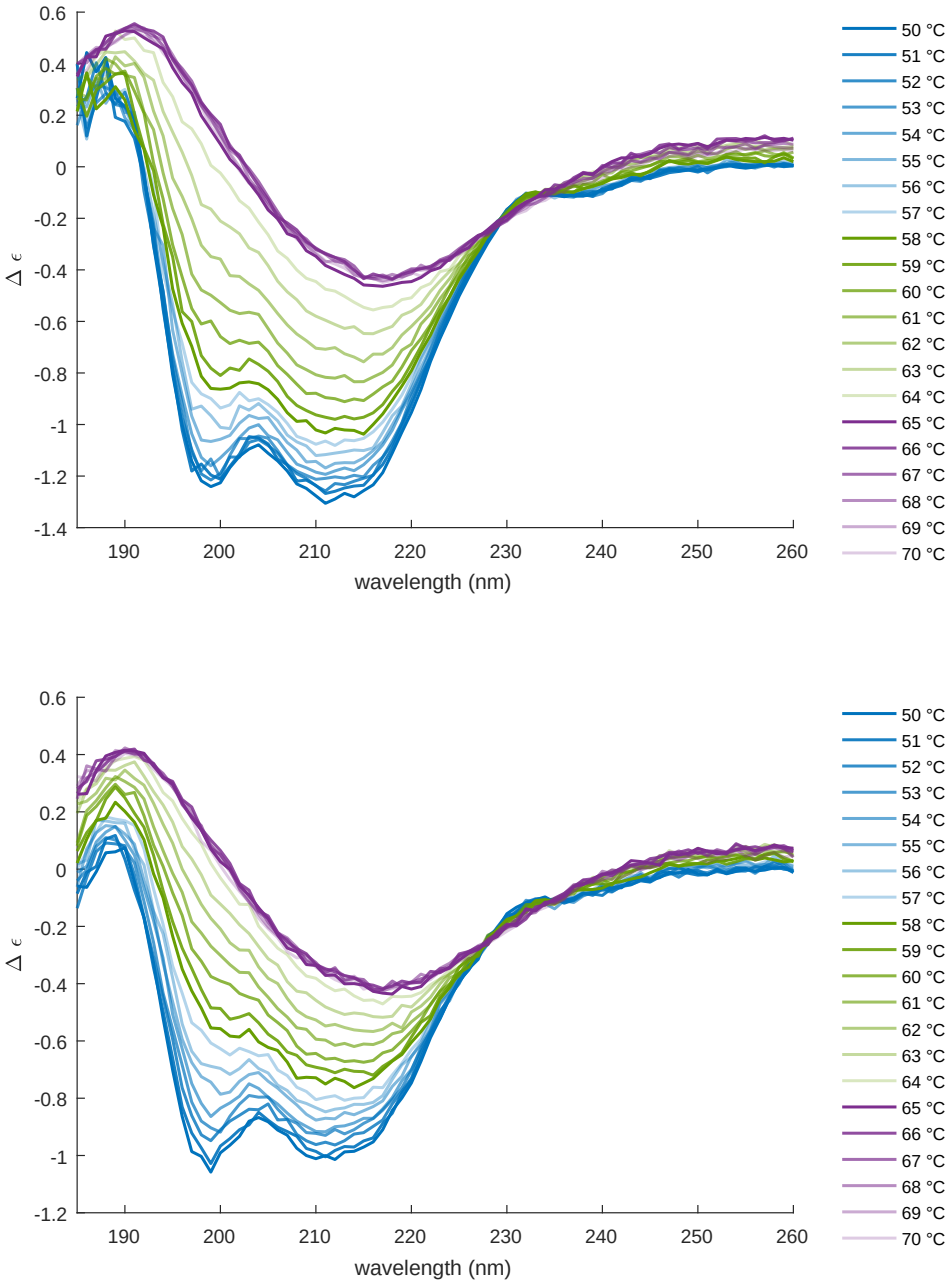

Figure A-7: CD thermal ramp heat treated released TTCF within a limited range. CD spectra between 260—185 nm were acquired for each temperature interval starting at 50°C up to 70°C with 1°C increments. Range was based on the native TTCF global run to provide accurate unfolding temperatures, T_m.

A.11 CD long-term

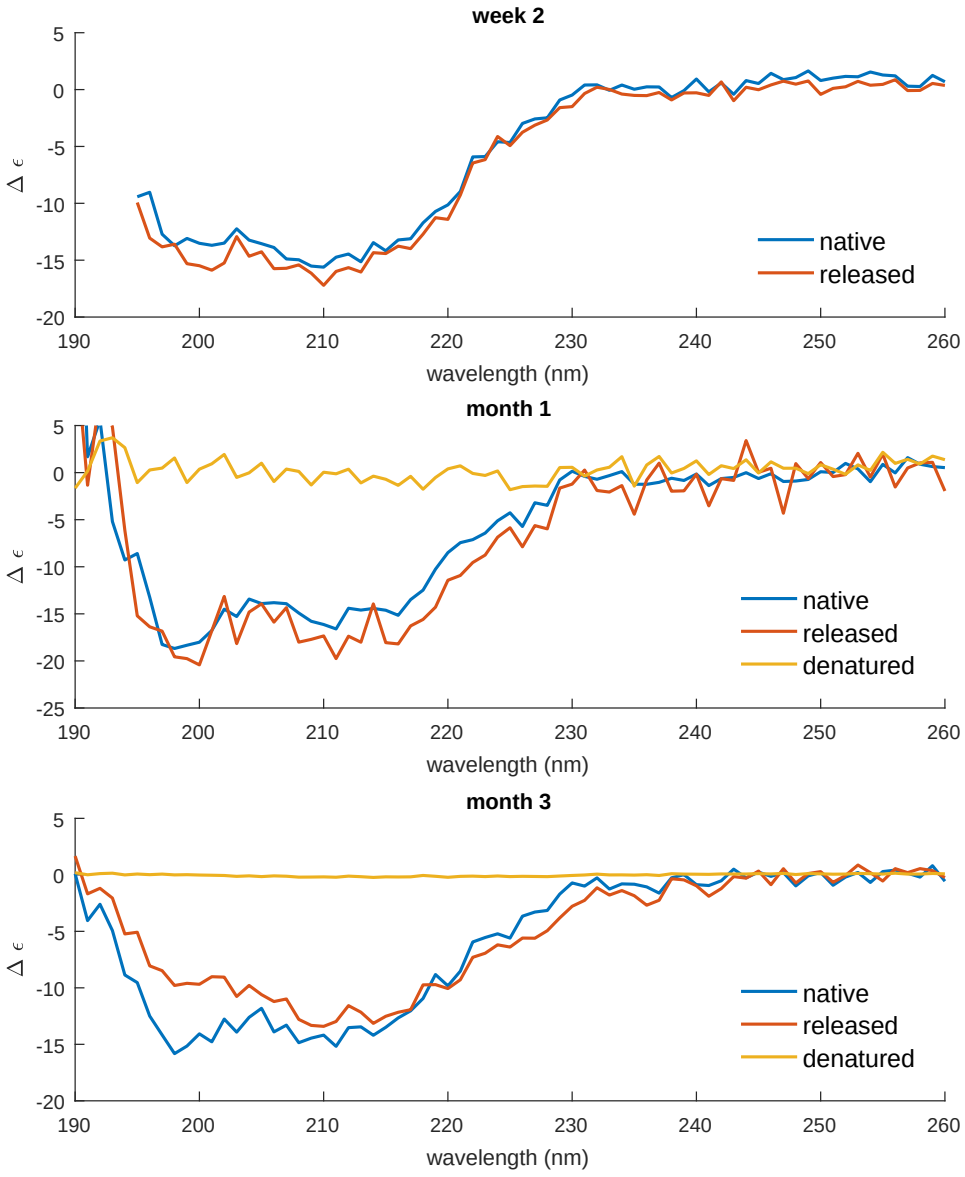

Figure A-8: CD long term, 2 weeks - 3 months. Spectra obtained from analysis of released TTCF at 2 weeks, 1 month and 3 months. Low resolution of the data is due to technical errors during sample preparation and instrument optimisation.

A.12 Lysozyme XRD parameters

X-ray data collection statistics

Spacegroup	P4322		
Unit cell dimensions (Å)	78.60	78.60	37.04
	90.00	90.00	90.00
Mosaicity	0.72		
Resolution range (last shell)	55.58 - 1.75		(1.82 - 1.75)
Total number of reflections	101347		
Number of unique reflections	11498		
Average redundancy (last shell)	8.81		(5.96)
Rmerge (last shell)	0.039		(0.128)
Rmeas (last shell)	0.041		(0.140)
RmeasA (I+, I- reflns kept apart) (last shell)	0.04		(0.144)
Reduced ChiSquared (last shell)	0.95		(0.69)
Output <I/sigI> (last shell)	37.6		(9.1)

Model refinement statistics

Resolution range (Å)		30.822 - 1.754
Number of protein atoms		1054
Number of solvent atoms		150
Rwork		0.149
Rfree		0.1944
RMS deviations		
	bonds (A°)	0.0089
	angles(deg)	1.181
MolProbity		1.22
Ramachandran		
	Favoured regions (%)	98.47
	Allowed (%)	1.53
	Outliets (%)	0.00

A.13 ELISA lysozyme in vivo

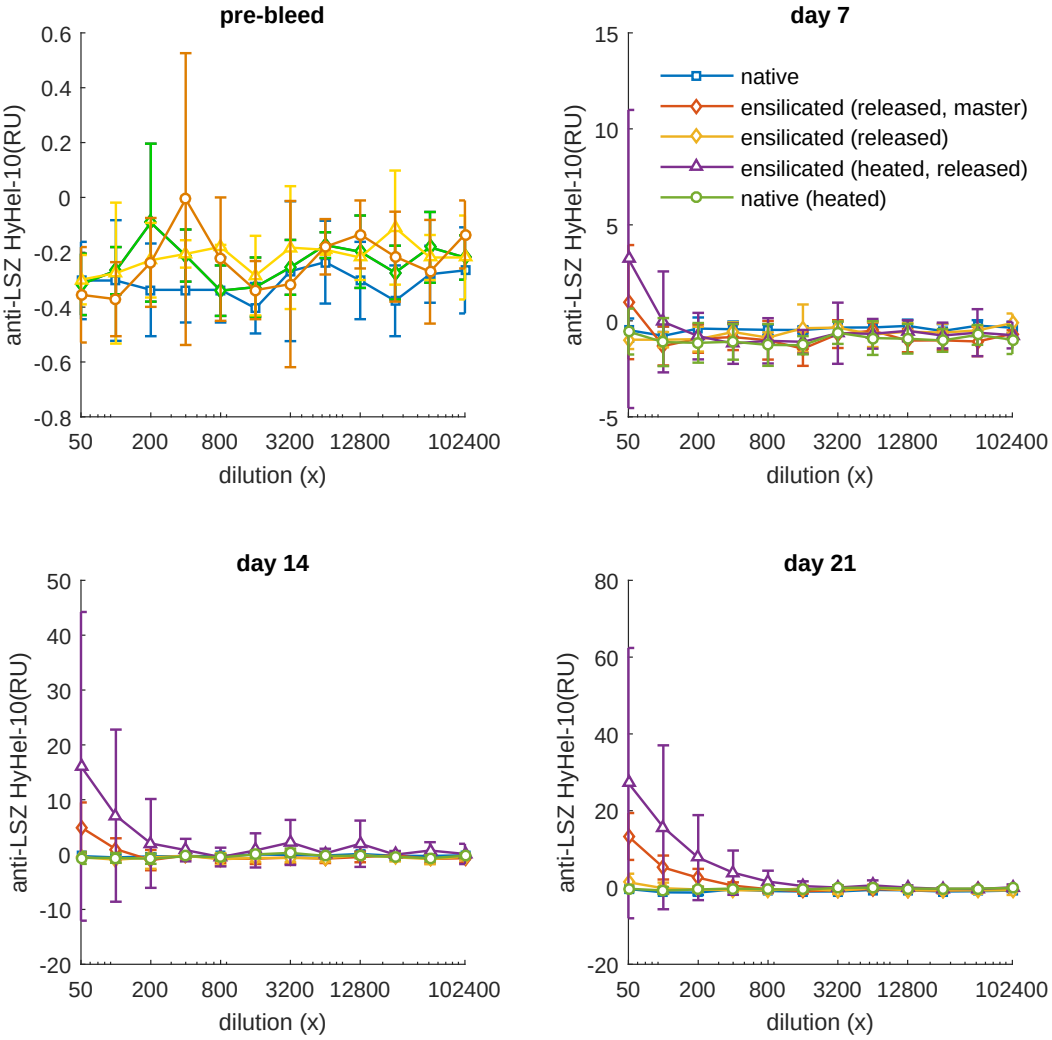

Figure A-9: ELISA serum lysozyme *in vivo* overview Serum responses of 5 mice/group injected with various types of lysozyme over a 6 week time period. HyHel-10 monoclonal antibody used as inter plate control for normalisation.

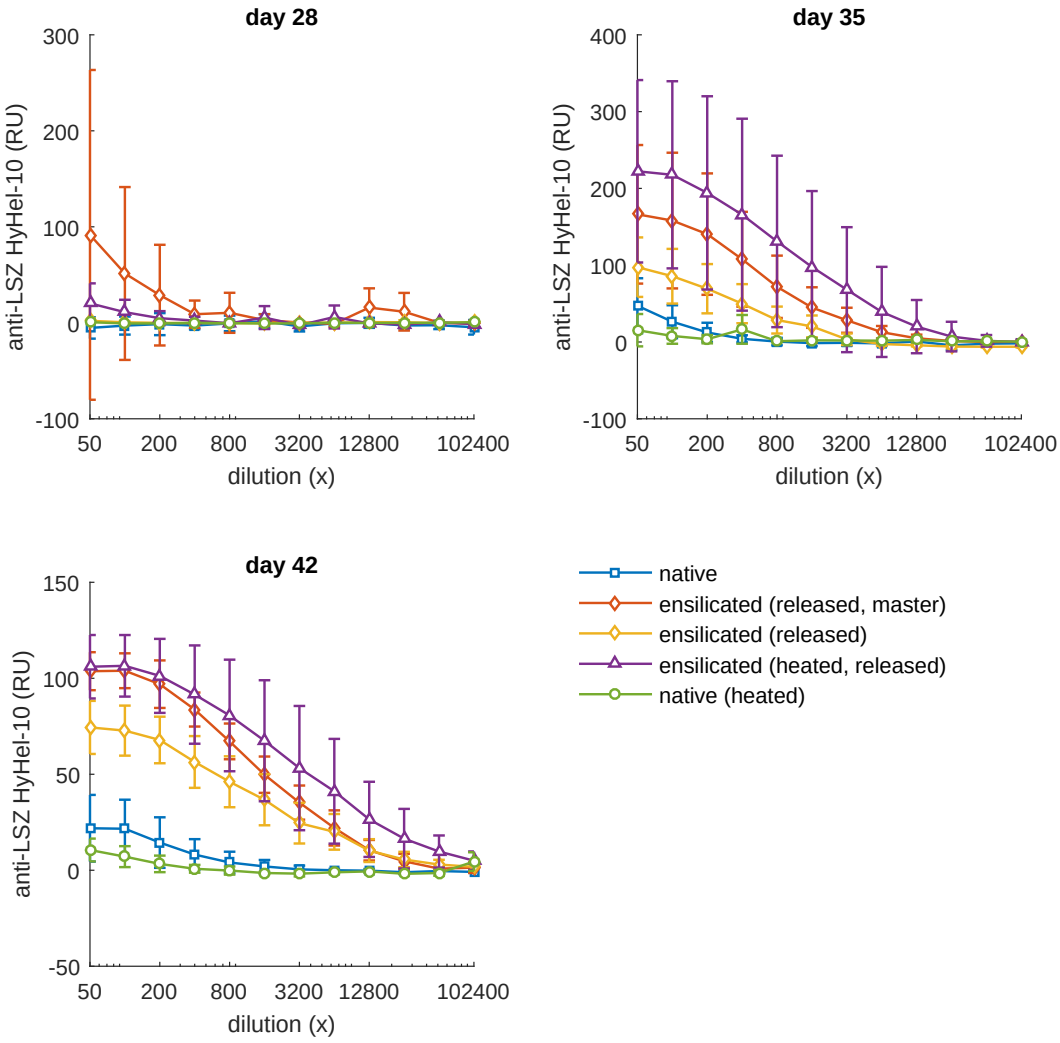

Figure A-10: ELISA serum lysozyme *in vivo* overview Serum responses of 5 mice/group injected with various types of lysozyme over a 6 week time period. HyHel-10 monoclonal antibody used as inter plate control for normalisation.

A.14 CD thermal ramp lysozyme

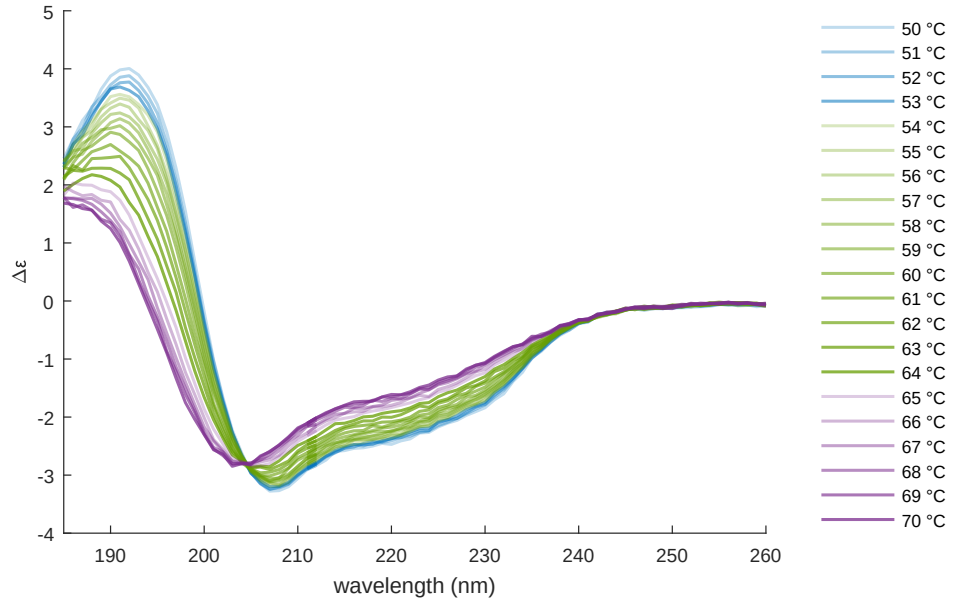

(a) native lysozyme

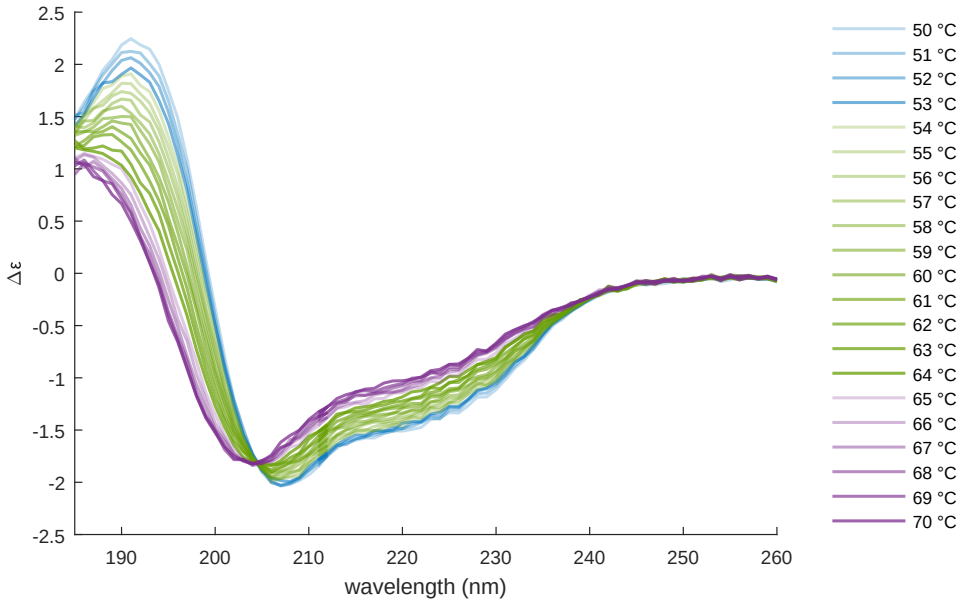

(b) released lysozyme

Figure A-11: CD thermal ramp native and released lysozyme in a limited range. CD spectra between 260—185 nm were acquired for each temperature interval starting at 60°C up to 80°C with 1°C increments. Range was based on the literature value to provide accurate unfolding temperatures, T_m.

References

[1] Edward Jenner. An inquiry into the causes and effects of the variolae vaccinae, a disease discovered in the western counties of england, particularly gloucestershire, and known by the name of the cow pox. *Springfield*, 1802.

[2] E. Liceaga. The Jenner Vaccine Well Preserved and Carefully Propagated is a Permanent Preservative against Smallpox. *Public Health Pap Rep*, 26:92–97, 1900.

[3] M. Zaffran. Vaccine transport and storage: environmental challenges. *Dev. Biol. Stand.*, 87:9–17, 1996.

[4] J Peetermans. Factors affecting the stability of viral vaccines. *Developments in biological standardization*, 87:97–101, 1996.

[5] Zaffran M. Galazka A, Milstien J. Thermostability of vaccines. Technical report, World Health Organization., 1998.

[6] M J Corbel. Reasons for instability of bacterial vaccines. *Developments in biological standardization*, 87:113–124, 1996.

[7] C J Burke, T A Hsu, and D B Volkin. Formulation, stability, and delivery of live attenuated vaccines for human use. *Critical reviews in therapeutic drug carrier systems*, 16:1–83, 1999.

[8] J F Newman, S Tirrell, C Ullman, P G Piatti, and F Brown. Stabilising oral polio-vaccine at high ambient temperatures. *Developments in biological standardization*, 87:103–111, 1996.

[9] H Lundbeck, B Håkansson, JS Lloyd, SK Litvinov, and F Assaad. A cold box for the transport and storage of vaccines. *Bulletin of the World Health Organization*, 56(3):427, 1978.

[10] S Berkley, M Chan, C Elias, A Fauci, A Lake, and J Phumaphi. *Global Vaccine Action Plan 2011-2020*. World Health Organization, 2012.

[11] WHO. Expanded programme on immunization: Vaccine vial monitor and open vial policy. questions and answers. Technical report, WHO, 1995.

[12] J S Lloyd. Improving the cold chain for vaccines. *WHO chronicle*, 31:13–18, January 1977. TJ: WHO CHRONICLE.

[13] GPVI. Vaccine vial monitors take guesswork out of immunization. *Vaccine & immunization news : the newsletter of the Global Programme for Vaccines and Immunization*, pages 7–8, June 1996. TJ: VACCINE AND IMMUNIZATION NEWS.

[14] PATH. Technology to save millions, extends vaccine outreach programs. vaccine management. *Vaccine weekly*, page 16, April 1996. TJ: VACCINE WEEKLY.

[15] John Lloyd and James Cheyne. The origins of the vaccine cold chain and a glimpse of the future. *Vaccine*, 35:2115–2120, Apr 2017.

[16] S. Subaiya, L. Dumolard, P. Lydon, M. Gacic-Dobo, R. Eggers, and L. Conklin. Global routine vaccination coverage, 2014. *MMWR Morb. Mortal. Wkly. Rep.*, 64(44):1252–1255, Nov 2015.

[17] F. L. Black. The role of herd immunity in control of measles. *Yale J Biol Med*, 55(3-4):351–360, 1982.

[18] P. Fine, K. Eames, and D. L. Heymann. "Herd immunity": a rough guide. *Clin. Infect. Dis.*, 52(7):911–916, Apr 2011.

[19] Sirirat Techathawat, Porpit Varinsathien, Aimorn Rasdjarmrearnsook, and Piyanit Tharmaphornpilas. Exposure to heat and freezing in the vaccine cold chain in thailand. *Vaccine*, 25(7):1328—1333, January 2007.

[20] Martin L Gold MS, Nayda CL, and Kempe AE. Electronic temperature monitoring and feedback to correct adverse vaccine storage in general practice. *Med J Aust.*, 171(2):83–4, Jul 19 1999.

[21] Carib Nelson, Paulo Froes, Anne Mie Van Dyck, Jeaneth Chavarría, Enrique Boda, Alberto Coca, Gladys Crespo, and Heinz Lima. Monitoring temperatures in the vaccine cold chain in bolivia. *Vaccine*, 25(3):433 – 437, Jan 2007.

[22] Li Liu, Hope L Johnson, Simon Cousens, Jamie Perin, Susana Scott, Joy E Lawn, Igor Rudan, Harry Campbell, Richard Cibulskis, Mengying Li, Colin Mathers, Robert E Black, Child Health Epidemiology Reference Group of WHO, and UNICEF. Global, regional, and national causes of child mortality: an updated systematic analysis for 2010 with time trends since 2000. *Lancet (London, England)*, 379:2151–2161, Jun 2012.

[23] WHO Expanded Programme on Immunization. Who policy statement : the use of opened vials of vaccine in subsequent immunization sessions. *Geneva : World Health Organization*, 1995. WHO/EPI/LHIS/95.01 6 p.

[24] World Health Organization. 2018 assessment report of the global vaccine action plan. strategic advisory group of experts on immunization. Geneva: World Health Organization; 2018 (WHO/IVB/18.11)., November 2018.

[25] Sarah Lane, Noni E. MacDonald, Melanie Marti, and Laure Dumolard. Vaccine hesitancy around the globe: Analysis of three years of who/unicef joint reporting form data-2015-2017. *Vaccine*, 36(26):3861–3867, June 2018.

[26] Melanie Marti, Monica de Cola, Noni E. MacDonald, Laure Dumolard, and Philippe Duclos. Assessments of global drivers of vaccine hesitancy in 2014—looking beyond safety concerns. *PLOS ONE*, 12(3):1–12, 03 2017.

[27] Helen Bedford, Katie Attwell, Margie Danchin, Helen Marshall, Paul Corben, and Julie Leask. Vaccine hesitancy, refusal and access barriers: The need for clarity in terminology. *Vaccine*, 36:6556–6558, Oct 2018.

[28] Noni MacDonald, Eve Dubé, and Robb Butler. Vaccine hesitancy terminology: A response to bedford et al. *Vaccine*, 2017.

[29] R. De Swardt, C. B. Ijsselmuiden, and M. E. Edginton. Vaccine cold-chain status in the elim health ward of gazankulu. *South African medical journal = Suid-Afrikaanse tydskrif vir geneeskunde*, 72:334–6, Sep 1987.

[30] T. A. Miles. The integrity of the vaccine cold chain in the hunter area of new south wales. *Australian journal of public health*, 17:169–71, Jun 1993.

[31] D. O. Simba and G. I. Msamanga. Use of cold-chain to assess vaccine exposure to adverse temperatures in rural tanzania. *East African medical journal*, 71:445–6, Jul 1994.

[32] Paloma Ortega Molina, Paloma Astasio Arbiza, Romana Albaladejo Vicente, M. Luisa Gomez Rabago, Jose Ramon de Juanes Pardo, and Vicente Dominguez Rojas. [vaccine storage cold chain at primary care centers in one area of madrid: keeping the chain intact and degree of knowledge]. *Revista espanola de salud publica*, 76:333–46, Jul-Aug 2002.

[33] Carib M. Nelson, Hariadi Wibisono, Hary Purwanto, Isa Mansyur, Vanda Moniaga, and Anton Widjaya. Hepatitis b vaccine freezing in the indonesian cold chain: evidence and solutions. *Bulletin of the World Health Organization*, 82:99–105, Feb 2004.

[34] Carmen Barber-Hueso, Oscar Rodriguez-Sanchez, Inmaculada Cervera-Perez, and Salvador Peiro. [the vaccine cold chain in a valencian health department (spain)]. *Gaceta sanitaria*, 23:139–43, Mar-Apr 2009.

[35] Dante Raglione, Gustavo Antonio Marcolongo Bezerra, Marta Heloisa Lopes, Maria Ligia Bacciotte Ramos Nerger, Tereza Cristina Guimaraes, and Ana Marli Christovam Sartori. [evaluation of the cold chain for vaccine conservation in primary healthcare centers in the south and midwest regions of sao paulo city, brazil, in 2011-2012]. *Epidemiologia e servicos de saude : revista do Sistema Unico de Saude do Brasil*, 25:65–74, Jan-Mar 2016.

[36] Siamon Gordon. Elie metchnikoff: father of natural immunity. *European journal of immunology*, 38:3257–64, Dec 2008.

[37] Philip A. Mackowiak. Recycling metchnikoff: probiotics, the intestinal microbiome and the quest for long life. *Frontiers in public health*, 1:52, Nov 2013.

[38] Scott L. Friedman. Focus. metchnikoff, macrophages and the metabolic syndrome. *Journal of hepatology*, 57:1–2, Jul 2012.

[39] Arthur M. Silverstein. Ilya metchnikoff, the phagocytic theory, and how things often work in science. In *Journal of leukocyte biology*, volume 90, pages 409–10, United States, Sep 2011.

[40] NL Warner, A Szenberg, and FM Burnet. The immunological role of different lymphoid organs in the chicken. *Australian Journal of Experimental Biology and Medical Science*, 40(5):373–388, 1962.

[41] Marc H. V. Van Regenmortel. What is a b-cell epitope? In *Epitope Mapping Protocols: Second Edition*, pages 3–20. Humana Press, Totowa, NJ, 2009.

[42] R. R. Porter. Chemical structure of gamma-globulin and antibodies. *British medical bulletin*, 19:197–201, Sep 1963.

[43] J. R. Marrack. The chemistry of antigens and antibodies. *The Journal of Physical Chemistry*, 38(7):989–989, 1933.

[44] Paavo Toivanen. Bursa of fabricius. In Peter J. Delves, editor, *Encyclopedia of Immunology (Second Edition)*, pages 393–396. Elsevier, Oxford, January 1998.

[45] D. H. Katz and B. Benacerraf. The regulatory influence of activated t cells on b cell responses to antigen. *Advances in immunology*, 15:1–94, 1972.

[46] CA Janeway, P Travers, and M Walport. *Immunobiology: The Immune System in Health and Disease. The major histocompatibility complex and its functions.* Garland Science, New York, 5th edition, 2001.

[47] J. F. Miller. Immunological function of the thymus. *Lancet (London, England)*, 2:748–9, Sep 1961.

[48] G Ramon. Sur la toxine et sur i'anatoxine diphtheriques. *Ann. Inst. Pasteur*, 38:1–10, 1924.

[49] J. Aucouturier, L. Dupuis, and V. Ganne. Adjuvants designed for veterinary and human vaccines. *Vaccine*, 19:2666–72, Mar 2001.

[50] Sunita Awate, Lorne A. Babiuk, and George Mutwiri. Mechanisms of action of adjuvants. *Frontiers in immunology*, 4:114–114, May 2013.

[51] Volker Gerdts. Adjuvants for veterinary vaccines–types and modes of action. *Berliner und Munchener tierarztliche Wochenschrift*, 128:456–463, 2015.

[52] A. T. Glenny, C. G. Pope, Hilda Waddington, and U. Wallace. Immunological notes. xvii-xxiv. *J. Pathol.*, 29(1):31–40, January 1926.

[53] JC Freund and JEP Hosmer. Sensitization and antibody formation after inejction of tubercle bacili and parafin oil. *Proc Soc Exp Biol Medical*, 1937.

[54] S.A. Plotkin and W.A. Orenstein. *Vaccines. 3rd edition.* Philadelphia: Saunders, 1999.

[55] C. B. Anfinsen and H. A. Scheraga. Experimental and theoretical aspects of protein folding. *Advances in protein chemistry*, 29:205–300, 1975.

[56] L.A. Urry, M.L. Cain, S.A. Wasserman, P.V. Minorsky, and J.B. Reece. *Campbell Biology, 11th Edition*. Pearson, 2017.

[57] Gregory J. Jr. Gatto Jeremy M. Berg, John L. Tymoczko and Lubert Stryer. *Biochemistry*. Macmillan Education, 2015.

[58] W. Kauzmann. Some factors in the interpretation of protein denaturation. In C.B. Anfinsen, M.L. Anson, Kenneth Bailey, and John T. Edsall, editors, *Advances in Protein Chemistry*, volume 14 of *Advances in Protein Chemistry*, pages 1 – 63. Academic Press, 1959.

[59] John T. Edsall. Hsien wu and the first theory of protein denaturation (1931). In C.B. Anfinsen, Frederic M. Richards, John T. Edsall, and David S. Eisenberg, editors, *Protein Stability*, volume 46 of *Advances in Protein Chemistry*, pages 1 – 5. Academic Press, 1995.

[60] Ken A. Dill, Sarina Bromberg, Kaizhi Yue, Hue Sun Chan, Klaus M. Ftebig, David P. Yee, and Paul D. Thomas. Principles of protein folding — a perspective from simple exact models. *Protein Science*, 4(4):561–602, 1995.

[61] S. Krimm. The hydrophobic effect: Formation of micelles and biological membranes, charles tanford, wiley-interscience, new york, 1980, 233 pp. price: $18.50. *Journal of Polymer Science: Polymer Letters Edition*, 18(10):687–687, 1980.

[62] A. Cooper. *Protein: A Comprehensive Treatise*, volume 2, chapter Thermodynamics of Protein Folding and Stability, pages 217–270. JAI Press Inc., 1999.

[63] J L Cleland, M F Powell, and S J Shire. The development of stable protein formulations: a close look at protein aggregation, deamidation, and oxidation. *Critical reviews in therapeutic drug carrier systems*, 10:307–377, 1993.

[64] K C Fox. Biopreservation. putting proteins under glass. *Science (New York, N.Y.)*, 267:1922–1923, March 1995.

[65] W Wang. Lyophilization and development of solid protein pharmaceuticals. *International journal of pharmaceutics*, 203:1–60, August 2000.

[66] H Willemer. Measurements of temperatures, ice evaporation rates and residual moisture contents in freeze-drying. *Developments in biological standardization*, 74:123–34; discussion 135–6, 1992.

[67] MJ Pikal. Freeze-drying of proteins. part i: process design. *Biopharm.*, 1990.

[68] J A House and J C Mariner. Stabilization of rinderpest vaccine by modification of the lyophilization process. *Developments in biological standardization*, 87:235–244, 1996.

[69] Thomas A. Jennings. *Lyophilization: Introduction and Basic Principle.* Informa Healthcare, 1999.

[70] F Franks. Freeze-drying: from empiricism to predictability. the significance of glass transitions. *Developments in biological standardization*, 74:9–18; discussion 19, 1992.

[71] Joan C. May Louis Rey, editor. *Freeze Drying/Lyophilization of Pharmaceutical and Biological Products.* Informa Healthcare, 2010.

[72] E E Worrall, J K Litamoi, B M Seck, and G Ayelet. Xerovac: an ultra rapid method for the dehydration and preservation of live attenuated rinderpest and peste des petits ruminants vaccines. *Vaccine*, 19:834–839, November 2000.

[73] J K Litamoi, G Ayelet, and M M Rweyemamu. Evaluation of the xerovac process for the preparation of heat tolerant contagious bovine pleuropneumonia (cbpp) vaccine. *Vaccine*, 23:2573–2579, April 2005.

[74] Jeffrey C Mariner, James Gachanja, Sheltone H Tindih, and Philip Toye. A thermostable presentation of the live, attenuated peste des petits ruminants vaccine in use in africa and asia. *Vaccine*, 35:3773–3779, June 2017.

[75] Johnson. Preparation of peptide and protein powders for inhalation. *Advanced drug delivery reviews*, 26:3–15, June 1997.

[76] Yuh-Fun Maa, Mahmoud Ameri, Cassandra Shu, Lendon G Payne, and Dexiang Chen. Influenza vaccine powder formulation development: spray-freeze-drying and stability evaluation. *Journal of pharmaceutical sciences*, 93:1912–1923, July 2004.

[77] H. W. Frijlink and A. H. De Boer. Dry powder inhalers for pulmonary drug delivery. *Expert opinion on drug delivery*, 1:67–86, Nov 2004.

[78] Juan Huang, Robert J Garmise, Timothy M Crowder, Kevin Mar, C Robin Hwang, Anthony J Hickey, John A Mikszta, and Vincent J Sullivan. A novel dry powder

influenza vaccine and intranasal delivery technology: induction of systemic and mucosal immune responses in rats. *Vaccine*, 23:794–801, December 2004.

[79] Duane T. Brandau, Latoya S. Jones, Christopher M. Wiethoff, Jason Rexroad, and C. Russell Middaugh. Thermal stability of vaccines. *Journal of Pharmaceutical Sciences*, 92(2):218–231, 2003.

[80] Matthew Auton, D Wayne Bolen, and Jörg Rösgen. Structural thermodynamics of protein preferential solvation: osmolyte solvation of proteins, aminoacids, and peptides. *Proteins*, 73:802–813, December 2008.

[81] Serge N Timasheff. Protein-solvent preferential interactions, protein hydration, and the modulation of biochemical reactions by solvent components. *Proceedings of the National Academy of Sciences of the United States of America*, 99:9721–9726, July 2002.

[82] Serge N Timasheff. Protein hydration, thermodynamic binding, and preferential hydration. *Biochemistry*, 41:13473–13482, November 2002.

[83] Jiang Hong, Michael W Capp, Charles F Anderson, Ruth M Saecker, Daniel J Felitsky, Melissa W Anderson, and M Thomas Record. Preferential interactions of glycine betaine and of urea with dna: implications for dna hydration and for effects of these solutes on dna stability. *Biochemistry*, 43:14744–14758, November 2004.

[84] Seishi Shimizu and Derek J Smith. Preferential hydration and the exclusion of cosolvents from protein surfaces. *The Journal of chemical physics*, 121:1148–1154, July 2004.

[85] J. Birner and J. R. Garnet. Thimerosal as a preservative in biological preparations. i. application of polarography to the determination of thimerosal in aqueous solutions and vaccines. *Journal of pharmaceutical sciences*, 53:1264–5, Oct 1964.

[86] E. O. Davisson, H. M. Powell, J. O. Macfarlane, R. Hodgson, R. L. Stone, and C. G. Culbertson. The preservation of poliomyelitis vaccine with stabilized merthiolate. *The Journal of laboratory and clinical medicine*, 47:8–19, Jan 1956.

[87] C. B. Gerichter and W. Silberstein. T.a.b. studies; merthiolate as preservative of vi-antigen in t.a.b. vaccine. ii. passive mouse protection. *Acta medica Orientalia*, 15:10–7, Jan 1956.

[88] D. Nagaki, K. Iwasaki, S. Homma, Y. Nakase, and T. Uchiyama. Studies on influenza virus. iii. studies on the influenza virus vaccine; immunization experiment of mice with the influenza virus vaccine inactivated by sodium ethylmercurithiosalicylate. *The Kitasato archives of experimental medicine*, 26:209–15, Dec 1953.

[89] E. A. Nelson and H. D. Anderson. Potencies of phenolized rabies vaccine improved by addition of merthiolate during inactivation. *Applied microbiology*, 1:135–7, May 1953.

[90] L. Greenberg and M. Detlor. Phenol and merthiolate as preservatives for diphtheria toxoid. *The Journal of pathology and bacteriology*, 65:616–8, Apr 1953.

[91] W. Silberstein and C. B. Gerichter. Merthiolate as preservative of vi-antigen in tab vaccine. i. active mouse protection. *Acta medica Orientalia*, 12:159–64, Jun 1953.

[92] Paul A Offit and Rita K Jew. Addressing parents' concerns: do vaccines contain harmful preservatives, adjuvants, additives, or residuals? *Pediatrics*, 112:1394–1397, December 2003.

[93] Joachim Mutter, Johannes Naumann, Rainer Schneider, Harald Walach, and Boyd Haley. Mercury and autism: accelerating evidence? *Neuro endocrinology letters*, 26:439–46, Oct 2005.

[94] B. Taylor. Vaccines and the changing epidemiology of autism. *Child: care, health and development*, 32:511–9, Sep 2006.

[95] Mieszko Olczak, Michalina Duszczyk, Pawel Mierzejewski, Teresa Wierzba-Bobrowicz, and Maria D. Majewska. Lasting neuropathological changes in rat brain after intermittent neonatal administration of thimerosal. *Folia neuropathologica*, 48:258–69, 2010.

[96] Mieszko Olczak, Michalina Duszczyk, Pawel Mierzejewski, Teresa Bobrowicz, and Maria Dorota Majewska. Neonatal administration of thimerosal causes persistent changes in mu opioid receptors in the rat brain. *Neurochemical research*, 35:1840–7, Nov 2010.

[97] Michalina Duszczyk-Budhathoki, Mieszko Olczak, Malgorzata Lehner, and Maria Dorota Majewska. Administration of thimerosal to infant rats increases overflow of glutamate and aspartate in the prefrontal cortex: protective role of dehydroepiandrosterone sulfate. *Neurochemical research*, 37:436–47, Feb 2012.

[98] I. Lowe and J. Southern. The antimicrobial activity of phenoxyethanol in vaccines. *Letters in applied microbiology*, 18:115–6, Feb 1994.

[99] Nityananda Sahoo, Ranjan Ku. Sahoo, Nikhil Biswas, Arijit Guha, and Ketousetuo Kuotsu. Recent advancement of gelatin nanoparticles in drug and vaccine delivery. *International Journal of Biological Macromolecules*, 81:317 – 331, 2015.

[100] Tanya Clapp, Paul Siebert, Dexiang Chen, and LaToya Jones Braun. Vaccines with aluminum-containing adjuvants: Optimizing vaccine efficacy and thermal stability, Feb 2011.

[101] M Ellmerer, L Schaupp, G A Brunner, G Sendlhofer, A Wutte, P Wach, and T R Pieber. Measurement of interstitial albumin in human skeletal muscle and adipose tissue by open-flow microperfusion. *American journal of physiology. Endocrinology and metabolism*, 278:E352–E356, February 2000.

[102] Gregory J. Quinlan, Greg S. Martin, and Timothy W. Evans. Albumin: biochemical properties and therapeutic potential. *Hepatology (Baltimore, Md.)*, 41:1211–9, Jun 2005.

[103] Sung-Min Ahn, Kyunghee Byun, Kun Cho, Jin Young Kim, Jong Shin Yoo, Deokhoon Kim, Sun Ha Paek, Seung U. Kim, Richard J. Simpson, and Bonghee Lee. Human microglial cells synthesize albumin in brain. *PloS one*, 3:e2829, Jul 2008.

[104] European Medicines Agency. Chmp position statement on creutzfeldt-jakob disease and plasma-derived and urine-derived medicinal products. Technical report, EMEA, 2011.

[105] R. Wu, M. M. Georgescu, F. Delpeyroux, S. Guillot, J. Balanant, K. Simpson, and R. Crainic. Thermostabilization of live virus vaccines by heavy water (d2o). *Vaccine*, 13:1058–63, Aug 1995.

[106] J. L. Melnick and C. Wallis. Effect of ph on thermal stabilization of oral poliovirus vaccine by magnesium chloride. *Proceedings of the Society for Experimental Biology and Medicine. Society for Experimental Biology and Medicine (New York, N.Y.)*, 112:894–7, Apr 1963.

[107] A. K. Srivastava. Stabilization of the attenuated poliovirus type 3 vaccine strain by sucrose. *Acta virologica*, 33:188–90, Mar 1989.

[108] M. Barme, B. Vacher, M. L. Ryhiner, and G. Chabannier. [thermostabilization of the lyophilized yellow fever vaccine 17-d. ii. pilot lots prepared under conditions of industrial production]. *Journal of biological standardization*, 15:67–72, Jan 1987.

[109] D. K. Sood, R. K. Aggarwal, S. B. Sharma, J. Sokhey, and H. Singh. Study on the stability of 17d-204 yellow fever vaccine before and after stabilization. *Vaccine*, 11:1124–8, 1993.

[110] C. Radha, P. Salotra, R. Bhat, and R. Bhatnagar. Thermostabilization of protective antigen–the binding component of anthrax lethal toxin. *Journal of biotechnology*, 50:235–42, Oct 1996.

[111] C. H. Chen, R. Wu, L. G. Roth, S. Guillot, and R. Crainic. Elucidating mechanisms of thermostabilization of poliovirus by d2o and mgcl2. *Archives of biochemistry and biophysics*, 342:108–16, Jun 1997.

[112] Mine R. Ikizler and Peter F. Wright. Thermostabilization of egg grown influenza viruses. *Vaccine*, 20:1393–9, Jan 2002.

[113] Samer Singh, Aparna Singh, Mohd Azhar Aziz, Syed Mohsin Waheed, Rajiv Bhat, and Rakesh Bhatnagar. Thermal inactivation of protective antigen of bacillus anthracis and its prevention by polyol osmolytes. *Biochemical and biophysical research communications*, 322:1029–37, Sep 2004.

[114] Robert Alcock, Matthew G. Cottingham, Christine S. Rollier, Julie Furze, Samodh D. De Costa, Marian Hanlon, Alexandra J. Spencer, Jared D. Honeycutt, David H. Wyllie, Sarah C. Gilbert, Migena Bregu, and Adrian V. S. Hill. Long-term thermostabilization of live poxviral and adenoviral vaccine vectors at supraphysiological temperatures in carbohydrate glass. *Science translational medicine*, 2:19ra12, Feb 2010.

[115] Fang Lv, Yu Lu, Zheng-Lin Hao, Yan-Hong Zhao, Li-Hang Zhang, Lei Feng, Jin Chen, Li-Li Wang, Rong Rui, and Ji-Bo Hou. Preparation and heat resistance study of porcine reproductive and respiratory syndrome virus sugar glass vaccine. *Vaccine*, 34:3746–50, Jul 2016.

[116] A. C. Chang and R. K. Gupta. Stabilization of tetanus toxoid in poly(dl-lactic-co-glycolic acid) microspheres for the controlled release of antigen. *Journal of pharmaceutical sciences*, 85:129–32, Feb 1996.

[117] O'Hagan. Microparticles and polymers for the mucosal delivery of vaccines. *Advanced drug delivery reviews*, 34:305–320, Dec 1998.

[118] W. Jiang and S. P. Schwendeman. Stabilization of a model formalinized protein antigen encapsulated in poly(lactide-co-glycolide)-based microspheres. *Journal of pharmaceutical sciences*, 90:1558–69, Oct 2001.

[119] Wenlei Jiang and Steven P. Schwendeman. Stabilization of tetanus toxoid encapsulated in plga microspheres. *Molecular pharmaceutics*, 5:808–17, Sep-Oct 2008.

[120] Stephany Y. Tzeng, Rohiverth Guarecuco, Kevin J. McHugh, Sviatlana Rose, Evan M. Rosenberg, Yingying Zeng, Robert Langer, and Ana Jaklenec. Thermostabilization of inactivated polio vaccine in plga-based microspheres for pulsatile release. *Journal of controlled release : official journal of the Controlled Release Society*, 233:101–13, Jul 2016.

[121] M J Alonso, S Cohen, T G Park, R K Gupta, G R Siber, and R Langer. Determinants of release rate of tetanus vaccine from polyester microspheres. *Pharmaceutical research*, 10:945–953, July 1993.

[122] M. S. Siva Sankar, V. Bhanuprakash, G. Venkatesan, D. P. Bora, M. Prabhu, and R. Yogisharadhya. Comparative efficacy of chemical stabilizers on the thermostabilization of a novel live attenuated buffalopox vaccine. *Biologicals : journal of the International Association of Biological Standardization*, 49:39–45, Sep 2017.

[123] Ralph K. Iler. *The Chemistry of Silica: Solubility, Polymerization, Colloid and Surface Properties and Biochemistry of Silica*. John Wiley and Sons, 1979.

[124] Hans-Jurgen Ensikat, Thorsten Geisler, and Maximilian Weigend. A first report of hydroxylated apatite as structural biomineral in loasaceae - plants' teeth against herbivores. *Scientific reports*, 6:26073, May 2016.

[125] B. E. Reimann, J. C. Leivin, and B. E. Volcani. Studies on the biochemistry and fine structure of silica shell formation in diatoms. ii. the structure of the cell wall of navicula pelliculosa (breb.) hilse. *Journal of phycology*, 2:74–84, Jun 1966.

[126] B. E. Reimann, J. C. Lewin, and B. E. Volcani. Studies on the biochemistry and fine structure of silica shell formation in diatoms. i. the structure of the cell wall of cylindrotheca fusiformis reimann and lewin. *The Journal of cell biology*, 24:39–55, Jan 1965.

[127] B. E. Reimann. Deposition of silica inside a diatom cell. *Experimental cell research*, 34:605–8, May 1964.

[128] Thomas C. Boothby, Hugo Tapia, Alexandra H. Brozena, Samantha Piszkiewicz, Austin E. Smith, Ilaria Giovannini, Lorena Rebecchi, Gary J. Pielak, Doug Koshland, and Bob Goldstein. Tardigrades use intrinsically disordered proteins to survive desiccation. *Molecular cell*, 65:975–984.e5, Mar 2017.

[129] Wen Jin and John D Brennan. Properties and applications of proteins encapsulated within sol–gel derived materials. *Analytica Chimica Acta*, 461(1):1–36, jun 2002.

[130] Gareth J. Owens, Rajendra K. Singh, Farzad Foroutan, Mustafa Alqaysi, Cheol-Min Han, Chinmaya Mahapatra, Hae-Won Kim, and Jonathan C. Knowles. Sol–gel based materials for biomedical applications. *Progress in Materials Science*, 77:1 – 79, 2016.

[131] R. F. S. Lenza, W. L. Vasconcelos, J. R. Jones, and L. L. Hench. Surface-modified 3d scaffolds for tissue engineering. *Journal of Materials Science: Materials in Medicine*, 13(9):837–842, September 2002.

[132] R. Li, A. E. Clark, and L. L. Hench. An investigation of bioactive glass powders by sol-gel processing. *J. App. Biomater.*, 2(4):231–239, December 1991.

[133] Fang Lu, Si-Han Wu, Yann Hung, and Chung-Yuan Mou. Size effect on cell uptake in well-suspended, uniform mesoporous silica nanoparticles. *Small*, 5(12):1408–1413, June 2009.

[134] Zhen-An Qiao, Ling Zhang, Mingyi Guo, Yunling Liu, and Qisheng Huo. Synthesis of mesoporous silica nanoparticles via controlled hydrolysis and condensation of silicon alkoxide. *Chem. Mater.*, 21(16):3823–3829, August 2009.

[135] Thomas Graham. Xxxv.–on the properties of silicic acid and other analogous colloidal substances. *J. Chem. Soc.*, 17(0):318–327, 1864.

[136] M Ebelmen. Recherches sur les combinaisons des acides borique et silicique avec les e´ thers. *Ann Chim Phys*, 1846.

[137] Walter A Patrick. Silica gel and process of making same., March 18 1919. US Patent 1,297,724.

[138] S. S. Kistler. Coherent expanded aerogels and jellies. *Nature*, 127:741, May 1931.

[139] C Jeffrey Brinker and George W Scherer. *Sol-gel science: the physics and chemistry of sol-gel processing*. Academic press, 2013.

[140] Rosaria Ciriminna, Marzia Sciortino, Giuseppe Alonzo, Aster de Schrijver, and Mario Pagliaro. From molecules to systems: Sol-gel microencapsulation in silica-based materials. *Chemical Reviews*, 111(2):765–789, feb 2011.

[141] Thomas Graham. Xxxv.-on the properties of silicic acid and other analogous colloidal substances. *J. Chem. Soc.*, 17:318–327, 1864.

[142] A. Carle and G. Rattone. Studio esperimentale sull'eziologia del tetano (experimental studies of the etiology of tetanus). *Giorn. Accad. Med. Torino*, 1(32):174–179, 1884.

[143] S. Kitasato. Ueber den tetanus bacillus (on the tetanus bacillus). *Z. Hyg. Infekt. Kr.*, 7:225–233, 1889.

[144] W E Van Heyningen. Tetanus. *Scientific American*, 218:69–73 passim, April 1968.

[145] W. H. Manwaring. Types of tetanus toxin. *California and western medicine*, 59(6):306–307, December 1943.

[146] K. Faber. Die pathogenie des tetanus (the pathogenesis of tetanus). *Berl. klin. Wochenschr.*, 27:717–720, 1890.

[147] G. Tizzoni and G. Cattani. Uber das tetanusgift (on tetanus toxin). *Zentralbl. Bakt.*, 8:69–73, 1890.

[148] D. M. Cowie and R. M. Greenthal. Studies on the nature of the action of non-specific protein in disease processes : Iii. non-specific proteins and soluble toxin (diphtheria-tetanus). *The Journal of medical research*, 43:21–8, Jan 1922.

[149] V. B. Brooks, D. R. Curtis, and J. C. Eccles. The action of tetanus toxin on the inhibition of motoneurones. *The Journal of Physiology*, 135(3):655–672, March 1957.

[150] V. B. Brooks, D. R. Curtis, and J. C. Eccles. Mode of action of tetanus toxin. *Nature*, 175:120–1, Jan 1955.

[151] A. M. Harvey. The peripheral action of tetanus toxin. *The Journal of physiology*, 96(3):348–365, August 1939.

[152] Sherrington Charles Scott. On reciprocal innervation of antagonistic muscles. -tenth note. *Proceedings of the Royal Society of London. Series B, Containing Papers of a Biological Character*, 79(532):337–349, July 1907.

[153] H. E. Roaf and C. S. Sherrington. Experiments in examination of the ;locked-jaw' induced by tetanus toxin. *The Journal of physiology*, 34(4-5):315–331, August 1906.

[154] U Eisel, W Jarausch, K Goretzki, A Henschen, J Engels, U Weller, M Hudel, E Habermann, and H Niemann. Tetanus toxin: primary structure, expression in e. coli, and homology with botulinum toxins. *The EMBO journal*, 5:2495–2502, October 1986.

[155] C Montecucco and G Schiavo. Mechanism of action of tetanus and botulinum neurotoxins. *Molecular microbiology*, 13:1–8, July 1994.

[156] G Schiavo, P Boquet, B R Dasgupta, and C Montecucco. Membrane interactions of tetanus and botulinum neurotoxins: a photolabelling study with photoactivatable phospholipids. *Journal de physiologie*, 84:180–187, 1990.

[157] C Fotinou, P Emsley, I Black, H Ando, H Ishida, M Kiso, K A Sinha, N F Fairweather, and N W Isaacs. The crystal structure of tetanus toxin hc fragment complexed with a synthetic gt1b analogue suggests cross-linking between ganglioside receptors and the toxin. *The Journal of biological chemistry*, 276:32274–32281, August 2001.

[158] Andreas Rummel, Steffen Bade, Jürgen Alves, Hans Bigalke, and Thomas Binz. Two carbohydrate binding sites in the h(cc)-domain of tetanus neurotoxin are required for toxicity. *Journal of molecular biology*, 326:835–847, February 2003.

[159] Andreas Rummel, Kirstin Häfner, Stefan Mahrhold, Natallia Darashchonak, Matthew Holt, Reinhard Jahn, Silke Beermann, Tino Karnath, Hans Bigalke, and Thomas Binz. Botulinum neurotoxins c, e and f bind gangliosides via a conserved binding site prior to stimulation-dependent uptake with botulinum neurotoxin f utilising the three isoforms of sv2 as second receptor. *Journal of neurochemistry*, 110:1942–1954, September 2009.

[160] Chen Chen, Zhuji Fu, Jung-Ja P Kim, Joseph T Barbieri, and Michael R Baldwin. Gangliosides as high affinity receptors for tetanus neurotoxin. *The Journal of biological chemistry*, 284:26569–26577, September 2009.

[161] Antony N. Antoniou and Colin Watts. Antibody modulation of antigen presentation: positive and negative effects on presentation of the tetanus toxin antigen via the murine b cell isoform of fcgammarii. *European journal of immunology*, 32:530–40, Feb 2002.

[162] Janne M. Toivonen, Sara Olivan, and Rosario Osta. Tetanus toxin c-fragment: the courier and the cure? *Toxins*, 2:2622–44, Nov 2010. NLM: Original Date-Completed: 20111110.

[163] O. Rossetto, M. Scorzeto, A. Megighian, and C. Montecucco. Tetanus neurotoxin. *Toxicon*, 66:59 – 63, 2013.

[164] Rupp B. Knapp M., Segelke B. The 1.61 angstrom structure of the tetanus toxin ganglioside binding region: Solved by mad and mir phase combination. *Am.Cryst.Assoc.*, 1998.

[165] Morten Thaysen-Andersen, Sys Borcher Jorgensen, Ellen Sloth Wilhelmsen, Jesper Westphal Petersen, and Peter Hojrup. Investigation of the detoxification mechanism of formaldehyde-treated tetanus toxin. *Vaccine*, 25:2213–27, Mar 2007.

[166] A Galazka and F Gasse. The present status of tetanus and tetanus vaccination. *Current topics in microbiology and immunology*, 195:31–53, 1995.

[167] J. L. Middlebrook and J. E. Brown. Immunodiagnosis and immunotherapy of tetanus and botulinum neurotoxins. *Clostridial Neurotoxins*, January 1995.

[168] E.I. Shmelyova, editor. *Study of stability of physical properties and biological activity of liquid and freeze dried adsorbed pertussis-diphtheria-tetanus vaccines. Proceedings of the symposium on stability and effectiveness of measles, poliomyelitis and pertussis vaccines.*, Zagreb, Yugoslavia, 1976. Yugoslav Academy of Sciences and Arts.

[169] World Health Organization. Expanded programme on immunization : The effects of freezing on the appearance, potency and toxicity of adsorbed and unadsorbed dpt vaccines = programme Élargi de vaccination : Effets de la congélation

sur l'aspect, l'activité et la toxicité des vaccins dtcoq adsorbés et non adsorbés. *Weekly Epidemiological Record = Relevé épidémiologique hebdomadaire*, pages 396–398, 1980.

[170] J. Aleksandrowicz, M. Drozdz, M. Fieka, and W. Kurzatkowski. Evaluation of the physico-chemical state of aluminium hydroxide in biopreparations stored at various conditions. *Medycyna doswiadczalna i mikrobiologia*, 42(3-4):163–170, 1990.

[171] Ümit Kartoğlu. *Insight and Control of Infectious Disease in Global Scenario*, chapter Temperature Sensitivity of the Diphtheria Containing Vaccines, pages 271–287. InTech, 2012.

[172] N F Fairweather and V A Lyness. The complete nucleotide sequence of tetanus toxin. *Nucleic acids research*, 14:7809–7812, October 1986.

[173] Thomas Binz and Andreas Rummel. Cell entry strategy of clostridial neurotoxins. *Journal of neurochemistry*, 109:1584–1595, June 2009.

[174] Seetharaman Jayaraman, Subramaniam Eswaramoorthy, Desigan Kumaran, and Subramanyam Swaminathan. Common binding site for disialyllactose and tri-peptide in c-fragment of tetanus neurotoxin. *Proteins*, 61:288–295, November 2005.

[175] Roya Khosravi-Eghbal, Ahmad Reza Mahmoudi, Mahmood Jeddi-Tehrani, Hodjatallah Rabbani, and Fazel Shokri. Comparative in vitro and in vivo assessment of toxin neutralization by anti-tetanus toxin monoclonal antibodies au - yousefi, mehdi. *Human Vaccines & Immunotherapeutics*, 10(2):344–351, February 2014.

[176] M R Wilkins, E Gasteiger, A Bairoch, J C Sanchez, K L Williams, R D Appel, and D F Hochstrasser. Protein identification and analysis tools in the expasy server. *Methods in molecular biology (Clifton, N.J.)*, 112:531–552, 1999.

[177] J A Bornhorst and J J Falke. Purification of proteins using polyhistidine affinity tags. *Methods in enzymology*, 326:245–254, 2000.

[178] Rui Yu, Shaoqiong Yi, Changming Yu, Ting Fang, Shuling Liu, Ting Yu, Xiaohong Song, Ling Fu, Lihua Hou, and Wei Chen. A conformational change of c fragment of tetanus neurotoxin reduces its ganglioside-binding activity but does not destroy its immunogenicity. *Clinical and vaccine immunology : CVI*, 18:1668–1672, Oct 2011.

[179] Caroline Bayart, Sébastien Peronin, Elisa Jean, Joseph Paladino, Philippe Talaga, and Marc Le Borgne. The combined use of analytical tools for exploring tetanus toxin and tetanus toxoid structures. *Journal of Chromatography B*, 1054:80–92, June 2017.

[180] O. Qazi, D. Sesardic, R. Tierney, Z. Soderback, D. Crane, B. Bolgiano, and N. Fairweather. Reduction of the ganglioside binding activity of the tetanus toxin HC fragment destroys immunogenicity: Implications for development of novel tetanus vaccines. *Infection and Immunity*, 74(8):4884–4891, jul 2006.

[181] E W Hewitt, A Treumann, N Morrice, P J Tatnell, J Kay, and C Watts. Natural processing sites for human cathepsin e and cathepsin d in tetanus toxin: implications for t cell epitope generation. *The Journal of Immunology*, 159(10):4693–9, 1997.

[182] A. J. Makoff, M. D. Oxer, M. A. Romanos, N. F. Fairweather, and S. Ballantine. Expression of tetanus toxin fragment c in e. coli: high level expression by removing rare codons. *Nucleic acids research*, 17:10191–202, Dec 1989.

[183] Germain L. Rosano and Eduardo A. Ceccarelli. Recombinant protein expression in escherichia coli: advances and challenges. *Front. Microbiol.*, 5, apr 2014.

[184] Friedrich Widdel. Theory and measurement of bacterial growth. *Di dalam Grundpraktikum Mikrobiologie*, 4(11):1–11, 2007.

[185] Fanglian He. Bca (bicinchoninic acid) protein assay. *Bio-protocol*, 1(5):e44, March 2011.

[186] Fukumi Hashimoto, Tsuneyoshi Horigome, Miyuki Kanbayashi, Kaoru Yoshida, and Hiroshi Sugano. An improved method for separation of low-molecular-weight polypeptides by electrophoresis in sodium dodecyl sulfate-polyacrylamide gel. *Analytical Biochemistry*, 129(1):192 – 199, 1983.

[187] Biorad. *Electrophoresis Guide, Interactive PDF, Rev B*. Biorad, NA. http://www.bio-rad.com/en-uk/applications-technologies/protein-electrophoresis-methods.

[188] C.N. Banwell. *Fundamentals of molecular spectroscopy*. European chemistry series. McGraw-Hill, 1966.

[189] Eugene A. Permyakov. The use of uv-vis absorption spectroscopy for studies of natively disordered proteins. In *Methods in Molecular Biology*, pages 421–433. Springer Science Business Media, 2012.

[190] S W Provencher and J Glackner. Estimation of globular protein secondary structure from circular dichroism. *Biochemistry*, 20:33–37, Jan 1981.

[191] I H van Stokkum, H J Spoelder, M Bloemendal, R van Grondelle, and F C Groen. Estimation of protein secondary structure and error analysis from circular dichroism spectra. *Analytical biochemistry*, 191:110–118, Nov 1990.

[192] Bijan Ranjbar and Pooria Gill. Circular dichroism techniques: biomolecular and nanostructural analyses- a review. *Chemical biology & drug design*, 74:101–120, Aug 2009.

[193] John R. Crowther. *The ELISA Guidebook*. Humana Press, 2009.

[194] Robert Hnasko, Alice Lin, Jeffery A McGarvey, and Larry H Stanker. A rapid method to improve protein detection by indirect elisa. *Biochemical and biophysical research communications*, 410:726–731, Jul 2011.

[195] Murphy. Static and dynamic light scattering of biological macromolecules: what can we learn? *Current opinion in biotechnology*, 8:25–30, Feb 1997.

[196] Jeffrey D Clogston and Anil K Patri. Zeta potential measurement. *Methods in molecular biology (Clifton, N.J.)*, 697:63–70, 2011.

[197] Marie-Bernadette Villiers, Françoise M. Gabert, Muriel R. Jacquier, Christian L. Villiers, and Maurice G. Colomb. Involvement of the zn-binding region of tetanus toxin in b and t recognition. influence of zn fixation. *Molecular Immunology*, 30(2):129–136, February 1993.

[198] I. Kerblat, S. Tongiani-Dahshan, C. Aude-Garcia, M.-B. Villiers, C. Drouet, and P. N. Marche. Tetanus toxin l chain is processed by major histocompatibility complex class i and class ii pathways and recognized by cd8+ or cd4+ t lymphocytes. *Immunology*, 100(2):178–184, June 2000.

[199] S. Demotz, C. Barbey, G. Corradin, A. Amoroso, and A. Lanzavecchia. The set of naturally processed peptides displayed by dr molecules is tuned by polymorphism of residue 86. *European journal of immunology*, 23:425–32, Feb 1993.

[200] P. Panina-Bordignon, A. Tan, A. Termijtelen, S. Demotz, G. Corradin, and A. Lanzavecchia. Universally immunogenic t cell epitopes: promiscuous binding to human mhc class ii and promiscuous recognition by t cells. *European journal of immunology*, 19:2237–42, Dec 1989.

[201] S. Demotz, A. Lanzavecchia, U. Eisel, H. Niemann, C. Widmann, and G. Corradin. Delineation of several dr-restricted tetanus toxin t cell epitopes. *Journal of immunology (Baltimore, Md. : 1950)*, 142:394–402, Jan 1989.

[202] Mehdi Yousefi, Fathollah Tahmasebi, Vahid Younesi, Alireza Razavi, Jalal Khoshnoodi, Ali Ahmad Bayat, Ebrahim Abbasi, Hodjatallah Rabbani, Mahmood Jeddi-Tehrani, and Fazel Shokri. Characterization of neutralizing monoclonal antibodies directed against tetanus toxin fragment c. *Journal of Immunotoxicology*, 11(1):28–34, January 2014.

[203] Yun-Chu Chen. *Ensilication and Thermal Stability of Proteins*. PhD thesis, University of Bath, 12 2017.

[204] J.C. Brinker and G.W. Scherer. *Sol-Gel Science*, chapter Hydrolysis and Condensation: Silicates, page 104. Elsevier, 1990.

[205] David J. Belton, Olivier Deschaume, and Carole C. Perry. An overview of the fundamentals of the chemistry of silica with relevance to biosilicification and technological advances. *The FEBS Journal*, 279(10):1710–1720, 2012.

[206] Daniel Otzen. The role of proteins in biosilicification. *Scientifica*, 2012:867562, 2012.

[207] Todd J Dolinsky, Jens E Nielsen, J Andrew McCammon, and Nathan A Baker. Pdb2pqr: an automated pipeline for the setup of poisson–boltzmann electrostatics calculations. *Nucleic acids research*, 32(suppl_2):W665–W667, 2004.

[208] MG Lerner and HA Carlson. Apbs plugin for pymol. *Ann Arbor: University of Michigan*, 2006.

[209] Samir Unni, Yong Huang, Robert M Hanson, Malcolm Tobias, Sriram Krishnan, Wilfred W Li, Jens E Nielsen, and Nathan A Baker. Web servers and services for electrostatics calculations with apbs and pdb2pqr. *Journal of computational chemistry*, 32(7):1488–1491, 2011.

[210] Arijit Mitra and J. Donald Rimstidt. Solubility and dissolution rate of silica in acid fluoride solutions. *Geochimica et Cosmochimica Acta*, 73(23):7045–7059, December 2009.

[211] Weilie Zhou, Robert Apkarian, Zhong Lin Wang, and David Joy. Fundamentals of scanning electron microscopy (sem). In *Scanning microscopy for nanotechnology*, pages 1–40. Springer, 2006.

[212] Brian C Smith. *Fundamentals of Fourier transform infrared spectroscopy*. CRC press, 2011.

[213] A Elliott and EJ Ambrose. Structure of synthetic polypeptides. *Nature*, 165(4206):921, 1950.

[214] Samuel Krimm and Jagdeesh Bandekar. Vibrational spectroscopy and conformation of peptides, polypeptides, and proteins. In *Advances in protein chemistry*, volume 38, pages 181–364. Elsevier, 1986.

[215] Heino Susi and D Michael Byler. Resolution-enhanced fourier transform infrared spectroscopy of enzymes. In *Methods in enzymology*, volume 130, pages 290–311. Elsevier, 1986.

[216] Philip J Launer. Infrared analysis of organosilicon compounds: Spectra-structure correlations, laboratory for materials. *Inc. Burnt Hills, New York*, page 12027, 1987.

[217] Jilie Kong and Shaoning Yu. Fourier transform infrared spectroscopic analysis of protein secondary structures. *Acta biochimica et biophysica Sinica*, 39(8):549–559, 2007.

[218] Caroline A Schneider, Wayne S Rasband, and Kevin W Eliceiri. Nih image to imagej: 25 years of image analysis. *Nature methods*, 9(7):671, 2012.

[219] Hon. J.W. Strutt. Lviii. on the scattering of light by small particles. *The London, Edinburgh, and Dublin Philosophical Magazine and Journal of Science*, 41(275):447–454, 1871.

[220] J. H. Hubbell, Wm. J. Veigele, E. A. Briggs, R. T. Brown, D. T. Cromer, and R. J. Howerton. Atomic form factors, incoherent scattering functions, and photon scattering cross sections. *Journal of Physical and Chemical Reference Data*, 4(3):471–538, 1975.

[221] J. H. Hubbell and I. O/verbo/. Relativistic atomic form factors and photon coherent scattering cross sections. *Journal of Physical and Chemical Reference Data*, 8(1):69–106, 1979.

[222] A. Guinier and G. Fournet. *Small-Angle Scattering of X-rays* . John Wiley & Sons, Inc., New York, 1955.

[223] M Kerker. *The Scattering of Light and Other Electromagnetic Radiation*. Academic Press, 1969.

[224] P. Moore. Small-angle scattering. information content and error analysis. *Journal of Applied Crystallography*, 13(2):168–175, 1980.

[225] D. F. R. Mildner Hall and P L. Small-angle scattering from porous solids with fractal geometry. *Journal of Physics D: Applied Physics*, 19(8):1535, 1986.

[226] L. A. Feigin and D. I. Svergun. *Structure Analysis by Small-Angle X-Ray and Neutron Scattering*. Springer, 1987.

[227] Yun-Chu Chen, Tristan Smith, Robert H Hicks, Aswin Doekhie, Francoise Koumanov, Stephen A Wells, Karen J Edler, Jean van den Elsen, Geoffrey D Holman, Kevin J Marchbank, and Asel Sartbaeva. Thermal stability, storage and release of proteins with tailored fit in silica. *Scientific reports*, 7:46568, April 2017.

[228] R. A. Pethrick. Polymers and neutron scattering, edited by j. s. higgins and h. c. benoit. oxford university press, oxford, 1994. pp. xix + 436, price £65.00. isbn 0-19-85-1003-9. *Polymer International*, 37(2):149–150, 1995.

[229] G.R. Kinsel, D.A. Skoog, F.J. Holler, and S.R. Crouch. *Fundamentals of Analytical Chemistry*. Thomson-Brooks/Cole, 2003.

[230] W. L. Bragg. The diffraction of short electromagnetic waves by a crystal. *Scientia*, 23(45):153, 1929.

[231] Debye P. Light scattering in soap solutions. *Annals of the New York Academy of Sciences*, 51(4):575–592, 1949.

[232] G. Porod. Die röntgenkleinwinkelstreuung von dichtgepackten kolloiden systemen. *Kolloid-Zeitschrift*, 133(1):51–51, oct 1953.

[233] Mark Basham, Jacob Filik, Michael T. Wharmby, Peter C. Y. Chang, Baha El Kassaby, Matthew Gerring, Jun Aishima, Karl Levik, Bill C. A. Pulford, Irakli Sikharulidze, Duncan Sneddon, Matthew Webber, Sarnjeet S. Dhesi, Francesco Maccherozzi, Olof Svensson, Sandor Brockhauser, Gabor Náray, and Alun W. Ashton. *Data Analysis WorkbeNch* (*DAWN*). *Journal of Synchrotron Radiation*, 22(3):853–858, May 2015.

[234] Theyencheri Narayanan, Michael Sztucki, Pierre Van Vaerenbergh, Joachim Léonardon, Jacques Gorini, Laurent Claustre, Franc Sever, John Morse, and Peter Boesecke. A multipurpose instrument for time-resolved ultra-small-angle and coherent X-ray scattering. *Journal of Applied Crystallography*, 51(6):1511–1524, Dec 2018.

[235] D. Schneidman-Duhovny, M. Hammel, J. A. Tainer, and A. Sali. Foxs, foxsdock and multifoxs: Single-state and multi-state structural modeling of proteins and their complexes based on saxs profiles. *Nucleic Acids Res*, 44(Web Server issue):W424–9, 2016.

[236] D. Schneidman-Duhovny, M. Hammel, J. A. Tainer, and A. Sali. Accurate saxs profile computation and its assessment by contrast variation experiments. *Biophys J*, 105(4):962–74, 2013.

[237] H. Fischer, M. de Oliveira Neto, H. B. Napolitano, I. Polikarpov, and A. F. Craievich. Determination of the molecular weight of proteins in solution from a single small-angle x-ray scattering measurement on a relative scale. *Journal of Applied Crystallography*, 43(1):101–109, 2010.

[238] Paul Meakin. The effects of rotational diffusion on the fractal dimensionality of structures formed by cluster–cluster aggregation. *The Journal of Chemical Physics*, 81(10):4637–4639, 1984.

[239] B.B. Mandelbrot. *The fractal geometry of nature*. W.H. Freeman, 1982.

[240] Dominique J. Tobler, Sam Shaw, and Liane G. Benning. Quantification of initial steps of nucleation and growth of silica nanoparticles: An in-situ saxs and dls study. *Geochimica et Cosmochimica Acta*, 73(18):5377–5393, 2009.

[241] Charlotte J. Mable, Matthew J. Derry, Kate L. Thompson, Lee A. Fielding, Oleksandr O. Mykhaylyk, and Steven P. Armes. Time-resolved saxs studies of

the kinetics of thermally triggered release of encapsulated silica nanoparticles from block copolymer vesicles. *Macromolecules*, 50(11):4465–4473, 2017.

[242] Janine L Burns, Yao-de Yan, Graeme J Jameson, and Simon Biggs. A light scattering study of the fractal aggregation behavior of a model colloidal system. *Langmuir*, 13(24):6413–6420, 1997.

[243] Dale W. Schaefer, James E. Martin, Pierre Wiltzius, and David S. Cannell. Fractal geometry of colloidal aggregates. *Phys. Rev. Lett.*, 52(26):2371–2374, June 1984.

[244] Christelle Mathé, Stéphanie Devineau, Jean-Christophe Aude, Gilles Lagniel, Stéphane Chédin, Véronique Legros, Marie-Hélène Mathon, Jean-Philippe Renault, Serge Pin, Yves Boulard, and Jean Labarre. Structural determinants for protein adsorption/non-adsorption to silica surface. *PLOS ONE*, 8(11):e81346, 2013.

[245] W.Neal Burnette. "western blotting": Electrophoretic transfer of proteins from sodium dodecyl sulfate-polyacrylamide gels to unmodified nitrocellulose and radiographic detection with antibody and radioiodinated protein a. *Analytical Biochemistry*, 112(2):195 – 203, 1981.

[246] Hong-Wen Gao, Qing Xu, Ling Chen, Shi-Long Wang, Yuan Wang, Ling-Ling Wu, and Yuan Yuan. Potential protein toxicity of synthetic pigments: Binding of poncean s to human serum albumin. *Biophysical Journal*, 94(3):906–917, February 2008.

[247] F. Delben and V. Crescenzi. Thermal denaturation of lysozyme. a differential scanning calorimetry investigation. *Biochim Biophys Acta*, 194(2):615–8, 1969.

[248] Susanne Matheus, Wolfgang Friess, and Hanns-Christian Mahler. Ftir and ndsc as analytical tools for high-concentration protein formulations. *Pharmaceutical research*, 23:1350–1363, June 2006.

[249] Christopher M. Johnson. Differential scanning calorimetry as a tool for protein folding and stability. *Archives of Biochemistry and Biophysics*, 531(1):100–109, 2013.

[250] B. Ibarra-Molero, A. N. Naganathan, J. M. Sanchez-Ruiz, and V. Munoz. Modern analysis of protein folding by differential scanning calorimetry. *Methods Enzymol*, 567:281–318, 2016.

[251] A. W. Coats and J. P. Redfern. Thermogravimetric analysis. a review. *Analyst*, 88:906–924, 1963.

[252] Lee Whitmore and B A Wallace. Protein secondary structure analyses from circular dichroism spectroscopy: methods and reference databases. *Biopolymers*, 89:392–400, May 2008.

[253] Norma J. Greenfield. Using circular dichroism collected as a function of temperature to determine the thermodynamics of protein unfolding and binding interactions. *Nature Protocols*, 1:2527, December 2006.

[254] N. Sreerama and R. W. Woody. Estimation of protein secondary structure from circular dichroism spectra: comparison of contin, selcon, and cdsstr methods with an expanded reference set. *Analytical biochemistry*, 287:252–60, Dec 2000.

[255] L. A. Compton and W. C. Jr Johnson. Analysis of protein circular dichroism spectra for secondary structure using a simple matrix multiplication. *Analytical biochemistry*, 155:155–67, May 1986.

[256] P. Manavalan and W. C. Jr Johnson. Variable selection method improves the prediction of protein secondary structure from circular dichroism spectra. *Analytical biochemistry*, 167:76–85, Nov 1987.

[257] David Mao, E. Wachter, and B. A. Wallace. Folding of the mitochondrial proton adenosine triphosphatase proteolipid channel in phospholipid vesicles. *Biochemistry*, 21(20):4960–4968, 1982. PMID: 6291595.

[258] E. W. Silverton, E. A. Padlan, D. R. Davies, S. Smith-Gill, and M. Potter. Crystalline monoclonal antibody fabs complexed to hen egg white lysozyme. *Journal of molecular biology*, 180:761–5, Dec 1984.

[259] Michele Cianci, John R. Helliwell, and Atsuo Suzuki. The interdependence of wavelength, redundancy and dose in sulfur SAD experiments. *Acta Crystallographica Section D*, 64(12):1196–1209, Dec 2008.

[260] K. Takada, N. Ohno, and T. Yadomae. Binding of lysozyme to lipopolysaccharide suppresses tumor necrosis factor production in vivo. *Infection and immunity*, 62:1171–5, Apr 1994.

[261] Leslie Brent. The discovery of immunologic tolerance. *Human Immunology*, 52(2):75 – 81, 1997.

[262] P. Shih, D. R. Holland, and J. F. Kirsch. Thermal stability determinants of chicken egg-white lysozyme core mutants: hydrophobicity, packing volume, and conserved buried water molecules. *Protein Sci*, 4(10):2050–62, 1995.

[263] Tatsuyuki Yamamoto, Noriko Fukui, Akihiro Hori, and Yoshihisa Matsui. Circular dichroism and fluorescence spectroscopy studies of the effect of cyclodextrins on the thermal stability of chicken egg white lysozyme in aqueous solution. *Journal of Molecular Structure*, 782(1):60–66, 2006.

[264] A. Blumlein and J. J. McManus. Reversible and non-reversible thermal denaturation of lysozyme with varying ph at low ionic strength. *Biochim Biophys Acta*, 1834(10):2064–70, 2013.

[265] Ozan S. Kumru, Sangeeta B. Joshi, Dawn E. Smith, C. Russell Middaugh, Ted Prusik, and David B. Volkin. Vaccine instability in the cold chain: Mechanisms, analysis and formulation strategies. *Biologicals*, 42(5):237 – 259, 2014.

[266] D. M. Matthias, J. Robertson, M. M. Garrison, S. Newland, and C. Nelson. Freezing temperatures in the vaccine cold chain: a systematic literature review. *Vaccine*, 25(20):3980–3986, May 2007.

[267] A.P. Silve. Size matters: A clear solution. Master's thesis, University of Bath, 2018.

[268] John H. Harreld, Takeo Ebina, Norihiko Tsubo, and Galen Stucky. Manipulation of pore size distributions in silica and ormosil gels dried under ambient pressure conditions. *Journal of Non-Crystalline Solids*, 298(2):241–251, March 2002.

[269] Tapan Kanti Das, Imran Khan, Denis L. Rousseau, and Joel M. Friedman. Temperature dependent quaternary state relaxation in sol-gel encapsulated hemoglobin. *Biospectroscopy*, 5(S5):S64–S70, January 1999.

[270] L. J. Juszczak and J. M. Friedman. Uv resonance raman spectra of ligand binding intermediates of sol-gel encapsulated hemoglobin. *The Journal of biological chemistry*, 274:30357–60, Oct 1999.

[271] Bakul C. Dave, Bruce Dunn, Joan Selverstone Valentine, and Jeffrey I. Zink. Sol-gel encapsulation methods for biosensors. *Anal. Chem.*, 66(22):1120A–1127A, November 1994.

[272] Alexey G. Kikhney and Dmitri I. Svergun. A practical guide to small angle x-ray scattering (saxs) of flexible and intrinsically disordered proteins. *FEBS Letters*, 589(19, Part A):2570–2577, September 2015.

[273] W. B. Ershler, A. L. Moore, and M. P. Hacker. Specific in vivo and in vitro antibody response to tetanus toxoid immunization. *Clinical and experimental immunology*, 49(3):552–558, September 1982.

[274] Guangchuan Wang, Hangyu Zhou, Qing-Gong Nian, Yuling Yang, Cheng-Feng Qin, and Ruikang Tang. Robust vaccine formulation produced by assembling a hybrid coating of polyethyleneimine-silica. *Chem. Sci.*, 7(3):1753–1759, 2016.

[275] Lucy Cliff. Thermal stability of silica encapsulated lysozyme. Master's thesis, University of Bath, 2018.

[276] Christopher Pudney. Measuring protein flexibility and conformational state, 2016. UK Patent 1604640.1.

[277] RE Woolley, A Kwok, S Parsons, HBL Jones, P Phaal, O Kassaar, DAM Catici, SA Wells, M Connolly, A Watts, JMH van den Elsen, and CR Pudney. Revealing protein conformation and stability using a quantitative understanding of biomolecular edge shift. Patented.

[278] Liam Wrigley. Ensilication and release of monoclonal antibodies. Master's thesis, University of Bath, 2016.

[279] Maria Pelliccia, Patrizia Andreozzi, Jayson Paulose, Marco D'Alicarnasso, Valeria Cagno, Manuela Donalisio, Andrea Civra, Rebecca M. Broeckel, Nicole Haese, Paulo Jacob Silva, Randy P. Carney, Varpu Marjomäki, Daniel N. Streblow, David Lembo, Francesco Stellacci, Vincenzo Vitelli, and Silke Krol. Additives for vaccine storage to improve thermal stability of adenoviruses from hours to months. *Nature Communications*, 7:13520, November 2016.